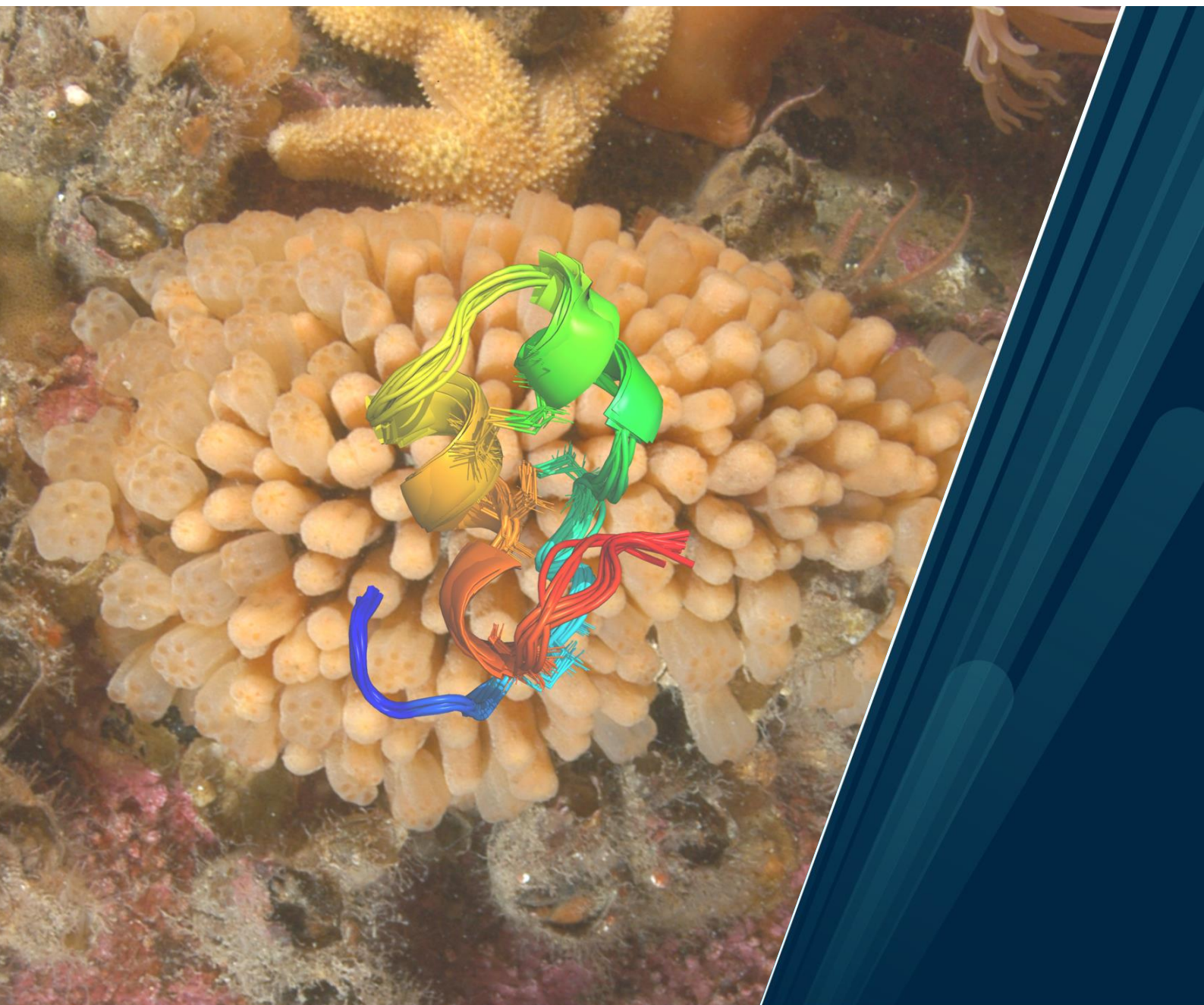Faculty of Biosciences, Fisheries and Economics

The Norwegian College of Fishery Science

Antimicrobial peptides from the Arctic ascidian *Synoicum turgens*

Ida K. Ø. Hansen

A dissertation for the degree of Philosophiae Doctor   April 2022

A dissertation for the degree of Philosophiae Doctor

Antimicrobial peptides from the Arctic ascidian *Synoicum turgens*

Ida Kristine Østnes Hansen

Tromsø, April 2022

ABSTRACT

The rise in frequency of antibiotic resistant pathogenic bacteria makes the need for new treatment options for previously curable bacterial infections ever more important. In the process of discovering and developing antibacterial agents, one powerful approach has been borrowing wisdom from nature. Antimicrobial peptides (AMPs) are critical components of the innate immune systems found in almost all eukaryotic life forms. Their mode of action includes disruption of the bacterial membrane and to trigger supporting immune responses. Due to these properties, AMPs are considered promising lead structures that can be further developed into commercially available antibiotics to treat or prevent human diseases caused by bacteria.

The work conducted in this thesis aims to discover and characterize novel antimicrobial peptides from the Arctic marine ascidian *Synoicum turgens* by using a marine bioprospecting approach. This includes collection, extraction and fractionation of biomass, antibacterial bioactivity testing and AMP isolation followed by chemical and biological characterization. For one isolated peptide class, truncated versions were prepared, aiming to produce shorter, linear variants with retained antimicrobial activity.

In **paper I**, turgencin A and B and their oxidized derivatives were discovered through bioassay-guided purification. These peptides had an unusual disulfide connectivity, rarely seen in marine AMPs. Both turgencin A and B were potently active against all assayed bacterial strains. Membrane assays showed that the peptides cause bacterial membrane disruption within a few seconds. Turgencin A and B also displayed some cytotoxic activity against two human cell lines. Oxidation of the methionine present in both peptides decreased the bioactivities in all assays.

Turgencin A, being the most potent AMP, was subject for sequence analysis and prediction of antimicrobial potential of different regions in **paper II**. Truncated and modified variants of turgencin A were synthetically produced to make smaller AMPs with the potential of being developed into antimicrobial drug leads. These 10-mer peptides, named StAMP-1–11, were made using an amino acid replacement strategy. Some of the Trp enriched peptides had similar bactericidal activity as the parent peptide turgencin A, and no cytotoxic activity against the mammalian cell lines.

During turgencin isolation, a series of other smaller peptides were discovered in the same extracts presumably with antimicrobial activity. These isolated and characterized ~2 kDa, cysteine-rich peptides (CRPs) (described in **paper III**), were named St-CRP-1 and St-CRP-2 and contained 18-19 amino acids. The St-CRPs shared a disulfide connectivity pattern with alpha-defensins, had a neutral net charge, moderate antibacterial activity and showed no cytotoxicity.

In addition, the introduction section provides background information on topics related to the thematic of the articles. This includes an introduction to bacteria, antibiotics and antibiotic resistance, AMPs, ascidians, and the marine environment.

ACKNOWLEDGEMENT

First, I would like to thank my team of supervisors, Prof. Tor Haug, and co-supervisors Prof. Klara Stensvåg and Assoc. Prof. Hans-Matti Blencke. Matti, thank you for your guidance and help with everything that has to do with single-celled organisms. Klara, the heart of our group, thank you for always keeping your door open even when your calendar begs you to lock it. Tor, thank you for your guidance and patience, and for many discussions about everything from work to football to parenting. It has been an honor to have a fellow Lofoting as my main supervisor.

I would also like to express my gratitude to Aaron J. C. Andersen for your help with isolation and MS-experiments. Thank you for spreading your Kiwi humor and being a good friend. Further, I would like to thank Runar for walking the marine bioprospecting path with me since 2006. You are a nightmare in discussions, but I would not be without them. Thank you to Hege for all help in the lab, and for letting everyone in building know when to take a coffee break through your awesome laughter.

To Prof. David Craik, thank you letting me work in your lab, and to Aaron Poth for all your help with peptide sequencing. Thank you to everyone in Craiks group for making my stay in Brisbane such an unforgettable adventure. I would also like to thank Jeanette, Espen, and everyone else in Marbio for letting me use your lab facilities, and always making me feel welcome when I come by. Thank you, Johan, for your remarkable NMR contributions, and for sharing your twin parenting experience.

To all my present and former colleges, both inside and outside the marine bioprospecting group, thank you for making such a good working environment. I look forward going to work every day because of you. Thank you to all my co-authors for your contributions, and to Aaron J. C., Sietske and Kine for proofreading my thesis. Thank you to fellow PhD students over all these years for good discussions, laughter, and coffee breaks. Due to limited space, I cannot list you all, but you know who you are. Thank you to all my friends for caring for my wellbeing, and for at least pretending to be interested in my PhD.

Finally, my gratitude goes to my family for all your love and support. Mum, the day is finally here. To my wonderful twin boys, you are the main reason this thesis is overdue, but you are also the best thing that happened to me during this PhD. My absolute biggest gratitude goes to my wife, Kine. Thank you for keeping up with me during this endless journey, for all your contributions to my work, and for being the best partner and mum to our kids. You are my rock. I love you!

Ida K. Ø. Hansen, Tromsø 23.03.2022.

LIST OF PAPERS

The following three publications form the basis of this thesis:

Paper I

Ida K. Ø. Hansen, Johan Isaksson, Aaron G. Poth, Kine Ø. Hansen, Aaron J.C. Andersen, Céline S. Richard, Hans-Matti Blencke, Klara Stensvåg, David J. Craik and Tor Haug
Isolation and characterization of antimicrobial peptides with unusual disulfide connectivity from the colonial ascidian *Synoicum turgens*
Marine Drugs (2020). doi: 10.3390/md18010051

Paper II

Ida K. Ø. Hansen, Tomas Lövdahl, Danijela Simonovic, Kine Ø. Hansen, Aaron J. C. Anderson, Hege Devold, Celine Richard, Jeanette H. Andersen, Morten B. Strøm and Tor Haug
Antimicrobial activity of small synthetic peptides based on the marine peptide turgencin A: Prediction of antimicrobial peptide sequences in a natural peptide and strategy for optimization of potency
International Journal of Molecular Sciences (2020). doi: 10.3390/ijms21155460

Paper III

Ida K. Ø. Hansen, Phil B. Rainsford, Johan Isaksson, Kine Ø. Hansen, Klara Stensvåg, Anastasia Albert, Terje Vasskog and Tor Haug
Isolation and characterization of St-CRPs: Cysteine-rich peptides from the Arctic marine ascidian *Synoicum turgens*
Manuscript

Contributions

	Paper I	Paper II	Paper III
Concept and idea	IKØH, KS, DJC, TH	IKØH, MBS, TH	IKØH, KS, TV, TH
Study design and methods	IKØH, AGP, CSMR	IKH, TL, DS, AJCA	IKØH, AA, TV, JI
Data gathering and interpretation	IKØH, CSMR, HMB, TH, AGP, AJCA, JI	IKØH, TL, DS, KØH, JHA, AJCA, HD, CSMR, AJCA, MBS, TH	IKØH, KØH, AA, TV, PBR, JI
Manuscript preparation	IKØH, JI, KØH, AJCA, CSMR, HMB, TH	IKØH, MBS, TH	IKØH, PBR, JI, TV, TH

1D NMR	One-dimensional nuclear magnetic resonance
2D NMR	Two-dimensional nuclear magnetic resonance
α	Alpha
ADAM	Database of anti-microbial peptides
APD	The antimicrobial peptide database
AMPs	Antimicrobial peptides
β	Beta
C18	Octadecyl
CAMP$_{R3}$	The collection of anti-microbial peptides
COSY	Correlation spectroscopy
CRPs	Cysteine-rich peptides
Da	Dalton
DAD	Diode array detector
ESI	Electrospray ionization
FA	Formic acid
FDA	The American food and drug administration
G+	Gram-positive
G-	Gram-negative
HPLC	High performance liquid chromatography
HR	High resolution
IL-10	Interleukin 10
LLE	Liquid-liquid extraction
LPS	Lipopolysaccharides
MIC	Minimal inhibitory concentration
MoA	Mode of action
MS	Mass spectrometry
m/z	Mass-to-charge
NCFS	Norwegian college of fishery sciences
PAM	Peptidylglycine α-amidating monooxygenase
PTM	Post-translational modification
RP	Reversed phase
SPE	Solid phase extraction
TFA	Trifluoroactic acid
TNF	Tumor necrosis factor
ToF	Time-of-flight
UHPLC	Ultra high-performance liquid chromatography
UiT	The Arctic University of Norway
UV	Ultraviolet
WHO	World Health Organization

LIST OF FIGURES

LIST OF TABLES

TABLE OF CONTENTS

1. INTRODUCTION

Antibiotics are bactericidal or bacteriostatic agents mainly used to treat or prevent pathogenic bacterial infections in humans and animals, while causing no harm to host cells [1]. Antibiotic therapy has made a profound impact on human health, enabling treatment of several leading causes of death in the pre-antibiotic era, like tuberculosis, which is caused by the pathogenic bacterium *Mycobacterium tuberculosis* [2]. However, selective evolutionary pressure inflicted on bacteria by extensive and improper use of antibiotics [3], has caused bacteria to develop resistance mechanisms in order to survive by neutralizing or destroying antibiotics [4]. This is threatening the continued efficacy of antibiotic agents. The World Health Organization (WHO) is terming this new phase the 'post-antibiotic era', where previously treatable infections become fatal due to diminishing treatment options [5]. The problem has been aggravated from downscaled efforts by the pharmaceutical industry to the development of new antibiotics [6]. Current estimates state that 700,000 people die annually due to antibiotic resistant bacterial infections [7]. This number is predicted to escalate as the availability of active antibiotic agents gradually lowers and resistant pathogenic bacteria spreads throughout the global population [8]. If not counteracted, this continued evolution and spread of antibiotic resistance in pathogens could prove to be a long-term public health menace [6].

In search of new antibiotics, nature remains the richest and most versatile source, as the large majority of antibiotics currently used in clinical therapy are natural products or derivatives thereof [9]. Antimicrobial peptides (AMPs) have become a promising focus area in antibiotic research [2]. These ribosomally synthesized peptides have properties which makes them desirable lead compounds for the development of new antibiotics, including high potency and a low tendency of resistance developing towards them [2, 10].

1.1 BACTERIA AND ANTIBIOTICS

Bacteria constitute a diverse group of omnipresent microorganisms, which are distinctly different from human cells [11]. They are prokaryotic, thus lacking membrane-bound organelles [12]. Their peptidoglycan cell walls have no homologous structures in vertebrates, their essential nutrients are different, and there is a large difference between eukaryotic and prokaryotic ribosomal RNAs [13]. Although most bacteria are harmless, beneficial, or even

necessary, some are opportunistic or pathogenic, raising the need for antibiotics to prevent or treat bacterial infections [14, 15].

1.1.1 Gram-positive and Gram-negative bacteria

Based on differences in the cell envelope structure, bacteria are commonly divided into two groups; Gram-positive (G+) and Gram-negative (G-) bacteria [16, 17]. A simplified illustration of the G+ and G- cell wall constructions is shown in Figure 1. Both G+ and G- bacteria have an inner cytoplasmic phospholipid bilayer membrane [18], but in G+ bacteria, a thick peptidoglycan layer surrounds this membrane. Embedded through and on the peptidoglycan layer are various lipoteichoic acids, which gives the surface of G+ bacteria a negative charge [19]. In G- bacteria, the cytoplasmic membrane is surrounded by a single layer of peptidoglycan, enclosed by an outer membrane. The outer membrane is distinctly different from the inner membrane as its outer leaflet consists of lipopolysaccharides (LPS) [20]. LPS is unique to G- bacteria and also renders the surface of G- bacteria negatively charged. Both G+ and G- cell envelopes contain transmembrane proteins carrying out a variety of functions, including export of waste, import of nutrients and cell signaling [18]. The cell walls of bacteria are highly complex, and the composition of its constituents may change in response to external factors [21]. E.g., more than 100 different LPS variants are predicted to be present in *Escherichia coli* alone [22]. The differences between the cell envelope of G+ and G- bacteria confer different properties to the two groups in response to external stress, including antibiotics. In addition, important examples of pathogenic bacteria not belonging to the G+ and G- classes exist. This includes the *Corynebacterineae* group, which *M. tuberculosis* belongs to [23]. The cell envelopes of these bacteria have characteristics of both G+ and G- bacteria [16].
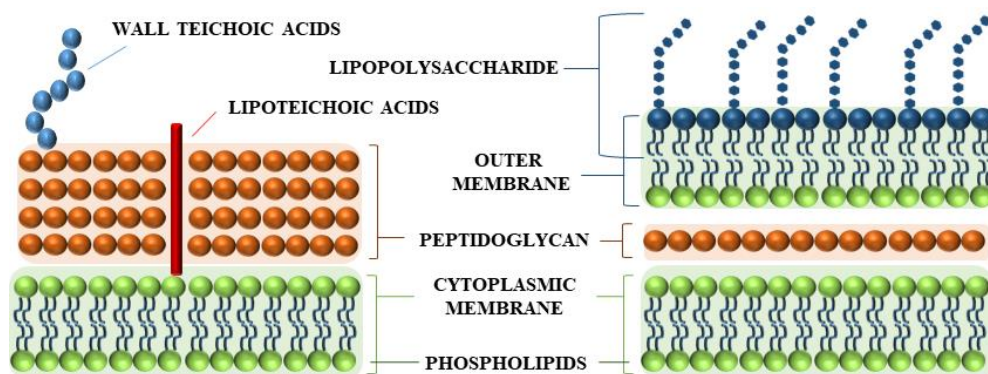
Figure 1: The cell wall of Gram-positive (left) and Gram-negative (right) bacteria [24].

1.1.2 Bacterial infections

Pathogenic bacteria can damage host cells directly, by using host cells as nutrition or through waste or toxin production, or indirectly through host immune response provocation [25]. At the beginning of the 20th century, several leading causes of death in humans were diseases caused by pathogenic microorganisms [26, 27]. Today, bacterial infections are significantly less prominent in terms of mortality rates, especially in developed countries. This is in large parts due to vaccination, improvement in sanitary practices, and the discovery and use of antibiotics [26]. However, WHO still estimates lower respiratory infections, diarrheal diseases and tuberculosis as the fourth, ninth and tenth top global cause of death in 2016 [28]. One of the bacterial diseases with the highest disease burden is tuberculosis, caused by *M. tuberculosis*, which kills between 1.3 and 2 million people every year [27].

1.1.3 Antibiotics

The development of antibiotics is one of the great discoveries of the 20th century. Today, human health and food production are heavily reliant on the effective use of these agents [26, 29, 30]. When antibiotics are used to treat a disease, the desired outcomes are to kill the bacteria or inhibit their growth rate sufficiently to allow the patients' immune system to combat the infection. Antibiotics may also be used prophylactically when the risk of infection is substantial for example during surgical procedures and for patients receiving chemotherapy and immunosuppressive drugs [31]. Prophylactic use of antibiotics in animal feed is also widespread in some countries [32]. The reasons behind this practice are several. It lowers the incidence of diseases, prevents spread of disease in aquaculture or animals and stimulates growth [33].

The differences between bacterial and mammalian cells represent targets for antibiotics. Traditional antibiotics kill or inhibit the growth of bacteria by targeting various biosynthetic processes, including synthesis of proteins, RNA, DNA, peptidoglycan (e.g. penicillins) and folic acid [34]. AMPs comprise a group of compounds with properties distinguishing them from the traditional antibiotics. In fact, AMPs are classified by the WHO as non-traditional antibiotics along with, for example, bacteriophages [35]. Unlike most conventional antibiotics, the mode of action (MoA) of AMPs includes destabilization of the bacterial cell wall and may also cause enhanced immune response in the user by acting as immunomodulatory agents [36].

1.1.4 Antibiotic resistance

Antibiotic resistance is a natural phenomenon where bacteria become resistant to the effects of a previously debilitating antibacterial agent [37]. Bacteria develop resistance to antibiotic agents through gene mutations. Most bacteria are haploid for the vast majority of their genes [38]. This, coupled with typically short generation times, allows mutations to emerge and accumulate rapidly [39]. Many of these genes are carried on mobile genetic elements (plasmids) transmittable to other bacteria, enabling acquirement of the genetic information encoding resistance from other bacteria via horizontal gene transmission [40]. As a result of widespread use of antibiotics in human medicine, as well as in other areas, like veterinary medicine and food production, the evolutionary pressure for the emergence of antibiotic resistance is great [41, 42]. Resistant bacteria may persist in the body, causing prolonged disease or potentially death, as well as an increased risk of infecting others [43]. Moreover, antibiotics support modern medicine. If they lose their effectiveness, key medical procedures, including surgery, caesarean section and treatments that suppress the immune system, such as chemotherapy, may prove fatal [44]. Due to economic and regulatory obstacles, development of new antibiotics by the pharmaceutical industry has steadily decreased over the past decades, further aggravating the problem [45, 46]. At the current rate of drug development versus emergence of antibiotic resistant bacteria, drug development programs are predicted to be insufficient to provide therapeutic coverage in 10 to 20 years [47]. Figure 2 gives a timeline of the deployment of selected antibiotics and when resistance towards the same agents was identified. This clearly illustrates the inevitability and rapidness of the emergence of antimicrobial resistance and highlights the need for continuous development of new antibacterial treatment options.

Bacteria use a wide variety of mechanisms to resist antibiotics [43]. These include prevention of access to drug targets e.g., via efflux pumps, altering the structure of antibiotic targets or direct inactivation of antibiotic e.g., by hydrolysis or phosphorylation [44]. Resistance mechanisms exist for all currently available antibiotics [48]. Bacteria possessing genes which allow them to resist antibiotics with different MoAs are termed multidrug resistant bacteria [49, 50].
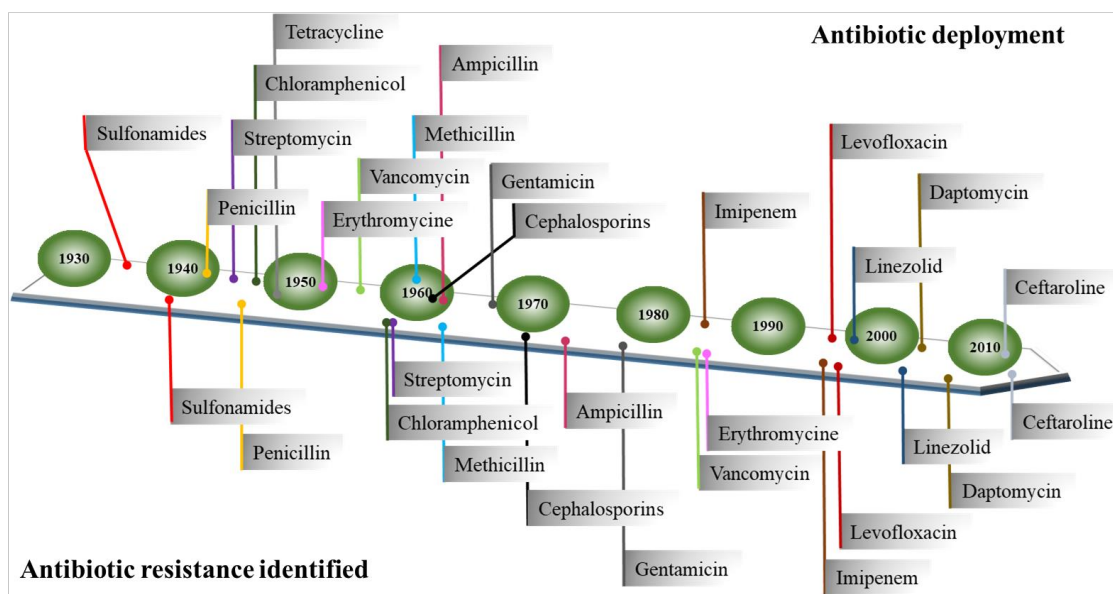
Figure 2: A timeline showing when selected antibiotics were deployed and when resistance against the same antibiotics was identified in pathogenic bacteria. Figure inspired by [43, 51].

1.2 ANTIMICROBIAL PEPTIDES (AMPs)

AMPs are a group of structurally diverse defense compounds encoded in the DNA of their proprietors, which form part of the innate immune system of most plants and animals [36, 52, 53]. Even bacteria produce AMPs (termed bacteriocins), most often to gain an advantage over other bacteria in the competition for food or over the same environmental niche [54]. The widespread distribution of these peptides underscores their critical benefits for the producing organism [55]. AMPs produced by multicellular organisms have evolved over millions of years through evolution as a result of coexistence with microbes. Despite the vast presence and ancient lineage of AMPs, they remain effective weapons to combat bacterial infections. To date, more than 3000 AMPs are registered in the antimicrobial peptide database (APD, https://aps.unmc.edu/), out of which more than 70% come from animals [56-58]. This class of compounds are now gaining increasing attention due to their potential of being developed into antibiotics to combat antibiotic resistant bacteria [59].

AMPs from the marine environment are highly diverse. Some similarities can however be found. In general, marine AMPs are found to contain cysteine [60]. Exceptions to this general observation are AMPs isolated from some tunicates [61]. Post-translational modifications (PTMs) are common in marine AMPs. This includes amidation of the C-terminus, in addition to more complex and extensive PTMs [61-63]. Many marine AMPs, for example the styelins isolated from *Styela clava*, are produced as isoforms, protein variants that originate from a

5

single gene or gene family. Marine derived AMPs are known to be less salt sensitive compared to terrestrial AMPs [64]. This may offer benefits as treatment to specific patient group e.g., patients suffering from cystic fibrosis, who have high salt concentrations in body fluids, thus inhibiting the function of human AMPs, such as human β-defensin-1 [65].

1.2.1 The primary structure of AMPs

The linear array of amino acids forming the primary structure of AMPs is encoded in the DNA of the producing organism [66]. While the encoding gene sequences are known to be highly diverse, some common features can be found in most AMPs. Most are relatively short (10 - 50 amino acids), are rich in basic amino acids rendering them an overall positive charge ranging from +2 to +11, and most contain a substantial portion of hydrophobic residues [67]. It is observed that the basic amino acids arginine and lysine are 50% more abundant in AMPs than in the overall genome, while the acidic amino acids glutamic acid and aspartic acid are about 75% less abundant than expected. In addition, hydrophobic residues are more abundant in AMPs compared to the overall genome [68].

1.2.2 The mature structure and post-translational modifications of AMPs

Following translation, the R-groups (side chains) of the amino acids force the molecules to twist and fold in a specific way. This results in formation of intramolecular hydrogen bonds between the amino hydrogen and carboxyl oxygen atoms in the peptide backbone, folding the peptide into its secondary structure [69]. The most common secondary structural elements observed in natural peptides are α-helixes and β-sheets [69].

Furthermore, the structure of AMPs may be altered through PTMs [70]. PTMs of AMPs include C-terminal amidation, oxidation, disulfide bridge formation, cyclization and halogenation [70]. PTMs appear to influence not only the activity of the peptide, but also their stability against protease degradation and denaturation. Following the final alterations, the peptides adopt their final three-dimensional structures. One example of an α-helical AMP subjected to substantial PTMs is styelin D (Figure 3) [61, 62]. This 32 amino acid peptide was isolated from hemocytes from the ascidian *Styela clava*.

| | 6-bromotryptophan | | Dihydroxyarginine | | Dihydroxylysine | | 3,4-dihydroxyphenylalanine | | 5-hydroxylysine |

Figure 3: The primary structure of styelin D, isolated from the ascidian *Styela clava* [61]. In total, 12 amino acids have undergone post-translational modifications (amino acids highlighted with color) and the C-terminal is amidated.

Disulfide bridges

Disulfide bridges, or disulfide bonds, forms between two cysteine thiol groups (Figure 4) resulting in a covalent bond between two sulfur atoms, as a result of a series of enzyme catalyzed reactions [71]. This introduces conformational constrains to the peptide backbone, which is known to improve stability, enabling the peptide to better resist environmental conditions like high temperature, acidic or basic conditions and may provide an increased peptide half-life [72]. For many peptides with one or more disulfide bridges, their presence is critical for the proper folding of the peptide and thus also often a prerequisite for achieving its biological function [73]. Many peptides with β-sheet secondary structures are stabilized with disulfide bridges [58].

Figure 4: The formation of a disulfide bridge between the side chains of two cysteine amino acids. The curved lines represent the continuation of the peptide backbone [74].

7

1.2.3 Mode of action of AMPs against bacteria

The best characterized MoA of AMPs against bacteria is direct interaction with bacterial membranes causing permeabilization and bacterial death. This is initiated by electrostatic interaction between the peptides' positively charged domain and the negatively charged outer surface of the bacteria. The hydrophobic domain of the peptide then interacts with and embeds into the lipophilic membrane core causing membrane disruption and collapse [75]. The mechanism in which the AMPs are inserted into the bacterial membrane depends on the structural features of the peptide. The most widely mentioned models describing how AMPs transverse bacterial membranes are the toroidal, barrel-stave and carpet models, illustrated in Figure 5 [76, 77]. In the toroidal model, AMPs are inserted into the bacterial membrane causing the two membrane leaflets to connect forming a continuous bend from the top to the bottom, similar to a toroidal hole [78, 79]. The barrel-stave model describes how stave shaped AMPs (most often α-helixes) are inserted perpendicularly through the membrane, forming a barrel-shaped hole [79]. In the carpet model, areas of the membrane are coated with AMPs. This causes membrane instability and eventually membrane disintegration and micelle formation [79].
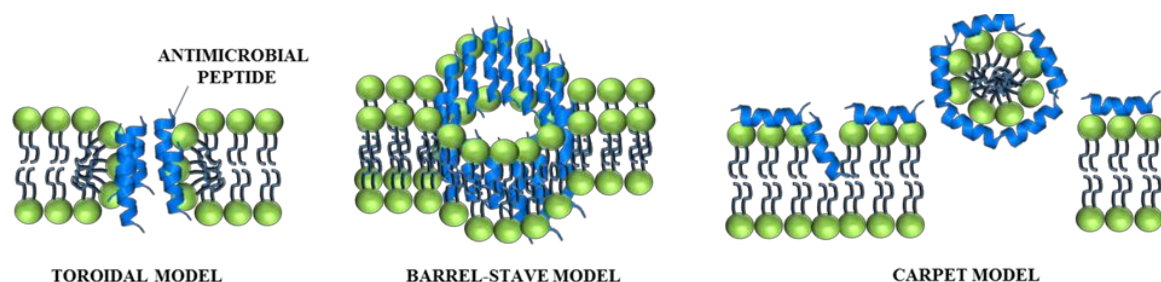
Figure 5: Illustrations of the different models by which antimicrobial peptides (AMPs) exert their activity on the bacterial membrane. Figure adapted from [80].

Interference with cell wall integrity was long believed to be the only MoA of AMPs. It is now, however, clear that AMPs are multifunctional compounds capable of a multitude of direct and indirect antibacterial actions (Figure 6). In addition to the direct effects on cell wall integrity, AMPs can disrupt membrane bound machineries (like ion channels), bind to receptors and affect internal targets in the bacteria [77]. AMPs have also been proven to cause indirect pathogen clearance by modulation of host immune responses. Responses include stimulation of chemotaxis, modulation of immune cell differentiation and initiation of adaptive immunity [81, 82]. As the sequence diversity, PTMs and 3D structures, as well as the

wide variety of activity models proposed for AMPs, it is likely that multiple MoAs occur simultaneously [75].
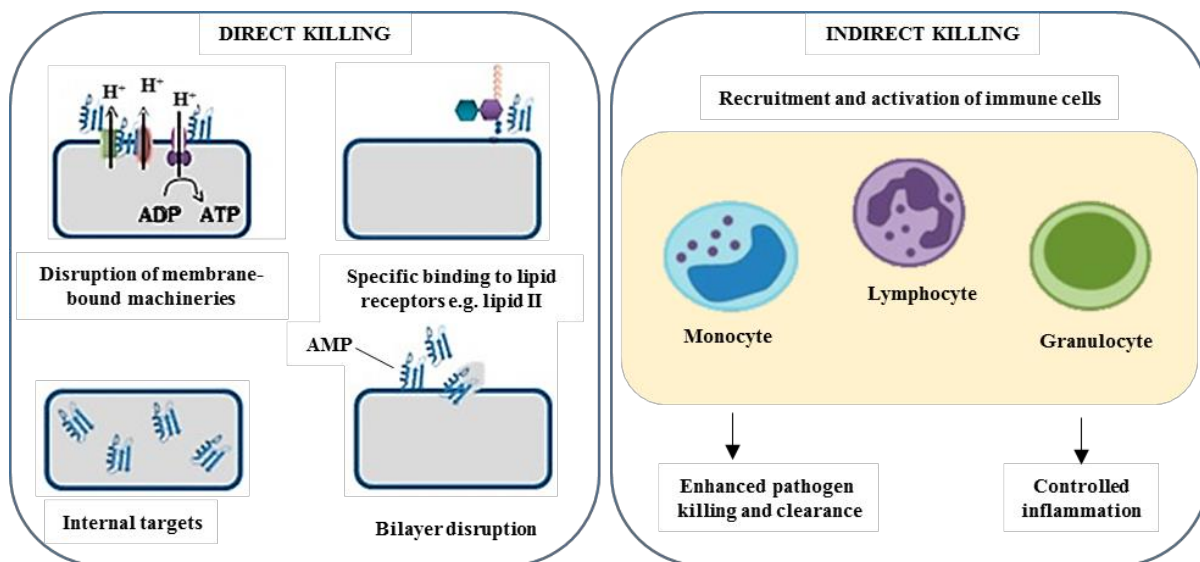
Figure 6: A schematic overview illustrating the different modes of action by which AMPs exert their antibacterial activities. Figure modified from [58].

1.2.4 Classification of AMPs

AMPs constitute a group of compounds, whose structure, origin, biosynthetic production pathway, localization within the producing organism, biological function, bioactivity, and MoAs are highly diverse. Consequently, AMPs may be classified in a wide variety of ways [83-85] and no official classification system exists. However, a widely used classification is based on their secondary structure, where AMPs are classified in the four broad classes (α-helixes, β-sheets, loop structures and extended structures) [36, 86-88]. Most AMPs belong to the first two classes [89].

<u>α-helixes</u>

In α-helical AMPs, the hydrophobic and hydrophilic portion are often segregated along the α-helical long axis, giving them a distinct amphipathic nature (Figure 7) [90, 91]. AMPs holding this structure are widespread in nature. This group usually adopts a disordered structure in aqueous solution but arranges in amphipathic helixes when interacting with membranes [92]. α–helical AMPs include arasin 1, isolated from hemocytes of the spider crab *Hyas araneus*

9

[93], the chrysophisins, isolated from the gills of the red sea bream *Chrysophrys major* [94] and astacidin 1, isolated from plasma of the freshwater crayfish *Pacifastacus leniusculus* [95].
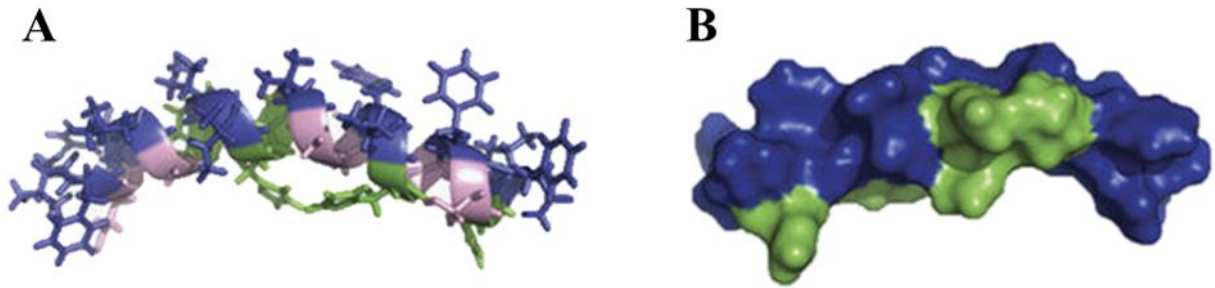
**Figure 7: The three-dimensional structure of the AMP clavanin A, isolated from the ascidian *Styela clava*. A) The peptide is twisted into an α-helical shape. The figure shows the peptide backbone portrayed as a cartoon overlaid with extended structure showing the protrusion of the R-groups. B) The surface structure of clavanin A. The hydrophilic and lipophilic regions are mainly clustered on different sides along the α-helical long axis. Color indications: pink = polar, green = cationic, and blue = hydrophobic residues. Figure modified from [96].**

β-sheets

This class refers to AMPs containing β-sheet sheets (Figure 8). This class includes the protegrins, which were first isolated from porcine leukocytes [97], the mammalian defensins [98] and the tachyplesins, isolated from hemocytes of horseshoe crabs [99]. Nearly all β-sheet AMPs contain disulfide bridges [58]. Compared to α-helical AMPs, β-sheet AMPs are less prone to undergo structural changes in response to changing chemical environments [100].
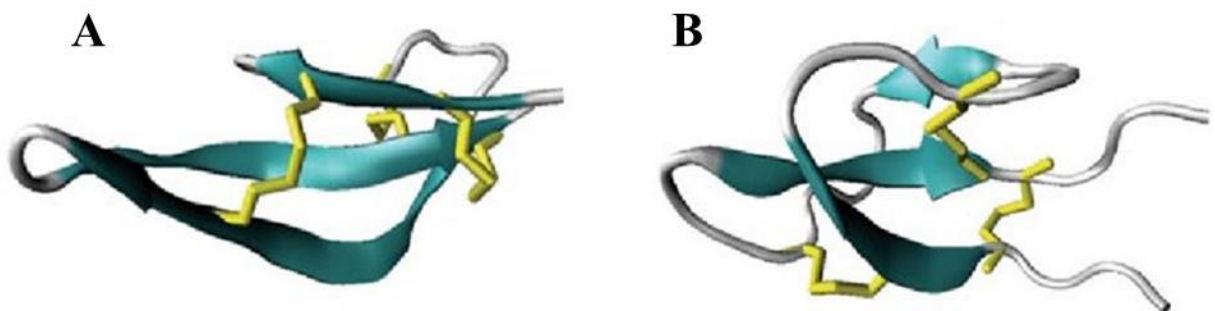
Figure 8: Structures of the mammalian AMPs, α-defensins: A) Human neutrophil peptide-4 [101] and B) cryptdin-4 [102]. The tertiary structures of both proteins are arranged with β-sheets (blue) supported by three disulfide bridges (yellow).

Loop and extended structures

Loop AMPs adopt a loop formation with one intramolecular disulfide bridge [103]. This class includes the bovine AMPs bactenecin [104] and lactoferricin [105]. Extended structures are characterized by the overexpression of one or more of the following amino acids: proline, tryptophan, arginine or histidine and do not fold into regular secondary structures [92]. Many extended AMPs are not active against bacterial membranes, but rather exert their activity through interaction with intracellular bacterial structures [106]. Indolicidin, a cationic 13 amino acid AMP, which is unusually rich in tryptophan and proline, belongs to this class [107]. So does apidaecin, produced by bees and wasps [108] and pyrrhocoricin produced by fire beetles [109].

1.2.5 Optimization of AMP structure through analog synthesis

Despite the many advantages of native AMPs, the challenges associated with these compounds have delayed their development into antibacterial drugs. In particular, the relationship between AMP structure and therapeutic index needs to be investigated and improved [110]. This can be done through chemical synthesis of AMP analogs and conduction of structure-activity/toxicity analysis. This will allow pinpointing of AMP pharmacophores and toxicophores, knowledge of which can be utilized to produce AMP analogues with improved therapeutic indexes [111]. In addition, by pinpointing the smallest amino acid domain exerting activity, costs associated with AMP production can be minimized. Analogs of natural AMPs produced through chemical synthesis are being reported to an increasing degree [90].

To help in this endeavor, several computer-aided design methods exist. These methods allow the pinpointing of regions within the full peptide sequence that are important for the antimicrobial activity of the peptides. These include the online prediction tool of the collection of anti-microbial peptides (CAMP$_{R3}$) web server [112] and tools in the database of anti-microbial peptides (ADAM) [113]. The peptide stretches with the highest overall predicted antimicrobial potential can then be used as a starting point for peptide synthesis. Furthermore, the synthetic peptide can be mutated at specific residues to examine the effect this has on antimicrobial activity [114]. If the peptide loses activity following the replacement of a specific amino acid, that residue is in some way necessary for its biological function. However, if the antibacterial potency improves, this provides valuable information regarding

which structural elements of the peptides that are important for the observed antibacterial activity and elevates the potential of this peptide as antibacterial drug-lead.

1.3 THE MARINE ENVIRONMENT

The ocean covers more than 70% of the earth's surface and is the home to more than 300,000 described species of plants and animals [115]. With an average depth of three kilometers, the habitable space under its surface is enormous [116]. One factor is common for all marine habitats, which is the presence of saltwater. Apart from this, the habitats are immensely diverse, stretching from the intertidal zones to deep-water trenches, from tropical sun- and nutrition-rich waters to the dark, cold, and ice-covered waters at the North Pole [117]. In the marine environment, 34 out of the 36 phyla of life are represented out of which 21 are exclusively marine [115]. The chemodiversity in marine species is significantly less studied compared to terrestrial chemodiversity, as terrestrial plants traditionally have been more easily accessible. Marine organisms truly emerged as a source of chemodiversity in the 1960s, with self-contained underwater breathing apparatus exploration, and later robot-sampling in oceanic depths [118]. Products coming from marine organisms could be used for various human applications, including cosmetics and skin care purposes, as nutraceuticals and as pharmaceuticals [119].

1.3.1 Marine bioprospecting and pharmaceuticals from marine sources

Bioprospecting is the systematic search for biochemical or genetic products in nature that can be developed into commercial products for pharmaceutical, agricultural, cosmetic and other applications [120]. For pharmaceutical development, natural products have played a particularly important role, with around 60% of all marketed drugs originating from nature [121]. This success can be explained by the different and diverse chemistry of natural products compared to compounds produced by combinatorial synthesis [122]. In addition, many natural products, especially those produced as defense molecules, have been developed through an evolutionary arms race between species, where the producer aims to prevent being overgrown or to repel predators or pathogens [123]. This is most often achieved by production of compounds with chemical properties allowing potent interactions with protein targets within the competing or attacking organism. Most drug targets in humans are of protein

12

nature, thus rationalizing the impressive success of natural products for pharmaceutical development [124, 125]. For antimicrobial drug development, natural products have been especially important [126]. In fact, around 70% of all marketed antibacterial agents originate from natural products [127]. These include β-lactams, aminoglycosides, tetracyclines and macrolides [44, 120].

In natural product based drug development, terrestrial plants have been most widely studied [121]. Therefore, many consider the marine environment the world's greatest untapped resource for new biodiversity and chemodiversity. As of March 3rd, 2022, 17 marine derived pharmaceuticals are approved for use by the American food and drug administration (FDA) or for use in Australia or China, and 29 are in the various stages of clinical development [9, 128]. One of the approved compounds is ziconotide, a synthetic form of a ω-conotoxine peptide, which is a constituent in the venom of the fish-eating marine snail *Conus magus* [129]. It consists of 25 amino acids, and its three-dimensional structure is supported by three disulfide bonds (Figure 9) [129]. The disulfide bridges give the secondary peptide structure its inherent stability and are imperative for the activity of the peptide. The final confirmation of the peptide is heavily influenced by the conformational constrains imposed by the disulfide bridges. It is approved for the treatment of chronic pain [130].
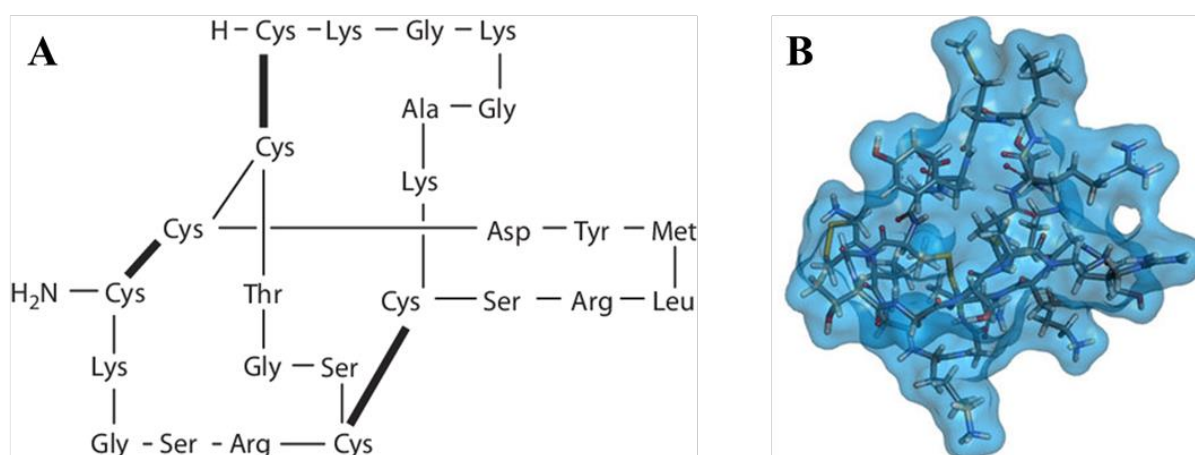
Figure 9: A) The structure of ziconotide includes three disulfide bridges (indicated by bold lines) [131]. B: The three-dimensional structure of ziconotide [132].

1.4 ASCIDIANS

The evolutionary connection of ascidians to vertebrates, also known as sea squirts, are animals belonging to the Ascidiacea class. The class includes Phlebobranchia, Aplousobranchia and Stolidobranchia, orders mainly distinguished by the physiology of their bronchial baskets [133, 134]. More than 3000 ascidian species are recorded, all of which live in the marine environment. Ascidians belong to the Chordata phylum, where both Tunicata (the subphylum of ascidians) and Vertebrata are subphyla [135].

1.4.1 Anatomy and biology of ascidians

Ascidians evolutionary connection to vertebrates can only be seen in their tadpole-like larvae stadium, which has a notochord [136, 137]. When the larvae metamorphose into an adult, the original nervous system and sensory organs degrade. Adult ascidians are thus invertebrates, most of which are sessile, soft-bodied filter feeders [138]. Adult ascidians exist either in solitaire, with little or no interactions with other individuals of their species, or as colonial animals, where many individuals live in close association. Colonial ascidians may share nutrients between themselves. Colonies may also share a common siphon where water is filtered through each individual and excreted through a larger, common siphon [139]. The anatomy of a solitary ascidian can be seen in Figure 10. Adult ascidians have a sac-like body with two openings, called siphons, allowing water to flow through the animal via a large bronchial basket. An endostyle, attached to the bronchial basket, secrets a mucous net required to trap particles suspended in the filtrated water [140]. An outer layer, called the tunic, made of the polysaccharide cellulose, encloses the animal.
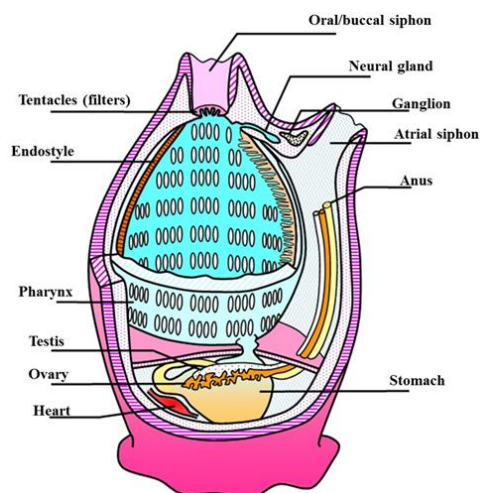

Figure 10: The anatomy of a solitary ascidian. Adapted from [141].

Entailed by the absence of a vertebrate column, ascidians do not possess the complex adaptive immune system found in vertebrates [142]. Thus, they do not have the long-term immunological memory mediated through lymphocyte immunity (T- and B-cells). However, ascidians thrives in the marine habitat, which is known to possess up to $10^5 - 10^6$ microbes/mL seawater [143]. Ascidians therefore require an efficient innate immune system to avoid being infected by pathogenic microbes. Immunity in ascidians is principally confined to non-specific inflammatory responses, at large mediated by circulating blood cells, including hemocytes, which are lymphocyte-like cells, phagocytes, and cytotoxic cells. These cells synthesize most of the pattern-recognition receptors, including toll-like receptors, required for immune defense [144]. In addition, ascidians are known to produce AMPs as a defense strategy. Ascidian AMPs may even be produced in the absence of external threats and stored in granules [145]. The ability of ascidians to produce AMPs as part of their innate immune response suggests that these peptides are amongst the earliest components of the immune system of the vertebrate lineage [146]. Ascidians also have a well-developed chemical defense strategy, mediated through the production of secondary metabolites [142, 147].

1.4.2 Bioactive compounds from ascidians

Peptides only constitute a small fraction (around 4%) of the natural products isolated from ascidians [148]. More than 1200 natural products have been isolated from ascidians [149]. The most reported compounds are classified as indoles (around 48%), followed by pyrocridine alkaloids (around 18%) and β-carboline alkaloids (around 8%). Regarding bioactivities, anti-tumor or anticancer are the most common bioactivities, reported for about 64% of the natural products isolated from ascidians. Antibacterial activity is the second most reported bioactivity, at 14% [148]. In addition to the AMPs described as part of this thesis, 16 ascidian derived AMPs have been reported. For some of these, synthetic analogues have been produced. The properties of the isolated AMPs are detailed in Table 1.

Table 1: Antimicrobial peptides reported from ascidians and their properties.

PEPTIDE	SPECIES	ISOLATED FROM	Aa[a]	NET CHARGE[b]	EFFECT	COMMENTS
Clavanin A – E [146]	*Styela clava*	Hemocytes	23	A - D: +5, E: +6	Antimicrobial[c, d, e], immunoregulatory [150]	α-helical, amphipathic, C-terminal amidated, no other PTMs.
Clavaspirin [151]	*Styela clava*	Pharyngeal tissue	23	+1	Antibacterial against G+ and G- bacteria[e], cytotoxic towards human and bovine erythrocytes	α-helical, C-terminal amidated, no other PTMs, cloned from cDNA library.
Dicynthaurin [152, 153]	*Halocynthia aurantium*	Hemocytes	60	+4	Antibacterial against G+ and G- bacteria[c], haemolytic towards human erythrocytes	α-helical, consists of two identical monomers linked through a disulfide bond.
Halocidin [154]	*Halocynthia aurantium*	Hemocytes	33	+1	Antibacterial against G+ and G- bacteria	Heterodimer. 18 and 15 aa monomers linked through a disulfide bond.
Halocyntin [155]	*Halocynthia papillosa*	Hemocytes	26	+2	Antibacterial against G+ and G- bacteria, haemolytic	α-helical
Papillosin [155]	*Halocynthia papillosa*	Hemocytes	34	+5	Antibacterial against G+ and G- bacteria	α-helical
Plicatamide [156, 157]	*Styela plicata*	Hemocytes	8	+1	Antibacterial against G+ and G- bacteria[c, f], haemolytic towards human erythrocytes	Smaller than most AMPs (octapeptide). one aa has undergone PTM.
Stylelin A – E [61, 62]	*Styela clava*	Hemocytes	32	A: +5, B: +4, C: +6, D: +9, E: +10	Antibacterial against G+ and G- bacteria[c], haemolytic against eukaryotic cells	α-helical, C-terminal amidated, undergone several post-translational modifications (PTM).

[a]Aa.: Amino acids, [b]Net charge at neutral pH calculated from ADP web site (http://aps.unmc.edu/AP/main.php), [c]mode-of-action includes bacterial membrane destabilization, [d]pH and salinity dependent antibacterial, antifungal, and anti-biofilm activities [96, 146, 158]. [e]The antibacterial effect is most prominent at acidic pH as this results in the protonation of histidine residues, hence increasing the positive charge of the proteins [151, 158, 159], [f]antibacterial activity reduced at reduced pH, indicating that electrostatic interactions do not play a major role in its activity.

1.4.3 Anticancer non-ribosomal peptides from ascidians

Two non-ribosomal peptides isolated from collected ascidian biomass have entered clinical trials [160-162]. The cyclic depsipeptide dehydrodidemnin B, also known as Aplidine® or plitidepsin, was isolated from the Mediterranean ascidian *Aplidum albicans* [163]. This non-ribosomal peptide, developed by the Spanish company PharmaMar, got market approval in Australia in 2018 for treatment of multiple myeloma [164]. The second non-ribosomal peptide, didemnin B, isolated from the Caribbean ascidian *Trididemnum cyanophorum* [165], was entered into clinical trials as an antineoplastic agent by the National Cancer Institute [166]. It completed phase II clinical trials, but further trials were not conducted due to anaphylactic reactions in patients [160].

1.4.4 Secondary metabolites from ascidians

In addition to the bioactive peptides, several small molecules with diverse bioactivities have been isolated from ascidians. This include the anti-tumor chemotherapy drug trabectedin (Yondelis®), which was approved for use by the European Union in 2007 and the FDA in 2015 [167]. Lurbinectedin (Zepzelca®), isolated from *Ecteinascidia turbinate*, was approved for use by the FDA in 2020 for adult patients with metastatic small cell lung cancer with disease progression on or after platinum-based chemotherapy [168]. In addition, several bioactive compounds have been reported. These include the well-known kinase inhibitor staurosporine, which was isolated from *Eudistoma toealensis* [169]. However, as this compound originally was isolated from the bacterium *Streptomyces staurosporeus* [170], it is believed to be produced by a microorganism living in symbiosis with the collected ascidian.

1.4.5 Bioactive compounds from *Synoicum* species

Synoicum species, belonging to the family Policlinidae, are all colonial ascidians [171] and known to be a rich source of novel compounds. Approximately 62 compounds have been isolated from *Synoicum* species, with origin from all over the world (Table 2). More than two thirds of these compounds are halogenated aromatic derivatives, and beside the heavily brominated tetraphenolic bis-spiroketals prunolide A and B from *Synoicum prunum* [172], they are all below 1000 Da. The bioactivity varies among the compounds; antibacterial [173],

antifungal [174], cytotoxic [175], anti-inflammatory [176], enzyme inhibitors [177], antiviral activity [172].

Table 2: Natural products isolated from *Synoicum* species around the world

SPECIES	REGION	COMPOUNDS	CHEMISTRY
S. adareanum	Antarctic	10	Ecdysteroids [178], macrolides [177, 179]
S. blochmanni	Spain	6	Furanones [175]
S. castellatum	Australia	1	Tetrahydrocannabinol [180]
S. globosum	South Africa	4	Furanones [181]
S. kuranui	New Zealand	5	Furanones [182, 183]
S. macroglossum	India	1	Alkaloid [184]
S. prunum	Australia	11	Tetraphenolic Bis-Spiroketals, alkaloids [172, 185]
S. pulmonaria	Norway	5	Alkaloids [174, 186, 187]
Synoicum n. sp.	New Zealand	1	Furanone [176]
Synoicum sp.	Korea	17	Furanones, esters [173, 188]
Synoicum sp.	India	1	Furanone [189]

1.4.6 *Synoicum turgens*

Synoicum turgens (Class Ascidiacea, order Aplousobranchia, family Polyclinidae) is a colonial ascidian. The species was first described by C. J. Phipps in 1774, when it was collected on a voyage towards the North Pole [190]. *S. turgens* is an Arctic species. Along the coast of the Norwegian mainland, it can only be found off the coast of the county, Troms and Finnmark. Apart from the work conducted in this thesis, no natural products have been reported coming from *S. turgens*.

18

2. AIMS OF THE THESIS

This project was done as part in the marine bioprospecting research group at the Norwegian College of Fishery Science, UiT, whose main focus are antimicrobial and antibiofilm marine natural compounds.

Primary aim

The main aim was to isolate and characterize AMPs from the marine ascidian *S. turgens* as natural innate defense molecules from a marine source.

Secondary aims

The secondary aims of the thesis were to further evaluate the potential of isolated peptides as templates for drug lead development by:

- Determining the structure of the isolated AMPs
- Investigating their antibacterial activities and mode-of-action
- Documenting their toxicity against mammalian cells
- Evaluating synthetic (truncated and modified) variants of a selected AMP for their antibacterial and cytotoxic activity
- Documenting whether the optimized peptides had other beneficial effects like antifungal and anti-inflammatory activities

3. SUMMARY OF PAPERS

Paper I

Isolation and characterization of antimicrobial peptides with unusual disulfide connectivity from the colonial ascidian *Synoicum turgens*

Ida K. Ø. Hansen, Johan Isaksson, Aaron G. Poth, Kine Ø. Hansen, Aaron J.C. Andersen, Céline S. Richard, Hans-Matti Blencke, Klara Stensvåg, David J. Craik and Tor Haug

- Two novel cysteine-rich AMPs were isolated, turgencin A and turgencin B and their oxidized derivatives, from the Arctic marine ascidian *Synoicum turgens*

- The peptides are post-translationally modified, containing six cysteines with an unusual disulfide connectivity of C1-C6, C2-C5, C3-C4 and an amidated C-terminus

- The turgencins contains methionine residues resulting in the isolation of peptides with different degrees of oxidation

- Turgencin A_{Mox1} displayed antimicrobial activity against the Gram-negative bacteria, *E. coli*, at 0.8 µM, and the Gram-positive bacteria, *B. subtilis*, at 0.4 µM. Turgencin B inhibited growth at 12.5 µM and 1.6 µM against the same strains

- Turgencin A_{Mox1} was cytotoxic against the melanoma cancer cell line A2058 (IC_{50} = 1.4 µM) and the human fibroblast cell line MRC-5 (IC_{50} = 4.8 µM). Turgencin B killed the same cells at 14.1 µM and 7.5 µM.

- Antimicrobial activity decreased the more methionine being oxidized

- In membrane assays, turgencin A_{Mox1} and turgencin B disrupted the bacterial membrane within seconds
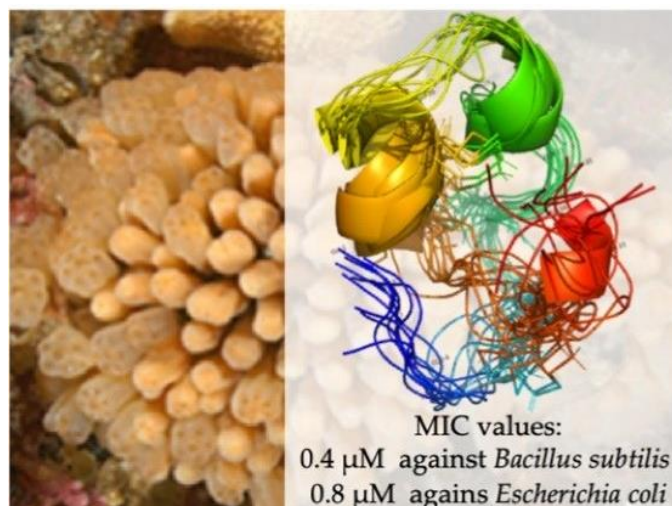

MIC values:
0.4 µM against *Bacillus subtilis*
0.8 µM agains *Escherichia coli*

Antimicrobial activity of small synthetic peptides based on the marine peptide turgencin A: prediction of antimicrobial peptide sequences in a natural peptide and strategy for optimization of potency

Ida K. Ø. Hansen, Tomas Lövdahl, Danijela Simonovic, Kine Ø. Hansen, Aaron J. C. Andersen, Hege Devold, Céline S. M. Richard, Jeanette H. Andersen, Morten B. Strøm and Tor Haug

- The aim of this study was to develop a truncated peptide with an antimicrobial drug lead potential, based on the sequence of the AMP turgencin A

- *In silico* analysis of turgencin A using various prediction software indicated an internal, cationic 10-mer sequence to be putatively antimicrobial.

- Based on this sequence, a 10-mer lead peptide named StAMP-1, without any cysteine residues, was synthesized and tested for antimicrobial activity

- StAMP-1 displayed weak antimicrobial activity, but by doing a systematic amino acid replacement strategy, a modified peptide was developed that retained the potency of the original peptide

- The optimized peptide, StAMP-9, displayed bactericidal activity, with minimal inhibitory concentrations of 5.5 µM against *S. aureus* and 2.7 µM against *E. coli*, and no cytotoxic effects against mammalian cells

- Preliminary experiments indicate the bacterial membranes as immediate and primary targets
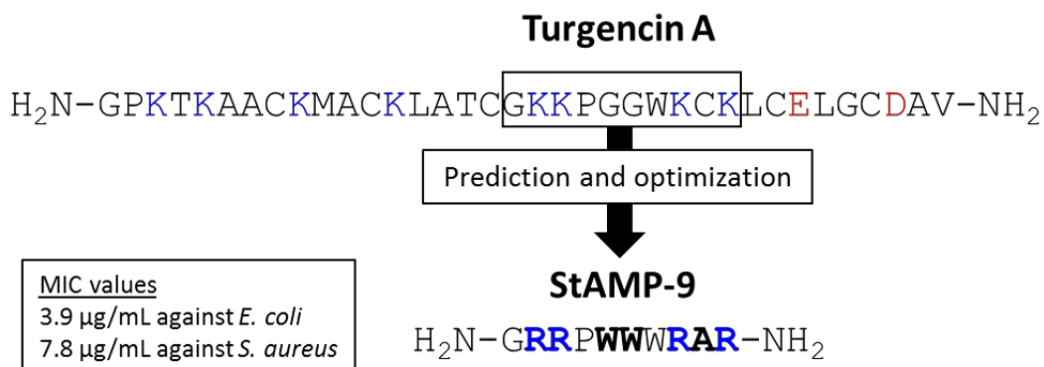
Paper III

Isolation and characterization of St-CRPs: Cysteine-rich peptides from the Arctic marine ascidian *Synoicum turgens*

Ida K. Ø. Hansen, Phil B. Rainsford, Johan Isaksson, Kine Ø. Hansen, Klara Stensvåg, Anastasia Albert, Terje Vasskog and Tor Haug

- Two novel cysteine-rich peptides (CRPs), St-CRP-1 and St-CRP-2, were isolated from *S. turgens*

- The sequences and structures of the peptides were solved with Edman degradation sequencing, mass spectrometry, and NMR analysis

- Both peptides were ~2 kDa, had neutral net charge, and were C-terminally amidated

- St-CRP-1 consisted of 18 amino acids, inhibited growth of two Gram-positive bacterial strains (*B. subtilis* and *C. glutamicum*) at 24.6 µM, and displayed no cytotoxic activity against two mammalian cell lines or the brine shrimp *Artemia salina*

- St-CRP-2, with 19 amino acids, inhibited the growth of *B. subtilis* at 49.2 µM

- The St-CRPs had a Cys1-Cys6, Cys2-Cys4, and Cys3-Cys5 disulfide connectivity, which is also found in alpha-defensins

4. DISCUSSION

Two of the papers included in this thesis (**paper I** and **III**) details the isolation and characterization of novel peptides from antibacterial fractions produced by solid-phase extraction of an aqueous extract of the Arctic marine ascidian *S. turgens*. In addition, a truncated analogue series of one of the peptides were produced and characterized in **paper II**. This was, to the best of my knowledge, the first report of natural compounds being isolated from *S. turgens*.

In **paper I**, four cationic peptides, with a disulfide connectivity of Cys1-Cys6, Cys2-Cys5, and Cys3-Cys4 were isolated. The most active oxiform of the turgencins, turgencin A$_{Mox1}$, produced MIC values at sub-µM concentrations against both G+ and G- bacteria, while at the same time displaying cytotoxicity against human malignant and non-malignant cells at low µM concentrations. In **paper II**, eleven truncated variants of turgencin A, named StAMP-1 to StAMP-11, devoid of cysteines, were produced based on sequence analysis and predictions of antimicrobial potential. The most potent variant, StAMP-9, regained most of the antimicrobial activity of the parent AMP while displaying significantly reduced cytotoxicity towards human cells. In **paper III**, two neutral peptides, with disulfide connectivity of Cys1-Cys6, Cys2-Cys4, and Cys3-Cys5, were isolated. These two peptides showed moderate antibacterial activity, and no toxicity against brine shrimps and two human cell lines. The most active peptide, St-CRP-1, had comparable bioactivity to the least active turgencin, the fully oxidized turgencin B, turgencin B$_{Mox2}$.

4.1 BIOACTIVITY GUIDED PURIFICATION

Most extracts from natural sources are highly complex, containing numerous compounds. Therefore, if an extract contains a compound that is of interest in sense of being a drug lead, this will exist in a complex mixture with other natural products. Bioactivity guided purification is an efficient strategy to eliminate compounds without a desired bioactivity, and to discover novel bioactive compounds. A common workflow is illustrated in Figure 11. This strategy will also, in some cases, lead to identification of novel bioactivity coming from known compounds [191]. The exact procedure of bioactivity guided purification varies, but the main objective is to make a highly complex mixture less complex, test for bioactivity and proceed with active extracts. The active extracts will go through further fractionation and

testing until the compound(s) causing the activity is purified and the bioactivity confirmed [192].
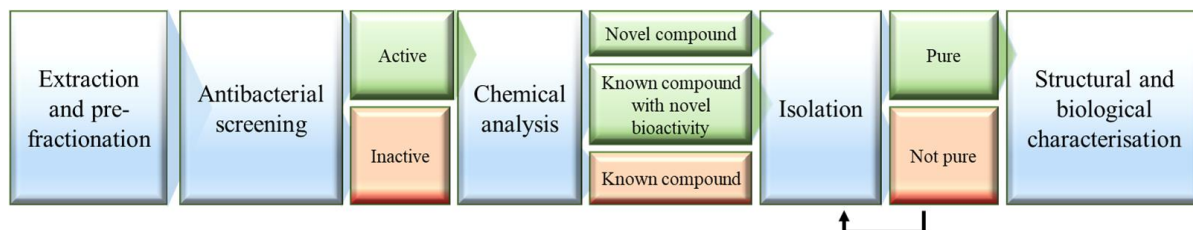
Figure 11: A common bioactivity guided purification workflow.

The peptides isolated in **paper I** and **III** are results of this procedure. Extracts and fractions from *S. turgens* were selected based on their antibacterial activity. When testing the purified turgencins, it was clear that the antibacterial activity in the HPLC fractions were mainly coming from these AMPs. This was not the case with the St-CRPs. The St-CRP containing HPLC fractions inhibited growth of several bacterial strains, and the St-CRPs were the major compounds in these fractions. When testing the purified peptides against the same panel of bacteria, they only exhibit moderate activity against two test strains. Whether the antibacterial activity in the HPLC fractions were due to minor amounts of other peptides or compounds, or synergy between the St-CRPs and these compounds is unknown. On the other hand, preliminary results detailed in section 4.3.3 at least addresses the potential of the St-CRPs working synergistically with other compounds, including the turgencins. Other species have been known to produce cocktails of neutral, anionic and cationic peptides, working on their own or in synergy with each other [193]. It has been observed that some combinations of peptides generate considerable increased antibacterial activity compared to the individual peptides alone, and suggested that such AMP cocktails might be beneficial when combating antimicrobial resistance [194]. In addition to the peptides isolated in **paper I** and **III**, extracts from *S. turgens* still contains several AMPs that have not been characterized yet. Perhaps the turgencins, or other cationic AMPs, damages the bacteria membrane and enables neutrally charged St-CRPs to work intracellularly.

As with most laboratory protocols, bioactivity guided purification has its weaknesses. Since compounds are proceeded with based on the bioactivity, the bioassays available in the laboratory determine which compounds that are isolated and may therefore also cause

compounds that can be used for other purposes to remain undetected. If the peptides from *S. turgens* were only tested for anti-inflammatory activity or anti-biofilm formation properties, they may never have been prioritized for isolation. Despite the moderate antibacterial activity of the St-CRPs in **paper III**, the main function in the animal itself could be protection against UV radiation, repelling predators, target pathogens that were not assayed as part of this work, or something completely different to combating pathogens. Also, if compounds have synergistic effect, the bioactivity might be reduced when they are separated. To avoid losing potentially valuable compounds, it would be wise to, in addition to acting on bioactivity, also isolate compounds that are abundant or have interesting chemistry (e.g. halogenated compounds). Another obstacle with bioactivity guided purification is that the concentration of a compound sometimes is too low to give results in bioassays. Low yield of bioactive compounds is in general a major hurdle in marine bioprospecting, where large amounts of marine biomass is required to get only a few mg of the active compound [167].

4.2 OXIDATION OF AMPs DURING SAMPLE HANDLING

The unique activities of a peptide are highly dependent on the side chain functionalities of its amino acids. Any structural change in the side chains may thus have a profound impact on peptide properties. Turgencin A has one, and turgencin B has two methionine residues. The thioether side chain of methionine is highly susceptible to oxidation, even by mild oxidants, and thus such oxidation is a widespread problem for methionine containing peptides [195]. Oxidation of methionine changes its polarity slightly, a shift expected to have profound structural and functional consequences. In **paper I**, turgencin variants with one and two Met-ox residues (+16/32 Da) were observed both with MS and nuclear magnetic resonance (NMR) spectroscopy. The peptides were dissolved in water as part of the isolation process and exposed to air during drying. It is thus hypothesized that most of the peptide fractions with oxidized methionine residues are formed during sample handling. The unoxidized variant of the most potent variant, turgencin with its methionine residue oxidized (turgencin A_{Mox1}), was not isolated in amounts allowing bioactivity evaluation, and therefore no comparison between the bioactivity of turgencin A with and without oxidated methionine could be made. Turgencin B and turgencin B with one (turgencin B_{Mox1}) and two (turgencin B_{Mox2}) oxidated methionines were all isolated in sufficient amount to evaluate their antibacterial properties (Table 3).

Table 3: The antibacterial activity of turgencin B, turgencin B$_{Mox1}$ and turgencinB$_{Mox2}$.

PEPTIDE	Antimicrobial activity (MIC, µM)				
	Corynebacterium glutamicum*	*Bacillus subtilis**	*Staphylococcus aureus**	*Escherichia coli***	*Pseudomonas aeruginosa***
Turgencin B (67% Mox0, 29% Mox1, 4% Mox2)	1.6	1.6	>100	12.5	25.0
Turgencin B$_{Mox1}$ (88% Mox1, 10% Mox2, 2% Mox0)	1.6	3.1	>100	25.0	>100
Turgencin B$_{Mox2}$ (97% Mox2, 3% Mox1)	25.0	25.0	>100	>100	>100

*Gram-positive, **Gram-negative

The data displayed in Table 3 clearly shows the detrimental effect of methionine oxidation on peptide activity. For the most sensitive strains, *C. glutamicum* and *B. subtilis*, the antibacterial potency dropped by a factor of ~15 from the unoxidized to the di-oxidized variant of turgencin B. As indicated in Table 3 for each peptide, the oxiforms could not be completely separated from each other. However, as most of the sample was the indicated peptide, the trend in bioactivity was clear.

Oxidations of methionine can be reduced by avoiding the use of oxidizing solvents to dissolve the peptides and minimizing the peptides exposure to air. These factors, in particular exposure to air, is hard to avoid during sample handling. Oxidation of methionine is a reversible covalent modification. Methionine sulfoxide can therefore be converted back to its native state using medicinal chemistry approaches or even enzymes [196]. These approaches to minimize or reverse methionine oxidation makes the whole process of AMP handling more labor intensive and were never tested as part of this thesis. However, in **paper II**, the linear sequence of turgencin A was analyzed using pre-trained AMP prediction tools that rely on various machine learning algorithms to predict the antimicrobial properties of shorter stretches of amino acids within the peptide. The central loop of turgencin A, containing the 10-amino acid stretch that served as a template for synthesis, did not contain methionine. After synthesis, some of these analogues were found to have adequate antibacterial properties, an analogue (named StAMP-9 in **paper II**) comparable to that of the turgencins against both G+ and G- bacteria. By production of analogues that does not contain methionine, the initial oxidation problem can be avoided, and the peptides can be handled without considering for example minimalizing their exposure to air.

4.3 AMPs AS LEAD STRUCTURES FOR ANTIBIOTIC DEVELOPMENT

Despite the efforts put into the development of antibiotics from natural AMPs, no ribosomal AMP is currently marketed as a drug. However, in 2021, 29 AMPs were in various stages of clinical development, with the majority intended for topical applications [197]. AMPs have many advantages, making them a desirable basis for development of antibiotic, but are simultaneously associated with several challenges.

4.3.1 Advantages

In addition to AMPs' desirable MoA (rapid microbial killing, immune modulation, and the ability to target quiescent cells), AMPs have several benefits as a basis for development of commercially available antibiotics. Compared to conventional antibiotics, interacting with one defined target, the antibacterial effect of most AMPs is caused by electrostatic attachment to the negatively charged bacterial surface followed by embedment into the membrane. AMPs therefore have a lower tendency to induce antibiotic resistance [198, 199]. These qualities are also found in turgencin A (net charge 7+), turgencin B (net charge 3+) (**paper I**), and the truncated synthetic peptides (net charge 5+) (**paper II**) which are all cationic peptides that rapidly disrupt the bacterial membrane. The reduced resistance tendency is in large due to the profound changes in bacterial membrane structure needed to confer the bacterial cell with resistance, while simultaneously preserving membrane functionality and structural integrity. Moreover, optimized peptide therapeutics are recognized for eliciting high specificity and efficacy, while at the same time being relatively safe and well tolerated as proteinaceous compounds are natural components in humans [200]. Degradation of the peptide drug yields simple amino acids, which can be recycled in the body in everyday metabolism such as protein synthesis [201]. The development and use of peptides as disease preventers or treatments are well established. There are currently more than 60 peptide-based drugs approved by the FDA and 120+ are in clinical trials [202, 203]. Peptides are used as supplements (e.g. insulin for patients with diabetes), as vaccines, for diagnostic applications, surfactants to treat respiratory distress syndrome in premature infants and as anticancer agents [204]. In addition, as peptides often are unique in form and function, the prospect of far-reaching patent protection is good.

4.3.2 Challenges

The pharmacokinetic properties generally associated with therapeutic peptides are predicted to be key limiting factors for AMPs as clinical candidates [111]. This includes low bioavailability due to extensive first pass metabolism by pre-systemic degradation enzymes following per oral administration and rapid degradation by proteolytic enzymes in the oral-intestinal tract and blood plasma when administered intravenously [201, 205]. Extensive metabolism, coupled with a general tendency to undergo rapid hepatic and renal clearance of amino acids, leaves AMPs with short half-lives [2, 206]. In addition, many AMPs show hemolytic or cytotoxic activity towards human cells [207, 208], as uncovered in **paper I** with turgencin A$_{Mox1}$ and turgencin B. Improvement of the pharmacokinetic and toxicological properties may require analogue production through medicinal chemistry efforts [2]. Furthermore, production of peptides with complex structures (for example peptides with disulfide bridges and PTMs) is associated with substantial production costs [209]. Both the turgencins (**paper I**) and the St-CRPs (**paper III**) consist of three disulfide bridges, and even though this is an advantage with regard to stabilizing the structure and improved thermodynamic stability [74], it complicates peptide synthesis. While the tendency of bacterial development of resistance towards AMPs is lower than for conventional antibiotics, resistance development is possible, as demonstrated in several experiments where bacteria were subjected to selective AMP selection pressure [210, 211]. The changes observed in AMP resistant bacteria includes modifications in membrane surface charge, utilization of efflux pumps and AMP acetylation. A special concern for AMP resistance has been the possibility of development of cross-resistance towards AMPs of the human endogenous innate immune system [212, 213].

4.3.3 AMPs from S. *turgens* and the truncated variants as antibiotic drug leads

In **paper I**, turgencin A was shown to have potent antibacterial activity against both G+ and G- bacteria. According to the 2020 report by WHO entitled "Antibacterial agents in clinical and preclinical development, infections by antibiotic resistant" [214], G- bacteria proposes a particular future concern, as very few antibiotic agents in clinical development are targeting G- bacteria. The activity of turgencin A against the G- strains *E. coli* (MIC = 0.8 μM) and *P. aeruginosa* (MIC = 1.6 μM) is therefore particularly interesting. An ideal antibiotic agent should treat or prevent pathogenic bacterial infections, while causing no harm to host cells. Turgencin A was shown to be cytotoxic, but the MIC values against the most sensitive

28

bacteria were 12 times lower than the IC_{50} value against the non-malignant fibroblast cell line MRC-5 (in the toxicological assay). It is however unlikely that this "therapeutic window" is broad enough to allow administration in humans at doses that can treat a G- pathogenic infection while simultaneously not causing any cytotoxicity towards human cells. Furthermore, the turgencin A is a complex molecule consisting of 36 amino acids and a structure tied together through three disulfide bonds. Production costs of a peptide with identical structure as the native peptide would be substantially higher than of a smaller, linear peptide.

The potent activity nominated the structure of turgencin A as the inspiration of analogues in the hopes of making variants with improved properties. In **paper II**, *in silico* analysis of turgencin A, using various prediction software, predicted an internal cationic 10-mer sequence in the loop region to be a promising candidate. Based in this analysis, several truncated and linear variants of turgencin A were produced (StAMP-1 to StAMP-11). These decapeptides had 72% less amino acids in their sequences compared to the 36 amino acids found in the native turgencin A. The sequence chosen for synthesis did not contain methionine, which is prone to oxidation, as this have proven to decrease the antimicrobial activity in turgencin B (**paper I**). It is plausible that turgencin A without methionine oxidation would increase the antimicrobial activity (and perhaps also the cytotoxic activity). In addition, all the cysteines were eliminated in the StAMPs, thus removing the possibility of the peptides to form intramolecular disulfide bridges, of which the turgencins have three. The StAMP series of peptides is thus both significantly smaller and have less complex structures compared to their natural precursor. The linear decapeptides can be produced relatively easily using standard peptide synthesis protocols. Importantly, the bioactivity of turgencin A_{Mox1} was fully recovered by several of the StAMP variants. While the antibacterial activity of the most potent variant StAMP-9 was slightly reduced compared to turgencin A_{Mox1} (Table 4), a massive improvement was made in terms of reduced toxicity against human cells. None of the StAMPs were cytotoxic against the human melanoma cell line A2058 and the human non-malignant lung fibroblast cell line MRC-5, or displayed hemolytic activity against sheep red blood cells at concentrations up to 250 µg/mL (= 165 – 237 µM), indicating that the peptides may be well tolerated in an *in vivo* setting.

Table 4: Selected antibacterial and cytotoxic activities of turgencin A_{Mox1} compared to its most potent truncated variant StAMP-9.

	Antimicrobial activity (MIC, µM)		Cytotoxic activity (IC$_{50}$, µM)	
PEPTIDE	*Bacillus megaterium**	*Escherichia coli***	A2058***	MRC-5****
Turgencin A_{Mox1}	0.1	0.8	1.4	4.8
StAMP-9	0.7	5.5	>175	>175

*Gram-positive, **Gram-negative, ***human melanoma cell line, ****non-malignant human lung fibroblasts

In addition, the antifungal activities of some of the StAMPs were comparable to those of turgencin A_{Mox1}. The MIC value of StAMP-8 against *Aurobasidium pollulans* was better (5.6 µM) than that of turgencin A (25 µM), while against *Rhodotorula* sp. the MIC value was better for turgencin A (6.3 µM) compared to StAMP-8 (11.1 µM).

Based on the antibacterial activity results of the St-CRPs in **paper III**, the peptides alone are not suited as antibiotics. This does not mean that their novel sequences do not have the potential of serving as a template for drug development. StAMP-1, which was synthesized based on the main sequence of turgencin A in **paper II**, had weak antibacterial properties. However, by substituting some of the amino acids in the sequence acquired major changes to the antibacterial activity. Similar synthesis based on the sequence of both St-CRPs from **paper III**, and turgencin B from **paper I**, might generate truncated peptides with high antimicrobial potential.

Another aspect worth mentioning when it comes to the St-CRPs is that they might have another antibacterial function than membrane disruption. Both peptides have neutral net charge, which is not optimal for attracting bacterial membrane. Most AMPs have a positive net charge that allows them to interact with the negatively charged bacterial membrane [75]. Preliminary results have shown that when combining the St-CRPs with a known bacterial membrane active peptide, the MIC values are decreased for both peptides (results not published). This gives reason to speculate whether the St-CRPs could possess synergy effect together with other peptides produced by the animal.

The potential of AMPs as candidate for development towards becoming an antimicrobial drug cannot be assessed by the antibacterial/antimicrobial and toxicological activity of the peptides

alone. The pharmacokinetic properties of therapeutic peptides are predicted to be a key limiting factor for AMPs as oral or intravascular clinical candidates. The lack of pharmacokinetic data for the peptides reported in **papers I – III** therefore represents a limitation for the evaluation of their clinical potential. Evaluation of the pharmacokinetic properties of the reported peptides were however outside the scope of the work performed as part of this work.

4.5 SYMBIOSIS

Many adhering invertebrates host a high abundance and diversity of microorganisms, which can include bacteria, archaea, fungi, and microalgae. For example, in some instances of marine sponges, 40% of the biomass volume of marine sponges has been reported to be of microorganisms [215]. Ascidians are known to be filter feeders, and microorganisms and other food particles in seawater are consumed as part of their nourishment [140]. Microscopic observations on the Antarctic ascidian, *Synoicum adareanum*, showed a dense microbial community inside the animal. This study was done as part of an investigation on whether the animal itself, or host-assosiated microorganisms, was the true producer of palmeroide A, an antimelanoma macrolide isolated from *S. adareanum* [216]. Many bioactive compounds originally isolated from ascidians or other invertebrates have later proved to be produced by microbial symbionts [170, 216, 217]. The true producer of the turgencins (**paper I**) and St-CRPs (**paper II**) from *S. turgens* have not yet been established. Having said that, most AMPs from ascidians have proved to be of eukaryotic origin, apart from bacteriocins [218]. Also, all turgencins and St-CRPs are C-terminally amidated. Amidation of the COOH-terminus is performed by peptidylglycine α-amidating monooxygenase (PAM), an enzyme only found in multicellular organisms and the green algae, *Chlamydomonas reinhardtii* [219, 220]. To confirm the true producer of the peptides in *S. turgens*, the genes of the animal should be isolated and characterized, but the lack of PAM in procaryotes at least points towards *S. turgens* as the true producer.

5. FUTURE STUDIES

As an increasing number of pathogenic bacteria are acquiring resistance towards currently available antibiotics, AMPs, with their extraordinary properties (such as broad-spectrum activity, rapid action and low tendency of resistance developed towards them), have emerged as promising candidates for development of new antibiotics. While the potential of AMPs such as the turgencins is interesting, several obstacles must be tackled before this basic new information can be used in lead compound development. These obstacles include development of variants with improved activity and without toxicity towards mammalian tissue, which can be produced and formulated into a pharmaceutical product. To accomplish this, further research into the pharmacophore and toxicophore of AMPs, and structural modifications that would improve their pharmacokinetic properties (for example increased half-life) is needed.

There is currently no information about the genome of *S. turgens*. A greater effort in genome sequencing and/or cDNA library construction would contribute to uncover the structure of AMPs produced by the ascidian. In addition to confirming the true producer of the peptides, it would be beneficial in regards of potential recombinant gene expression and production of the peptides. A higher yield of the peptides would allow further bioactivity testing, such as antibacterial activity testing against antibiotic resistant strains and testing for antiparasitic and antiviral activities.

New, modified variants of all peptides from *S. turgens* should be synthesized. This could generate simpler structures with improved antibacterial potency, and low cytotoxicity against human cells. An alternative to the synthetic work done in this thesis one could experiment with designing truncated peptides with D-amino acids instead of L-amino acids, or cyclic versions. This could make the peptides less prone to proteolytic degradation.

6. CONCLUSIONS

The efforts conducted as part of this thesis led to the isolation of four novel AMPs: turgencin A and B, and St-CRP-1 and 2, along with several oxidized versions of the turgencins. Solving the structure of the peptides revealed that the turgencins contained 35-36 amino acids and an unusual cysteine connectivity. Turgencin A_{mox1} and turgencin B displayed potent antibacterial activity, but also toxic activity against mammalian cells. The oxidized versions of turgencin B were less toxic, but also had less antibacterial activity. The St-CRPs contained 18-19 amino acids and had the same cysteine connectivity as the α-defensins. They showed only moderate activity against bacteria.

Using turgencin A as a template, 11 smaller truncated and modified versions (10-mers) of the peptide were produced. Some of these synthesized peptides showed equal antibacterial activity as the full mature peptide, and low cytotoxicity. Both the turgencins, and the most antimicrobial 10-mer peptides, seemed to be membrane active.

Altogether, these efforts expand our knowledge regarding the diversity of AMPs from marine sources in general, and marine ascidians in particular, and about innate defense molecules of the Arctic *S. turgens*.

7. REFERENCES

1. Cully, M., Public health: The politics of antibiotics. *Nature* **2014,** 509, (7498), S16-S17.
2. Aoki, W.; Ueda, M., Characterization of antimicrobial peptides toward the development of novel antibiotics. *Pharmaceuticals* **2013,** 6, (8), 1055-1081.
3. Prestinaci, F.; Pezzotti, P.; Pantosti, A., Antimicrobial resistance: A global multifaceted phenomenon. *Pathog. Glob. Health* **2015,** 109, (7), 309-318.
4. Munita, J. M.; Arias, C. A., Mechanisms of antibiotic resistance. *Microbiol. Spectr.* **2016,** 4, (2).
5. World Health Organization, Antimicrobial resistance: Global report on surveillance. 2014.
6. Fair, R. J.; Tor, Y., Antibiotics and bacterial resistance in the 21st century. *Perspect. Med. Chem.* **2014,** 6, 25-64.
7. Jasovský, D.; Littmann, J.; Zorzet, A.; Cars, O., Antimicrobial resistance - A threat to the world's sustainable development. *Ups. J. Med. Sci.* **2016,** 121, (3), 159-164.
8. Michael, C. A.; Dominey-Howes, D.; Labbate, M., The antimicrobial resistance crisis: Causes, consequences, and management. *Front. Public Health* **2014,** 2, 145.
9. Newman, D. J.; Cragg, G. M.; Snader, K. M., Natural products as sources of new drugs over the period 1981-2002. *J. Nat. Prod.* **2003,** 66, (7), 1022-1037.
10. Yeaman, M. R.; Yount, N. Y., Mechanisms of antimicrobial peptide action and resistance. *Pharmacol. Rev.* **2003,** 55, (1), 27-55.
11. Vellai, T.; Vida, G., The origin of eukaryotes: The difference between prokaryotic and eukaryotic cells. *Proc. Biol. Sci.* **1999,** 266, (1428), 1571-1577.
12. Sela, I.; Wolf, Y. I.; Koonin, E. V., Theory of prokaryotic genome evolution. *Proc. Natl. Acad. Sci. USA* **2016,** 113, (41), 11399-11407.
13. Hong, W.; Zeng, J.; Xie, J., Antibiotic drugs targeting bacterial RNAs. *Acta Pharm. Sin. B* **2014,** 4, (4), 258-265.
14. Uzman, A., *Molecular biology of the cell (4th ed.): Alberts, B., Johnson, A., Lewis, J., Raff, M., Roberts, K., and Walter, P*. 2003; Vol. 31, p 212-214.
15. Wilson, J. W.; Schurr, M. J.; LeBlanc, C. L.; Ramamurthy, R.; Buchanan, K. L.; Nickerson, C. A., Mechanisms of bacterial pathogenicity. *Postgrad. Med. J.* **2002,** 78, (918), 216-224.
16. Silhavy, T. J.; Kahne, D.; Walker, S., The bacterial cell envelope. *CSH Perspect. Biol.* **2010,** 2, (5), a000414.
17. Gram, C., Ueber die isolirte Farbung der schizomyceten in schnitt-und trockenpraparaten. *Fortschr. Med.* **1884,** 2, 185-189.
18. Doerrler, W. T., Lipid trafficking to the outer membrane of Gram-negative bacteria. *Mol. Microbiol.* **2006,** 60, (3), 542-552.
19. Schneewind, O.; Missiakas, D., Lipoteichoic acid synthesis and function in Gram-positive bacteria. In *Biogenesis of Fatty Acids, Lipids and Membranes*, Geiger, O., Ed. Springer International Publishing: Cham, **2017**; pp 1-18.
20. Chatterjee, S. N.; Chaudhuri, K., Gram-negative bacteria: The cell membranes. In *Outer membrane vesicles of bacteria*, Springer Berlin Heidelberg: Berlin, Heidelberg, **2012**; pp 15-34.
21. Furse, S.; Scott, D. J., Three-dimensional distribution of phospholipids in Gram-negative bacteria. *Biochemistry* **2016,** 55, (34), 4742-4747.
22. Miyadai, H.; Tanaka-Masuda, K.; Matsuyama, S.-i.; Tokuda, H., Effects of lipoprotein overproduction on the induction of DegP (HtrA) involved in quality control in the *Escherichia coli* periplasm. *J. Biol. Chem.* **2004,** 279, (38), 39807-39813.
23. Fu, L. M.; Fu-Liu, C. S., Is *Mycobacterium tuberculosis* a closer relative to Gram-positive or Gram-negative bacterial pathogens? *Tuberculosis* **2002,** 82, (2-3), 85-90.
24. Epand, R. M.; Walker, C.; Epand, R. F.; Magarvey, N. A., Molecular mechanisms of membrane targeting antibiotics. *BBA-Biomembranes* **2016,** 1858, (5), 980-987.

25. Casadevall, A.; Pirofski, L. A., Virulence factors and their mechanisms of action: the view from a damage-response framework. *J. Water. Health.* **2009,** 7 Suppl 1, S2-S18.

26. Jones, D. S.; Podolsky, S. H.; Greene, J. A., The burden of disease and the changing task of medicine. *N. Engl. J. Med.* **2012,** 366, (25), 2333-2338.

27. Smith, I., *Mycobacterium tuberculosis* pathogenesis and molecular determinants of virulence. *Clin. Microbiol. Rev.* **2003,** 16, (3), 463-496.

28. World Health Organization, The top 10 causes of death. https://www.who.int/news-room/fact-sheets/detail/the-top-10-causes-of-death (30.12.2021),

29. Kirchhelle, C., Pharming animals: A global history of antibiotics in food production (1935–2017). *Palgrave Commun.* **2018,** 4, (1), 96.

30. Hao, H.; Cheng, G.; Iqbal, Z.; Ai, X.; Hussain, H. I.; Huang, L.; Dai, M.; Wang, Y.; Liu, Z.; Yuan, Z., Benefits and risks of antimicrobial use in food-producing animals. *Front. Microbiol.* **2014,** 5, 288-288.

31. Enzler, M. J.; Berbari, E.; Osmon, D. R., Antimicrobial prophylaxis in adults. *Mayo Clinic Proc.* **2011,** 86, (7), 686-701.

32. Landers, T. F.; Cohen, B.; Wittum, T. E.; Larson, E. L., A review of antibiotic use in food animals: Perspective, policy, and potential. *Public Health Rep.* **2012,** 127, (1), 4-22.

33. Cabello, F. C., Heavy use of prophylactic antibiotics in aquaculture: A growing problem for human and animal health and for the environment. *Environ. Microbiol.* **2006,** 8, (7), 1137-1144.

34. Uddin, T. M.; Chakraborty, A. J.; Khusro, A.; Zidan, B. M. R. M.; Mitra, S.; Emran, T. B.; Dhama, K.; Ripon, M. K. H.; Gajdács, M.; Sahibzada, M. U. K.; Hossain, M. J.; Koirala, N., Antibiotic resistance in microbes: History, mechanisms, therapeutic strategies and future prospects. *J. Infect. Public Heal.* **2021,** 14, (12), 1750-1766.

35. World Health Organization, *Antibacterial agents in clinical development: an analysis of the antibacterial clinical development pipeline*; Geneva, Switzerland, **2019**.

36. Bahar, A. A.; Ren, D., Antimicrobial peptides. *Pharmaceuticals* **2013,** 6, (12), 1543-1575.

37. MacGowan, A.; Macnaughton, E., Antibiotic resistance. *Medicine* **2017,** 45, (10), 622-628.

38. Dyson, P., Bacterial and bacteriophage genetics (4th edn). *Heredity* **2001,** 86, 117.

39. Pray, L., Antibiotic resistance, mutation rates and MRSA. *Nat. Sci. Educ.* **2008,** 1, (1), 30.

40. Partridge, S. R.; Kwong, S. M.; Firth, N.; Jensen, S. O., Mobile genetic elements associated with antimicrobial resistance. *Clin. Microbiol. Rev.* **2018,** 31, (4), e00088-17.

41. Holmes, A. H.; Moore, L. S. P.; Sundsfjord, A.; Steinbakk, M.; Regmi, S.; Karkey, A.; Guerin, P. J.; Piddock, L. J. V., Understanding the mechanisms and drivers of antimicrobial resistance. *Lancet* **2016,** 387, (10014), 176-187.

42. Polly, S. M., The antibiotic paradox: How miracle drugs are destroying the miracle. *JAMA* **1993,** 270, (3), 384-385.

43. Zaman, S. B.; Hussain, M. A.; Nye, R.; Mehta, V.; Mamun, K. T.; Hossain, N., A review on antibiotic resistance: Alarm bells are ringing. *Cureus* **2017,** 9, (6), e1403.

44. Davies, J.; Davies, D., Origins and evolution of antibiotic resistance. *Microbiol. Mol. Biol. R.* **2010,** 74, (3), 417-433.

45. Simpkin, V. L.; Renwick, M. J.; Kelly, R.; Mossialos, E., Incentivising innovation in antibiotic drug discovery and development: progress, challenges and next steps. *J. Antibiot.* **2017,** 70, (12), 1087-1096.

46. Power, E., Impact of antibiotic restrictions: The pharmaceutical perspective. *Clin. Microbiol. Infec.* **2006,** 12, 25-34.

47. Rice, L. B., The clinical consequences of antimicrobial resistance. *Curr. Opin. Microbiol.* **2009,** 12, (5), 476-481.

48. Harbottle, H.; Thakur, S.; Zhao, S.; White, D. G., Genetics of antimicrobial resistance. *Anim. Biotechnol.* **2006,** 17, (2), 111-124.

49. Li, B.; Webster, T. J., Bacteria antibiotic resistance: New challenges and opportunities for implant-associated orthopedic infections. *J. Orthop. Res.* **2018,** 36, (1), 22-32.

50.   Nikaido, H., Multidrug resistance in bacteria. *Annu. Rev. Biochem.* **2009,** 78, 119-146.

51.   Clatworthy, A. E.; Pierson, E.; Hung, D. T., Targeting virulence: A new paradigm for antimicrobial therapy. *Nat. Chem. Biol.* **2007,** 3, (9), 541-548.

52.   Zhang, L.-j.; Gallo, R. L., Antimicrobial peptides. *Curr. Biol.* **2016,** 26, (1), R14-R19.

53.   Bulet, P.; Stocklin, R.; Menin, L., Anti-microbial peptides: From invertebrates to vertebrates. *Immunol. Rev.* **2004,** 198, 169-184.

54.   Yang, S.-C.; Lin, C.-H.; Sung, C. T.; Fang, J.-Y., Antibacterial activities of bacteriocins: Application in foods and pharmaceuticals. *Front. Microbiol.* **2014,** 5, 241-241.

55.   Patel, S.; Akhtar, N., Antimicrobial peptides (AMPs): The quintessential 'offense and defense' molecules are more than antimicrobials. *Biomed. Pharmacother.* **2017,** 95, 1276-1283.

56.   Wang, G.; Li, X.; Wang, Z., APD3: The antimicrobial peptide database as a tool for research and education. *Nucleic Acids Res.* **2016,** 44, (D1), D1087-1093.

57.   Wang, Z.; Wang, G., APD: The antimicrobial peptide database. *Nucleic Acids Res.* **2004,** 32, D590-592.

58.   Kumar, P.; Kizhakkedathu, J. N.; Straus, S. K., Antimicrobial peptides: Diversity, mechanism of action and strategies to improve the activity and biocompatibility *in Vivo*. *Biomolecules* **2018,** 8, (1), 4.

59.   de la Fuente-Núñez, C.; Silva, O. N.; Lu, T. K.; Franco, O. L., Antimicrobial peptides: Role in human disease and potential as immunotherapies. *Pharmacol. Therapeut.* **2017,** 178, 132-140.

60.   Sperstad, S. V.; Haug, T.; Blencke, H. M.; Styrvold, O. B.; Li, C.; Stensvag, K., Antimicrobial peptides from marine invertebrates: challenges and perspectives in marine antimicrobial peptide discovery. *Biotechnol. Adv.* **2011,** 29, (5), 519-530.

61.   Taylor, S. W.; Craig, A. G.; Fischer, W. H.; Park, M.; Lehrer, R. I., Stylelin D, an extensively modified antimicrobial peptide from ascidian hemocytes. *J. Biol. Chem.* **2000,** 275, (49), 38417-26.

62.   Lee, I. H.; Cho, Y.; Lehrer, R. I., Stylelins, broad-spectrum antimicrobial peptides from the solitarytunicate, *Styela clava*. *Comp. Biochem. Phys. B* **1997,** 118, (3), 515-521.

63.   Noga, E. J.; Stone, K. L.; Wood, A.; Gordon, W. L.; Robinette, D., Primary structure and cellular localization of callinectin, an antimicrobial peptide from the blue crab. *Dev. Comp. Immunol.* **2011,** 35, (4), 409-415.

64.   Falanga, A.; Lombardi, L.; Franci, G.; Vitiello, M.; Iovene, M. R.; Morelli, G.; Galdiero, M.; Galdiero, S., Marine antimicrobial peptides: Nature provides templates for the design of novel compounds against pathogenic bacteria. *Int. J. Mol. Sci.* **2016,** 17, (5), 785.

65.   Goldman, M. J.; Anderson, G. M.; Stolzenberg, E. D.; Kari, U. P.; Zasloff, M.; Wilson, J. M., Human beta-defensin-1 is a salt-sensitive antibiotic in lung that is inactivated in cystic fibrosis. *Cell* **1997,** 88, (4), 553-560.

66.   Spänig, S.; Heider, D., Encodings and models for antimicrobial peptide classification for multi-resistant pathogens. *BioData Min.* **2019,** 12, (1), 7.

67.   Mahlapuu, M.; Håkansson, J.; Ringstad, L.; Björn, C., Antimicrobial peptides: An emerging category of therapeutic agents. *Front. Cell. Infect. Mi.* **2016,** 6, 194-194.

68.   Wimley, W. C., Describing the mechanism of antimicrobial peptide action with the interfacial activity model. *ACS Chem. Biol.* **2010,** 5, (10), 905-917.

69.   Morales, P.; Jiménez, M. A., Design and structural characterisation of monomeric water-soluble α-helix and β-hairpin peptides: State-of-the-art. *Arch. Biochem. Biophys.* **2019,** 661, 149-167.

70.   Wang, G., Post-translational modifications of natural antimicrobial peptides and strategies for peptide engineering. *Curr. Biotechnol.* **2012,** 1, (1), 72-79.

71.   Patil, N. A.; Tailhades, J.; Hughes, R. A.; Separovic, F.; Wade, J. D.; Hossain, M. A., Cellular disulfide bond formation in bioactive peptides and proteins. *Int. J. Mol. Sci.* **2015,** 16, (1), 1791-1805.

72. Cook, K. M.; Hogg, P. J., Post-translational control of protein function by disulfide bond cleavage. *Antioxid. Redox Sign.* **2013,** 18, (15), 1987-2015.

73. Haag, A. F.; Kerscher, B.; Dall'Angelo, S.; Sani, M.; Longhi, R.; Baloban, M.; Wilson, H. M.; Mergaert, P.; Zanda, M.; Ferguson, G. P., Role of cysteine residues and disulfide bonds on the activity of a legume root nodule-specific, cysteine-rich peptide. *J. Biol. Chem.* **2012,** 287, (14), 10891-10798.

74. Bulaj, G., Formation of disulfide bonds in proteins and peptides. *Biotechnol. Adv.* **2005,** 23, (1), 87-92.

75. Lee, T.-H.; Hall, K. N.; Aguilar, M.-I., Antimicrobial peptide structure and mechanism of action: A focus on the role of membrane structure. *Curr. Top. Med. Chem.* **2016,** 16, (1), 25-39.

76. Galdiero, S.; Falanga, A.; Berisio, R.; Grieco, P.; Morelli, G.; Galdiero, M., Antimicrobial peptides as an opportunity against bacterial diseases. *Curr. Med. Chem.* **2015,** 22, 1665-1677.

77. Brogden, K. A., Antimicrobial peptides: Pore formers or metabolic inhibitors in bacteria? *Nat. Rev. Microbiol.* **2005,** 3, (3), 238-250.

78. Sengupta, D.; Leontiadou, H.; Mark, A. E.; Marrink, S. J., Toroidal pores formed by antimicrobial peptides show significant disorder. *Biochim. Biophys. Acta* **2008,** 1778, (10), 2308-2317.

79. López-Meza, J. E.; Ochoa-Zarzosa, A.; Barboza-Corona, J. E.; Bideshi, D. K., Antimicrobial peptides: Current and potential applications in biomedical therapies. *BioMed Res. Int.* **2015,** 2015, 367243-367243.

80. Park, S.-C.; Park, Y.; Hahm, K.-S., The role of antimicrobial peptides in preventing multidrug-resistant bacterial infections and biofilm formation. *Int. J. Mol. Sci.* **2011,** 12, (9), 5971-5992.

81. Hancock, R. E.; Nijnik, A.; Philpott, D. J., Modulating immunity as a therapy for bacterial infections. *Nat. Rev. Microbiol.* **2012,** 10, (4), 243-254.

82. Lai, Y.; Gallo, R. L., AMPed up immunity: How antimicrobial peptides have multiple roles in immune defense. *Trends Immunol.* **2009,** 30, (3), 131-141.

83. Tam, J. P.; Wang, S.; Wong, K. H.; Tan, W. L., Antimicrobial peptides from plants. *Pharmaceuticals* **2015,** 8, (4), 711-757.

84. Zasloff, M., Antimicrobial peptides of multicellular organisms. *Nature* **2002,** 415, (6870), 389-395.

85. Hollmann, A.; Martinez, M.; Maturana, P.; Semorile, L. C.; Maffia, P. C., Antimicrobial peptides: interaction with model and biological membranes and synergism with chemical antibiotics. *Front. Chem.* **2018,** 6, 204-204.

86. Powers, J.-P. S.; Hancock, R. E. W., The relationship between peptide structure and antibacterial activity. *Peptides* **2003,** 24, (11), 1681-1691.

87. Seo, M.-D.; Won, H.-S.; Kim, J.-H.; Mishig-Ochir, T.; Lee, B.-J., Antimicrobial peptides for therapeutic applications: A review. *Molecules* **2012,** 17, (10), 12276-12286.

88. Tincu, J. A.; Taylor, S. W., Antimicrobial peptides from marine invertebrates. *Antimicrob. Agents Ch.* **2004,** 48, (10), 3645-3654.

89. Wang, J.; Dou, X.; Song, J.; Lyu, Y.; Zhu, X.; Xu, L.; Li, W.; Shan, A., Antimicrobial peptides: Promising alternatives in the post feeding antibiotic era. *Med. Res. Rev.* **2019,** 39, (3), 831-859.

90. Ciumac, D.; Gong, H.; Hu, X.; Lu, J. R., Membrane targeting cationic antimicrobial peptides. *J. Colloid Interf. Sci.* **2019,** 537, 163-185.

91. Chen, Y.; Guarnieri, M. T.; Vasil, A. I.; Vasil, M. L.; Mant, C. T.; Hodges, R. S., Role of peptide hydrophobicity in the mechanism of action of alpha-helical antimicrobial peptides. *Antimicrob. Agents Ch.* **2007,** 51, (4), 1398-1406.

92. Mishra, A. K.; Choi, J.; Moon, E.; Baek, K. H., Tryptophan-rich and proline-rich antimicrobial peptides. *Molecules* **2018,** 23, (4), 815.

93. Stensvag, K.; Haug, T.; Sperstad, S. V.; Rekdal, O.; Indrevoll, B.; Styrvold, O. B., Arasin 1, a proline-arginine-rich antimicrobial peptide isolated from the spider crab, *Hyas araneus*. *Dev. Comp. Immunol.* **2008,** 32, (3), 275-85.

94.   Iijima, N.; Tanimoto, N.; Emoto, Y.; Morita, Y.; Uematsu, K.; Murakami, T.; Nakai, T., Purification and characterization of three isoforms of chrysophsin, a novel antimicrobial peptide in the gills of the red sea bream, *Chrysophrys major*. *Eur. J .Biochem.* **2003,** 270, (4), 675-686.

95.   Lee, S. Y.; Lee, B. L.; Soderhall, K., Processing of an antibacterial peptide from hemocyanin of the freshwater crayfish *Pacifastacus leniusculus*. *J. Biol. Chem.* **2003,** 278, (10), 7927-33.

96.   Silva, O. N.; Alves, E. S.; de la Fuente-Nunez, C.; Ribeiro, S. M.; Mandal, S. M.; Gaspar, D.; Veiga, A. S.; Castanho, M. A.; Andrade, C. A.; Nascimento, J. M.; Fensterseifer, I. C.; Porto, W. F.; Correa, J. R.; Hancock, R. E.; Korpole, S.; Oliveira, A. L.; Liao, L. M.; Franco, O. L., Structural studies of a lipid-binding peptide from tunicate hemocytes with anti-biofilm activity. *Sci. Rep.* **2016,** 6, 27128.

97.   Kokryakov, V. N.; Harwig, S. S. L.; Panyutich, E. A.; Shevchenko, A. A.; Aleshina, G. M.; Shamova, O. V.; Korneva, H. A.; Lehrer, R. I., Protegrins: Leukocyte antimicrobial peptides that combine features of corticostatic defensins and tachyplesins. *FEBS Lett.* **1993,** 327, (2), 231-236.

98.   Sahl, H.-G.; Pag, U.; Bonness, S.; Wagner, S.; Antcheva, N.; Tossi, A., Mammalian defensins: Structures and mechanism of antibiotic activity. *J. Leukocyte Biol.* **2005,** 77, (4), 466-475.

99.   Nakamura, T.; Furunaka, H.; Miyata, T.; Tokunaga, F.; Muta, T.; Iwanaga, S.; Niwa, M.; Takao, T.; Shimonishi, Y., Tachyplesin, a class of antimicrobial peptide from the hemocytes of the horseshoe crab (*Tachypleus tridentatus*). Isolation and chemical structure. *J. Biol. Chem.* **1988,** 263, (32), 16709-16713.

100.   Büyükkiraz, M. E.; Kesmen, Z., Antimicrobial peptides (AMPs): A promising class of antimicrobial compounds. *J. Appl. Microbiol.* **2022,** 132, (3), 1573-1596.

101.   Szyk, A.; Wu, Z.; Tucker, K.; Yang, D.; Lu, W.; Lubkowski, J., Crystal structures of human α-defensins HNP4, HD5, and HD6. *Protein Sci.* **2006,** 15, (12), 2749-2760.

102.   Jing, W.; Hunter, H. N.; Tanabe, H.; Ouellette, A. J.; Vogel, H. J., Solution structure of cryptdin-4, a mouse paneth cell α-defensin. *Biochemistry* **2004,** 43, (50), 15759-15766.

103.   Midura-Nowaczek, K.; Markowska, A., Antimicrobial peptides and their analogs: searching for new potential therapeutics. *Perspect. Med. Chem.* **2014,** 6, 73-80.

104.   Madhongsa, K.; Pasan, S.; Phophetleb, O.; Nasompag, S.; Thammasirirak, S.; Daduang, S.; Taweechaisupapong, S.; Lomize, A. L.; Patramanon, R., Antimicrobial action of the cyclic peptide bactenecin on *Burkholderia pseudomallei* correlates with efficient membrane permeabilization. *PLoS Neglect. Trop. D.* **2013,** 7, (6), e2267.

105.   Jenssen, H.; Andersen, J. H.; Uhlin-Hansen, L.; Gutteberg, T. J.; Rekdal, Ø., Anti-HSV activity of lactoferricin analogues is only partly related to their affinity for heparan sulfate. *Antivir. Res.* **2004,** 61, (2), 101-109.

106.   Scocchi, M.; Tossi, A.; Gennaro, R., Proline-rich antimicrobial peptides: converging to a non-lytic mechanism of action. *Cell. Mol. Life Sci.* **2011,** 68, (13), 2317-2330.

107.   Sitaram, N.; Subbalakshmi, C.; Nagaraj, R., Indolicidin, a 13-residue basic antimicrobial peptide rich in tryptophan and proline, interacts with Ca(2+)-calmodulin. *Biochem. Bioph. Res. Co.* **2003,** 309, (4), 879-884.

108.   Li, W. F.; Ma, G. X.; Zhou, X. X., Apidaecin-type peptides: biodiversity, structure-function relationships and mode of action. *Peptides* **2006,** 27, (9), 2350-9.

109.   Taniguchi, M.; Ochiai, A.; Kondo, H.; Fukuda, S.; Ishiyama, Y.; Saitoh, E.; Kato, T.; Tanaka, T., Pyrrhocoricin, a proline-rich antimicrobial peptide derived from insect, inhibits the translation process in the cell-free *Escherichia coli* protein synthesis system. *J. Biosci. Bioeng.* **2016,** 121, (5), 591-598.

110.   Haney, E. F.; Hancock, R. E. W., Peptide design for antimicrobial and immunomodulatory applications. *Biopolymers* **2013,** 100, (6), 572-583.

111.   Lau, J. L.; Dunn, M. K., Therapeutic peptides: Historical perspectives, current development trends, and future directions. *Bioorgan. Med. Chem.* **2018,** 26, (10), 2700-2707.

112. Waghu, F. H.; Barai, R. S.; Gurung, P.; Idicula-Thomas, S., CAMP$_{R3}$: A database on sequences, structures and signatures of antimicrobial peptides. *Nucleic Acids Res.* **2016,** 44, (D1), D1094-D1097.

113. Lee, H.-T.; Lee, C.-C.; Yang, J.-R.; Lai, J. Z. C.; Chang, K. Y., A large-scale structural classification of antimicrobial peptides. *BioMed Res. Int.* **2015,** 2015, 475062.

114. Solstad, R. G.; Johansen, C.; Stensvåg, K.; Strøm, M. B.; Haug, T., Structure-activity relationship studies of shortened analogues of the antimicrobial peptide EeCentrocin 1 from the sea urchin *Echinus esculentus*. *J. Pept. Sci.* **2020,** 26, (2), e3233.

115. Donia, M.; Hamann, M. T., Marine natural products and their potential applications as anti-infective agents. *Lancet. Infect. Dis.* **2003,** 3, (6), 338-348.

116. Rowley, D. B., Oceanic axial depth and age-depth distribution of oceanic lithosphere: Comparison of magnetic anomaly picks versus age-grid models. *Lithosphere* **2018,** 11, (1), 21-43.

117. Costello, M. J.; Chaudhary, C., Marine biodiversity, biogeography, deep-sea gradients, and conservation. *Curr. Biol.* **2017,** 27, (11), R511-R527.

118. Pawlik J. R.; Amsler C. D.; Ritson-Williams R; McClintock J. B.; Baker B. J.; V.J., P., *Marine chemical ecology: A science born of scuba*. Smithsonian Institution Scholarly Press: **2013**; Vol. 39, p 53-69.

119. Pomponi, S. A., The bioprocess–technological potential of the sea. *J. Biotechnol.* **1999,** 70, (1), 5-13.

120. Khan, R. A., Natural products chemistry: The emerging trends and prospective goals. *Saudi Pharm. J.* **2018,** 26, (5), 739-753.

121. Dias, D. A.; Urban, S.; Roessner, U., A historical overview of natural products in drug discovery. *Metabolites* **2012,** 2, (2), 303-36.

122. Pascolutti, M.; Quinn, R. J., Natural products as lead structures: chemical transformations to create lead-like libraries. *Drug Discov. Today* **2014,** 19, (3), 215-221.

123. Hong, J., Natural product diversity and its role in chemical biology and drug discovery. *Curr. Opin. Chem. Biol.* **2011,** 15, (3), 350-354.

124. Xu, H.; Xu, H.; Lin, M.; Wang, W.; Li, Z.; Huang, J.; Chen, Y.; Chen, X., Learning the drug target-likeness of a protein. *Proteomics* **2007,** 7, (23), 4255-4263.

125. Hopkins, A. L.; Groom, C. R., The druggable genome. *Nat. Rev. Drug Discov.* **2002,** 1, (9), 727-730.

126. Newman, D. J.; Cragg, G. M., Natural products as sources of new drugs from 1981 to 2014. *J. Nat. Prod.* **2016,** 79, (3), 629-661.

127. Patridge, E.; Gareiss, P.; Kinch, M. S.; Hoyer, D., An analysis of FDA-approved drugs: natural products and their derivatives. *Drug Discov. Today* **2016,** 21, (2), 204-7.

128. The marine pharmaceutical pipeline. http://marinepharmacology.midwestern.edu/clinPipeline.htm (04.10.2021),

129. McGivern, J. G., Ziconotide: A review of its pharmacology and use in the treatment of pain. *Neuropsych. Dis. Treat.* **2007,** 3, (1), 69-85.

130. Staats, P. S.; Yearwood, T.; Charapata, S. G.; Presley, R. W.; Wallac, M. S.; Byas-Smith, M.; Fisher, R.; Bryce, D. A.; Mangieri, E. A.; Luther, R. R.; Mayo, M.; McGuire, D.; Ellis, D., Intrathecal ziconotide in the treatment of refractory pain in patients with cancer or aids: A randomized controlled trial. *JAMA* **2004,** 291, (1), 63-70.

131. Ternon, E.; Thomas, O., Toxins from marine invertebrates. In *Seafood and freshwater toxins: Pharmacology, physiology, and detection*, Boca Raton, **2014**; p 77.

132. Zambelli, V. O.; Pasqualoto, K. F. M.; Picolo, G.; Chudzinski-Tavassi, A. M.; Cury, Y., Harnessing the knowledge of animal toxins to generate drugs. *Pharmacol. Res.* **2016,** 112, 30-36.

133. Zeng, L.; Jacobs, M. W.; Swalla, B. J., Coloniality has evolved once in stolidobranch ascidians. *Integr. Comp. Biol.* **2006,** 46, (3), 255-268.

134. Tsagkogeorga, G.; Turon, X.; Hopcroft, R. R.; Tilak, M.-K.; Feldstein, T.; Shenkar, N.; Loya, Y.; Huchon, D.; Douzery, E. J. P.; Delsuc, F., An updated 18S rRNA phylogeny of tunicates based on mixture and secondary structure models. *BMC Evol. Biol.* **2009,** 9, (1), 187.

135. Shenkar, N.; Swalla, B. J., Global diversity of Ascidiacea. *PLoS One* **2011,** 6, (6), e20657.

136. Sommer, F.; Awazu, S.; Anton-Erxleben, F.; Jiang, D.; Klimovich, A. V.; Klimovich, B. V.; Samoiˇlovich, M. P.; Satou, Y.; Krüss, M.; Gelhaus, C.; Kürn, U.; Bosch, T. C. G.; Khalturin, K., Blood system formation in the urochordate *Ciona intestinalis* requires the variable receptor vCRL1. *Mol. Biol. Evol.* **2012,** 29, (10), 3081-3093.

137. Sasakura, Y.; Mita, K.; Ogura, Y.; Horie, T., Ascidians as excellent chordate models for studying the development of the nervous system during embryogenesis and metamorphosis. *Dev. Growth Differ.* **2012,** 54, (3), 420-37.

138. Nishino, A., Morphology and physiology of the ascidian nervous systems and the effectors. In *Transgenic ascidians*, Sasakura, Y., Ed. Springer Singapore: Singapore, **2018;** pp 179-196.

139. Goodbody, I., The physiology of ascidians. In *Advances in marine biology*, Russell, F. S.; Yonge, M., Eds. Academic Press: **1975;** Vol. 12, pp 1-149.

140. Petersen, J. K., Ascidian suspension feeding. *J. Exp. Mar. Biol. Ecol.* **2007,** 342, (1), 127-137.

141. Urochordates - Sea Squirts, Salps and Larvaceans. https://cronodon.com/BioTech/Urochordates.html (06.04.2022),

142. Franchi, N.; Ballarin, L., Immunity in protochordates: The tunicate perspective. *Front. Immunol.* **2017,** 8, 674.

143. Jensen, P. R.; Fenical, W., Marine bacterial diversity as a resource for novel microbial products. *J. Ind. Microbiol.* **1996,** 17, (5), 346-351.

144. Colucci-Guyon, E.; Tinevez, J.-Y.; Renshaw, S. A.; Herbomel, P., Strategies of professional phagocytes *in vivo*: unlike macrophages, neutrophils engulf only surface-associated microbes. *J. Cell Sci.* **2011,** 124, (18), 3053-3059.

145. Di Bella, M. A.; Fedders, H.; De Leo, G.; Leippe, M., Localization of antimicrobial peptides in the tunic of *Ciona intestinalis* (Ascidiacea, Tunicata) and their involvement in local inflammatory-like reactions. *Results Immunol.* **2011,** 1, (1), 70-75.

146. Lee, I. H.; Zhao, C.; Cho, Y.; Harwig, S. S. L.; Cooper, E. L.; Lehrer, R. I., Clavanins, α-helical antimicrobial peptides from tunicate hemocytes. *FEBS Lett.* **1997,** 400, (2), 158-162.

147. Blunt, J. W.; Carroll, A. R.; Copp, B. R.; Davis, R. A.; Keyzers, R. A.; Prinsep, M. R., Marine natural products. *Nat. Prod. Rep.* **2018,** 35, (1), 8-53.

148. Palanisamy, S. K.; Rajendran, N. M.; Marino, A., Natural products diversity of marine ascidians (Tunicates; Ascidiacea) and successful drugs in clinical development. *Nat. Prod. Bioprospect.* **2017,** 7, (1), 1-111.

149. Dou, X.; Dong, B., Origins and bioactivities of natural compounds derived from marine ascidians and their symbionts. *Mar. Drugs* **2019,** 17, (12), 670.

150. Lima, S. M. F.; Freire, M. S.; Gomes, A. L. O.; Cantuária, A. P. C.; Dutra, F. R. P.; Magalhães, B. S.; Sousa, M. G. C.; Migliolo, L.; Almeida, J. A.; Franco, O. L.; Rezende, T. M. B., Antimicrobial and immunomodulatory activity of host defense peptides, clavanins and LL-37, *in vitro*: An endodontic perspective. *Peptides* **2017,** 95, 16-24.

151. Lee, I. H.; Zhao, C.; Nguyen, T.; Menzel, L.; Waring, A. J.; Sherman, M. A.; Lehrer, R. I., Clavaspirin, an antibacterial and haemolytic peptide from *Styela clava*. *J. Pept. Res.* **2001,** 58, (6), 445-56.

152. Lee, I. H.; Lee, Y. S.; Kim, C. H.; Kim, C. R.; Hong, T.; Menzel, L.; Boo, L. M.; Pohl, J.; Sherman, M. A.; Waring, A.; Lehrer, R. I., Dicynthaurin: an antimicrobial peptide from hemocytes of the solitary tunicate, *Halocynthia aurantium*. *BBA-Gen. Subjects* **2001,** 1527, (3), 141-148.

153. Bringezu, F.; Majerowicz, M.; Maltseva, E.; Wen, S.; Brezesinski, G.; Waring, A. J., Penetration of the antimicrobial peptide dicynthaurin into phospholipid monolayers at the liquid–air interface. *Chembiochem* **2007,** 8, (9), 1038-1047.

154. Jang, W. S.; Kim, K. N.; Lee, Y. S.; Nam, M. H.; Lee, I. H., Halocidin: a new antimicrobial peptide from hemocytes of the solitary tunicate, *Halocynthia aurantium*. *FEBS Lett.* **2002,** 521, (1-3), 81-86.

155. Galinier, R.; Roger, E.; Sautiere, P. E.; Aumelas, A.; Banaigs, B.; Mitta, G., Halocyntin and papillosin, two new antimicrobial peptides isolated from hemocytes of the solitary tunicate, *Halocynthia papillosa*. *J. Pept. Sci.* **2009,** 15, (1), 48-55.

156. Tincu, J. A.; Menzel, L. P.; Azimov, R.; Sands, J.; Hong, T.; Waring, A. J.; Taylor, S. W.; Lehrer, R. I., Plicatamide, an antimicrobial octapeptide from *Styela plicata* hemocytes. *J. Biol. Chem.* **2003,** 278, (15), 13546-53.

157. Tincu, J. A.; Craig, A. G.; Taylor, S. W., Plicatamide: A lead to the biosynthetic origins of the tunichromes? *Biochem. Bioph. Res. Co.* **2000,** 270, (2), 421-424.

158. Lee, I. H.; Cho, Y.; Lehrer, R. I., Effects of pH and salinity on the antimicrobial properties of clavanins. *Infect. Immun.* **1997,** 65, (7), 2898-2903.

159. van Kan, E. J. M.; Ganchev, D. N.; Snel, M. M. E.; Chupin, V.; van der Bent, A.; de Kruijff, B., The peptide antibiotic clavanin A interacts strongly and specifically with lipid bilayers. *Biochemistry* **2003,** 42, (38), 11366-11372.

160. Motzer, R.; Scher, H.; Bajorin, D.; Sternberg, C.; Bosl, G. J., Phase II trial of Didemnin B in patients with advanced renal cell carcinoma. *Invest. New Drug.* **1990,** 8, (4), 391-2.

161. Mittelman, A.; Chun, H. G.; Puccio, C.; Coombe, N.; Lansen, T.; Ahmed, T., Phase II clinical trial of didemnin B in patients with recurrent or refractory anaplastic astrocytoma or glioblastoma multiforme (NSC 325319). *Invest. New Drug.* **1999,** 17, (2), 179-182.

162. Tourneau, C. L.; Raymond, E.; Faivre, S., Aplidine: A paradigm of how to handle the activity and toxicity of a novel marine anticancer poison. *Curr. Pharm. Design* **2007,** 13, (33), 3427-3439.

163. Nuijen, B.; Bouma, M.; Henrar, R. E. C.; Floriano, P.; Jimeno, J. M.; Talsma, H.; Kettenes-van den Bosch, J. J.; Heck, A. J. R.; Bult, A.; Beijnen, J. H., Pharmaceutical development of a parenteral lyophilized formulation of the novel antitumor agent aplidine. *PDA J. Pharm. Sci. Tech.* **2000,** 54, (3), 193-208.

164. Dyshlovoy, S. A.; Honecker, F., Marine compounds and cancer: The first two decades of XXI century. *Mar. Drugs* **2020,** 18, (1), 20.

165. Rinehart, K. L.; Gloer, J. B.; Cook, J. C.; Mizsak, S. A.; Scahill, T. A., Structures of the didemnins, antiviral and cytotoxic depsipeptides from a Caribbean tunicate. *J. Am. Chem. Soc.* **1981,** 103, (7), 1857-1859.

166. Chun, H. G.; Davies, B.; Hoth, D.; Suffness, M.; Plowman, J.; Flora, K.; Grieshaber, C.; Leyland-Jones, B., Didemnin B. The first marine compound entering clinical trials as an antineoplastic agent. *Invest. New Drug.* **1986,** 4, (3), 279-84.

167. Lindequist, U., Marine-derived pharmaceuticals – challenges and opportunities. *Biomol. Ther.* **2016,** 24, (6), 561-571.

168. Patel, S.; Petty, W. J.; Sands, J. M., An overview of lurbinectedin as a new second-line treatment option for small cell lung cancer. *Ther. Adv. Med. Oncol.* **2021,** 13, 17588359211020529.

169. Schupp, P.; Eder, C.; Proksch, P.; Wray, V.; Schneider, B.; Herderich, M.; Paul, V., Staurosporine derivatives from the ascidian *Eudistoma toealensis* and Its predatory flatworm *Pseudoceros* sp. *J. Nat. Prod.* **1999,** 62, (7), 959-962.

170. Omura, S.; Iwai, Y.; Hirano, A.; Nakagawa, A.; Awaya, J.; Tsuchya, H.; Takahashi, Y.; Masuma, R., A new alkaloid AM-2282 of *Streptomyces* origin. Taxonomy, fermentation, isolation and preliminary characterization. *J. Antibiot.* **1977,** 30, (4), 275-282.

171. Braun, K.; Leubner, F.; Stach, T., Phylogenetic analysis of phenotypic characters of Tunicata supports basal Appendicularia and monophyletic Ascidiacea. *Cladistics* **2020,** 36, (3), 259-300.

172. Carroll, A. R.; Healy, P. C.; Quinn, R. J.; Tranter, C. J., Prunolides A, B, and C: Novel tetraphenolic bis-spiroketals from the Australian ascidian *Synoicum prunum*. *The Journal of Organic Chemistry* **1999,** 64, (8), 2680-2682.

173. Won, T. H.; Jeon, J.-e.; Kim, S.-H.; Lee, S.-H.; Rho, B. J.; Oh, D.-C.; Oh, K.-B.; Shin, J., Brominated aromatic furanones and related esters from the ascidian *Synoicum* sp. *J. Nat. Prod.* **2012,** 75, (12), 2055-2061.

174. Tadesse, M.; Strøm, M. B.; Svenson, J.; Jaspars, M.; Milne, B. F.; Tørfoss, V.; Andersen, J. H.; Hansen, E.; Stensvåg, K.; Haug, T., Synoxazolidinones A and B: Novel bioactive alkaloids from the ascidian *Synoicum pulmonaria*. *Org. Lett.* **2010,** 12, (21), 4752-4755.

175. Ortega, M. a. J.; Zubía, E.; Ocaña, J. M.; Naranjo, S.; Salvá, J., New rubrolides from the ascidian *Synoicum blochmanni*. *Tetrahedron* **2000,** 56, (24), 3963-3967.

176. Pearce, A. N.; Chia, E. W.; Berridge, M. V.; Maas, E. W.; Page, M. J.; Webb, V. L.; Harper, J. L.; Copp, B. R., *E/Z*-rubrolide O, an anti-inflammatory halogenated furanone from the New Zealand ascidian *Synoicum* n. sp. *J. Nat. Prod.* **2007,** 70, (1), 111-113.

177. Noguez, J. H.; Diyabalanage, T. K. K.; Miyata, Y.; Xie, X.-S.; Valeriote, F. A.; Amsler, C. D.; McClintock, J. B.; Baker, B. J., Palmerolide macrolides from the Antarctic tunicate *Synoicum adareanum*. *Bioorgan. Med. Chem.* **2011,** 19, (22), 6608-6614.

178. Miyata, Y.; Diyabalanage, T.; Amsler, C. D.; McClintock, J. B.; Valeriote, F. A.; Baker, B. J., Ecdysteroids from the Antarctic tunicate *Synoicum adareanum*. *J. Nat. Prod.* **2007,** 70, (12), 1859-1864.

179. Diyabalanage, T.; Amsler, C. D.; McClintock, J. B.; Baker, B. J., Palmerolide A, a cytotoxic macrolide from the Antarctic tunicate *Synoicum adareanum*. *J. Am. Chem. Soc.* **2006,** 128, (17), 5630-5631.

180. Carroll, A. R.; Bowden, B. F.; Coll, J. C., Studies of Australian Ascidians. III. A New Tetrahydrocannabinol Derivative From the Ascidian <I>Synoicum castellatum</I>. *Aust. J. Chem.* **1993,** 46, (7), 1079-1083.

181. Sikorska, J.; Parker-Nance, S.; Davies-Coleman, M. T.; Vining, O. B.; Sikora, A. E.; McPhail, K. L., Antimicrobial rubrolides from a South African species of *Synoicum* tunicate. *J. Nat. Prod.* **2012,** 75, (10), 1824-1827.

182. Bracegirdle, J.; Stevenson, L. J.; Page, M. J.; Owen, J. G.; Keyzers, R. A., Targeted isolation of rubrolides from the New Zealand marine tunicate *Synoicum kuranui*. *Marine Drugs* **2020,** 18, (7), 337.

183. Bracegirdle, J.; Stevenson, L. J.; Sharrock, A. V.; Page, M. J.; Vorster, J. A.; Owen, J. G.; Ackerley, D. F.; Keyzers, R. A., Hydrated rubrolides from the New Zealand tunicate *Synoicum kuranui*. *J. Nat. Prod.* **2021,** 84, (2), 544-547.

184. Ravinder, K.; Vijender Reddy, A.; Krishnaiah, P.; Ramesh, P.; Ramakrishna, S.; Laatsch, H.; Venkateswarlu, Y., Isolation and synthesis of a novel β-carboline guanidine derivative tiruchanduramine from the Indian ascidian *Synoicum macroglossum*. *Tetrahedron Lett.* **2005,** 46, (33), 5475-5478.

185. Holland, D. C.; Prebble, D. W.; Er, S.; Hayton, J. B.; Robertson, L. P.; Avery, V. M.; Domanskyi, A.; Kiefel, M. J.; Hooper, J. N. A.; Carroll, A. R., α-synuclein aggregation inhibitory prunolides and a dibrominated β-carboline sulfamate from the ascidian *Synoicum prunum*. *J. Nat. Prod.* **2022,** 85, (2), 441-452.

186. Tadesse, M.; Svenson, J.; Jaspars, M.; Strøm, M. B.; Abdelrahman, M. H.; Andersen, J. H.; Hansen, E.; Kristiansen, P. E.; Stensvåg, K.; Haug, T., Synoxazolidinone C; a bicyclic member of the synoxazolidinone family with antibacterial and anticancer activities. *Tetrahedron Lett.* **2011,** 52, (15), 1804-1806.

187. Tadesse, M.; Svenson, J.; Sepčić, K.; Trembleau, L.; Engqvist, M.; Andersen, J. H.; Jaspars, M.; Stensvag, K.; Haug, T., Isolation and synthesis of pulmonarins A and B, acetylcholinesterase inhibitors from the colonial ascidian *Synoicum pulmonaria*. *J. Nat. Prod.* **2014,** 77, (2), 364-369.

188.   Bae, J.; Cho, E.; Park, J. S.; Won, T. H.; Seo, S.-Y.; Oh, D.-C.; Oh, K.-B.; Shin, J., Isocadiolides A–H: Polybrominated aromatics from a *Synoicum* sp. ascidian. *J. Nat. Prod.* **2020,** 83, (2), 429-437.

189.   Smitha, D.; Kumar, M. M. K.; Ramana, H.; Rao, D. V., Rubrolide R: A new furanone metabolite from the ascidian *Synoicum* of the Indian Ocean. *Nat. Prod. Res.* **2014,** 28, (1), 12-17.

190.   Phipps, C. J., *A voyage towards the North Pole undertaken by His Majesty's command 1773*. W. Bowyer and J. Nichols for J. Nourse: London, **1774**.

191.   Hanssen, K. Ø.; Andersen, J. H.; Stiberg, T.; Engh, R. A.; Svenson, J.; GenevièRe, A.-M.; Hansen, E., Antitumoral and mechanistic studies of ianthelline isolated from the Arctic sponge *Stryphnus fortis*. *Anticancer Res.* **2012,** 32, (10), 4287-4297.

192.   Ebada, S. S.; Edrada, R. A.; Lin, W.; Proksch, P., Methods for isolation, purification and structural elucidation of bioactive secondary metabolites from marine invertebrates. *Nat. Protoc.* **2008,** 3, (12), 1820-1831.

193.   Nicolas, P.; El Amri, C., The dermaseptin superfamily: A gene-based combinatorial library of antimicrobial peptides. *BBA-Biomembranes* **2009,** 1788, (8), 1537-1550.

194.   Yu, G.; Baeder, D. Y.; Regoes, R. R.; Rolff, J., Combination effects of antimicrobial peptides. *Antimicrob. Agents Ch.* **2016,** 60, (3), 1717-1724.

195.   Kim, G.; Weiss, S. J.; Levine, R. L., Methionine oxidation and reduction in proteins. *Biochim. Biophys. Acta* **2014,** 1840, (2), 901-905.

196.   Suzuki, S.; Kodera, Y.; Saito, T.; Fujimoto, K.; Momozono, A.; Hayashi, A.; Kamata, Y.; Shichiri, M., Methionine sulfoxides in serum proteins as potential clinical biomarkers of oxidative stress. *Sci. Rep.* **2016,** 6, 38299-38299.

197.   Sierra, J. M.; Fuste, E.; Rabanal, F.; Vinuesa, T.; Vinas, M., An overview of antimicrobial peptides and the latest advances in their development. *Expert Opin. Biol. Th.* **2017,** 17, (6), 663-676.

198.   Wang, S.; Zeng, X.; Yang, Q.; Qiao, S., Antimicrobial peptides as potential alternatives to antibiotics in food animal industry. *Int. J. Mol. Sci.* **2016,** 17, (5), 603.

199.   Roncevic, T.; Puizina, J.; Tossi, A., Antimicrobial peptides as anti-infective agents in pre-post-antibiotic era? *Int. J. Mol. Sci.* **2019,** 20, (22), 5713.

200.   Leader, B.; Baca, Q. J.; Golan, D. E., Protein therapeutics: a summary and pharmacological classification. *Nat. Rev. Drug Discov.* **2008,** 7, (1), 21-39.

201.   Hall, M. P., Biotransformation and *in vivo* stability of protein biotherapeutics: Impact on candidate selection and pharmacokinetic profiling. *Drug Metab. Dispos.* **2014,** 42, (11), 1873-1880.

202.   Fosgerau, K.; Hoffmann, T., Peptide therapeutics: current status and future directions. *Drug Discov. Today* **2015,** 20, (1), 122-8.

203.   Kaspar, A. A.; Reichert, J. M., Future directions for peptide therapeutics development. *Drug Discov. Today* **2013,** 18, (17-18), 807-17.

204.   Uhlig, T.; Kyprianou, T.; Martinelli, F. G.; Oppici, C. A.; Heiligers, D.; Hills, D.; Calvo, X. R.; Verhaert, P., The emergence of peptides in the pharmaceutical business: From exploration to exploitation. *EuPA Open Proteom.* **2014,** 4, 58-69.

205.   Marr, A. K.; Gooderham, W. J.; Hancock, R. E. W., Antibacterial peptides for therapeutic use: Obstacles and realistic outlook. *Curr. Opin. Pharmacol.* **2006,** 6, (5), 468-472.

206.   Jenssen, H.; Aspmo, S. I., Serum stability of peptides. *Methods Mol. Biol.* **2008,** 494, 177-186.

207.   Helmerhorst, E. J.; Reijnders, I. M.; van 't Hof, W.; Veerman, E. C.; Nieuw Amerongen, A. V., A critical comparison of the hemolytic and fungicidal activities of cationic antimicrobial peptides. *FEBS Lett.* **1999,** 449, (2-3), 105-110.

208.   Strandberg, E.; Tiltak, D.; Ieronimo, M.; Kanithasen, N.; Wadhwani, P.; Ulrich Anne, S., Influence of C-terminal amidation on the antimicrobial and hemolytic activities of cationic α-helical peptides. *Pure Appl. Chem.* **2007,** 79, (4), 717-728.

209.   Li, Y., Recombinant production of antimicrobial peptides in *Escherichia coli*: A review. *Protein Expres. Purif.* **2011,** 80, (2), 260-267.

210. Lofton, H.; Pranting, M.; Thulin, E.; Andersson, D. I., Mechanisms and fitness costs of resistance to antimicrobial peptides LL-37, CNY100HL and wheat germ histones. *PLoS One* **2013,** 8, (7), e68875.

211. Pränting, M.; Negrea, A.; Rhen, M.; Andersson, D. I., Mechanism and fitness costs of PR-39 resistance in *Salmonella enterica* serovar typhimurium LT2. *Antimicrob. Agents Ch.* **2008,** 52, (8), 2734-2741.

212. Malekkhaiat Häffner, S.; Malmsten, M., Influence of self-assembly on the performance of antimicrobial peptides. *Curr. Opin. Colloid In.* **2018,** 38, 56-79.

213. Dobson, A. J.; Purves, J.; Rolff, J., Increased survival of experimentally evolved antimicrobial peptide-resistant *Staphylococcus aureus* in an animal host. *Evol. Appl.* **2014,** 7, (8), 905-912.

214. World Health Organization, *Antibacterial agents in clinical and preclinical development: An overview and analysis*; Geneva, Switzerland, **2020**.

215. Webster, N. S.; Taylor, M. W., Marine sponges and their microbial symbionts: love and other relationships. *Environ. Microbiol.* **2012,** 14, (2), 335-346.

216. Riesenfeld, C. S.; Murray, A. E.; Baker, B. J., Characterization of the microbial community and polyketide biosynthetic potential in the palmerolide-producing tunicate *Synoicum adareanum*. *J. Nat. Prod.* **2008,** 71, (11), 1812-1818.

217. Davidson, S. K.; Allen, S. W.; Lim, G. E.; Anderson, C. M.; Haygood, M. G., Evidence for the biosynthesis of bryostatins by the bacterial symbiont "*Candidatus Endobugula sertula*" of the Bryozoan *Bugula neritina*. *Appl. Environ. Microb.* **2001,** 67, (10), 4531-4537.

218. Matos, A.; Domínguez-Pérez, D.; Almeida, D.; Agüero-Chapin, G.; Campos, A.; Osório, H.; Vasconcelos, V.; Antunes, A., Shotgun proteomics of ascidians tunic gives new insights on host-microbe interactions by revealing diverse antimicrobial peptides. *Mar. Drugs* **2020,** 18, (7), 362.

219. Merkler, D. J., C-Terminal amidated peptides: Production by the *in vitro* enzymatic amidation of glycine-extended peptides and the importance of the amide to bioactivity. *Enzyme Microb. Tech.* **1994,** 16, (6), 450-456.

220. Mains, R. E.; Blaby-Haas, C.; Rheaume, B. A.; Eipper, B. A., Changes in corticotrope gene expression upon increased expression of peptidylglycine α-amidating monooxygenase. *Endocrinology* **2018,** 159, (7), 2621-2639.

Paper I

Article

Isolation and Characterization of Antimicrobial Peptides with Unusual Disulfide Connectivity from the Colonial Ascidian *Synoicum turgens*

Ida K. Ø. Hansen [1,*] [ID], **Johan Isaksson** [2] [ID], **Aaron G. Poth** [3] [ID], **Kine Ø. Hansen** [4] [ID], **Aaron J. C. Andersen** [1] [ID], **Céline S. M. Richard** [1], **Hans-Matti Blencke** [1], **Klara Stensvåg** [1], **David J. Craik** [3] and **Tor Haug** [1,*]

[1] Norwegian College of Fishery Science, Faculty of Biosciences, Fisheries and Economics, UiT The Arctic University of Norway, Breivika, N-9037 Tromsø, Norway; aaron.j.andersen@uit.no (A.J.C.A.); celine.s.richard@uit.no (C.S.M.R.); hans-matti.blencke@uit.no (H.-M.B.); klara.stensvag@uit.no (K.S.)

[2] Department of Chemistry, UiT The Arctic University of Norway, Breivika, N-9037 Tromsø, Norway; johan.isaksson@uit.no

[3] Institute for Molecular Bioscience, The University of Queensland, Brisbane 4072, Queensland, Australia; a.poth@imb.uq.edu.au (A.G.P.); d.craik@imb.uq.edu.au (D.J.C.)

[4] Marbio, UiT The Arctic University of Norway, Breivika, N-9037, Tromsø, Norway; kine.o.hanssen@uit.no

[*] Correspondence: ida.k.hansen@uit.no (I.K.Ø.H.); tor.haug@uit.no (T.H.); Tel.: +47-77-64-92-66 (I.K.Ø.H.); +47-77-64-60-71 (T.H.)

Abstract: This study reports the isolation of two novel cysteine-rich antibacterial peptides, turgencin A and turgencin B, along with their oxidized derivatives, from the Arctic marine colonial ascidian *Synoicum turgens*. The peptides are post-translationally modified, containing six cysteines with an unusual disulfide connectivity of Cys^1-Cys^6, Cys^2-Cys^5, and Cys^3-Cys^4 and an amidated C-terminus. Furthermore, the peptides contain methionine residues resulting in the isolation of peptides with different degrees of oxidation. The most potent peptide, turgencin A_{Mox1} with one oxidized methionine, displayed antimicrobial activity against both Gram-negative and Gram-positive bacteria with a minimum inhibitory concentration (MIC) as low as 0.4 μM against selected bacterial strains. In addition, the peptide inhibited the growth of the melanoma cancer cell line A2058 (IC_{50} = 1.4 μM) and the human fibroblast cell line MRC-5 (IC_{50} = 4.8 μM). The results from this study show that natural peptides isolated from marine tunicates have the potential to be promising drug leads.

Keywords: marine; ascidian; peptide; antimicrobial; methionine oxidation

1. Introduction

The emergence of pathogenic microorganisms' resistance to conventional antibiotics has become a serious medical concern [1]. This natural microbial adaptation strategy [2] has been provoked by selective pressure exerted by extensive inappropriate use of antimicrobial agents, both for medical and non-medical purposes [3]. Diminished efforts in the development of novel antimicrobials by the pharmaceutical industry have further aggravated this problem [4,5]. Renewed efforts in the search for novel forms of antimicrobial treatments are now seen. Endogenous antimicrobial peptides (AMPs) are considered exciting candidates to address this challenge due to their innate properties of broad antimicrobial spectra, highly selective toxicities, and the increased difficulty for microbes in developing resistance towards them compared to conventional small molecule antimicrobial agents [6].

AMPs (also called host defense peptides, HDPs) are ancient effector molecules of the innate defense system, and are present in every life form [7,8]. Their evolutionary conservation among eukaryotes highlights their importance in the first-line of defense against invading pathogens [9]. They generally consist of 10 to 50 amino acids, have an amphiphilic three-dimensional structure and a net positive charge at physiological pH [7]. AMPs are arranged into highly heterogeneous structures [6], grouped into linear α-helical peptides, β-sheets stabilized by intramolecular disulfide bridges, and extended structures [10]. Unlike conventional antibiotics, which typically target specific cellular pathways necessary for microbial survival or reproduction [11], it is widely accepted that most AMPs exert their effect by targeting and destabilizing the lipopolysaccharide layer of the cell membrane, which is ubiquitous in microorganisms. The cationic AMP portion targets the anionic microbial membrane through unspecific electrostatic interaction. This is followed by membrane embedding of the hydrophobic portion, causing membrane disruption and cell death [12–14]. This non-specific targeting of an essential microbial component lowers the chance of resistance development towards AMPs, for which the bacteria need to change the entire membrane lipid composition, a costly solution for most microbes [9]. In addition, AMPs at large do not react with the lipophilic outer leaflet of mammalian cell membranes, hence their low tendency to be toxic towards human cells [15]. However, AMPs with antitumor activities have also been isolated [16].

The oceans cover 71% of the earth's surface and comprise 50–80% of the total global biodiversity [17]. Many marine invertebrates are sessile and soft bodied, lacking the sophisticated adaptable immune systems seen in vertebrates. Despite this, these organisms thrive, suggesting that their innate immune systems are effective and robust. It is now known that this apparent contradiction can be explained by the activities exerted by AMPs [18]. Compared to terrestrial AMPs, marine-derived AMPs are often adapted to high salt concentration conditions, enabling them to form stronger electrostatic interactions with bacterial membranes, thus making marine-derived AMPs more potent [19,20]. AMPs have been found in a wide range of marine invertebrates, including mollusks [21], crustaceans [22], sponges [23], and cnidarians [24]. A number of α-helical AMPs have also been isolated from a number of ascidians (belonging to the subphylum *Urochordata*, bearing all the chordate hallmarks in its larval form), including the phenylalanine-rich styelins and the histidine-rich clavanins from *Styleaclava* [25,26] and halocynthin and papillosin from *Halocynthia papillosa* [27]. Furthermore, two cysteine-containing α-helical AMPs have been isolated from *H. aurantium*: the homodimer dicynthaurin [28] and the heterodimer halocidin [29].

As part of our ongoing search for new compounds with antimicrobial activity from marine invertebrates, the aqueous extract of the colonial ascidian *Synoicum turgens* was examined for its content of AMPs. *Synoicum* species have previously awarded several bioactive secondary metabolites, including the cytotoxic palmerolide macrolides [30,31], the β-carboline guanidine alkaloid tiruchanduramine with α-glucosidase inhibitory activity [32,33], and the synoxazolidinones and pulmonarines with various bioactivities from *S. pulmonaria* [34–37]. To the best of our knowledge, no AMPs have been isolated and characterized from *Synoicum* species.

In the present study, we isolated, purified and characterized four novel AMPs, named turgencin A$_{Mox1}$, turgencin B, turgencin B$_{Mox1}$, and turgencin B$_{Mox2}$ from the Arctic ascidian *S. turgens*. The peptides were screened for antimicrobial activity against both Gram-negative and Gram-positive bacterial strains, and for cytotoxic activities against selected human cell lines. The goal of this study was to find new peptides with a potential for treating microbial infections.

2. Results and Discussion

2.1. Peptide Purification and Mass Spectrometry Analysis

Solvent extraction of the *S. turgens* specimens using 60% (v/v) acetonitrile (MeCN) at low temperature produced two liquid phases, an MeCN-rich organic phase and a salt-rich aqueous phase. This separation is caused by the high salt content within marine samples, which is immiscible with

MeCN at low temperature [38]. Salt was subsequently removed from the aqueous extract using solid phase extraction (SPE), yielding eluates with compounds of varying polarity. Antimicrobial screening of the SPE eluates and the organic extract revealed that the 40 and 80% MeCN SPE eluates displayed the highest antibacterial activity (Table S1 in the SI). The 80% MeCN SPE eluate was further fractionated by preparative reversed-phase high performance liquid chromatography (RP-HPLC), guided by a diode array detector (DAD) measuring UV-vis absorption at 220 and 280 nm. The obtained fractions were tested for antibacterial activity and the active fractions were analyzed by ultra-high performance liquid chromatography coupled to a quadrupole time-of-flight mass spectrometer (UHPLC-QTOF-MS). Several HPLC fractions displayed antibacterial activity and four bioactive peptides were extensively purified by RP-HPLC (Figure 1). The four peptides were also shown to be present in the 40% MeCN SPE eluate, but in lower quantities (data not shown). The peptides were present in all *S. turgens* samples regardless of where and when the biomass was collected.
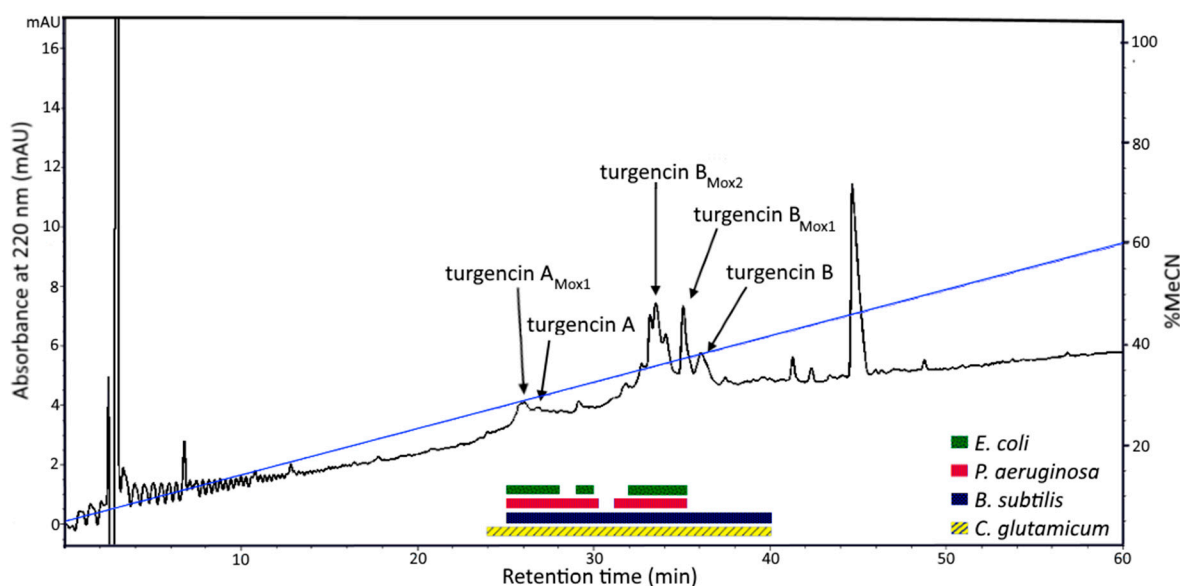
Figure 1. Preparative RP-HPLC-DAD spectrum at 220 nm of the 80% MeCN SPE eluate of *S. turgens*. HPLC fractions displaying antibacterial activity are shown in boxes below the chromatogram and peak fractions containing antibacterial peptides are marked with arrows. The blue line shows the linear gradient (5-60%) of acetonitrile (MeCN) dissolved with 0.1% formic acid (FA). Note: RP— reversed-phase; HPLC—high performance liquid chromatography; DAD—diode array detector; SPE—solid phase extraction.

The four isolated peptides (turgencin A_{Mox1}, turgencin B, turgencin B_{Mox1}, turgencin B_{Mox2}) were analyzed by UHPLC-QToF-MS to determine their monoisotopic molecular masses and isotope patterns, and to provide fragmentation ions in tandem mass spectrometry (MS/MS) (Figure S1 in the SI). This analysis resulted in the determination of monoisotopic masses of 3705.79, 3538.58, 3554.58, and 3570.58 Da, for turgencin A_{Mox1}, turgencin B, turgencin B_{Mox1}, turgencin B_{Mox2}, respectively (Table S2 in the SI).

2.2. Sequence Analysis

The peptides turgencin A_{Mox1} and turgencin B_{Mox2} were subjected to reduction/alkylation and N-terminal Edman degradation sequencing. A partial N-terminal sequence (34 residues: GPKTKAACKMACKLATCGKKPGGWKCKLCELGCD) was obtained for turgencin A_{Mox1}. The calculated monoisotopic mass of this sequence (3520.68 Da, assuming three disulfide bridges) was determined to be 185.11 Da less than the measured monoisotopic mass, indicating a missing dipeptide C-terminally. Reduction and alkylation with iodoacetamide, followed by enzymatic

digestion with Glu-C, RP-HPLC, and Edman degradation sequencing of selected HPLC fractions produced the fragment LGCDAV, which represents the C-terminal sequence from position 31 to 36. MS analysis proved this fragment (*m/z* 633.29, corresponding to $[M+H]^+$ and containing one carboxyamidomethylcysteine) to be amidated C-terminally. The monoisotopic mass of the 36-residue sequence (3689.80 Da, assuming three disulfide bridges and a C-terminally amidated valine) was determined to be 16 Da above the measured monoisotopic mass. This can be explained by an oxidized methionine (Met-ox) residue in position 10 (+15.9949 amu for monoisotopic oxygen). Extracted ion chromatograms of the SPE eluates proved the presence of a peptide with a monoisotopic mass of 3689.80 Da, also indicating the presence of the non-oxidized version of the peptide, turgencin A. By comparing MS/MS data of turgencin A and turgencin A_{Mox1}, in addition to the mass difference of 16 Da between them, it could be concluded that turgencin A is the non-oxidized version of turgencin A_{Mox1} (Figure S2 in the SI).

Edman degradation analysis of turgencin B_{Mox2} produced a 35 residue N-terminal sequence (GIKEMLCNMACAQTVCKKSGGPLCDTCQAACKALG) containing six cysteines and two methionine residues. The calculated monoisotopic mass of this sequence (3539.61 Da, assuming three disulfide bridges) was 30.96 Da greater than the measured monoisotopic mass. This can be explained by two Met-ox residues (+31.99 Da) and a C-terminally amidated glycine (−0.98 Da). MS/MS analysis of turgencin B and turgencin B_{Mox1} confirmed that these peptides are non-oxidized and mono-oxidized variants of turgencin B, respectively. The analysis also showed that the mono-oxidized peptide was mainly oxidized at the methionine residue in position 5 (Figure S3 in the SI).

The retention times of both turgencin A, turgencin B, and their oxidized derivatives also correspond with their oxidation states (Figure S4 in the SI), as oxidation of methionine has been shown to decrease peptide retention time in RP-HPLC [39].

Although the primary sequence and peptide length differ between the two mature peptides (Figure 2), there are some similarities. Both peptides contain six cysteine residues with the same cysteine pattern (C-C-C-C-C-C, i.e. no adjacent cysteines) and two identical sequence motifs (CXMAC and KKXGG), indicating identical cysteine connectivity. The peptides are both C-terminally amidated, and cationic with isoelectric points (pI) of 9.24 (turgencin A) and 8.33 (turgencin B). The peptides were not identified to belong to any of the 45 major AMP families present in $CAMP_{R3}$ database using the CAMPSign tool [40]. Furthermore, the basic local alignment search tool (BLAST) and homology searches of the oligopeptide sequences resulted in no overall sequence similarity to other known peptides or proteins. The peptides were therefore considered as novel antimicrobial peptides and named turgencins after the species from which they were isolated.

```
Turgencin A       G P K T K  AA C K M  A C K L A T C G K K P G G W K C K L C E L G C D A V  –NH₂
Turgencin A_Mox1  G P K T K  AA C K Mₒ A C K L A T C G K K P G G W K C K L C E L G C D A V  –NH₂
Turgencin B       G I K E M  L _ C N M A C A Q T V C _ K K S G G P L C D T C Q A A C K A L  G–NH₂
Turgencin B_Mox1  G I K E Mₒ L _ C N M A C A Q T V C _ K K S G G P L C D T C Q A A C K A L  G–NH₂
Turgencin B_Mox2  G I K E Mₒ L _ C N Mₒ A C A Q T V C _ K K S G G P L C D T C Q A A C K A L  G–NH₂
```

Figure 2. Sequence alignment of turgencin A and B, and their oxidized derivatives. Gaps (_) are introduced to maximize the alignment. Cysteine residues are marked in bold, oxidized methionine residues are marked with M_o, and identical amino acids are shaded in grey.

Peptides with Met-ox residues (+16/32 Da) could be observed both with MS/MS and nuclear magnetic resonance (NMR) spectroscopy. Although the HPLC chromatograms indicated that the peptides could easily be separated, it proved difficult to separate the oxidized forms of the peptides from the non-oxidized forms. This is probably due to oxidation occurring in the different purification steps, which was to a degree unavoidable. Such oxidation is a common problem in methionine containing peptides [41]. NMR analysis of the purified peptide fractions revealed that turgencin A_{Mox1} contained 28% turgencin A_{Mox0}, turgencin B contained 29% turgencin B_{Mox1} and 4% turgencin B_{Mox2}, turgencin B_{Mox1} contained 10% turgencin B_{Mox2} and 2% turegncin B_{Mox0}, and turgencin B_{Mox2}

contained 3% turgencin B_{Mox1}.Turgencin A was not isolated in sufficient amounts for purity analysis using NMR. MS/MS data analyzed over time of the purified peptide showed small changes of the different oxidation states (data not shown). Despite this temporal variation, samples were purified in sufficient amounts for structural determination and peptide sequencing. The variation of methionine oxidation was greater in turgencin B due to the presence of two methionine residues in its sequence, resulting in potentially two possible peptide variants having one Met-ox residue. Tandem MS analysis of turgencin B_{Mox1} indicates that the first methionine is preferentially oxidized, with an absence of a b5 ion for the GIKEM ion at *m/z* 559.29, and a significant signal at *m/z* 575.28 corresponding to the b5 for $GIKEM_o$ (Figure S3 in the SI). This preference for oxidation at position 5 is likely due to steric effects as the position of the methionine in position 9 was revealed by NMR to be protected within the peptide structure, compared to the more exposed methionine in position 5.

Methionine residues in peptides are highly susceptible to oxidation even by mild oxidants [42]. This causes a change in the polarity of the amino acid residue, from non-polar to polar, a shift expected to have profound structural and functional consequences [43]. This reaction is known to take place in vivo and to occur during the process of sample preparation and peptide isolation [44]. Whether oxidation of the methionines of turgencin A and B is actively catalyzed by the enzymatic machinery of *S. turgens* is unknown. However, as the herein reported peptides were dissolved in water as part of the isolation process and exposure to air during the drying processes, it is hypothesized that the majority of the peptide fractions with oxidized methionine residues are formed as a result of sample handling. Turgencin A_{Mox1}, turgencin B_{Mox1}, and turgencin B_{Mox2} are thus believed to be oxidized artefacts of their corresponding unoxidized parent peptides (turgencin A and turgencin B).

2.3. Structure Determination

Two-dimensional NMR data was collected for turgencin A_{Mox1},turgencin B, turgencin B_{Mox1}, and turgencin B_{Mox2} in 90:10 H_2O/D_2O.

Turgencin A_{Mox1} forms a folded structure in water, resulting in a dispersed ^{15}N-HSQC spectrum (Figure S5 in the SI). The resonance dispersion is however less pronounced than for turgencin B (compare Figure S6 in the SI), which appears to have a significant amount of random coil character. The peptide sequence is also significantly less varied than the sequence of turgencin B. For example, seven out of 36 amino acids are lysine. This results in increased spectral overlap, making structural correlations more difficult to deduce unambiguously. The chemical shift assignments were successfully assigned using ^{15}N-^1H and ^{13}C-^1H HSQC, HMBC, TOCSY and HSQC-TOCSY spectra. The sequential assignment was completed through NOE-hopping supported by high-resolution HMBC of the carbonyl region in the carbon dimension where possible (Tables S3 and S4 in the SI). Based on the chemical shift assignments, the protein backbone dihedral angle prediction program TALOS+ was used to predict the secondary structure, resulting in all residues being predicted to be in an unfolded conformation. A quick assessment of the assignable NOE correlations revealed that there were very few structurally important long-range contacts in turgencin A_{Mox1} to base a structure calculation on. For these reasons a full structure determination was not further pursued.

All turgencin B fractions produced near-identical, well-dispersed natural abundance ^{15}N-HSQCs, indicating that they share largely common folded structures that are not substantially affected by the varying numbers of methionine sulfoxides. The turgencin B_{Mox2} data set was the purest fraction of the turgencin B samples and was therefore selected for further structural studies (Figure S6 in the SI). The peptide backbone and side chains were successfully assigned using the same procedure as described above for turgencin A_{Mox1} (Tables S5 and S6 in the SI). The sequential NOESY correlations are summarized in Figure 3.
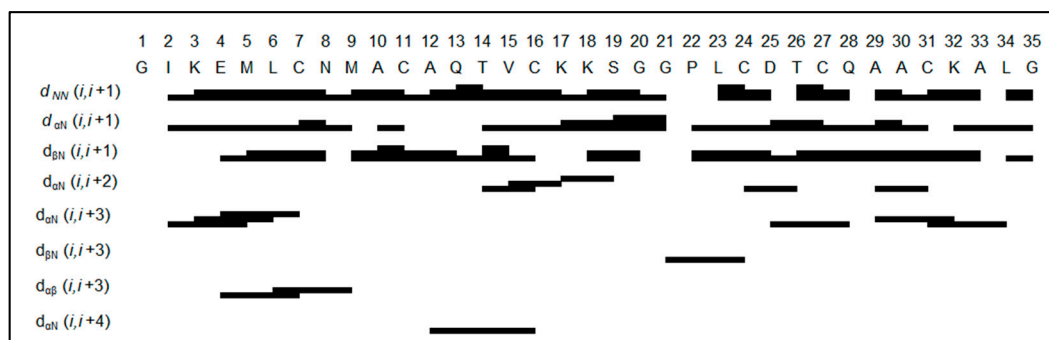
Figure 3. Summary of the sequential NOESY correlations of turgencin B$_{Mox2}$. A total of 69 through-space correlations between neighboring, or near-neighboring, residues were extracted from NOESY experiments using 100, 200, and 300 ms mixing times. The line width in the figure corresponds to the strength of the correlation: the thicker the line, the stronger the NOE. For 'i, i+2' and longer range correlations, the lines indicate residue pairs displaying inter-residue correlations.

In total, 108 sequential and 84 long range NOEs were assigned, integrated and classified as strong, medium or weak, applying upper-limit constraints of 2.5, 3.7 and 5.0 Å respectively. Out of these, 16 directly involved alpha- or beta protons of cysteines, which are of extra importance for determining the cysteine connectivity of the peptide. The NOE patterns with relatively strong NN(i,i+1) correlations compared to αN(i,i+1) suggest some helical character, especially when αN(i,i+3) is also detectable. However, there is no long stretch of pronounced alpha helix indicated from the NOE pattern, and, in terms of absolute intensity of the NN(i,i+1) correlations relative to the reference correlations, the helix secondary structure is populated but not a stable fold of the peptide.

TALOS+ was used to predict the secondary structure from the secondary chemical shifts relative to the random coil shifts, using H, NH, CA, CB and CO as input, resulting in a predicted loop-type fold for all residues (Figure S7 in the SI). It should be noted here that the cysteines are relatively evenly distributed in the sequence, and being oxidized their chemical shifts will be different from reduced cysteines. The influence of the disulfide bonds on the quality of the TALOS+ predictions, which is based on the secondary chemical shifts, is unknown to us. The absence of stretches of clear secondary structure was supported by the majority of residues that could be measured [45,46] with $^3J_{HNHa}$ between 6.0 and 7.5 Hz, which is an indication of conformational averaging between ~4 Hz couplings from θ of -60° (alpha helix) and ~9 Hz from θ in (−120)–(−140)° (beta sheet) (Figure S8 in the SI). All couplings belonging to the stretch of residues between 5 and 12 could only be measured with the TOCSY line width method [45] owing to the structural heterogeneity from the methionine oxidation isomers in combination with the anti-phase pattern of the DQF/E.COSY cross-peaks resulting in severe cancellation. For these reasons, phi and psi dihedral angles were not restrained in the structural calculations, and NOE contacts were treated conservatively with loose restraints to allow conformational flexibility.

To establish the disulfide connectivity pattern by NMR, a preliminary 3D structure was calculated without defining any disulfide bonds. Three iterations of simulated annealing and constraint refinement were performed using an extended starting structure with all cysteines in the reduced form. Out of 100 calculated structures, the 10 lowest energy structures were analyzed for inter-cysteine distances. The ensemble is shown in Figure 4a,b. In the ensemble, the average distances from each cysteine sulfur to every other cysteine sulfur was extracted, indicating a C1-C6/C2-C5/C3-C4 disulfide pattern (Figure 4c).
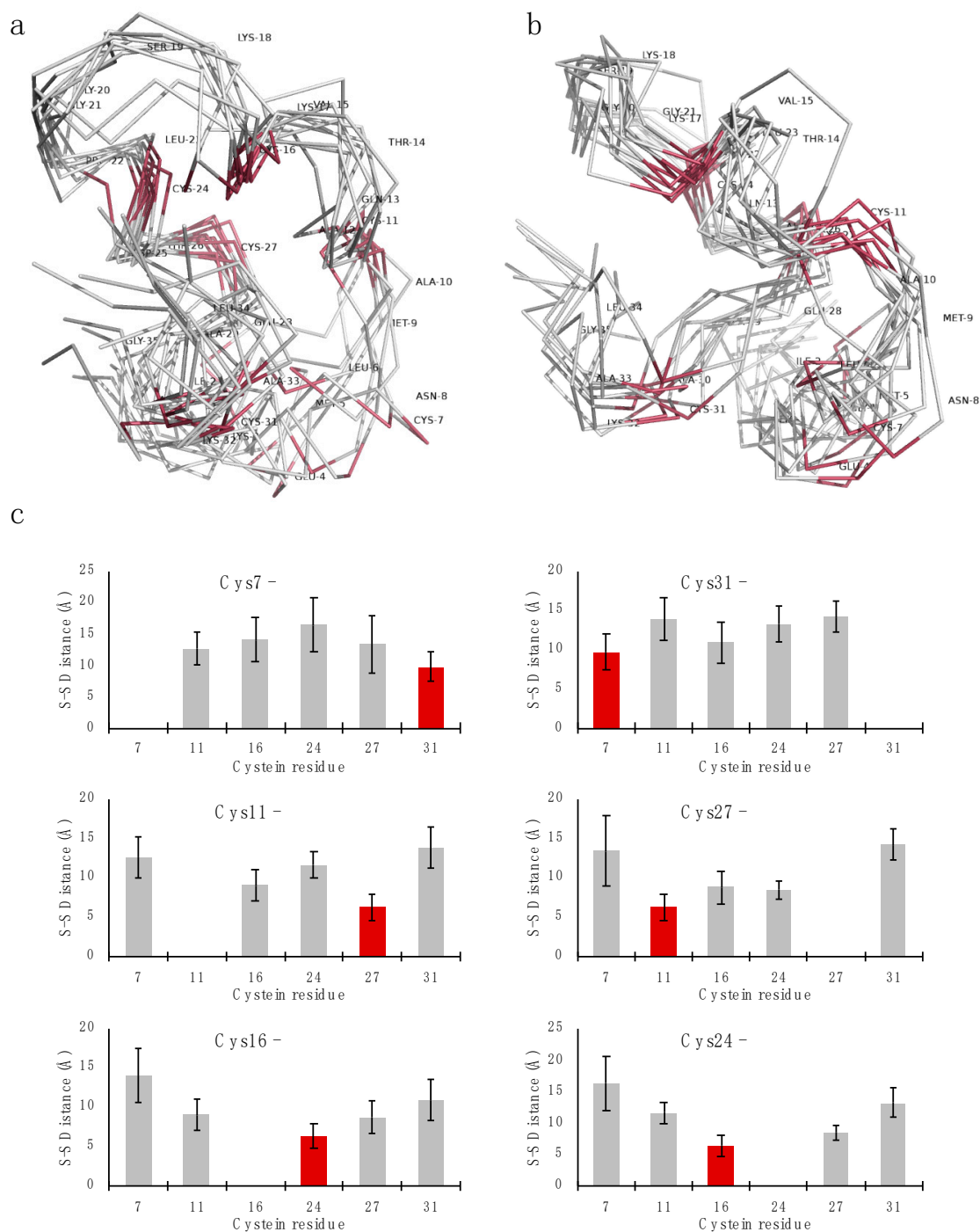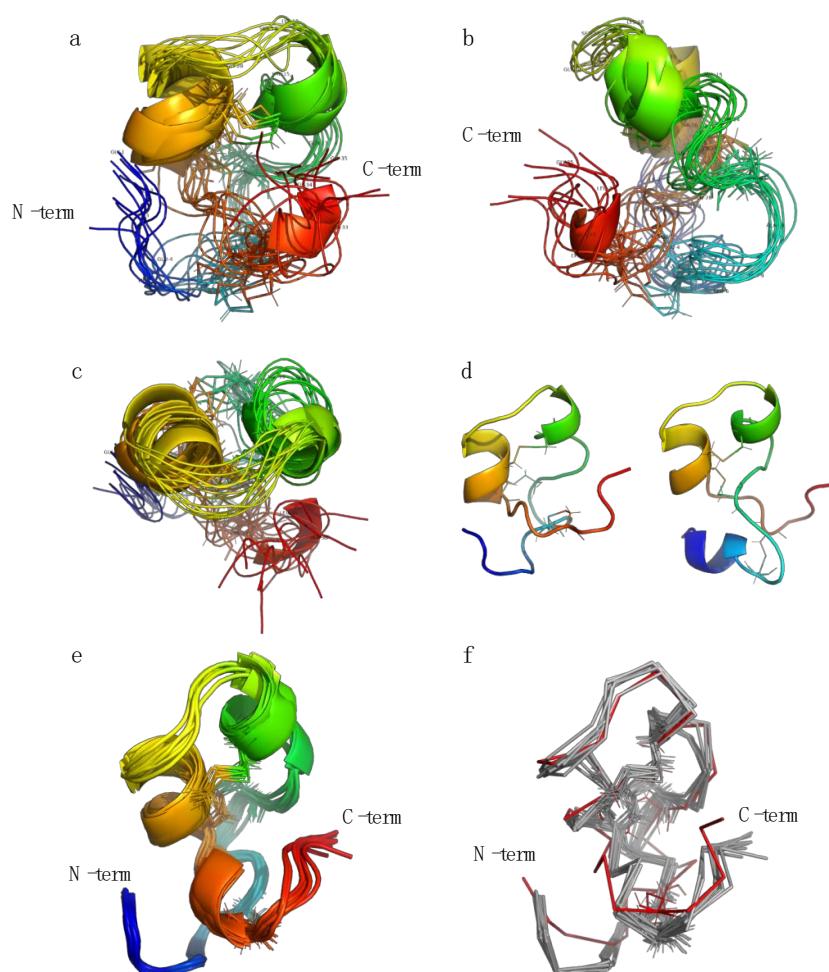
Figure 4. Lowest-energy structure ensembles and average inter-cysteine distances for turgencin B$_{\text{Mox2}}$. Panels (**a**) and (**b**) show two views of the 10 lowest energy structure ensembles from simulated annealing with reduced disulfide bonds. Panel (**c**) plots illustrate the average distances from each cysteine sulfur to every other cysteine sulfur, indicating a C1-C6/C2-C5/C3-C4 disulfide pattern, as highlighted with red bars.

The disulfide connectivity determined as above was introduced into the structure refinement and the most important stereospecific methyl assignments (valine and leucine) were resolved using the computed structures iteratively. Owing to the intrinsic heterogeneity of the data due to the epimeric oxidized methionines (resulting in four configurational isomers from the combined M5 and M9 chiralities) together with the conformational dynamics, further structural refinement was not pursued

past this point. A production run of 500 structures of the main disulfide pattern was calculated using the same simulated annealing protocol, using the best structure with reduced cysteines as starting structure. Several other disulfide connectivity patterns were evaluated in test calculations in terms of energies and evaluated in Figure S9 in the SI. As a more extensive control calculation, 500 structures of the most viable alternative pattern were also calculated using the final production constraints, resulting in overall less-favorable energies (Figure S10 in the SI).

Evaluation of the lowest energy structures revealed two major clusters of conformations, each having distinct folds at their termini and also affecting the outer disulfide bond. The major conformation (~75%) resides in a counter-clockwise twist while the minor conformation (~25%) is in a clockwise twist. Energetically there is no significant difference between the clusters. The 10 lowest energy structures of the major conformation are presented in Figure 5. A comparison overview of the two conformations is presented in Figure 5d.

Figure 5. The 10 lowest energy structure ensembles of the major turgencin B_{Mox2} conformers produced by the simulated annealing protocol using the C1-C6/C2-C5/C3-C4 disulfide pattern. Panel (**a**) illustrates the front view, (**b**) side view and (**c**) top view. In panel (**d**) the major conformation (left) is aligned with the minor conformation (right) to illustrate the difference between terminal folds. In the displayed scene the C-terminus folds on top of the N-terminus in the major conformation as opposed to the minor conformation in which the C-terminus is behind the N-terminus. Panel (**e**) shows one representative low energy nuclear magnetic resonance (NMR) structure subjected to 10 ns free molecular dynamics in explicit water and panel (**f**) illustrates a comparison between the NMR structure and the molecular dynamics (MD) structures: in both cases extracted from the final nanosecond of the simulation.

Structural analysis of the fold reveals that even without constraining any backbone dihedrals, there is a clear tendency to adopt an alpha helix fold for residues 15-18 and 23-27, driven by the NOE constraints alone. These residues do indeed have stronger NOE cross peaks from NH(n) to NH(n-1) than NH(n) to HA(n-1), which is characteristic for alpha helix secondary structure motifs. In many calculated structures there is a helix-like character of various parts of the N-terminal stretch from residue 6-14, and of the C-terminal stretch from 27-31. We interpret this as being a helix fold that is accessible and populated by the peptide in water, but also one that is unstable. Speculatively, the helix fold may very well be an active form that is stabilized by interactions with lipid membranes or other co-factors present in its native environment.

To ensure that the NMR structure was not overly constrained into an unfavorable conformation by the experimental constraints, one representative low energy structure was subjected to an unconstrained 10 ns molecular dynamics (MD) simulation in explicit water, monitoring the energies, conformation and fluctuations. The structure was not significantly different from its starting point and the core residues (defined as residues 6-32, thus ignoring the free termini) stabilized at approximately 1.5 Å backbone rmsd compared to the starting structure (Figure 5e–f and Figures S11 and S12 in the SI). It is noteworthy that the free simulations reinforced the helical character of the peptide rather than unfolding the NMR structure.

To further support the disulfide connectivity of turgencin B as determined by NMR, we attempted to solve it through partial reduction and alkylation, followed by analysis with LC-MS/MS. This however proved to be challenging as the herein used protocol rendered the peptide intact or with all disulfide bridges reduced regardless of incubation conditions evaluated, including varying temperature and length of exposure to the reducing agent.

The disulfide connectivity of the turgencins (C1-C6/C2-C5/C3-C4) is different from the well-characterized human α-defensins (C1-C6/C2-C4/C3-C5) and β-defensins (C1-C5/C2-C4/C3-C6) [47]. However, the overall structural motif of a C1-C6/C2-C5/C3-C4 disulfide linked peptide forming a helix-loop-helix-like structure has been previously observed in peptides from plants, like the viscotoxins from mistletoe [48,49] and crambin from the annual oil seed plant *Crambe abyssinica* [50–52]. These, as well as other previously reported C1-C6/C2-C5/C3-C4 peptides, like beta-defensin-like structures from Chinese sea turtles [53,54], typically have two adjacent cysteines involved in separate disulfide bridges and a stabilizing separate structural motif. Turgencin B does however have more evenly distributed cysteines where the C3-C4 pair stabilized the loop and the C2-C5 pair stabilizes the putative helices at the other end. The outermost C1-C6 pair does not have any obvious structural role other than stabilizing the ends. The role of the outermost disulfide bridge, as well as a more stable fold, might be revealed when the peptide interacts with a lipid bilayer or a co-factor. Structurally, turgencin B is not closely related to previously published peptides with the same cysteine patterns (listed in Table S7), but there are some overarching similarities, primarily to the viscotoxins, which are lysine-rich (and hence positively charged) and share the helix-loop-helix motif. However, the evolutionary relationship between the turgencins and other AMPs can only be fully revealed after characterization of their genes. Unfortunately, our attempts to construct a cDNA library have not yet been successful, probably due to degraded RNA (access only to frozen material).

2.4. Biological Activity

All isolated peptides showed antibacterial activity but to differing degrees (Table 1), with turgencin A_{Mox1} being the most potent peptide. The minimum inhibitory concentrations (MICs) of turgencin A_{Mox1} against *Corynebacterium glutamicum* and *Bacillus subtilis* were as low as 0.4 μM, and the MIC against *Escherichia coli* was 0.8 μM. In addition, turgencin A_{Mox1} affected eukaryotic cell viability, exhibiting an IC_{50} value against the human melanoma cancer cell line A2058 of 1.4 μM, and an IC_{50} against the non-malignant human fibroblast cell line MRC-5 of 4.8 μM. These results show that turgencin A_{Mox1} is cytotoxic, but the MIC against the most sensitive bacteria is still 12 times lower than the IC_{50} against the non-malignant cell line.

Table 1. Antimicrobial and cytotoxic activity of the isolated turgencins.

Peptide	Antimicrobial Activity (MIC; μM)					Cytotoxic Activity (IC$_{50}$; μM)	
	C. g.	*B. s.*	*S. a.*	*E. c.*	*P. a.*	A2058	MRC-5
Turgencin A$_{Mox1}$ (72% Mox1, 28% Mox0)	0.4	0.4	6.3	0.8	1.6	1.4	4.8
Turgencin B (67% Mox0, 29% Mox1, 4% Mox2)	1.6	1.6	>100.0	12.5	25.0	4.1	7.5
Turgencin B$_{Mox1}$ (88% Mox1, 10% Mox2, 2% Mox0)	1.6	3.1	>100.0	25.0	>100.0	27.4	>50.0
Turgencin B$_{Mox2}$ (97% Mox2, 3% Mox1)	25.0	25.0	>100.0	>100.0	>100.0	>50.0	>50.0

C.g.—Corynebacterium glutamicum, B.s.—Bacillus subtilis, S.a.—Staphylococcus aureus, E.c.—Escherichia coli, P.a.—Pseudomonas aeruginosa, A2058—Human melanoma cancer cell line and MRC-5—Non-malignant human fibroblast cell line.

The bioactivities of turgencin B and the two oxidized analogues (turgencin B$_{Mox1}$ and turgencin B$_{Mox2}$) vary depending on the total number and positions of the oxidations. It was found that there was an inverse relationship between the numbers of methionine sulfoxides harbored by the turgencins and their respective bioactivities, a common feature among peptides with methionine oxidation [55]. According to NMR analysis, methionine oxidation did not cause significant changes in the conformation of the peptides. Methionine oxidation changes the polarity of this amino acid residue from non-polar to polar. The observed reduction in bioactivity in the oxidized variants of turgencin B compared to turgencin B$_{Mox0}$ may be caused by a break in the lipophilic section of the peptide, resulting in insufficient affinity for the lipophilic portion of the bacterial and mammalian cell envelope, consequently reducing the antibacterial and cytotoxic effects of the oxidized variants. Despite this inverse relationship, when comparing antimicrobial activity and cell viability it might be argued that turgencin B$_{Mox1}$, with one Met-ox, might be a better drug-lead candidate than the unoxidized turgencin B. Even though the antibacterial effect of turgencin B$_{Mox1}$ is slightly lower than that of turgencin B, turgencin B$_{Mox1}$ did not affect the non-malignant cell line at the highest concentration tested (50 μM). With both methionines oxidized, as in turgencin B$_{Mox2}$, the MICs across all cell lines were considerably higher. The un-oxidized turgencin A might therefore be even more potent than turgencin A$_{Mox1}$, which has one Met-ox. Unfortunately, only minor amounts of turgencin A were observed during liquid chromatography-mass spectrometry (LC-MS) analysis (Figure S2), and the peptide could therefore not be isolated in sufficient quantities to allow for assessment of its bioactivities. These changes in bioactivity indicate that peptides containing methionine may be poor drug candidates. Niederhafner et al. [55] replaced methionine with norleucine in the peptide melectin and improved its antimicrobial activity, but it also increased the cytotoxic activity towards red blood cells from rats. Thus, although it is outside the scope of the current study, future work should investigate whether analogues without methionines exhibit improved bioactivity profiles.

2.5. Real-time Measurement of Immediate Effect on Membrane Integrity and Viability

Bacterial biosensors (*B. subtilis* and *E. coli*, both carrying the pCSS962 plasmid with the LucGR gene) were used to assess the immediate membrane disruptive properties of turgencin A$_{Mox1}$ and turgencin B. The strains express eukaryotic luciferase and will emit a luminescence peak if their membranes are disrupted and externally added D-luciferin is allowed to diffuse into the cell [56]. The luminescence measurements of *B. subtilis* after exposure to turgencins or chlorhexidine are shown in Figure 6. Both peptides affected the bacterial membrane integrity of *B. subtilis*. Although no increase in light emission was observed, except for chlorhexidine, a decrease in light intensity was observed for both peptides. Exposure to the natural peptide turgencin A$_{Mox1}$ (Figure 6) decreased luminescence by ~50% after 1 minute at a concentration of 50 μM (corresponding to 125 × MIC). Turgencin B exposure reduced light emission even more profoundly and much faster. Within 10 s of the addition of the peptide at a concentration of 50 μM, bacterial luminescence was reduced by 97%. Additionally, the

effect was clearly dose dependent. At concentrations above 6.25 μM (4 × MIC) turgencin B reduced relative luminescence by more than 50% within 1 minute (Figure 6). For fast-acting membrane active substances, it was not possible to resolve the initial peak in light emission as the lag time between addition of the cells to the analyte and first plate reading is approximately 10 s due to constraints of the plate reader. Therefore, only the subsequent drop below background luminescence could be observed. Our results indicate that addition of the peptide elicits a rapid effect on cell viability. None of the peptides displayed any pronounced effect on the membrane of *E. coli*; only a weak effect of turgencin B at 50 μM (4 × MIC) concentration was observed (data not shown). Chlorhexidine, an antiseptic agent known for its membrane-disruptive properties [57], produced an immediate increase in luminescence (caused by an increased influx of D-luciferin into the cells) and subsequently a decrease at concentrations of 12.5 μM and above (Figure 6).
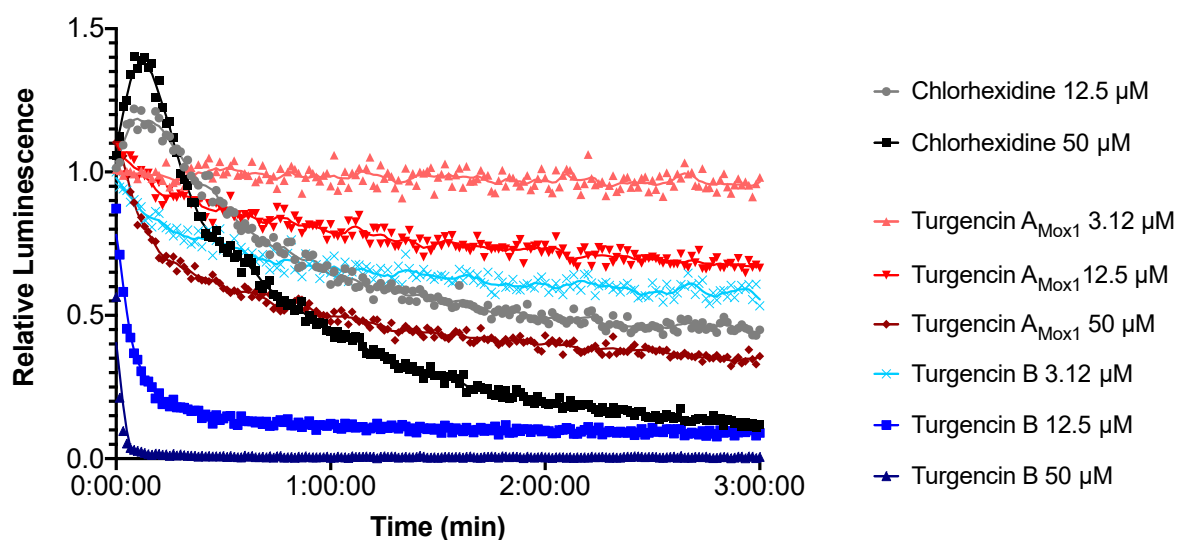
Figure 6. Kinetics of the antimicrobial effect on membrane integrity as measured by relative luminescence emission in *B. subtilis* (pCSS962). Cells were treated with turgencin A_{Mox1} (shades of red), turgencin B (shades of blue) or chlorhexidine. Each data point is the mean of three independent measurements normalized to the water negative control. Chlorhexidine was used as positive control and its addition in the assay elicited an initial peak in luminescence followed by a rapid drop below the background typical of membrane active substances. Turgencin A_{Mox1} reduced light emission at concentrations above 12.5 μM while turgencin B reduces light emission more efficiently and at concentrations of 3.12 μM and above. Note that the starting point depicts the start of luminescence measurement, not the combination of cells and analyte, which occurs approximately 10 s prior.

In order to independently confirm the bactericidal effect observed in the membrane integrity assays, real-time cell viability assay was performed using bacterial biosensors carrying either a chromosomally integrated (*B. subtilis* 168) or a plasmid-borne (*E. coli* K12) *lux* operon. Both strains express a bacterial luciferase and fatty acid reductases for regeneration of long-chain fatty aldehydes, which serve as substrates for light production. Light production is therefore linked to several metabolic processes, which in turn depend on the regeneration of reduction equivalents and adenosine triphosphate (ATP) [58,59]. While light production indicates active metabolism, loss of light production indicates a decrease in metabolic activity, and hence, reduced viability of the cells.

The immediate effect of turgencins on the viability of *B. subtilis* is presented in Figure 7. The results show that they both affect the viability of the Gram-positive strain within the assay period. Turgencin A_{Mox1} and turgencin B caused more than a 50% decrease in light production after 3 min of incubation at concentrations above 25 μM (12.5 × MIC) and 6.25 μM (4 × MIC), respectively. Furthermore, the observed effect was dose-dependent, with decreased light production observed at higher concentrations. Chlorhexidine treatment caused >50% reduction in light production at concentrations of 6.25 μM and

above (10 × MIC, unpublished results). The decrease in light emission within 3 min at concentrations above the MIC confirms that cell viability is affected relatively fast. The same experiment conducted in *E. coli* showed that, in contrast to chlorhexidine, the turgencin peptides did not affect the viability of this strain within the 3 min assay period at 50 μM concentrations (Figure 8).
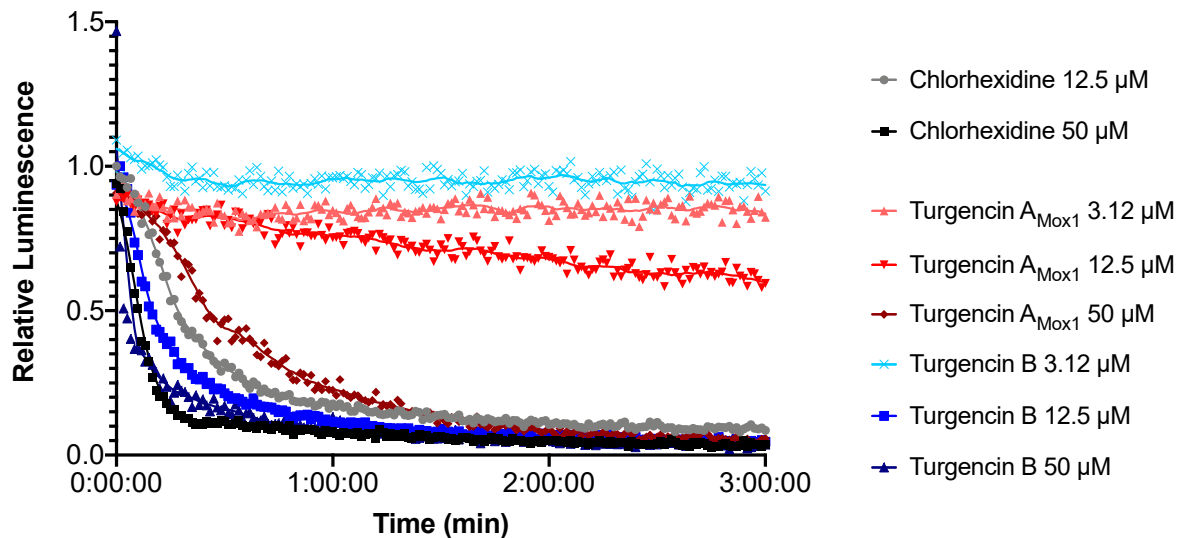
Figure 7. Kinetics of antimicrobial effect on viability of *B. subtilis* as relative luminescence emission from *luxABCDE* treated with turgencin A_{Mox1} (shades of red) and turgencin B (shades of blue). Each data point is the mean of three independent measurements normalized to the water negative control. Chlorhexidine and water were used as positive and negative controls, respectively.
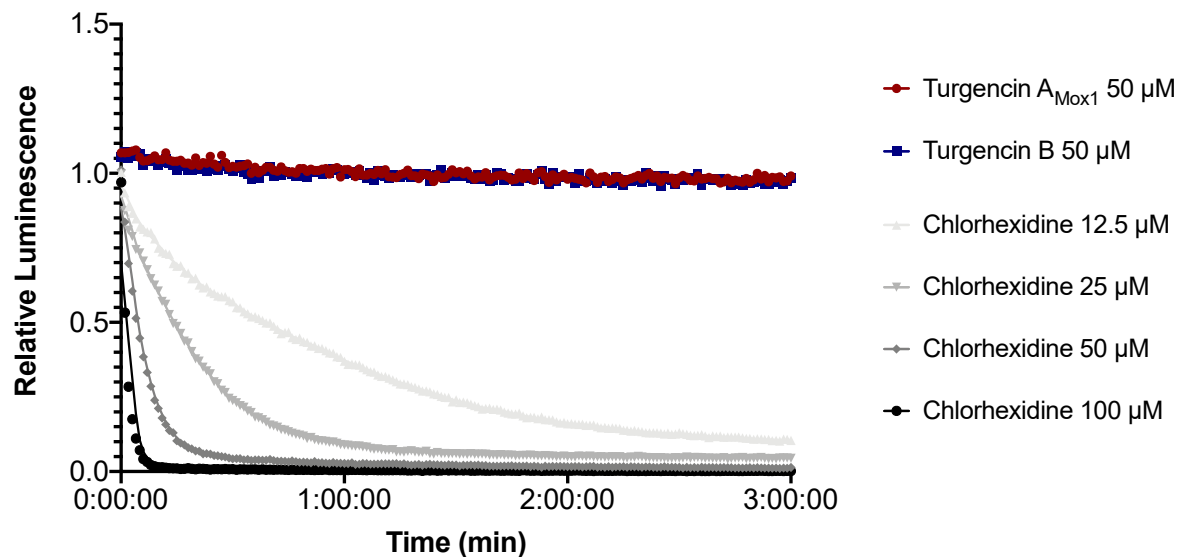
Figure 8. Kinetics of the relative luminescence emission by *E. coli* expressing a *luxCDABE* operon (pCGLS-11) treated with turgencin A_{Mox1} or turgencin B. Each data point is the mean of three independent measurements. Chlorhexidine and water were used as positive and negative controls, respectively.

3. Materials and Methods

3.1. Materials

Live specimens of the sea squirt *Synoicum turgens* (Phipps, 1774) were collected off the coast of Svalbard in October 2011 (79°31′N, 18°45′E) and August 2016 (79°33′N, 18°37′E) by divers at 20–30 m

depth, and outside of Bjørnøya in May 2009 (74°28′N, 18°44′E) by divers at 20 m depth and by Agassiz trawl (74°20′N, 19°20′E) at 47 m depth. All four samples were identified by Robert A. Johansen at the Norwegian national biobank (Marbank), frozen separately at −20 °C at sea, lyophilized, and again frozen until extraction. Voucher specimens (reference numbers: M11HEL0441, M16HEL1403, M09JAN0062-4 and M09JAN0059) were deposited in Marbank, Tromsø, Norway.

3.2. Extraction of Antimicrobial Peptides

Freeze-dried samples (100 g) were extracted twice with five volumes (v/w) of 60% (v/v) MeCN (HPLC-grade, Sigma-Aldrich, Steinheim, Germany) containing 0.1% trifluoroacetic acid (TFA; Sigma-Aldrich) for 24 h at 4 °C. The combined supernatants were incubated at −20 °C for approximately 1 h allowing two liquid phases, an organic, MeCN-rich phase and an aqueous, salt-rich phase to be formed and separated. The aqueous phase was dried in a ScanSpeed 40 vacuum centrifuge (LabogeneApS, Denmark), and resuspended in 0.05% TFA/H_2O (v/v) to a concentration of 100 mg/mL. Salt was removed from the aqueous phase by SPE, as previously described [60]. Briefly, the extracts were loaded onto reversed-phase C18 35cc Sep-Pak Vac cartridges (Waters, MA, USA) equilibrated with 0.05% TFA/H_2O (v/v). After washing with acidified water, the analytes were eluted with 10, 20, 30, 40, and 80% (v/v) MeCN containing 0.05% TFA (v/v). The SPE eluates were dried in a ScanSpeed 40 vacuum centrifuge, resuspended in MQ-H_2O (Millipore, MA, USA), and tested for antimicrobial activity.

Antimicrobial SPE eluates (the 40 and 80% MeCN eluate) were further fractionated by preparative high-performance liquid chromatography (HPLC) on an Agilent 218 Preparative LC system coupled to an Agilent 1260 infinity DAD with an Agilent 440-LC fraction collector (Matriks, Oslo, Norway). Separation was achieved using a Waters XBridge BEH C18 Prep Column (10 × 250 mm, 5 μm) column. The mobile phase consisted of two eluents: eluent A, H_2O with 0.1% formic acid (FA, Pro-analysis, Sigma-Aldrich), and eluent B, MeCN with 0.1% FA. The peptides were separated using a linear gradient of 5-60% eluent B over 60 min, with a flow rate of 6 mL/min. Fractions (6 mL) were collected at regular 1 min intervals, which were then dried in a ScanSpeed 40 vacuum centrifuge, resuspended in MQ-H_2O, and tested for antimicrobial activity.

Active HPLC fractions were submitted to an Agilent 1290 Infinity UHPLC system, coupled to an Agilent high resolution 6540B quadrupole time-of-flight (Q-ToF) mass spectrometer with a dual electrospray ionization (ESI) source, controlled by MassHunter software (Matriks), for identification of the bioactive constituents. The MS analysis revealed semi-purified peptides which required further purification using an analytical HPLC-DAD-MS system consisting of a 600 Pump, a 2996 Photodiode Array UV detector, a 3100 single quadrupole mass detector, and a 2767 sample manager (Waters, MA, USA). The system was controlled by MassLynx 4.1 and FractionLynx application manager. A linear gradient was developed for optimal separation, consisting of 20–36% MeCN (with 0.1% FA) over 24 min and a flow rate of 6 mL/min using a Waters XBridge BEH C18 Prep Column (10 × 250 mm, 5 μm). The resulting ion chromatograms of the peptides were used to determine the retention times (RTs; i.e. relative hydrophobicity) of the bioactive peptides. Fractions containing semi-purified peptides were collected using the "timed-event" function of the MassLynx software. Peptide fractions were pooled, dried in a ScanSpeed 40 vacuum centrifuge, and resuspended in MQ-H_2O. Purity was checked with analytical HPLC, UHPLC-QToF-MS and NMR, and the antimicrobial activity was profiled.

3.3. Peptide Sequencing

Primary structure determination of the peptides turgencin A_{Mox1} and turgencin B_{Mox2} was performed at Eurosequence (Groningen, The Netherlands, www.eurosequence.nl). The complete sequence of turgencin B_{Mox2} was obtained solely by Edman degradation sequencing, whereas the sequence of turgencin A_{Mox1} was obtained by a combination of N-terminal Edman degradation, reduction and alkylation of the peptide with iodacetamide, followed by Glu-C digestion, separation of fragments by RP-HPLC, and finally analyzing the obtained fragments by Edman degradation and

MS/MS. The peptide sequences have been submitted to the UniProt Knowledgebase with the accession numbers C0HLN5 (turgencin A) and C0HLN6 (turgencin B).

3.4. Partial Reduction and Alkylation

Lyophilized turgencin B (0.5 mg) was partially reduced in 210 μL of 0.17 M citrate buffer (32 mg/mL citric acid, 50 mg/mL trisodium citrate dihydrate) (pH 3.0). Peptide sample was then combined 1:1 with cold (4 °C) 10 mM tris(2-carboxyethyl)phosphine (11.4 mg/mL) solution in 0.17 M citrate buffer (pH 3.0). One sample of turgencin B was incubated at 40 °C, a second sample at room temperature, and a third sample at 4 °C. Aliquots of 50 μL were taken out at different timepoints (10, 20, 30, 45, 60, 90, 120 and 240 min) from all three samples. Upon sampling, each reaction solution was immediately added to 0.6 mg of pre-prepared N-ethylmaleimide (NEM) and incubated for 15 min at 37 °C before acidification through addition of 300 μL of 1% FA. After this step, salt was removed from all samples using C18 ZipTips (Millipore), and eluted in 10 μL of 80% MeCN with 1% FA. Following this, 100 μL of 0.5 M ammonium bicarbonate (pH 8.0) was added. Samples were fully reduced by adding 35 μL of 100 mM dithiothreitol, deoxygenated with N_2, and incubated at 60 °C for 30 min. Afterwards, they were alkylated by adding 35 μL of 250 mM iodoacetamide for 15 min at room temperature. The reduced and alkylated samples were analyzed on a Nexera UHPLC (Shimadzu) coupled to a TripleToF 5600 MS (AB Sciex).

3.5. NMR Spectroscopy and Calculations

All NMR experiments were performed on a Bruker Avance III HD spectrometer equipped with an inverse four-channel probe with cryogenic enhancement for ^1H, ^2H and ^{13}C (TCI) operating at 600 MHz for ^1H (Bruker Biospin, Switzerland). When applicable, gradient-selected experiments with adiabatic pulse sequences were used. The experiments acquired for the studied peptides were Presat, Excitation sculpting, Carbon, ^{15}N-HSQC, ^{13}C-HSQC, HMBC, band-selective HMBC (carbonyl hires), H_2BC, HSQCTOCSY (60 ms DIPSI), NOESY (100, 200, 300 ms mixing time), ROESY (100 ms spinlock), DQF-COSY, E.COSY and TOCSY (20, 60, 100 ms DIPSI). Acquisition and processing were done in Topspin 3.5pl7 using standard pulse sequences (Bruker Biospin, Switzerland). The NMR samples were prepared by dissolving 1–2 mg of peptide in 120 μL ultra-pure water and adding a drop of D_2O in a 3 mm Shigemi tube matched for D_2O. Spectral assignments and integrations were performed in CARA 1.8.4.2. Secondary structure prediction was made in TALOS+.

Structures were generated using XPLOR-NIH 2.52. Starting structures were created as extended chains and folded using standard simulated annealing protocol (2000 K, 20000 cooling steps in vacuo) using NMR-derived constraints without connecting any disulfide bonds. Low energy folds were then used to generate disulfide connected starting structures for the final refinements. Finally, production runs of 500 cycles of simulated annealing was used to generate the reported structure ensemble. Representative low energy structures were then solvated in an orthorhombic water box of explicit SPC water and neutralized by adding 3 Cl- ions, with $10 \times 10 \times 10$ Å clearance from the peptide atoms using the Desmond package in Maestro v11.4.011, MMshare v4.0.011, release 2017-4 for the Schrodinger suite. The structure was minimized (min 10 SD steps/3 LBFGS vectors) before a 10 ns free MD (2 fs timesteps, 9.0 Å electrostatics cutoff) was simulated under constant pressure and temperature (300 K Nose-Hoover thermostat, Martyna-Tobias-Klein barostat). The NMR data of this paper are available at the Biological Magnetic Resonance Data Bank under accession number 50153.

3.6. Microbial Strains and Antibacterial Activity Assays

The Gram-negative bacteria *E. coli* (*E.c*, ATCC 25922) and *P. aeruginosa* (*P.a*, ATCC 27853), and the Gram-positive bacteria *S. aureus* (*S.a*, ATCC 9144), *C. glutamicum* (*C.g*, ATCC 13032), and *B. subtilis* (*B.s*, ATCC 23857) were used as test bacteria. Cultures stored in glycerol at −80 °C were transferred to Mueller–Hinton (MH) plates (Difco Laboratories, Detroit, MI, USA) and incubated at room temperature for two days. One colony from each bacterial strain was transferred to 5 mL MH broth and shaken at

600 rpm overnight. From these vials of actively growing bacteria, 20 μL were transferred to 5 mL MH broth and shaken for 2 h at room temperature. The antibacterial assays were performed as previously described [61], but with the following exception; bacterial cultures were diluted with medium to $2.5–3.0 \times 10^4$ bacteria/mL concentrations. An aliquot of 50 μL (1250–1500 bacterial cells) was added to each well in 96 microwell plates (Thermo Fisher Scientific, Denmark), preloaded with sample solution (peptides or eluates) and controls (water, medium or antibiotic). The plates were incubated at 35 °C for 24 h, using an EnVisionMultilable Reader, controlled by EnVision Manager (PerkinElmer, United Kingdom) to measure the optical density (OD_{595}) every hour. The minimum inhibitory concentration (MIC) was set to the point a sample showed >90% reduction in OD_{595} after 24 h compared to the growth control (bacteria plus MQ-H_2O). Oxytetracycline (Sigma-Aldrich, Steinheim, Germany) in a serial dilution was used as a positive (antibacterial) control (40-0.04 μM). All experiments were performed in triplicates. The highest peptide concentration tested against the bacteria was 100 μM, and the lowest was 0.02 μM.

3.7. Real-time Assay Measuring Immediate Membrane Disruption

A real-time membrane integrity assay (modified from [56]) was performed using *B. subtilis* 168 (ATCC 23857) and *E. coli* K12 (ATCC MC1061), both carrying the plasmid pCSS962 with the eukaryotic luciferase gene *lucGR*. The luciferase enzyme is dependent on D-luciferin as substrate to emit light. Externally added D-luciferin (MW 280 Da) does not penetrate intact cell membranes efficiently. However, disruption of the bacterial membrane integrity (like pore-formation) will lead to the influx of luciferin and subsequently induce bacterial light emission. After reaching a peak, the light intensity will reduce and drop below normal values (intact cell membranes) due to reduced cell numbers.

B. subtilis and *E. coli* were cultured overnight in MH broth supplemented with 5 μg/mL chloramphenicol (Merck KGaA, Darmstadt, Germany) and a mixture of 20 μg/mL chloramphenicol / 100 μg/mL ampicillin, respectively, before being centrifuged at 4500 rpm for 10 min. The supernatant was removed, and the pellet resuspended in MH broth to give an OD_{600} of 0.1. D-luciferin potassium salt (Synchem Inc., Elk Grove Village, IL, USA) at a final concentration of 1 mM was added to the bacterial cultures and the background luminescence was measured. Twofold dilutions (final assay concentration of 50–1.6 μM) of turgencin A_{Mox1} and B dissolved in MQ-H_2O were prepared and added (10 μL) to black round-bottom 96-well microtiter plates (Nunc, Roskilde, Denmark). Chlorhexidine acetate (Fresenius Kabi, Halden, Norway), at assay concentrations of 200–12.5 μM, was used as a positive control, whereas MQ-H_2O was used as a negative control. The plates were loaded into a Synergy H1 Hybrid Reader (BioTek, Winooski, VT, USA). Aliquots (90 μL, to give a total assay volume of 100 μL) of the prepared bacteria suspension were added to the test wells by an automatic injector and luminescence emission was recorded every second for 180 s. All experiments were performed in triplicate and all values were normalized to untreated water controls.

3.8. Real-time Assay Measuring Bacterial Cell Viability

A real-time cell viability assay (modified from [62]) was performed using *B. subtilis* 168 and *E. coli* K12, carrying a chromosomal integration of an optimized *lux*ABCDE operon controlled by the constitutive promoter P*veg* [63] or the plasmid pCGLS-11 [64] with the *luxCDABE*operon from *Xenorhabdus luminescens*, respectively. These strains express luciferase constitutively and emit light as long as they are alive (i.e. have a functioning metabolism). Thus, adding a bactericidal compound will result in reduced light emission due to reduced cell viability and/or cell number. *B subtilis* and *E. coli* were cultured overnight in MH broth supplemented with 5 μg/mL chloramphenicol and 100 μg/mL ampicillin, respectively, before being centrifuged at 4500 rpm for 10 min. The supernatant was removed, and the pellet resuspended in MH broth to give an OD_{600} of 0.1. Twofold dilutions (10 μL) of turgencin A_{Mox1} and turgencin B (assay concentrations: 50–1.6 μM) and the positive control chlorhexidine acetate (assay concentrations: 200–12.5 μM) were added to black round-bottom 96-well

microtiter plates (Nunc). MQ-H$_2$O was used as a negative control. The plates were loaded into the Synergy H1 Hybrid Reader and aliquots (90 μL, to give a total assay volume of 100 μL) of the bacteria suspension were added to the test wells by an automatic injector. Luminescence emission was subsequently measured every second for 180 s. All experiments were performed in triplicate. The measurements were normalized to the untreated water controls.

3.9. Human Cell Viability Assay

The human melanoma cancer cell line A2058 (ATCC CRL-11147TM) and the non-malignant human fibroblast cell line MRC-5 (ATCC CCL-171) were cultured in Roswell Park Memorial Institute-1640 (RPMI; VWR, West Chester, PA, USA) medium, supplemented with 10% heat-inactivated fetal bovine serum (FBS; VWR, West Chester, PA, USA) at 37 °C in a humidified atmosphere of 5% CO$_2$. The inhibitory effect of the peptides on the proliferation on A2058 and MRC-5 were assessed. Cells were plated in 96-well microtiter plates at an initial density of 2000 (A2058) or 4000 (MRC-5) cells per well and allowed an overnight period for attachment. Cell media were then removed and replaced with fresh RPMI media containing ranging concentrations of the peptides. Cells were then incubated for 72 h at 37 °C. To each well 10 μL AqueousOne (Promega, Madison, WI, USA) was added 1 h before the end of the incubation period. Absorbance was measured at 485 nm. Cells in compound-free RPMI medium were used as a negative control and cells treated with 0.1% Triton®X-100 reagent (Sigma Aldrich, Steinheim, Germany) were used as a positive control. All experiments were performed in triplicate and repeated three times.

4. Conclusions

We report the isolation, structural and biochemical characterization of several novel cysteine rich AMPs from *S. turgens*. From a structural perspective, neither of the peptides, turgencin A and turgencin B, was found to exhibit sequence homology to any previously reported peptides, even with the same disulfide connectivity, however they do display overarching similarities to the lysine-rich viscotoxins which are also positively charged and share the helix-loop-helix motif. Antimicrobial activities and cytotoxicities across various oxiforms of these new peptides varied considerably, and hence future studies should elaborate and examine the importance of the methionine residues for the bioactivities of turgencins. To our knowledge, the turgencins are the first cysteine-rich AMPs ever isolated and characterized from ascidians/tunicates.

Author Contributions: I.K.Ø.H., K.Ø.H. and C.S.M.R. performed the biological activity experiments; I.K.Ø.H., K.Ø.H., C.S.M.R., H.-M.B. and T.H. conceived the biological experiments and analyzed data; I.K.Ø.H., A.G.P., and A.J.C.A., conceived the MS experiments and analyzed data; J.I., designed, interpret and analyzed the NMR experiments; I.K.Ø.H., J.I., K.Ø.H., A.J.C.A., C.S.M.R., H-M.B and T.H. wrote the paper. K.S., D.J.C. and T.H. contributed to the conception of the work and supervised the whole project. All authors read and approved the final manuscript.

Conflicts of Interest: The authors declare no conflict of interest.

References

1. World Health Organization. Global Action Plan on Antimicrobial Resistance. Available online: http://www.who.int/antimicrobial-resistance/publications/global-action-plan/en/ (accessed on 14 September 2019).
2. Wright, G.D. The antibiotic resistome: The nexus of chemical and genetic diversity. *Nat. Rev. Microbiol.* **2007**, *5*, 175–186. [CrossRef] [PubMed]
3. Magiorakos, A.P.; Srinivasan, A.; Carey, R.B.; Carmeli, Y.; Falagas, M.E.; Giske, C.G.; Harbarth, S.; Hindler, J.F.; Kahlmeter, G.; Olsson-Liljequist, B.; et al. Multidrug-resistant, extensively drug-resistant and pandrug-resistant bacteria: An international expert proposal for interim standard definitions for acquired resistance. *Clin. Microbiol. Infec.* **2012**, *18*, 268–281. [CrossRef] [PubMed]
4. Projan, S.J. Why is big Pharma getting out of antibacterial drug discovery? *Curr. Opin. Microbiol.* **2003**, *6*, 427–430. [CrossRef] [PubMed]
5. Brogan, D.M.; Mossialos, E. Systems, not pills: The options market for antibiotics seeks to rejuvenate the antibiotic pipeline. *Soc. Sci. Med.* **2016**, *151*, 167–172. [CrossRef]
6. Hancock, R.; Patrzykat, A. Clinical development of cationic antimicrobial peptides: From natural to novel antibiotics. *Curr. Drug Targets Infect. Disord.* **2002**, *2*, 79–83. [CrossRef]
7. Hancock, R.E.W.; Sahl, H.-G. Antimicrobial and host-defense peptides as new anti-infective therapeutic strategies. *Nat. Biotechnol.* **2006**, *24*, 1551–1557. [CrossRef]
8. Ganz, T. The role of antimicrobial peptides in innate immunity. *Integr. Comp. Biol.* **2003**, *43*, 300–304. [CrossRef]
9. Zasloff, M. Antimicrobial peptides of multicellular organisms. *Nature* **2002**, *415*, 389–395. [CrossRef]
10. Nguyen, L.T.; Haney, E.F.; Vogel, H.J. The expanding scope of antimicrobial peptide structures and their modes of action. *Trends Biotechnol.* **2011**, *29*, 464–472. [CrossRef]
11. Peach, K.C.; Bray, W.M.; Winslow, D.; Linington, P.F.; Linington, R.G. Mechanism of action-based classification of antibiotics using high-content bacterial image analysis. *Mol. Biosyst.* **2013**, *9*, 1837–1848. [CrossRef]
12. Pasupuleti, M.; Schmidtchen, A.; Malmsten, M. Antimicrobial peptides: Key components of the innate immune system. *Crit. Rev. Biotechnol.* **2012**, *32*, 143–171. [CrossRef] [PubMed]
13. Matsuzaki, K. Why and how are peptide–lipid interactions utilized for self-defense? Magainins and tachyplesins as archetypes. *BBA Biomembr.* **1999**, *1462*, 1–10. [CrossRef]
14. Pushpanathan, M.; Gunasekaran, P.; Rajendhran, J. Antimicrobial peptides: Versatile biological properties. *Int. J. Pept.* **2013**, *2013*, 1–15. [CrossRef] [PubMed]
15. Yeaman, M.R.; Yount, N.Y. Mechanisms of antimicrobial peptide action and resistance. *Pharmacol. Rev.* **2003**, *55*, 27–55. [CrossRef]
16. Deslouches, B.; Di, Y.P. Antimicrobial peptides with selective antitumor mechanisms: Prospect for anticancer applications. *Oncotarget* **2017**, *8*, 46635–46651. [CrossRef]
17. Millero, F.J. Descriptive oceanography. In *Chemical Oceanography*, 4th ed.; CRC Press Taylor & Francis Group: Boca Raton, FL, USA, 2013.
18. Buchmann, K. Evolution of innate immunity: Clues from invertebrates via fish to mammals. *Front. Immunol.* **2014**, *5*, 459. [CrossRef]
19. Falanga, A.; Lombardi, L.; Franci, G.; Vitiello, M.; Iovene, M.R.; Morelli, G.; Galdiero, M.; Galdiero, S. Marine antimicrobial peptides: Nature provides templates for the design of novel compounds against pathogenic bacteria. *Int. J. Mol. Sci.* **2016**, *17*, 785. [CrossRef]

20. Fedders, H.; Michalek, M.; Grötzinger, J.; Leippe, M. An exceptional salt-tolerant antimicrobial peptide derived from a novel gene family of haemocytes of the marine invertebrate *Ciona intestinalis*. *Biochem. J.* **2008**, *416*, 65–75. [CrossRef]

21. Venier, P.; Varotto, L.; Rosani, U.; Millino, C.; Celegato, B.; Bernante, F.; Lanfranchi, G.; Novoa, B.; Roch, P.; Figueras, A.; et al. Insights into the innate immunity of the Mediterranean mussel *Mytilus Galloprovincialis*. *BMC Genom.* **2011**, *12*, 69. [CrossRef]

22. Stensvåg, K.; Haug, T.; Sperstad, S.V.; Rekdal, Ø.; Indrevoll, B.; Styrvold, O.B. Arasin 1, a proline–arginine-rich antimicrobial peptide isolated from the spider crab, *Hyas araneus*. *Dev. Comp. Immunol.* **2008**, *32*, 275–285. [CrossRef]

23. Wiens, M.; Schröder, H.C.; Korzhev, M.; Wang, X.-H.; Batel, R.; Müller, W.E.G. Inducible ASABF-type antimicrobial peptide from the sponge *Suberites domuncula*: Microbicidal and hemolytic activity in vitro and toxic effect on molluscs in vivo. *Mar. Drugs* **2011**, *9*, 1969–1994. [CrossRef] [PubMed]

24. Vidal-Dupiol, J.; Ladrière, O.; Destoumieux-Garzón, D.; Sautière, P.-E.; Meistertzheim, A.-L.; Tambutté, E.; Tambutté, S.; Duval, D.; Fouré, L.; Adjeroud, M.; et al. Innate immune responses of a scleractinian coral to vibriosis. *J. Biol. Chem.* **2011**, *286*, 22688–22698. [CrossRef] [PubMed]

25. Lee, I.H.; Cho, Y.; Lehrer, R.I. Styelins, broad-spectrum antimicrobial peptides from the solitary tunicate, *Styela Clava*. *Comp. Biochem. Phys. B* **1997**, *118*, 515–521. [CrossRef]

26. Lee, I.H.; Zhao, C.; Cho, Y.; Harwig, S.S.L.; Cooper, E.L.; Lehrer, R.I. Clavanins, α-helical antimicrobial peptides from tunicate hemocytes. *FEBS Lett.* **1997**, *400*, 158–162. [CrossRef]

27. Galinier, R.; Roger, E.; Sautiere, P.-E.; Aumelas, A.; Banaigs, B.; Mitta, G. Halocyntin and papillosin, two new antimicrobial peptides isolated from hemocytes of the solitary tunicate, *Halocynthia Papillosa*. *J. Pept. Sci.* **2009**, *15*, 48–55. [CrossRef] [PubMed]

28. Lee, I.H.; Lee, Y.S.; Kim, C.H.; Kim, C.R.; Hong, T.; Menzel, L.; Boo, L.M.; Pohl, J.; Sherman, M.A.; Waring, A.; et al. Dicynthaurin: An antimicrobial peptide from hemocytes of the solitary tunicate. *Halocynthia aurantium*. *BBA Gen. Subj.* **2001**, *1527*, 141–148. [CrossRef]

29. Jang, W.S.; Kim, K.N.; Lee, Y.S.; Nam, M.H.; Lee, I.H. Halocidin: A new antimicrobial peptide from hemocytes of the solitary tunicate, *Halocynthia aurantium*. *FEBS Lett.* **2002**, *521*, 81–86. [CrossRef]

30. Diyabalanage, T.; Amsler, C.D.; McClintock, J.B.; Baker, B.J. Palmerolide A, a cytotoxic macrolide from the Antarctic tunicate *Synoicum adareanum*. *J. Am. Chem. Soc.* **2006**, *128*, 5630–5631. [CrossRef]

31. Noguez, J.H.; Diyabalanage, T.K.K.; Miyata, Y.; Xie, X.-S.; Valeriote, F.A.; Amsler, C.D.; McClintock, J.B.; Baker, B.J. Palmerolide macrolides from the Antarctic tunicate *Synoicum adareanum*. *Bioorgan. Med. Chem.* **2011**, *19*, 6608–6614. [CrossRef]

32. Buck, M.L.; Evans, D.M.; Evans, V.A.; Herkt, D.; Sharp, H.; Hollinshead, J.; Mitschang, F.; Murphy, P.J.; Nash, R.J.; Wenbourne, J. A synthesis of tiruchanduramine and a reinvestigation of its glycosidase inhibitory activity. *Tetrahedron* **2017**, *73*, 4545–4548. [CrossRef]

33. Ravinder, K.; Vijender Reddy, A.; Krishnaiah, P.; Ramesh, P.; Ramakrishna, S.; Laatsch, H.; Venkateswarlu, Y. Isolation and synthesis of a novel β-carboline guanidine derivative tiruchanduramine from the Indian ascidian *Synoicum macroglossum*. *Tetrahedron Lett.* **2005**, *46*, 5475–5478. [CrossRef]

34. Tadesse, M.; Strøm, M.B.; Svenson, J.; Jaspars, M.; Milne, B.F.; Tørfoss, V.; Andersen, J.H.; Hansen, E.; Stensvåg, K.; Haug, T. Synoxazolidinones A and B: Novel bioactive alkaloids from the ascidian *Synoicum pulmonaria*. *Org. Lett.* **2010**, *12*, 4752–4755. [CrossRef] [PubMed]

35. Tadesse, M.; Svenson, J.; Jaspars, M.; Strøm, M.B.; Abdelrahman, M.H.; Andersen, J.H.; Hansen, E.; Kristiansen, P.E.; Stensvåg, K.; Haug, T. Synoxazolidinone C; a bicyclic member of the synoxazolidinone family with antibacterial and anticancer activities. *Tetrahedron Lett.* **2011**, *52*, 1804–1806. [CrossRef]

36. Tadesse, M.; Svenson, J.; Sepčić, K.; Trembleau, L.; Engqvist, M.; Andersen, J.H.; Jaspars, M.; Stensvåg, K.; Haug, T. Isolation and synthesis of pulmonarins A and B, acetylcholinesterase inhibitors from the colonial ascidian *Synoicum pulmonaria*. *J. Nat. Prod.* **2014**, *77*, 364–369. [CrossRef]

37. Trepos, R.; Cervin, G.; Hellio, C.; Pavia, H.; Stensen, W.; Stensvåg, K.; Svendsen, J.-S.; Haug, T.; Svenson, J. Antifouling compounds from the sub-arctic ascidian *Synoicum pulmonaria*: Synoxazolidinones A and C, pulmonarins A and B, and synthetic analogues. *J. Nat. Prod.* **2014**, *77*, 2105–2113. [CrossRef]

38. Gu, Y.; Shih, P.-H. Salt-induced phase separation can effectively remove the acetonitrile from the protein sample after the preparative RP-HPLC. *Enzym. Microb. Technol.* **2004**, *35*, 592–597. [CrossRef]

39. Lao, Y.W.; Gungormusler-Yilmaz, M.; Shuvo, S.; Verbeke, T.; Spicer, V.; Krokhin, O.V. Chromatographic behavior of peptides containing oxidized methionine residues in proteomic LC–MS experiments: Complex tale of a simple modification. *J. Proteom.* **2015**, *125*, 131–139. [CrossRef]

40. Waghu, F.H.; Barai, R.S.; Idicula-Thomas, S. Leveraging family-specific signatures for AMP discovery and high-throughput annotation. *Sci. Rep.* **2016**, *6*, 24684. [CrossRef]

41. Squier, T.C.; Bigelow, D.J. Protein oxidation and age-dependent alterations in calcium homeostasis. *Front. Biosci.* **2000**, *5*, d504–d526. [CrossRef]

42. Kim, G.; Weiss, S.J.; Levine, R.L. Methionine oxidation and reduction in proteins. *BBA Gen. Subj.* **2014**, *1840*, 901–905. [CrossRef]

43. Nguyen, G.K.T.; Lim, W.H.; Nguyen, P.Q.T.; Tam, J.P. Novel cyclotides and uncyclotides with highly shortened precursors from *Chassalia chartacea* and effects of methionine oxidation on bioactivities. *J. Biol. Chem.* **2012**, *287*, 17598–17607. [CrossRef] [PubMed]

44. Suzuki, S.; Kodera, Y.; Saito, T.; Fujimoto, K.; Momozono, A.; Hayashi, A.; Kamata, Y.; Shichiri, M. Methionine sulfoxides in serum proteins as potential clinical biomarkers of oxidative stress. *Sci. Rep.* **2016**, *6*, 38299. [CrossRef] [PubMed]

45. Wang, Y.; Nip, A.M.; Wishart, D.S. A simple method to quantitatively measure polypeptide JHNHα coupling constants from TOCSY or NOESY spectra. *J. Biomol. NMR* **1997**, *10*, 373–382. [CrossRef] [PubMed]

46. Ludvigsen, S.; Andersen, K.V.; Poulsen, F.M. Accurate measurements of coupling constants from two-dimensional nuclear magnetic resonance spectra of proteins and determination of φ-angles. *J. Mol. Biol.* **1991**, *217*, 731–736. [CrossRef]

47. Schneider, J.J.; Unholzer, A.; Schaller, M.; Schäfer-Korting, M.; Korting, H.C. Human defensins. *J. Mol. Med.* **2005**, *83*, 587–595. [CrossRef]

48. Romagnoli, S.; Ugolini, R.; Fogolari, F.; Schaller, G.; Urech, K.; Giannattasio, M.; Ragona, L.; Molinari, H. NMR structural determination of viscotoxin A3 from *Viscum album* L. *Biochem. J.* **2000**, *350*, 569–577. [CrossRef]

49. Pal, A.; Debreczeni, J.E.; Sevvana, M.; Gruene, T.; Kahle, B.; Zeeck, A.; Sheldrick, G.M. Structures of viscotoxins A1 and B2 from European mistletoe solved using native data alone. *Acta Crystallogr. D* **2008**, *64*, 985–992. [CrossRef]

50. Ahn, H.-C.; Juranić, N.; Macura, S.; Markley, J.L. Three-dimensional structure of the water-insoluble protein crambin in dodecylphosphocholine micelles and its minimal solvent-exposed surface. *J. Am. Chem. Soc.* **2006**, *128*, 4398–4404. [CrossRef]

51. Teeter, M.M. Water structure of a hydrophobic protein at atomic resolution: Pentagon rings of water molecules in crystals of crambin. *Proc. Natl. Acad. Sci. USA* **1984**, *81*, 6014–6018. [CrossRef]

52. Chen, J.C.H.; Hanson, B.L.; Fisher, S.Z.; Langan, P.; Kovalevsky, A.Y. Direct observation of hydrogen atom dynamics and interactions by ultrahigh resolution neutron protein crystallography. *Proc. Natl. Acad. Sci. USA* **2012**, *109*, 15301–15306. [CrossRef]

53. Chattopadhyay, S.; Sinha, N.K.; Banerjee, S.; Roy, D.; Chattopadhyay, D.; Roy, S. Small cationic protein from a marine turtle has β-defensin-like fold and antibacterial and antiviral activity. *Proteins* **2006**, *64*, 524–531. [CrossRef] [PubMed]

54. Lakshminarayanan, R.; Vivekanandan, S.; Samy, R.P.; Banerjee, Y.; Chi-Jin, E.O.; Teo, K.W.; Jois, S.D.S.; Kini, R.M.; Valiyaveettil, S. Structure, self-assembly, and dual role of a β-defensin-like peptide from the Chinese soft-shelled turtle eggshell matrix. *J. Am. Chem. Soc.* **2008**, *130*, 4660–4668. [CrossRef] [PubMed]

55. Niederhafner, P.; Bednárová, L.; Buděšínský, M.; Šafařík, M.; Ehala, S.; Ježek, J.; Borovičková, L.; Fučík, V.; Čeřovský, V.; Slaninová, J. Melectin MAPs: The influence of dendrimerization on antimicrobial and hemolytic activity. *Amino Acids* **2010**, *39*, 1553–1561. [CrossRef] [PubMed]

56. Virta, M.; Åkerman, K.E.O.; Saviranta, P.; Oker-Blom, C.; Karp, M.T. Real-time measurement of cell permeabilization with low-molecular-weight membranolytic agents. *J. Antimicrob. Chemoth.* **1995**, *36*, 303–315. [CrossRef] [PubMed]

57. Kuyyakanond, T.; Quesnel, L.B. The mechanism of action of chlorhexidine. *FEMS Microbiol. Lett.* **1992**, *100*, 211–215. [CrossRef] [PubMed]

58. Galluzzi, L.; Karp, M. Whole cell strategies based on lux genes for high throughput applications toward new antimicrobials. *Comb. Chem. High Throughput Scr.* **2006**, *9*, 501–514.

59. Galluzzi, L.; Karp, M. Intracellular redox equilibrium and growth phase affect the performance of luciferase-based biosensors. *J. Biotechnol.* **2007**, *127*, 188–198. [CrossRef]

60. Haug, T.; Kjuul, A.K.; Stensvåg, K.; Sandsdalen, E.; Styrvold, O.B. Antibacterial activity in four marine crustacean decapods. *Fish Shellfish Immunol.* **2002**, *12*, 371–385. [CrossRef]

61. Solstad, R.G.; Li, C.; Isaksson, J.; Johansen, J.; Svenson, J.; Stensvåg, K.; Haug, T. Novel antimicrobial peptides EeCentrocins 1, 2 and EeStrongylocin 2 from the edible sea urchin *Echinus esculentus* have 6-br-trp post-translational modifications. *PLoS ONE* **2016**, *11*, e0151820. [CrossRef]

62. Vesterlund, S.; Paltta, J.; Lauková, A.; Karp, M.; Ouwehand, A.C. Rapid screening method for the detection of antimicrobial substances. *J. Microbiol. Meth.* **2004**, *57*, 23–31. [CrossRef]

63. Radeck, J.; Kraft, K.; Bartels, J.; Cikovic, T.; Dürr, F.; Emenegger, J.; Kelterborn, S.; Sauer, C.; Fritz, G.; Gebhard, S.; et al. The *Bacillus* BioBrick Box: Generation and evaluation of essential genetic building blocks for standardized work with *Bacillus subtilis*. *J. Biol. Eng.* **2013**, *7*, 29. [CrossRef] [PubMed]

64. Frackman, S.; Anhalt, M.; Nealson, K.H. Cloning, organization, and expression of the bioluminescence genes of *Xenorhabdus luminescens*. *J Bacteriol* **1990**, *172*, 5767–5773. [CrossRef] [PubMed]

Supporting information

Isolation and characterization of antimicrobial peptides with unusual disulfide connectivity from the colonial ascidian *Synoicum turgens*

Ida K. Ø. Hansen [1], Johan Isaksson [2], Aaron G. Poth[3], Kine Ø. Hansen [4], Aaron J. C. Andersen [1], Céline S. Richard [1], Hans-Matti Blencke[1], Klara Stensvåg[1], David J. Craik[3] and Tor Haug [1]

[1] Norwegian College of Fishery Science, Faculty of Biosciences, Fisheries and Economics, UiT The Arctic University of Norway, Breivika, N-9037 Tromsø, Norway

[2] Department of Chemistry, UiT The Arctic University of Norway, Breivika, N-9037 Tromsø, Norway

[3] Institute for Molecular Bioscience, The University of Queensland, Brisbane 4072, Queensland, Australia

[4] Marbio, UiT The Arctic University of Norway, Breivika, N-9037, Tromsø, Norway

Table of contents

Figure S1. MS spectra of the isotope patterns of the purified peptides turgencin A$_{Mox1}$, turgencin B, turgencin B$_{Mox1}$ and turgencin B$_{Mox2}$. The [M+4H]$^{4+}$ ions are highlighted, and the monoisotopic signals of these ions were used for calculation of the monoisotopic masses of the peptides.
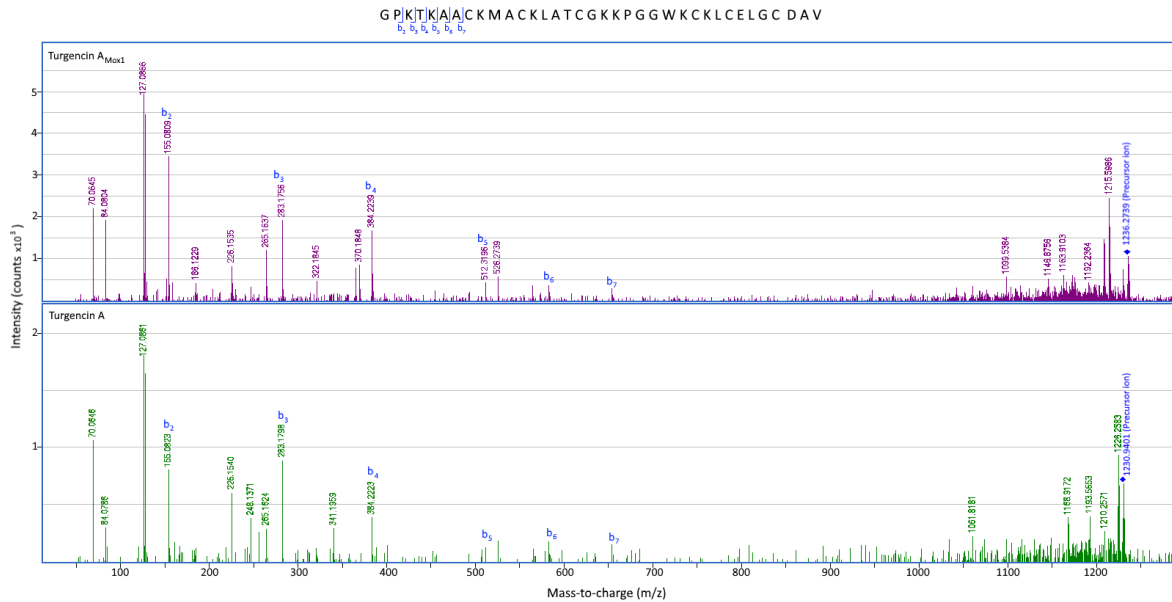
Figure S2. MS/MS spectra of the [M+3H]$^{3+}$ precursor ions *m/z* 1236.27 and *m/z* 1230.94 of the intact peptides of turgencin A and turgencin A$_{Mox1}$ respectively.
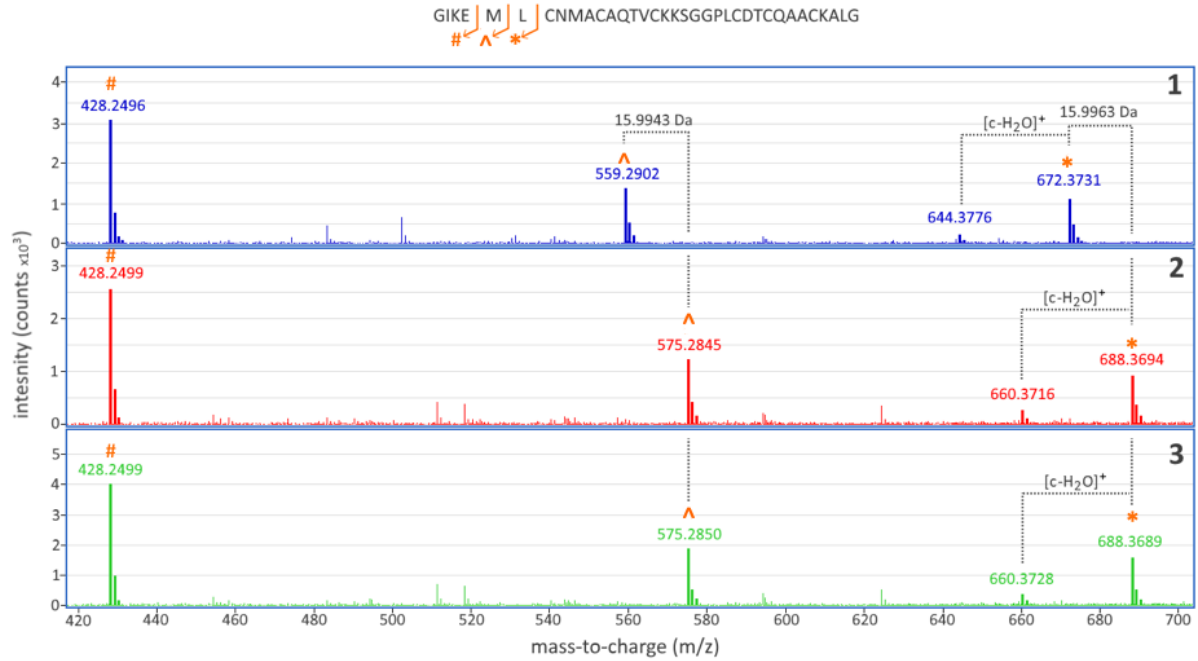
Figure S3. MS/MS spectra of the [M+4H]$^{4+}$ precursor ions, highlighting the differing oxidation states of Met5 across three turgencin B oxiforms, zoomed in between m/z 420-700. Spectrum 1 is of turgencin B (precursor m/z 885.65), spectrum 2 illustrates the oxidation of turgencin B$_{Mox1}$ (precursor m/z 889.65), and spectrum 3 is of turgencin B$_{Mox2}$ (precursor m/z 893.65).
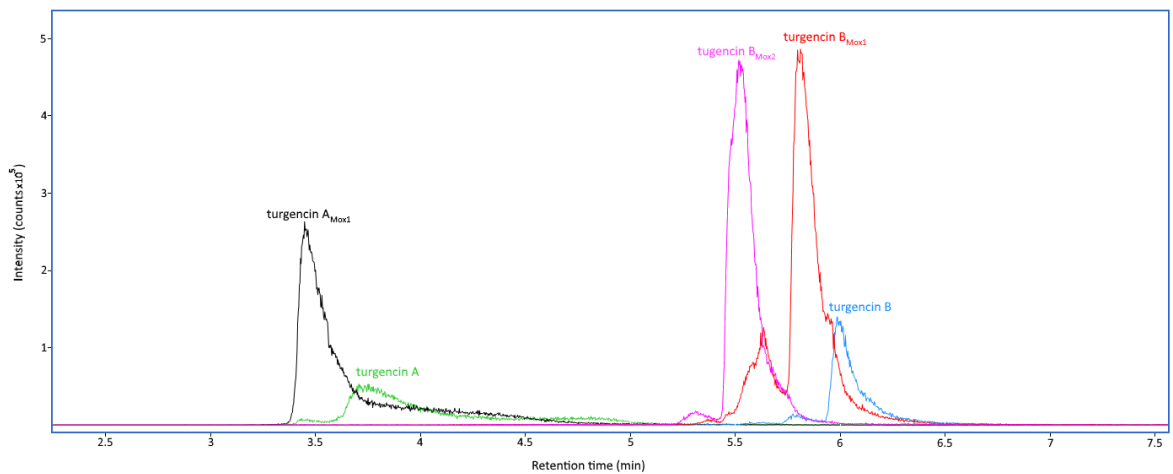
Figure S4. Reversed-phase HPLC separation of turgencin A, B and their oxidized derivatives. Peptides with methionine oxidation exhibit shorter retention times, corresponding with decreased hydrophobicity.
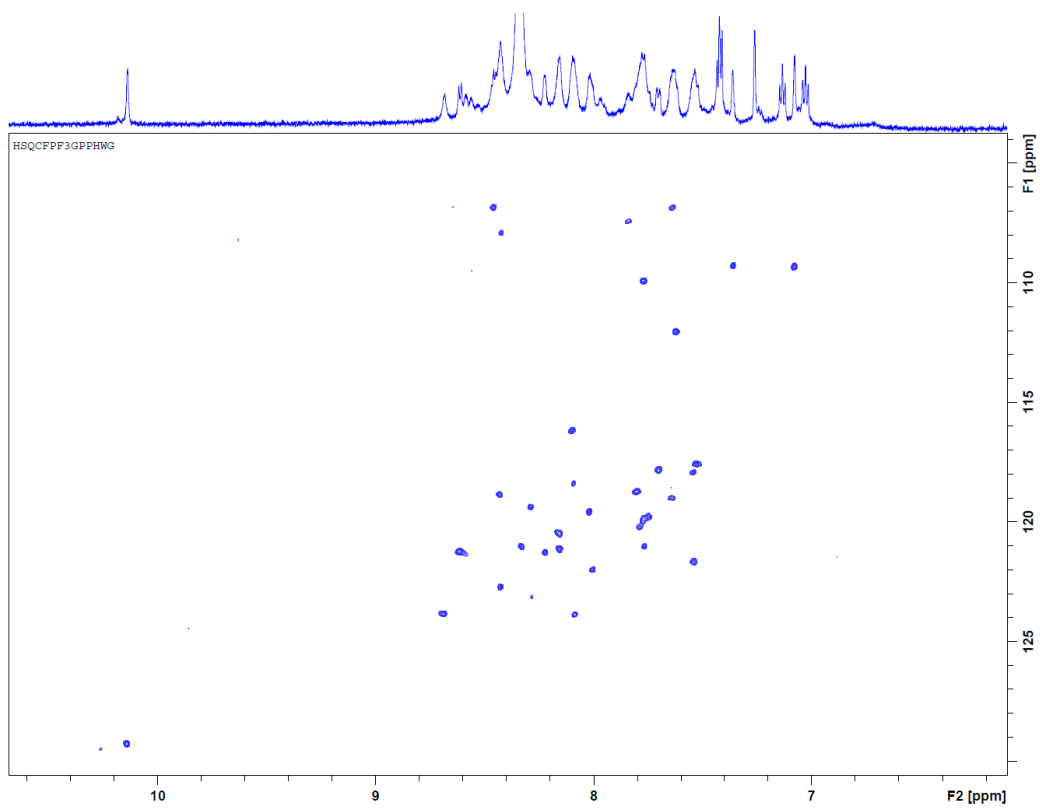
Figure S5. ^{15}N-HSQC (at natural abundance) of turgencin A$_{Mox1}$ in water.
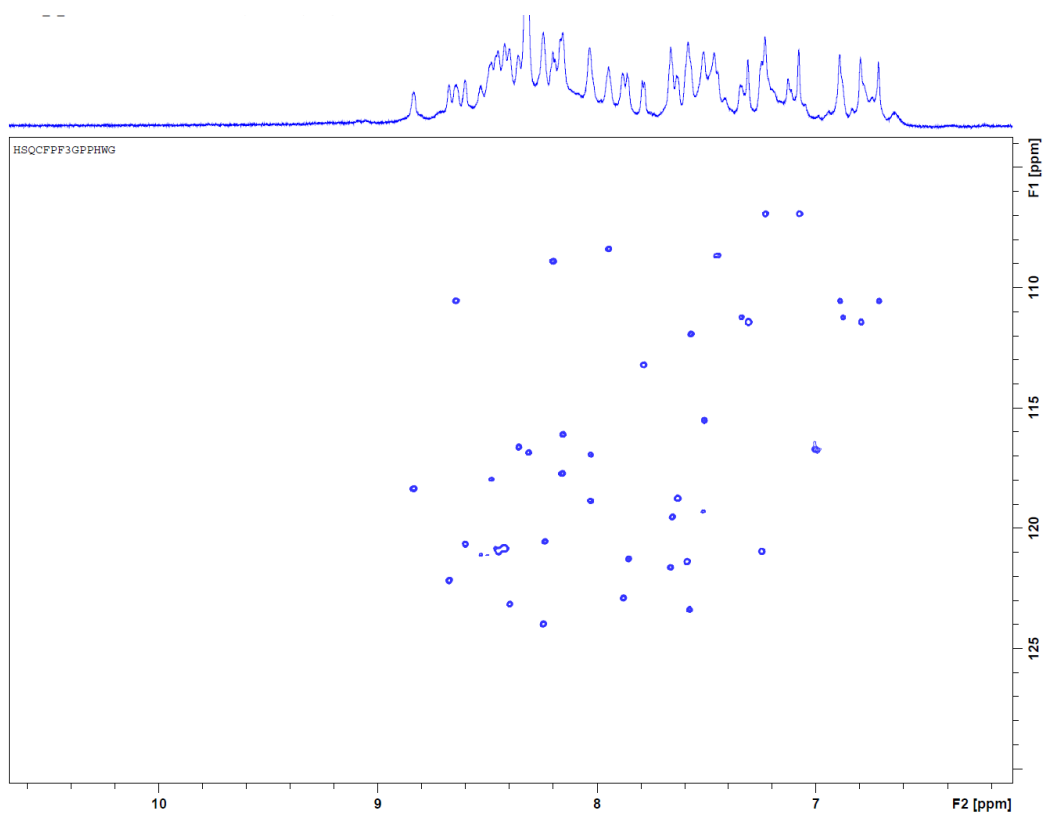
Figure S6. ^{15}N-HSQC (at natural abundance) of turgencin B$_{Mox2}$ in water.
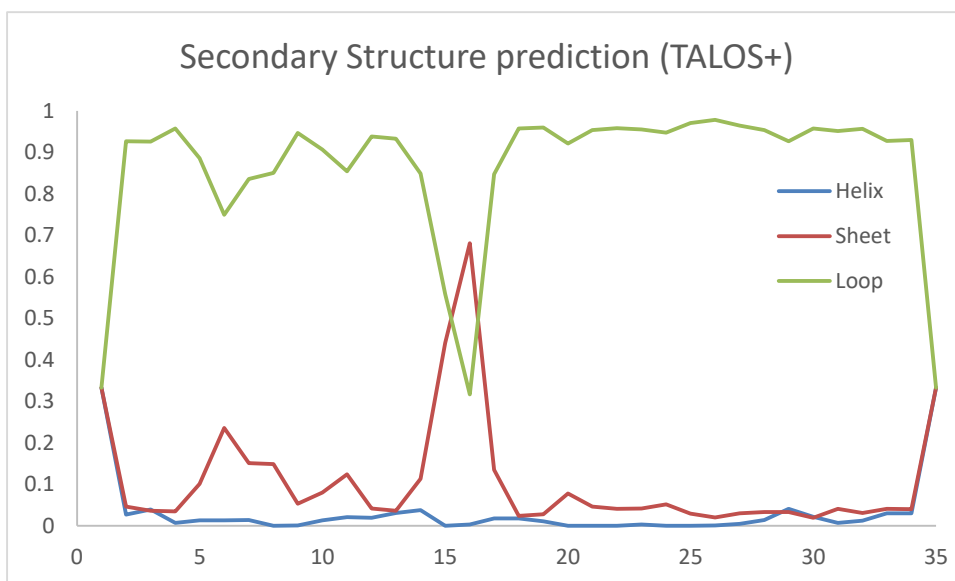
Figure S7. TALOS+ predicted secondary structure of turgencin B$_{Mox2}$ based on all available chemical shifts (HN, N, C, CA, CB, HA, HB). Overall patch of secondary fold is predicted. One residue (C16) is predicted as β-sheet with low confidence, however this is likely an effect of the disulfide bond affecting the chemical shifts.
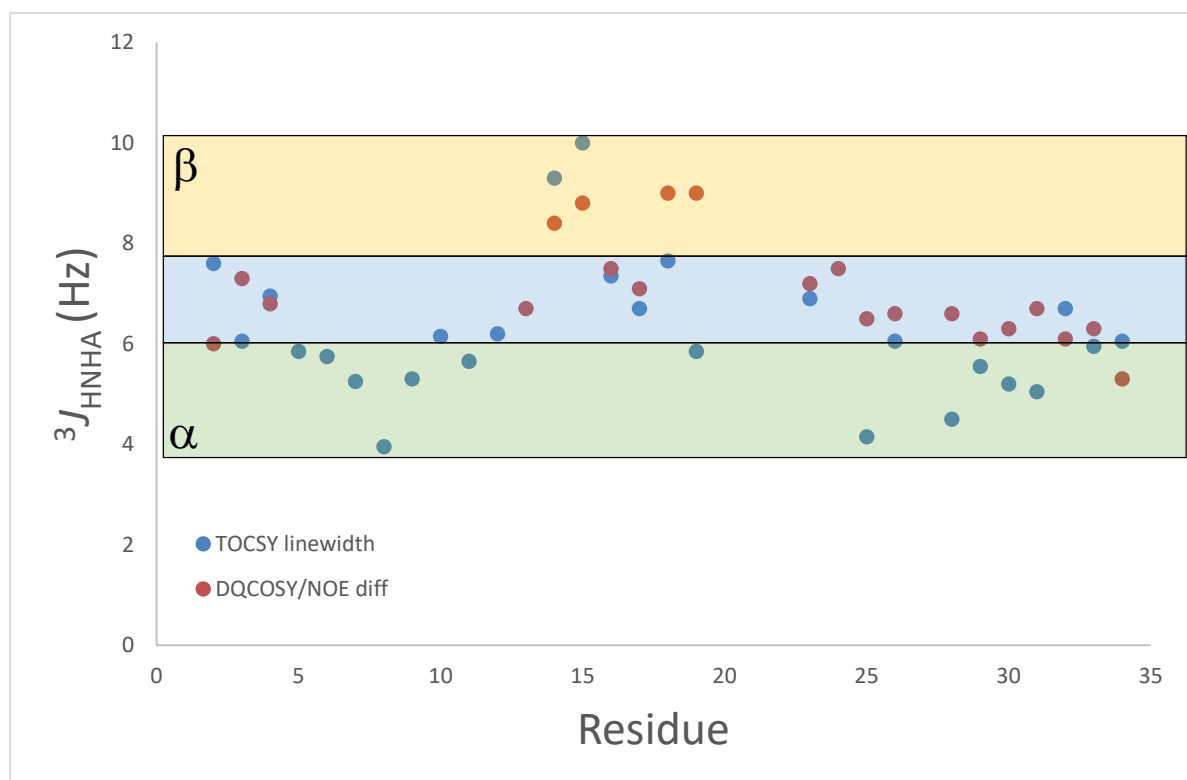
Figure S8. The $^3J_{HNHA}$ coupling constants for turgencin B$_{Mox2}$ structure estimated using two methods using the TOCSY line widths and the sum/diff displacement of DQF-COSY and NOESY slices. The results indicate access to helical structures (green area) for both sides of the turn, but the couplings also suggest significant conformational averaging (blue area).
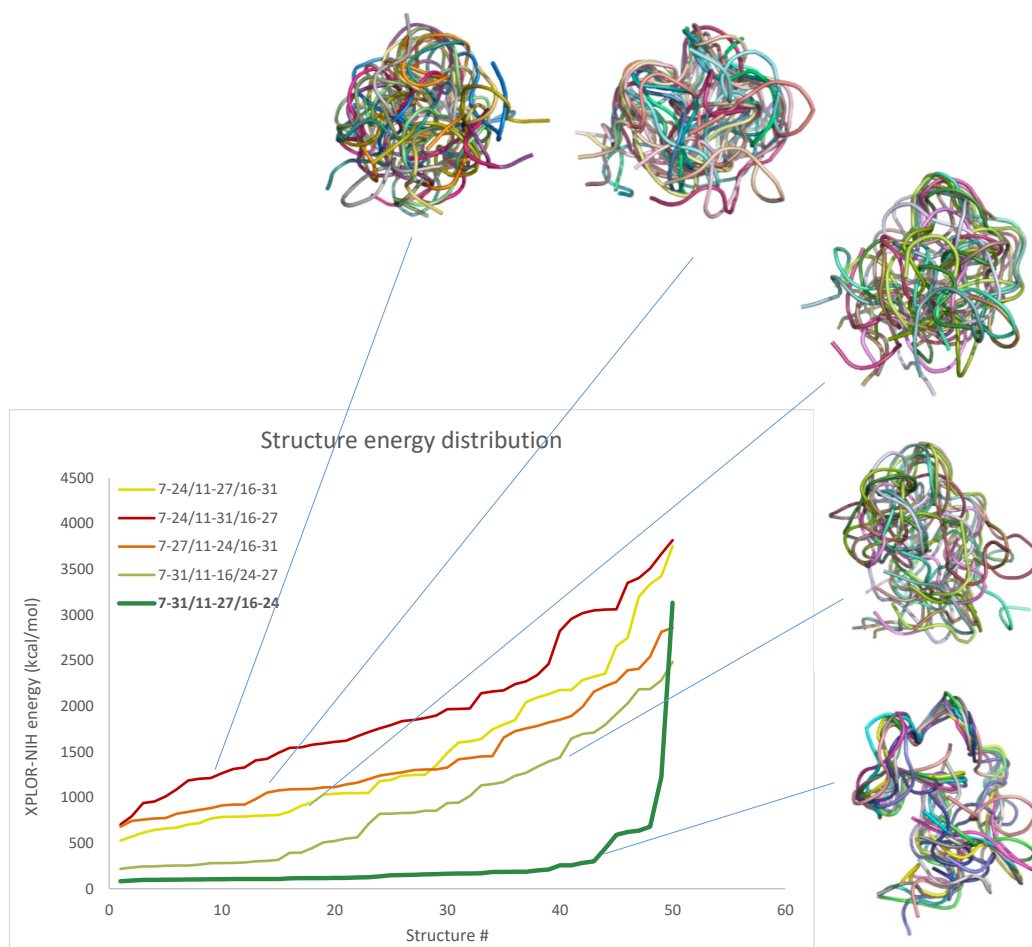
Figure S9. Early test calculations of turgencin B$_{Mox2}$ using crude constraints to evaluate different disulfide patterns using crude constraints. 10 out of 50 structures of each simulation are superimposed, picked at even intervals from the energy profile.
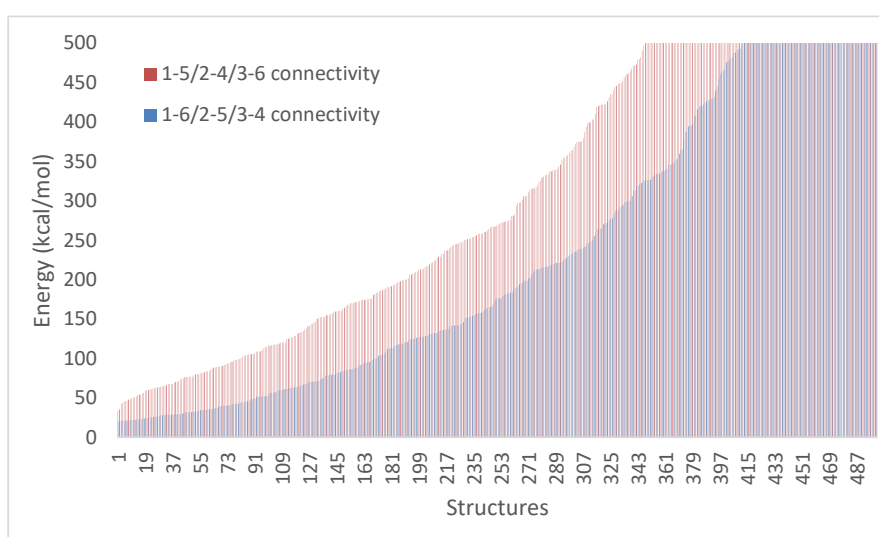
Figure S10. The most viable alternative disulfide pattern of turgencin B$_{Mox2}$ compared to the found pattern in terms of energy of 500 calculated simulated annealing structures using the final constraints.
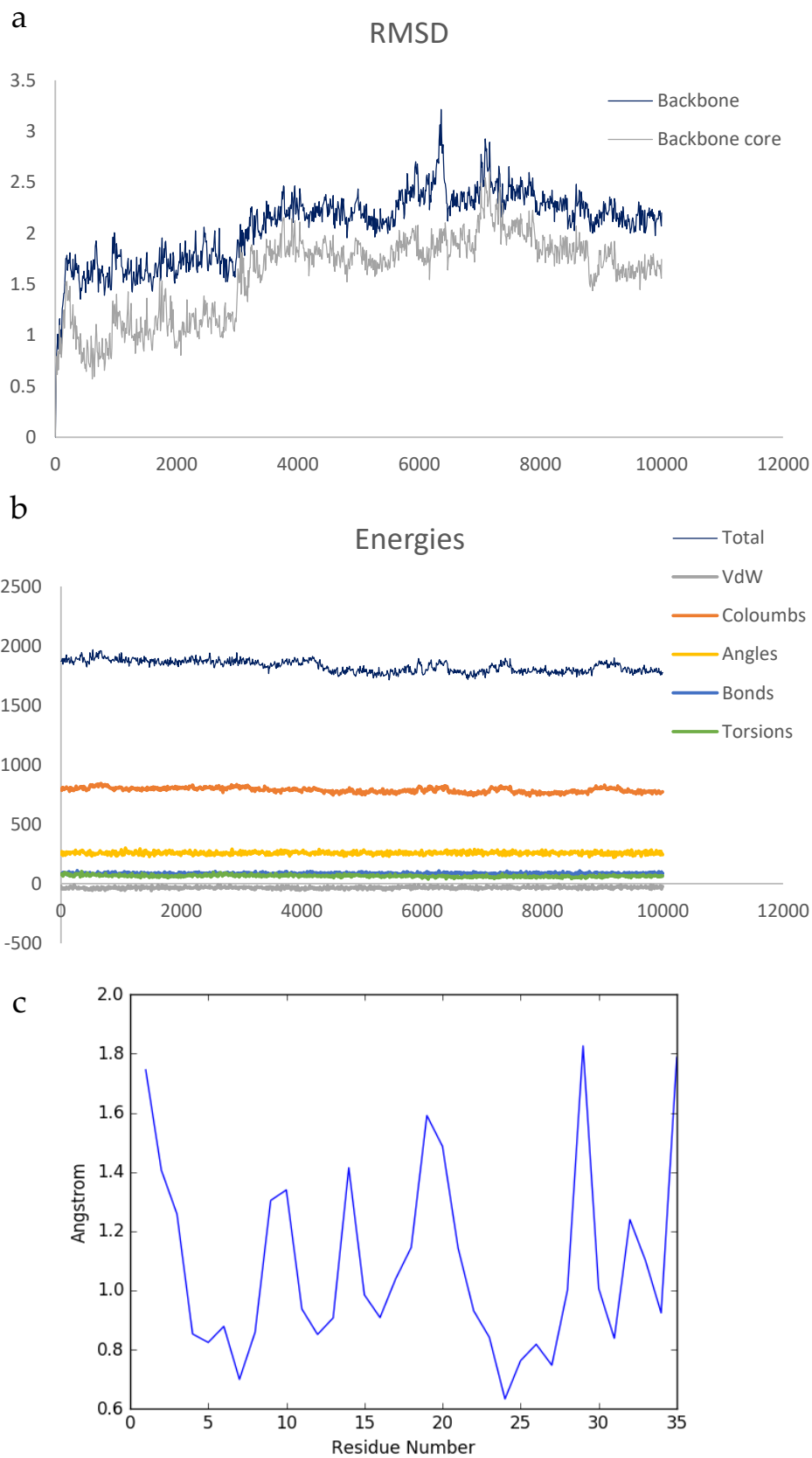
Figure S11. The (a) RMSD relative to the starting frame, (b) energies of turgencin B$_{Mox2}$ and (c) the RMSF of the backbone during the free MD trajectory.
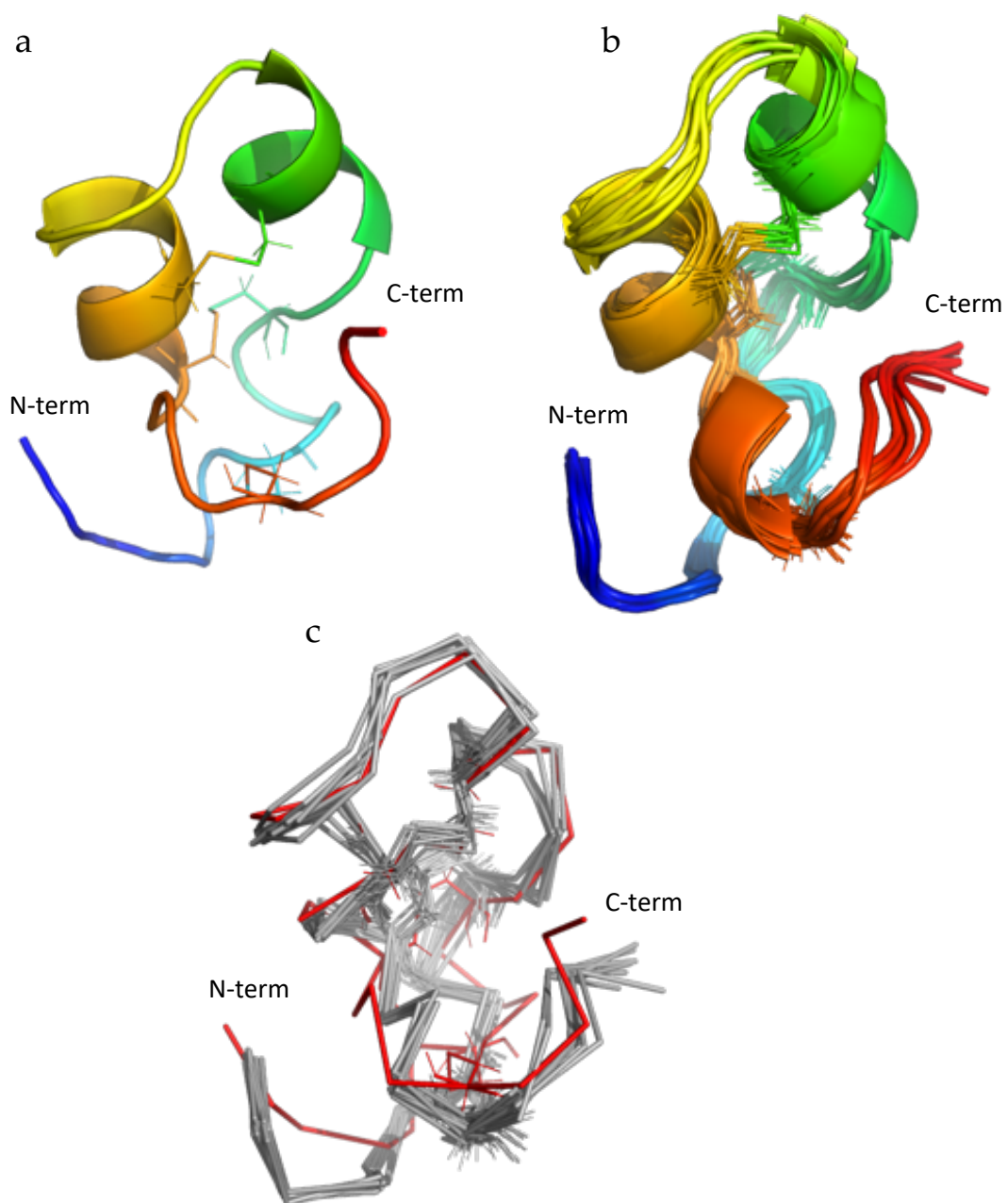
Figure S12. Comparison of NMR and molecular dynamics structures for turgencin B$_{Mox2}$. (a) The representative NMR structure of turgencin B$_{Mox2}$ selected for MD simulations, and (b) an ensemble sampling the last nanosecond of the simulation. Backbone core (res 6-32) RMSD ~ 1.5 Å. (c) The NMR and MD structures superimposed and displayed with ribbons.

Table S1. Antimicrobial activity of solid phase extract (SPE) fractions and the organic extract. Bacterial test strains: *C. g. - Corynebacterium glutamicum, B. s. - Bacillus subtilis, S. a. - Staphylococcus aureus, E. c. - Escherichia coli, P. a. - Pseudomonas aeruginosa.*

	Antimicrobial activity (MIC; mg/mL)				
Extract	*C. g.*	*B. s.*	*S. a.*	*E. c.*	*P. a.*
10% MeCN SPE	1.25	5.00	5.00	10.00	5.00
20% MeCN SPE	2.50	2.50	5.00	5.00	5.00
30% MeCN SPE	0.16	0.16	2.50	5.00	5.00
40% MeCN SPE	0.04	0.08	2.50	5.00	2.50
80% MeCN SPE	0.31	0.31	2.50	5.00	2.50
Organic	2.50	2.50	10.00	>10.00	>10.00

Table S2. Calculated and measured monoisotopic *m/z* $[M+4H]^{4+}$ ions of turgencin A, turgencin B, and their oxidized derivatives.

Peptide	Calculated monoisotopic mass $[M+4H]^{4+}$	Measured monoisotopic mass $[M+4H]^{4+}$	Error (ppm)
Turgencin A	923.4568	923.4574	0.65
Turgencin A$_{Mox1}$	927.4555	927.4562	0.71
Turgencin B	885.6526	885.6536	1.11
Turgencin B$_{Mox1}$	889.6529	889.6532	0.34
Turgencin B$_{Mox2}$	893.6501	893.6518	1.92

Table S3. Proton chemical shift assignments for turgencin A_{Mox1} in water.

Residue	H (ppm)	Hα(ppm)	Hβ (ppm)	Hγ(ppm)	Others (ppm)
GLY*1*	8.56	3.91/3.92			
PRO*2*		4.38	2.24/1.84	2.00/1.94	α:3.50/3.52
LYS*3*	8.61	4.32	1.80/1.70	1.39/1.43	α:1.57/1.58, α:2.90
THR*4*	7.62	4.34	4.41	1.18	
LYS*5*	8.68	3.97	1.82/1.74	1.38/1.40	α:1.66, α:2.94
ALA*6*	8.34	3.99	1.34		
ALA*7*	8.00	4.12	1.39		
CYS*8*	8.16	4.18	3.39/2.96		
LYS*9*	8.58	3.66	1.80/1.69	1.23/1.22	α:1.58/1.56, α:2.90
MET*10*	8.16	4.12	2.25	2.94/2.86	α: 1.57, α: 2.62
ALA*11*	7.96	4.14	1.49		
CYS*12*	8.10	4.45	3.06/3.12		
LYS*13*	8.08	3.72	1.99/1.88	1.29	α:1.55, α:2.86
LEU*14*	7.63	4.07	1.70/1.55	1.68	α1:0.78, α2:0.83
ALA*15*	7.77	4.31	1.41		
THR*16*	7.77	4.39	4.06	1.04	
CYS*17*	8.29	4.21	3.21/2.81		
GLY*18*	8.43	3.77/3.74			
LYS*19*	7.80	4.26	1.81/1.67	1.36/1.41	α:1.59, α:2.91
LYS*20*	7.70	4.75	1.75/1.64	1.26	α:1.63, α:2.90
PRO*21*		4.74	1.89/2.38	1.99/1.90	α:3.58/3.34
GLY*22*	8.46	3.67/4.01			
GLY*23*	7.64	3.76/4.15			
TRP*24*	8.42	4.34	3.36/3.18		α1:7.26, α1:10.13, α3:7.43, α2:7.13, α2: 7.41,αα3: 7.02
LYS*25*	8.02	3.54	1.42/1.26	0.89/0.84	α:1.40, α:2.80
CYS*26*	4.17	3.01/2.97			
LYS*27*	7.78	3.96	1.74/1.80	1.37/1.29	α:1.54, α:2.84
LEU*28*	8.09	3.92	1.46/1.41	1.44	α:0.78/0.74
CYS*29*	7.77	4.15	3.34/2.98		
GLU*30*	8.43	3.69	2.06/1.88	1.90/2.60	
LEU*31*	8.22	4.12	1.72/1.55	1.68	α:0.82/0.81
GLY*32*	7.84	3.86/3.85			
CYS*33*	7.54	4.66	3.07/2.97		
ASP*34*	7.74	4.47	2.68		
ALA*35*	7.54	4.27	1.40		
VAL*36*	7.53	3.98	2.08	γ1:0.92, γ2:0.85	

Table S4. Carbon chemical shift assignments for turgencin A$_{Mox1}$ in water.

Residue	N (ppm)	Cα(ppm)	Cβ (ppm)	Cγ(ppm)	Others (ppm)
GLY1	109.48	40.56			
PRO2		60.50	29.59	24.34	α:46.89
LYS3	121.19	53.92	30.14	22.24	α:26.21, α:39.33
THR4	111.99	58.48	68.09	19.07	
LYS5	123.81	57.34	29.02	22.26	α:26.72, α:39.32
ALA6	120.98	52.30	15.32		
ALA7	121.95	52.09	15.47		
CYS8	121.10	57.05	35.14		
LYS9	121.30	57.72	30.13	24.40	α:26.28, α:39.30
MET10	120.45	52.02	23.24	48.40	α:26.3, α:36.80
ALA11	123.40	52.42	14.53		
CYS12	116.13	54.33	35.66		
LYS13	123.81	56.97	29.22	22.05	α:26.27,αα:39.18
LEU14	118.52	53.97	39.30	24.20	α1:20.19, α2:21.16
ALA15	120.99	50.92	16.46		
THR16	109.91	61.20	66.78	18.18	
CYS17	119.35	55.29	40.47		
GLY18	118.81	43.86			
LYS19	118.69	54.01	30.64	22.21	α:26.29,αα:39.33
LYS20	117.80	50.79	30.37	22.04	α:26.25, α:39.34
PRO21		61.75	28.76	24.43	α:47.84
GLY22	106.81	42.12			
GLY23	106.85	42.17			
TRP24	122.69	57.01	25.95	108.03	α1:124.59, α2:126.89, α2:126.20, α3:117.93, α2:121.91, α2:112.01, α3:119,26, Nα1:129.22
LYS25	119.54	56.94	28.99	22.57	α:26.31, α:39.15
CYS26	118.96	55.75	36.82		
LYS27	120.16	56.37	29.55	22.18	α:26.125, α:39.22
LEU28	118.33	54.77	39.04	23.94	α:21.82/20.81
CYS29	119.87	52.41	35.34		
GLU30	107.90	57.71	26.49	34.96	
LEU31	121.21	54.92	39.28	24.20	α:22.07

GLY_32_	107.37	43.87		
CYS_33_	117.92	56.11	33.55	
ASP_34_	119.77	53.49	37.87	
ALA_35_	121.58	50.23	16.27	
VAL_36_	117.53	59.61	29.45	γ1:17.82, γ2:18.46

Table S5. Proton chemical shift assignments for turgencin B$_{Mox2}$ in water.

Residue	H (ppm)	Hα(ppm)	Hβ (ppm)	Hγ(ppm)	Others (ppm)
GLY_1_	7.63	3.65, 3.77	-	-	-
ILE_2_	8.65	3.94	1.79	1.19, 1.42, CH$_3$: 0.86	δCH$_3$: 0.81
LYS_3_	8.43	3.88	1.67, 1.76	1.32, 1.47	δCH$_2$:1.60, εCH$_2$: 2.89
GLU_4_	8.41	3.82	1.94, 1.98	2.17, 2.25	-
MET_5_	8.01	4.20	2.21, 2.28	2.84, 3.01	εCH$_3$: 2.58
LEU_6_	8.50	3.97	1.420, 1.749	1.74	δCH$_3$: 0.75, 0.77
CYS_7_	7,83	4.20	2.820, 3.254	-	-
ASN_8_	8.57	4.20	2.701, 2.748	-	-
MET_9_	8.22	4.14	2.24	2.73, 3.02	εCH$_3$: 2.57
ALA_10_	7.86	4.21	1.48	-	-
CYS_11_	8.01	4.27	3.04, 3.07		-
ALA_12_	8.22	3.73	1.42	-	-
GLN_13_	7.55	4.19	2.06, 2.20	2.40, 2.48	εNH$_2$: 6.85, 7.31
THR_14_	7.43	4.50	4.26	1.16	-
VAL_15_	8.81	4.09	2.09	0.98, 1.04	-
CYS_16_	8.13	4.89	2.76, 3.31	-	-
LYS_17_	7.23	3.99	1.70	1.30	δCH$_2$:1.60, εCH$_2$: 2.90
LYS_18_	8.13	4.17	1.70, 1.80	1.31	δCH$_2$:1.60, εCH$_2$: 2.89
SER_19_	7.77	4.37	3.76, 3.83	-	-
GLY_20_	8.18	3.82, 4.12	-	-	-
GLY_21_	8.62	3.85, 4.44	-	-	-

PRO22	-	4.26	1.87, 2.30	1.90, 1.98	δCH2: 3.54, 3.68
LEU23	8.46	4.09	1.34, 1.70	1.60	δCH3: 0.80, 0.84
CYS24	7.50	4.19	3.16, 3.21	-	-
ASP25	8.39	4.25	2.62, 2.67	-	-
THR26	8.34	3.86	4.08	1.17	-
CYS27	7.56	4.16	3.01, 3.36	-	-
GLN28	8.29	3.93	1.99, 2.02	2.22, 2.61	-
ALA29	8.38	4.02	1.41	-	-
ALA30	7.64	4.15	1.46	-	-
CYS31	7.49	4.55	3.00, 3.08	-	-
LYS32	7.63	4.03	1.79, 1.85	1.36, 1.49	δCH2:1.59, εCH2: 2.86
ALA33	7.57	4.21	1.37	-	-
LEU34	7.61	4.15	1.45, 1.75	1.78	δCH3: 0.78, 0.82
GLY35	7.93	3.78, 3.87	-	-	terminal-NH2: 7.05, 7.21

Table S6. Carbon chemical shift assignments for turgencin B$_{Mox2}$ in water.

Residue	N (ppm)	Cα(ppm)	Cβ (ppm)	Cγ(ppm)	Others (ppm)
GLY1	-	61.014	-	-	-
ILE2	122.15	60.82	35.45	14.68, 25.64	δCH3: 10.32
LYS3	120.82	57.24	29.27	22.65	δCH2: 26.37 εCH2: 39.28
GLU4	120.90	57.43	26.15	33.18	-
MET5	118.83	55.76	23.13	48.73	εCH3: 36.56
LEU6	121.07	55.31	38.68	23.92	δCH3: 19.85, 22.68
CYS7	121.22	57.19	32.11	-	-
ASN8	120.64	54.04	35.91	-	-
MET9	120.49	55.60	22.93	47.84	εCH3: 36.547
ALA10	122.84	52.64	14.45	-	-
CYS11	116.93	54.80	35.20	-	-
ALA12	123.91	52.69	15.50	-	-
GLN13	111.92	53.47	27.05	31.25	δCO: 177.40
THR14	108.63	57.095	67.66	18.38	-
VAL15	118.30	61.24	29.56	17.42, 19.53	-
CYS16	116.07	52.91	41.12	-	-

LYS_17_	120.89	56.09	30.06	22.133	δCH₂: 26.35 εCH₂: 39.32
LYS_18_	117.66	54.22	29.95	22.18	δCH₂: 26.34 εCH₂: 39.29
SER_19_	113.19	55.42	61.55	-	-
GLY_20_	108.86	42.22		-	-
GLY_21_	110.51	42.04		-	-
PRO_22_	-	62.77	29.46	24.59	δCH₂: 47.00
LEU_23_	117.91	55.08	38.44	24.45	δCH₃: 20.31, 22.08
CYS_24_	119.23	55.88	36.38	-	-
ASP_25_	120.78	54.79	36.90	-	-
THR_26_	116.55	63.82	66.02	18.78	-
CYS_27_	123.34	58.41	35.90	-	-
GLN_28_	116.81	56.55	25.79	32.02	-
ALA_29_	123.12	52.24	15.11	-	-
ALA_30_	121.61	51.88	14.65	-	-
CYS_31_	115.49	52.02	32.63	-	-
LYS_32_	119.51	55.41	29.82	22.31	δCH₂: 26.24, εCH₂: 39.20
ALA_33_	121.34	50.37	15.71	-	-
LEU_34_	118.72	53.19	39.37	23.84	δCH₃: 20.26, 23.08
GLY_35_	108.32	42.36	-	-	-

Table S7. Peptides sharing the same disulfide connectivity as turgencin B (C1-C6/C2-C5/C3-C4).

AMP	#aa	Sequence and protein data bank (PDB) ID	Species	Ref.
Turgencin B	35	GIKEMLCNMACAQTVCKKSGGPLCDTCQAACKAL-NH₂	*Synoicum turgens* (ascidian)	This work
TEWP	36	pEKKCPGRCTLKCGKHERPTLPYNCGKYICCVPVKVK (PDB: 2B5B)	*Caretta caretta* (Loggerhead sea turtle)	[1]
Pelovaterin	42	DDTPSSRCGSGGWGPCLPIVDLLCIVHVTVGCSGGFG CCRIG (PDB: 2JR3)	*Pelodiscus sinensis* (Chinese softshell turtle)	[2]
Caenopore-5	81	RSALSCQMCELVVKKYEGSADKDANVIKKDFDAECK KLFHTIPFGTRECDHYVNSKVDPIIHELEGGTAPKDVC TKLNECP (PDB: 2JS9)	*Caenorhabditis elegans* (nematode)	[3]
NK-lysin	78	GLICESCRKIIQKLEDMVGPQPNEDTVTQAASRVCDK MKILRGVCKKIMRTFLRRISKDILTGKKPQAICVDIKIC KE (PDB: 1NKL)	*Sus scrofa* (pig)	[4]
RTD-1	18	GFCRCLCRRGVCRCICTR (cyclic, 3 DSB + head to tail peptide bonds) (PDB: 2LYF)	*Macaca mulatta* (Rhesus monkey)	[5], [6]
Viscotoxin A3	46	KSCCPNTTGRNIYNACRLTGAPRPTCAKLSGCKIISGST CPSDYPK (PDB: 1ED0)	*Viscum album* (mistletoe)	[7] (sequence), [8] (activity)

References

1. Chattopadhyay, S.; Sinha, N. K.; Banerjee, S.; Roy, D.; Chattopadhyay, D.; Roy, S., Small cationic protein from a marine turtle has β-defensin-like fold and antibacterial and antiviral activity. *Proteins* **2006,** 64, 524-531.
2. Lakshminarayanan, R.; Vivekanandan, S.; Samy, R. P.; Banerjee, Y.; Chi-Jin, E. O.; Teo, K. W.; Jois, S. D. S.; Kini, R. M.; Valiyaveettil, S., Structure, self-assembly, and dual role of a β-defensin-like peptide from the Chinese soft-shelled turtle eggshell matrix. *J. Am. Chem. Soc.* **2008,** 130, 4660-4668.
3. Mysliwy, J.; Dingley, A. J.; Stanisak, M.; Jung, S.; Lorenzen, I.; Roeder, T.; Leippe, M.; Grötzinger, J., Caenopore-5: The three-dimensional structure of an antimicrobial protein from *Caenorhabditis elegans*. *Developmental & Comparative Immunology* **2010,** 34, 323-330.
4. Liepinsh, E.; Andersson, M.; Ruysschaert, J.-M.; Otting, G., Saposin fold revealed by the NMR structure of NK-lysin. *Nature Structural Biology* **1997,** 4, 793-795.
5. Tang, Y.-Q.; Yuan, J.; Ösapay, G.; Ösapay, K.; Tran, D.; Miller, C. J.; Ouellette, A. J.; Selsted, M. E., A cyclic antimicrobial peptide produced in primate leukocytes by the ligation of two truncated α-defensins. *Science* **1999,** 286, 498-502.
6. Selsted, M. E., θ-defensins: Cyclic antimicrobial peptides produced by binary ligation of truncated α-defensins. *Current Protein & Peptide Science* **2004,** 5, 365-371.
7. Romagnoli, S.; Ugolini, R.; Fogolari, F.; Schaller, G.; Urech, K.; Giannattasio, M.; Ragona, L.; Molinari, H., NMR structural determination of viscotoxin A3 from *Viscum album L*. *Biochem. J.* **2000,** 350, 569-577.
8. Giudici, A. M.; Regente, M. C.; Villalaín, J.; Pfüller, K.; Pfüller, U.; De La Canal, L., Mistletoe viscotoxins induce membrane permeabilization and spore death in phytopathogenic fungi. *Physiologia Plantarum* **2004,** 121, 2-7.

Paper II

Article

Antimicrobial Activity of Small Synthetic Peptides Based on the Marine Peptide Turgencin A: Prediction of Antimicrobial Peptide Sequences in a Natural Peptide and Strategy for Optimization of Potency

Ida K. Ø. Hansen [1,*] , **Tomas Lövdahl** [2] , **Danijela Simonovic** [2] , **Kine Ø. Hansen** [3] ,
Aaron J. C. Andersen [1] , **Hege Devold** [1] , **Céline S. M. Richard** [1] , **Jeanette H. Andersen** [3] ,
Morten B. Strøm [2] and **Tor Haug** [1,*]

[1]   Norwegian College of Fishery Science, Faculty of Biosciences, Fisheries and Economics, UiT The Arctic
      University of Norway, 9037 Tromsø, Norway; ajca@dtu.dk (A.J.C.A.); hege.devold@uit.no (H.D.);
      celine.s.richard@uit.no (C.S.M.R.)
[2]   Department of Pharmacy, Faculty of Health Sciences, UiT The Arctic University of Norway, 9037 Tromsø,
      Norway; tlovdahl88@hotmail.com (T.L.); danijela.simonovic@uit.no (D.S.); morten.strom@uit.no (M.B.S.)
[3]   Marbio, Faculty of Biosciences, Fisheries and Economics, UiT The Arctic University of Norway, Breivika,
      N-9037 Tromsø, Norway; kine.o.hanssen@uit.no (K.Ø.H.); jeanette.h.andersen@uit.no (J.H.A.)
*   Correspondence: ida.k.hansen@uit.no (I.K.Ø.H.); tor.haug@uit.no (T.H.)

check for
updates

Abstract: Turgencin A, a potent antimicrobial peptide isolated from the Arctic sea squirt *Synoicum turgens*, consists of 36 amino acid residues and three disulfide bridges, making it challenging to synthesize. The aim of the present study was to develop a truncated peptide with an antimicrobial drug lead potential based on turgencin A. The experiments consisted of: (1) sequence analysis and prediction of antimicrobial potential of truncated 10-mer sequences; (2) synthesis and antimicrobial screening of a lead peptide devoid of the cysteine residues; (3) optimization of in vitro antimicrobial activity of the lead peptide using an amino acid replacement strategy; and (4) screening the synthesized peptides for cytotoxic activities. In silico analysis of turgencin A using various prediction software indicated an internal, cationic 10-mer sequence to be putatively antimicrobial. The synthesized truncated lead peptide displayed weak antimicrobial activity. However, by following a systematic amino acid replacement strategy, a modified peptide was developed that retained the potency of the original peptide. The optimized peptide **StAMP-9** displayed bactericidal activity, with minimal inhibitory concentrations of 7.8 µg/mL against *Staphylococcus aureus* and 3.9 µg/mL against *Escherichia coli*, and no cytotoxic effects against mammalian cells. Preliminary experiments indicate the bacterial membranes as immediate and primary targets.

Keywords: Arctic; ascidian; antimicrobial; synthetic; peptide; *Synoicum turgens*

1. Introduction

Antibiotic-resistant bacteria are emerging as a major global health problem and are considered one of the biggest future medical threats to humankind. Many pathogenic bacteria previously susceptible to antibiotics are now becoming nearly impossible to combat [1–3]. The increasing number of immunocompromised patients (AIDS, cancer and transplant recipient patients) and the rising number of elderly further aggravate the problem, as they often need effective antibiotics to treat infections caused by opportunistic bacteria [4–6]. Currently, infections caused by antibiotic-resistant bacteria are estimated to cause more than 700,000 deaths annually and the number is rising [7]. Due to a long-term

focus on the modification of existing conventional antibiotics by the pharmaceutical industry, rather than development of novel treatment options, modern medicine is now in dire need of a solution to the problem [8]. Antimicrobial peptides have, in the last three decades, gained increasing attention as promising candidates to solve the challenges of antibiotic resistance [9].

Natural AMPs usually consist of less than 60 amino acid residues, which occur mainly in the natural L-configuration, and have molecular masses below 10 kDa [10,11]. AMPs normally have a substantial portion of hydrophobic residues (≥30%) and most are cationic, with a net charge of +2 to +9 [12]. The segregated arrangement of the hydrophobic and cationic amino acids gives AMPs an amphipathic nature, a feature allowing interaction with and embedding into anionic microbial cell membranes, causing bacterial death [13]. Thus, the presence of positive charges (mainly caused by the cationic amino acids Lys and Arg) in combination with hydrophobic residues have a fundamental role in the mechanism of action of these potent compounds [14]. Compared to conventional antibiotics, AMPs are substantially less prone to resistance development due to their mode of action, and they exert their killing activity faster (within seconds to minutes) [15]. AMPs often show a wide range of antimicrobial bioactivities, acting as antibacterial, antifungal and antiparasitic agents, and are often highly membrane-selective [11]. Furthermore, linear AMPs can easily be synthesized due to their relatively small size [16]. In this regard, the possibility for AMPs to overtake the title of next-generation antibiotics looks realistic [17]. However, to date, no AMP has reached the antibiotic market, although many AMPs are in clinical trials [18]. The biggest challenges faced in the development of AMPs into drugs are high production costs (especially for large and disulfide-rich peptides), lack of proteolytic stability, and unfavorable toxicology profile when administered systemically [3,17]. To overcome these issues, the pharmacophore of AMPs and the structural features causing toxicity must be identified to enable the production of peptides with improved therapeutic indexes. Furthermore, pharmacophore identification will lower production costs, as only substructures of the peptides need to be produced. This knowledge can be acquired through synthesis of analogues followed by bioactivity testing and structure–activity relationship studies. In fact, recent studies have shown that potent, short (<15 amino acids), linear AMPs (devoid of cysteines), can be successfully produced [3,19]. Certain characteristics have also proved to play a critical role for the activity of these peptides, like the balance between the positive charge, hydrophobicity, and content of lipophilic bulky residues such as Trp [19]. These peptides have shown effectiveness against bacterial infections in vivo [20], as well as improved stability in serum [21]. By experience, shortened peptides derived from natural AMPs can retain relevant biological activities [22,23]. Consequently, they are excellent candidates as lead peptides for developing novel antimicrobial drugs [2].

Recently, we have characterized two novel AMPs, turgencin A and turgencin B, from the Arctic sea squirt *Synoicum turgens* (Phipps, 1774) [24]. The turgencins are composed of 35–36 amino acid residues with six Cys residues engaged in three disulfide bridges with connectivity of Cys1-Cys6, Cys2-Cys5, and Cys3-Cys4, making them challenging to synthesize and explore as drug leads. The aim of the present study was to make a truncated AMP derivative based on turgencin A with drug lead potential. We recognized an internal stretch (residues 18–27) of turgencin A having an unusual amino acid PGGW central core, flanked by two lysine residues on each end, making it highly cationic. We therefore hypothesized that this 10-residue-long sequence could be used for the generation of a novel antimicrobial lead peptide. The antimicrobial potential of this first lead peptide **StAMP-1** was verified using publicly accessible and pre-trained AMP prediction tools that rely on various machine learning algorithms [25,26] before being synthesized and tested. First, a single-cysteine residue within the sequence was replaced by alanine to avoid potential and unpredictable dimerization. Subsequently, an amino acid replacement strategy was chosen to improve the antimicrobial activity of **StAMP-1**. This involved enrichment of the central core (PGGW) of the peptide with Trp residues, causing an increase in the hydrophobic ratio while leaving the cationic residues unchanged (i.e., ensure a high net positive charge). After optimizing hydrophobicity and exploring sequence effects through the preparation of peptides **StAMP-2-8**, an increase in antimicrobial potency was further explored by

synthesizing two peptides, **StAMP-9** and **StAMP-10**, where all four Lys residues were substituted by Arg. Finally, the effects on the antimicrobial activity of Leu and Trp as lipophilic residues was compared by synthesis of **StAMP-11**.

2. Results and Discussion

2.1. Sequence Analysis and AMP Prediction

Turgencin A is a potent AMP consisting of 36 amino acid residues with six cysteines forming three intramolecular disulfide bridges. Sequence homology with turgencin B indicates that these bridges are formed between Cys8-Cys33, Cys12-Cys29 and Cys17-Cys26 (Figure 1) [24]. By experience, short peptide segments derived from larger natural AMPs can partly be responsible for the detected activity [22,23,27], and thus be promising lead sequences for drug development. By visual inspection and similarity searches in various AMP databases (for review, see Liu et al. [28]), we recognized a cationic region within turgencin A (sequence 18–27, GKKPGGWKCK) with a 4-amino acid central core sequence PGGW (Figure 1) which was found in some abaecins, a well-known family of AMPs found in insects [29]. Hydrophobic Trp residues are widely accepted as contributors to the bioactivity of AMPs [30,31], and both Pro and Gly residues are known to break up α-helical sequences [32]. Turgencin A also contains an N-terminal Gly residue, which is found to be beneficial in many AMPs [33,34]. We therefore hypothesized that this 10-residue sequence could be used for the generation of novel antimicrobial lead peptides. To support our hypothesis, a linear version of turgencin A (denoted turgencin A_{lin}), where all Cys were replaced by Ala, was examined using the online prediction tool of the collection of antimicrobial peptides ($CAMP_{R3}$) web server (Figure 1). $CAMP_{R3}$ contains information on conserved AMP sequence signatures captured as patterns and Hidden Markov Models (HMMs), and currently the database contains 10,247 sequences and 114 family-specific signatures of AMPs [25].
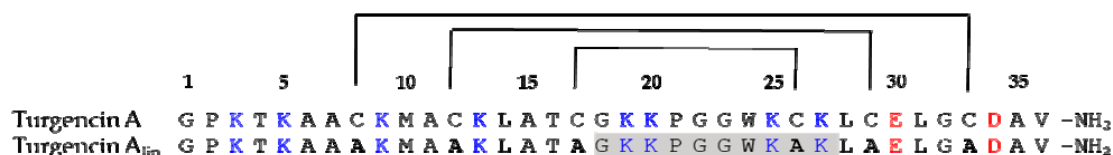
Figure 1. Amino acid sequences and disulfide bond connectivity of turgencin A and its linear derivative turgencin A_{lin} where all Cys residues were replaced by Ala (shown in bold). The potential 10-residue lead peptide sequence containing the PGGW core is shaded in grey.

The antimicrobial potential of shortened, overlapping peptides (10-mers), using a sliding window strategy, was predicted by utilizing all four available prediction models: support vector machine (SVM), random forests (RF), artificial neural network (ANN), and discriminant analysis (DA). SVM, RF and DA predict and state a peptide's probability of having antimicrobial properties in values between 0 (low probability) and 1 (high probability), with values above 0.5 defined as being most likely to be bioactive, whereas the ANN model makes a qualitative statement of either AMP or non-AMP (NAMP). The antimicrobial potential of these peptides was also predicted using a different SVM model available through ADAM, another comprehensive AMP database, containing 7007 unique sequences. In this model, a higher value indicates higher probability for antimicrobial activity. [26]. Out of the 27 sequences analyzed, only one sequence (sequence 18–27, GKKPGGWKAK) was predicted to be antimicrobial by all four models in AMP_{R3}, including the RF classifier, and by the SVM model in ADAM (Table 1). Although several other peptides were predicted to be antimicrobial by the SVM, DA and ANN models, only one additional sequence (the neighboring sequence, 19–28) was predicted to be active by the RF model (RF value > 0.5). A number of AMP prediction tools have been designed attempting to discriminate AMPs from non-AMPs (NANP) (reviewed by Liu et al. [28]). Among ten web-based AMP prediction tools, the $CAMP_{R3}$ (RF) tool was recently shown to outperform other web-based prediction models, followed by $CAMP_{R3}$ (SVM) and ADAM (SVM) [35]. The Lys residues, which are spread

through the turgencin A sequence, provide a positive charge to the peptide. Thus characteristic is known to be important for the activity of most AMPs. Of notice, the two 10-mer sequences predicted to be active by the RF model were also the two peptides with the highest net positive charge (+4) (Table 1). Furthermore, the peptide sequence, 18–27 (GKKPGGWKAK), was calculated to have a Boman index of 1.52, the highest among all the predicted peptides, but still in the middle range among AMPs [36]. The Boman Index is an estimate of protein-binding potential, calculated on the basis of cyclohexane-to-water partition coefficient of the respective amino acid side chains divided by the total number of amino acid residues within the peptide [36]. A high index value (>2.48) indicates a multifunctional peptide with high binding potential (e.g., hormones). A low index value (≤1) indicates a potential AMP with less side effects (e.g., low hemolytic activity) [36]. Based on the above predictions, the C-terminally amidated sequence 18–27 (GKKPGGWKAK; hereafter named **StAMP-1**) was selected as the first lead peptide to be synthesized, screened for antimicrobial activity, and further optimized employing an amino acid replacement strategy. Through single-residue substitutions, additional peptides were rationally designed with the purpose of increasing the hydrophobic ratio, i.e., overall hydrophobicity, and to investigate sequence specific effects. This resulted in the production of ten additional truncated turgencin A analogs, **StAMP-2-11**.

Table 1. Characteristics and in silico antimicrobial activity prediction of 10-mer peptide sequences modelled from Turgencin A$_{lin}$; a linear version of turgencin A where the Cys residues were replaced by Ala. The highlighted sequence 18–27 (GKKPGGWKAK) in bold was the only sequence that was predicted to be antimicrobial by all four in silico models.

Peptide Region	Sequence	Net Charge	Hydro-Phobic Ratio (%)	Boman Index (kcal/mol)	CAMP$_{R3}$ [1]				ADAM [2]
					SVM	RF	ANN	DA	SVM
1–10	GPKTKAAAKM	+3	40	1.04	1.000	0.479	AMP	0.681	1.49
2–11	PKTKAAAKMA	+3	50	0.96	0.548	0.439	NAMP	0.343	1.95
3–12	KTKAAAKMAA	+3	60	0.78	0.131	0.443	AMP	0.325	2.53
4–13	TKAAAKMAAK	+3	60	0.78	0.972	0.439	AMP	0.170	2.53
5–14	KAAAKMAAKL	+3	70	0.03	0.478	0.428	AMP	0.797	2.59
6–15	AAAKMAAKLA	+2	80	−0.70	0.980	0.363	AMP	0.785	2.64
7–16	AAKMAAKLAT	+2	70	−0.26	0.989	0.358	AMP	0.483	2.41
8–17	AKMAAKLATA	+2	70	−0.26	0.947	0.325	AMP	0.312	2.41
9–18	KMAAKLATAG	+2	60	−0.17	0.330	0.281	AMP	0.254	2.13
10–19	MAAKLATAGK	+2	60	−0.17	0.651	0.270	AMP	0.135	2.13
11–20	AAKLATAGKK	+3	50	0.61	0.615	0.425	AMP	0.786	2.07
12–21	AKLATAGKKP	+3	40	0.79	0.751	0.376	AMP	0.535	1.29
13–22	KLATAGKKPG	+3	30	0.87	0.244	0.377	AMP	0.647	1.58
14–23	LATAGKKPGG	+2	30	0.23	0.736	0.379	AMP	0.649	2.16
15–24	ATAGKKPGGW	+2	30	0.49	0.075	0.282	AMP	0.781	2.52
16–25	TAGKKPGGWK	+3	20	1.22	0.880	0.398	AMP	0.591	2.53
17–26	AGKKPGGWKA	+3	30	0.78	0.490	0.427	AMP	0.930	2.85
18–27	**GKKPGGWKAK**	+4	20	1.52	0.968	0.559	AMP	0.884	2.85
19–28	KKPGGWKAKL	+4	30	1.12	0.165	0.566	AMP	0.815	2.61
20–29	KPGGWKAKLA	+3	40	0.38	0.027	0.448	AMP	0.689	2.44
21–30	PGGWKAKLAE	+1	40	0.51	0.017	0.190	AMP	0.018	2.00
22–31	GGWKAKLAEL	+1	50	0.02	0.325	0.238	AMP	0.041	2.37
23–32	GWKAKLAELG	+1	50	0.02	0.444	0.241	AMP	0.041	2.37
24–33	WKAKLAELGA	+1	60	0.21	0.205	0.252	NAMP	0.024	2.04
25–34	KAKLAELGAD	0	50	0.00	0.004	0.293	NAMP	0.002	1.47
26–35	AKLAELGADA	−1	60	0.28	0.281	0.329	NAMP	0.003	1.44
27–36	KLAELGADAV	−1	60	0.80	0.799	0.373	NAMP	0.007	0.56

[1] CAMP$_{R3}$: collection of anti-microbial peptides; SVM: support vector machines; RF: random forests; ANN: artificial neural networks; and DA: discriminant analysis. [2] ADAM: a database of AMPs.

2.2. Peptide Design and Antibacterial Screening

A high net-positive charge is vital for many cationic AMPs, predominantly with regard to initial electrostatic interaction with the anionic microbial cell surfaces and subsequent disruption of the bacterial cell membrane or intracellular translocation [30,37,38]. The lead peptide **StAMP-1** and all

proceeding peptides were therefore synthesized with an amidated C-terminal end, which provides an increase in net positive charge by +1 by masking the otherwise anionic C-terminal carboxylate group. The original turgencin A peptide is also amidated C-terminally [24]. An amidated C-terminus can also provide resistance to the action of carboxypeptidases, as shown for the well-known AMP magainin [39]. An overview of the synthesized **StAMP-1-11** peptides and their physicochemical characteristics is presented in Table 2.

Table 2. Sequences and physicochemical properties of the synthesized **StAMP-1-11** peptides. **StAMP-1** corresponds to the C-terminal amidated first lead peptide sequence 18–27.

Peptide	Sequence [1]	Monoisotopic Mass (Da)		Net Charge	Boman Index (kcal/mol)	Hydro-Phobic Ratio (%)	Rt [3]
		Theoretical	Measured [2]				
StAMP-1	GKKPGGWKAK-NH2	1054.64	1054.64	+5	1.52	20	0.40
StAMP-2	GKKWGGWKAK-NH2	1143.67	1143.67	+5	1.29	30	1.75
StAMP-3	GKKPWGWKAK-NH2	1183.70	1183.70	+5	1.38	30	2.17
StAMP-4	GKKPGWWKAK-NH2	1183.70	1183.70	+5	1.38	30	2.05
StAMP-5	GKKWWGWKAK-NH2	1272.72	1272.72	+5	1.15	40	5.21
StAMP-6	GKKWGWWKAK-NH2	1272.72	1272.72	+5	1.15	40	5.39
StAMP-7	GKKPWWWKAK-NH2	1312.76	1312.76	+5	1.24	40	5.70
StAMP-8	GKKWWWWKAK-NH2	1401.78	1401.78	+5	1.01	50	8.77
StAMP-9	GRRPWWWRAR-NH2	1424.78	1424.78	+5	4.99	40	6.65
StAMP-10	GRRWWWWRAR-NH2	1513.81	1513.81	+5	4.76	50	9.20
StAMP-11	GRRPLLLRAR-NH2	1205.79	1205.79	+5	4.21	40	2.54

[1] Amino acid substitutions are shown in bold, [2] Measured by high-resolution mass spectrometry, [3] Retention time (min) on an analytical RP-HPLC C$_{18}$-column using a fixed mobile phase gradient.

As predicted by four models in the CAMP$_{R3}$ web server, **StAMP-1** displayed antibacterial activity in vitro (Table 3). However, the prediction models do not predict the exact antimicrobial potency of a given peptide sequence, they only predict the probability of being an AMP. As shown in Table 3, **StAMP-1** displayed low antibacterial activity (MIC = 250 µg/mL) and only against two out of seven test strains: the Gram-positive (G+) bacteria *Bacillus megaterium* and *Corynebacterium glutamicum*. The reason for the weak antibacterial activity was suspected to be a too low hydrophobic ratio (20%, Table 2). According to the APD3 database, the average hydrophobic ratio of AMPs deposited in the database is about 41.5% [40]. Higher hydrophobicity would ease the penetration of the peptide into the lipid environment of the microbial membranes. However, the hydrophobicity should not be too high, making the peptide insoluble in aqueous environments. On the other hand, according to a recent study [19], short AMPs have different features compared to larger AMPs. Short AMPs do not seem to need structural requirements like high α-helicity, a specific hydrophobic moment, an explicit partitioning of charge and hydrophobicity, or a high frequency of particular amino acids or amino acid pairs (e.g., Arg-Trp or Arg-Arg pairs) within the peptide sequence. For short cationic AMPs, a balance between positive charge and hydrophobicity seems to be more important, and some, but not too many, Trp residues seem to be advantageous [19]. In silico prediction of antimicrobial activity of very short peptides may, therefore, currently be challenging.

The above-mentioned design of **StAMP-2-11** involved enrichment with one (**StAMP-2/3/4**) or two (**StAMP-5/6/7**) lipophilic tryptophan residues in the central core (PGGW) of the first lead peptide **StAMP-1** while leaving the cationic residues (positive charge) unchanged. The substitution of Pro4, Gly5 or Gly6 with a single Trp (**StAMP-2/3/4**) resulted in increased hydrophobic ratio (30%, Table 2) and increased antibacterial activity against three to four of seven bacterial strains, but still only activity against G+ bacteria (and fungi; discussed below) (Table 3). All three peptides (**StAMP-2/3/4**) were highly potent against *B. megaterium*, and out of these three peptides, **StAMP-4** was the overall most potent peptide, having a MIC value of 3.9 µg/mL against both *B. megaterium* and *C. glutamicum*.

Table 3. Antimicrobial activities of turgencin A and the synthesized **StAMP-1–11** peptides.

	Antimicrobial Activity (MIC; μg/mL) [1]									
	Gram-Pos					Gram-Neg		Fungi		
Peptide	Bm	Bs	Cg	Ml	Sa	Ec	Pa	Ap	Ca	Rh
Turgencin A [2]	0.5	1.5	1.5	8.0	23.3	3.0	5.9	92.6	46.3	23.2
StAMP-1	250	>250	250	>250	>250	>250	>250	>250	>250	>250
StAMP-2	3.9	125	31.3	250	>250	>250	>250	62.5	125	62.5
StAMP-3	3.9	>250	15.6	250	>250	>250	>250	62.5	125	62.5
StAMP-4	3.9	125	3.9	125	>250	>250	>250	62.5	62.5	31.3
StAMP-5	1.0	15.6	2.0	15.6	>250	31.3	250	31.3	31.3	15.6
StAMP-6	1.0	3.9	3.9	62.5	250	62.5	>250	62.5	62.5	31.3
StAMP-7	1.0	3.9	2.0	31.3	125	31.3	250	15.6	31.3	15.6
StAMP-8	3.9	7.8	7.8	15.6	125	62.5	125	7.8	15.6	15.6
StAMP-9	1.0	3.9	2.0	3.9	7.8	7.8	31.3	31.3	31.3	15.6
StAMP-10	3.9	7.8	7.8	15.6	62.5	15.6	31.3	62.5	62.5	15.6
StAMP-11	7.8	>250	31.3	62.5	>250	>250	>250	250	125	31.3
Indolicidin	3.1	6.3	1.6	12.5	12.5	25.0	>250	25.0	100	25.0
Oxytetracycline	0.6	10.0	0.2	1.3	0.04	1.3	2.5	n.t [3]	n.t	n.t.
Triclosan	n.t	n.t	n.t	n.t	n.t	n.t	n.t	3.1	3.1	1.6

[1] Microbial strains: Bm—*Bacillus megaterium*, Bs—*Bacillus subtilis*, Cg—*Corynebacterium glutamicum*, Ml—*Micrococcus luteus*, Sa—*Staphylococcus aureus*, Ec—*Escherichia coli*, Pa—*Pseudomonas aeruginosa*, Ap—*Aurobasidium pollulans*, Ca—*Candida albicans*, Rh—*Rhodotorula* sp. [2] Antibacterial data for turgencin A against Bs, Cg, Sa, Ec and Pa are derived from Hansen et al. [24]. [3] nt: Not tested.

Introducing two Trp residues in the PGGW core (**StAMP-5/6/7**), and thereby increasing the hydrophobicity to 40% (Table 2), resulted in further improved antibacterial activity and measurable activity against Gram-negative (G-) bacteria. **StAMP-7**, having a total of three consecutive Trp residues, was overall the most potent peptide in this series, and the only peptide showing antibacterial activity against all test strains to date. **StAMP-7** displayed MIC values in the range of 1.0–125 μg/mL against G+ strains and MIC values of 31.3–250 μg/mL against G- strains (Table 3). The least sensitive bacterial strains within each class were *Staphylococcus aureus* (G+) and *Pseudomonas aeruginosa* (G-), in which *P. aeruginosa* often is the least susceptible strain to many AMPs [24]. Gly does not have a side chain and therefore provides increased flexibility within the sequence of AMPs. This feature does not seem to be of importance to **StAMP-7**, in which both Gly residues in the PGGW core were replaced by Trp. The substitution of Pro4 with Trp in both **StAMP-5** and **StAMP-6** resulted in a lower increase in antimicrobial activity and may indicate a role of Pro4 in peptide folding. Among the two Gly residues, the replacement of Gly5 with Trp (resulting in **StAMP-5**) seemed to result in an improvement in antibacterial activity compared to replacement of Gly6 with Trp (resulting in **StAMP-6**). In general, the antimicrobial activity increased when the overall hydrophobicity of the peptides increased, as measured by RP-HPLC and as shown by the in silico calculations (Table 2). However, increasing the hydrophobicity further by substituting all amino acids in the central core with Trp, giving **StAMP-8** with four consecutive Trp's and a WWWW core, did not result in a major increase in antibacterial activity except against *P. aeruginosa* (MIC = 125 μg/mL, Table 3). Other studies have shown that there should be a balance between positive charge, hydrophobicity and the amount of tryptophan in small peptides. Peptides with an imbalance between these properties have proven to give weak activity [19]. A hydrophobicity window for the optimal antibacterial activity of AMPs has also been observed by others [41].

After optimizing hydrophobicity and positioning of the inserted tryptophan residues, an attempt to further increase the antimicrobial potential of **StAMP-7** was performed by synthesizing a derivative where all four Lys residues were substituted by Arg. The results for **StAMP-9** where Lys2, Lys3, Lys8 and Lys10 were replaced by Arg resulted in 4-fold increase in antibacterial activity against *Escherichia coli* and an 8-fold increase against *P. aeruginosa*, as well as a 16-fold increase in activity against

S. aureus. Overall, the MIC values of the Arg-enriched peptide **StAMP-9** ranged from 1.0 to 31.3 µg/mL against all seven bacterial test strains. An increase in antimicrobial activity when replacing Lys with Arg is reported for other Trp-rich AMPs [14]. The hydrophobicity of **StAMP-9** was further increased by replacing Pro4 with Trp, resulting in **StAMP-10** with a WWWW core and a hydrophobic ratio of 50% (Table 2). As observed above for **StAMP-8**, this did not result in an improvement in antimicrobial activity, but the contrary, except against *P. aeruginosa* where the activity of **StAMP-9** and **StAMP-10** were similar (Table 3). Leu is, in some scales, reported to supersede Trp in hydrophobicity [42,43], and as a final peptide we made the Leu analog of the most potent peptide **StAMP-9,** resulting in the peptide **StAMP-11**. As shown in Table 3, **StAMP-11**, where all Trp residues were replaced by Leu, showed low antimicrobial activity, except against *B. megaterium* (MIC = 7.8 µg/mL). Thus, the putative high hydrophobicity of Leu was not enough to displace the more advantageous bulkiness of Trp with respect to antimicrobial activity.

When inspecting all the prepared 10-mer peptide sequences, it was noteworthy that the most potent antibacterial peptides within each series retained the Pro4 residue, as shown for **StAMP-4**, **StAMP-7**, and **StAMP-9**, and to some extent also **StAMP-11**. Pro is reported to be an α-helix breaker and that may serve a special function in the peptides by forming a hinge between the three first N-terminal GKK-residues and the following Trp enriched core sequence. In the present peptides, this may have been an important structural feature affecting the overall conformation of the Pro4 containing peptides upon interaction with bacterial membranes. In silico prediction of the antimicrobial potential of the designed 10-mer peptides showed that they were all proposed to be active (Table S1). However, whereas **StAMP-9** was the overall most potent peptide in the antimicrobial screening, **StAMP-8** showed the overall highest scores in the prediction. However, as previously mentioned, the prediction models do not predict the antimicrobial potency of a given sequence, only the probability of being antimicrobial.

2.2.1. Bacterial Killing Experiments

Overall, **StAMP-9** displayed the most potent antibacterial activity of the peptides that were synthesized (Table 3). To evaluate whether the peptide only inhibited growth (bacteriostatic) or killed the bacteria (bactericidal), **StAMP-9** was subjected to a bacterial killing experiment. The G+ bacteria *Bacillus subtilis* and the G- bacteria *E. coli* were selected for the experiment. As illustrated by the bar chart in Figure 2, no colony-forming units (CFU) were formed on the plates treated with overnight cultures that had been incubated with MIC (3.9 µg/mL for *B. subtilis* and 7.8 µg/mL for *E. coli*) or higher concentrations of the peptide. These results suggested that **StAMP-9** was bactericidal at MIC against both bacteria. Lower concentrations of **StAMP-9** produced approximately the same amount of CFU as the control (bacteria and water) after 24 h of incubation.
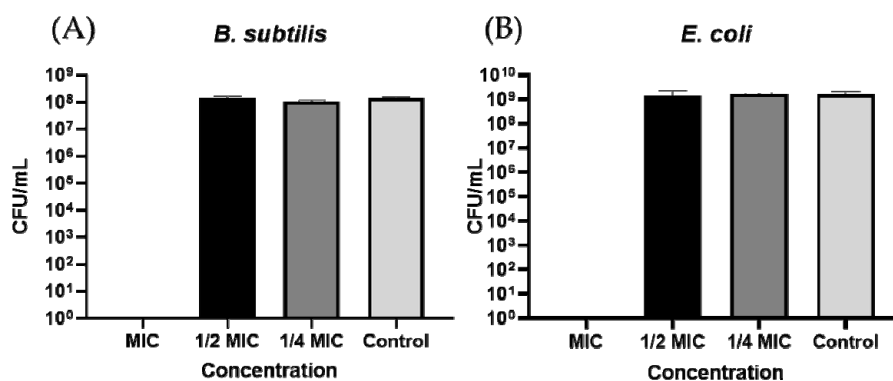

Figure 2. Bactericidal activity of **StAMP-9** against (**A**) *B. subtilis* and (**B**) *E. coli*. Colony-forming units (CFU) per mL were counted after treatment with MIC, 1/2 MIC, 1/4 MIC and no treatment (Control). Each bar presents the mean of three replicates ± SD.

2.2.2. Membrane Integrity and Viability Investigations

Based on the results from antibacterial screening and the bacterial killing experiment, **StAMP-6-10** were further studied for their immediate effect on the membrane integrity and viability on *B. subtilis* 168 and *E. coli* K12. In the integrity assay, both bacteria are carrying the luciferase *luc*GR gene within the plasmid pCSS962. When a compound disrupts the membrane, externally added D-luciferin can diffuse into the cells and function as a substrate for the luciferase enzyme. This, in turn, causes the emission of light as relative luminescence units (RLU), a signal whose strength is relative to the degree of membrane disruption in living cells. If the test compound affects the membrane sufficiently to cause bacterial death, the RLU signal will increase until the bacterial ATP storage is empty. At this time, the RLU signal will decrease in line with the decreasing ATP concentrations, as the enzymatic reaction gradually stops. D-luciferin does not cross intact membranes at a neutral pH [44]. Following membrane disruption, the RLU will reach its peak and start to decrease due to reduced cell numbers. In the assay setup used herein, RLU was measured over a period of 3 min. The short time period was selected as many membrane disruptive compounds usually affect the bacterial membranes immediately [24,45,46].

StAMP-6-7 affected the membrane integrity of *B. subtilis* at 50 µg/mL (RLU ~ 1.5) (Figure 3). However, since the light emission was not decreasing over time, the membrane disruption was not severe enough that the bacteria were killed within the measured time period. As both peptides gave MIC values of 3.9 µg/mL against the same strain, this might indicate that **StAMP-6-7** had an additional target in *B. subtilis*, or that the membrane disruption process took longer time than 3 min. Concentrations below 50 µg/mL did not affect the membrane.
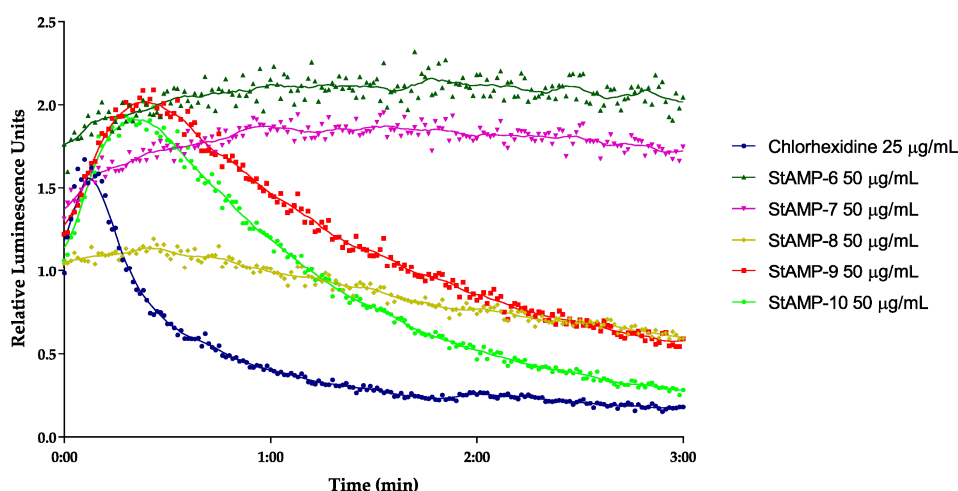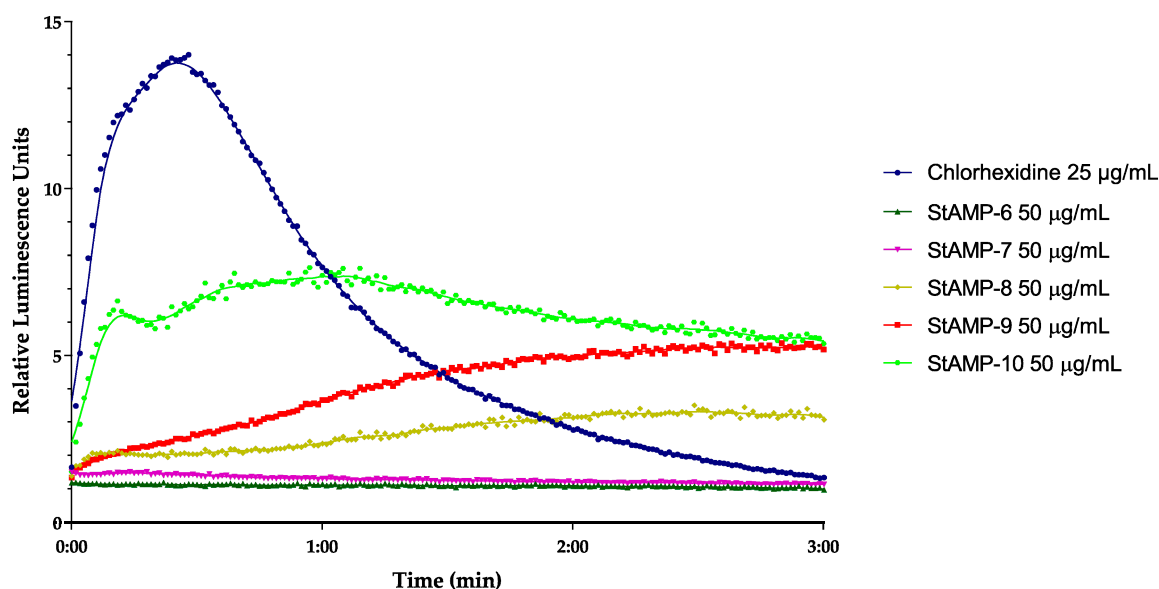

Figure 3. Kinetics of the antimicrobial effect on membrane integrity as measured by relative luminescence emission in *B. subtilis* 168 (pCSS962) in presence of D-luciferin. **StAMP-6-10** and the reference antimicrobial agent chlorhexidine was added to the bacteria. Chlorhexidine served as a positive (membranolytic) control and water as a negative (untreated) control. Each datapoint is the mean of three independent measurements normalized to the negative control.

StAMP-8-10 showed a stronger disruptive effect on bacterial membrane integrity of *B. subtilis* at 50 µg/mL. As shown in Figure 3, an increase in light emission was observed for all three peptides, but with a significantly weaker maximum peak intensity for **StAMP-8** compared to **StAMP-9-10**. The increasing light emission was followed by a continuing decrease in RLU. Compared to the control chlorhexidine, a bacterial agent known for its membrane disruptive properties [47], **StAMP-8-10** required a longer reaction time before disrupting the membrane. Chlorhexidine acetate has a molecular weight of 625.5 g/mol, making the concentration 25 µg/mL (40 µM) most comparable with the highest tested concentration for the peptides (50 µg/mL ~ 33–39 µM). As shown in Figure 3, it took approximately 30 s before a decrease in light intensity was observed in *B. subtilis* after adding **StAMP-8-10**. **StAMP-8**

affected the membrane at 25 μg/mL (Figure S1), **StAMP-9** at 12.5 μg/mL (Figure S2), and **StAMP-10** affected the membrane down to 6.3 μg/mL (Figure S3). These results strongly suggest that both chlorhexidine and **StAMP-8-10** had the bacterial membrane of *B. subtilis* as their main target, but the molecular mechanisms leading to membrane disruption might be different.

StAMP-6-7 had no effect on light emission at any of the concentrations tested when looking at the membrane integrity of *E. coli* (data not shown). **StAMP-8-10** affected the bacterial membrane of *E. coli* K12 at 50 μg/mL. As shown in Figure 4, all three peptides increased the light emission, but their membrane integrity effect on the *E. coli* was less prominent than the effect on *B. subtilis* when considering the decrease in light over time. The light emission was slowly decreasing after 1 min of **StAMP-10** exposure, but when exposed to **StAMP-8** and **StAMP-9** the light emission was not decreasing within the measured time period. **StAMP-8-9** influenced the *E. coli* membrane down to 25 μg/mL (Figures S4 and S5), and **StAMP-10** at 12.5 μg/mL (Figure S6).

A real-time cell viability assay was used to investigate the bactericidal effect of **StAMP-6-10**. *B. subtilis* 168 contains a chromosomally integrated *lux* operon, and *E. coli* K12 a plasmid-borne *lux* operon. Both strains emit light as long as they have an active metabolism. If a compound reduces the metabolic activity of the bacteria it will reduce the viability of the cells. The results of the viability assay are shown in Figures 5 and 6. These results independently confirmed the bactericidal effect observed in the membrane integrity assays. **StAMP-6-7** had a minor effect on the viability of both *B. subtilis* and *E. coli* at 50 μg/mL. The decrease in light emission caused by **StAMP-8-10** shown in both assays confirmed that these three peptides killed both strains at 50 μg/mL, but not as rapidly as the control chlorhexidine. The same activity observed for **StAMP-8-10** in the membrane integrity assay was also observed in both viability assays (Figures S7–S12). Chlorhexidine showed a dose-dependent activity in both integrity and viability assay against both bacteria tested (Figures S13–S16). Only at the lowest concentration tested (0.8 μg/mL), was there no observed membrane activity for these assays.

Figure 4. Kinetics of the antimicrobial effect on membrane integrity as measured by relative luminescence emission in *E. coli* K12 (pCSS962) in presence of D-luciferin. **StAMP-6-10** and the reference antimicrobial agent chlorhexidine was added to the bacteria. Chlorhexidine and water were used as positive and negative control. Each datapoint is the mean of three independent measurements normalized to the water control.
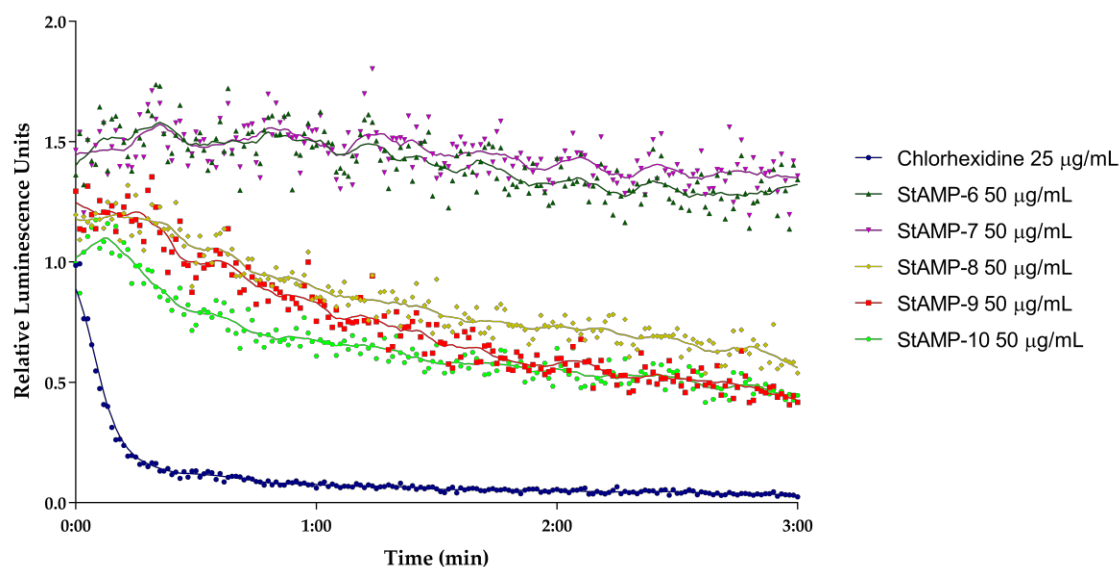
Figure 5. Kinetics of the antimicrobial effect on viability of *B. subtilis* 168 as measured by relative luminescence emission from the luxABCDE operon after adding **StAMP-6-10** to the bacteria. Chlorhexidine served as a positive control and water as a negative control. Each datapoint was the mean of three independent measurements normalized to the negative control.
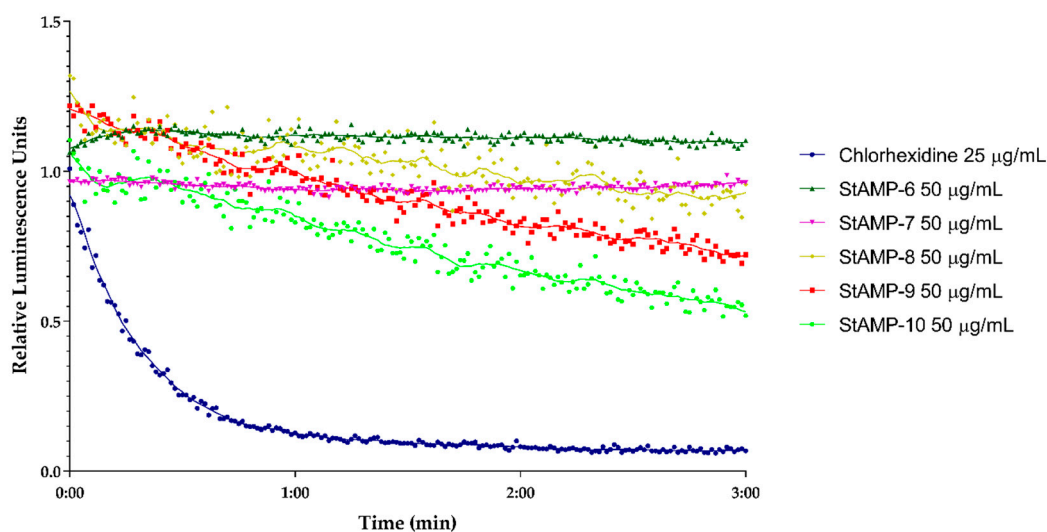
Figure 6. Kinetics of the antimicrobial effect on viability of *E. coli* K12 (pCGLS-11) as measured by relative luminescence emission from the *lux*CDABE operon after adding **StAMP-6-10**. Chlorhexidine served as a positive control and water as a negative control. Each datapoint was the mean of three independent measurements normalized to the negative control.

2.3. Antifungal Activity

The synthesized peptides were subjected to antifungal screening against the molds *Aureobasidium pullulans* and *Rhodotorula* sp., and the yeast *Candida albicans* (Table 3). The first lead peptide **StAMP-1** was inactive (MIC > 250 µg/mL) against all three fungal strains tested. As observed during the antibacterial screening, increased hydrophobicity of the peptides (due to Trp substitutions) generally increased the antifungal activity, with **StAMP-8** being the most potent peptide (MIC = 7.8–15.6 µg/mL) in this mutant series. In contrast to antibacterial activity, replacement of all Lys residues in **StAMP-7** with Arg, resulting in **StAMP-9,** did not improve the antifungal activity against the three fungal strains tested. Fungal membranes are more zwitterionic compared to the negatively charged bacterial membranes [48], and these differences naturally could make the membranes vulnerable to different antimicrobials.

2.4. Hemolytic, Cytotoxic and Anti-Inflammatory Properties

The peptides (**StAMP-1-11)** were assayed for hemolytic activity against sheep red blood cells, cytotoxic activity against the human melanoma cell line A2058 and the non-malignant human lung fibroblast cell line MRC-5, and their ability to inhibit LPS induced TNF-α production by the human acute leukemia monocytic THP-1 cell line. None of the synthesized peptides displayed any hemolytic activity (<1% hemolysis) against sheep red blood cells at concentrations up to 250 µg/mL. No cytotoxic or anti-inflammatory activities were detected for any of the peptides, even at the highest concentration tested (100 µg/mL). The results from these assays indicate that the peptides may be well tolerated in an in vivo setting.

3. Materials and Methods

3.1. Sequence Analysis and Peptide Design

The 36 amino acids sequence of turgencin A, a Cys-rich AMP isolated from the marine ascidian *S. turgens* [24], served as a starting point for the sequence analysis. All Cys residues were replaced by Ala prior to in silico prediction of antimicrobial potential of 10-residue sequences of the linear version of turgencin A, using the online prediction tool on the Collection of Anti-Microbial Peptides (CAMP$_{R3}$) server (http://www.camp3.bicnirrh.res.in/predict/) [25]. A sliding window strategy (using a window size of ten amino acid residues) was used to locate putative AMP stretches within the full peptide sequence. The peptide segments were analyzed by means of four prediction models: support vector machines (SVM), random forests (RF), artificial neural network (ANN), and discriminant analysis (DA). The antimicrobial potential of the peptides were also predicted using the SVM model in a database of antimicrobial peptides (ADAM) (http://bioinformatics.cs.ntou.edu.tw/ADAM/svm_tool.html) [26]. Physicochemical properties and primary sequence homology to known AMPs were investigated using the calculator, predictor, and BLAST tools of the antimicrobial peptide database (APD3) (http://aps.unmc.edu/AP/) [40]. The synthesized peptides were named with the acronym StAMP (*S. turgens* antimicrobial peptide) followed by a progressive number. The peptide sequence with the highest overall predicted AMP score from all models was the sequence GKKPGGWKAK, which became our first lead peptide **StAMP-1** and basis for further studies. As for turgencin A, the lead peptide **StAMP-1** and the following peptides synthesized were C-terminally amidated to increase the overall net-positive charge of the peptide series. In order to improve antimicrobial activity, an amino acid modification and replacement strategy was chosen for a set of derivatives. Firstly, a Trp enrichment strategy within the central core (PGGW) of the lead peptide was chosen to increase the overall hydrophobicity. Secondly, all four Lys residues were substituted by Arg, and finally a peptide was made with the Trp residues replaced by Leu. All designed StAMPs were subjected to AMP prediction to validate the in silico models used and described above (Table S1 in the SI).

3.2. Peptide Synthesis

The peptides were synthesized by microwave assisted fluorenylmethoxycarbonyl solid-phase peptide synthesis (Fmoc-SPSS), using a Biotage® Initiator+Alstra™ (Uppsala, Sweden) fully automated peptide synthesizer. Fmoc-amino acids and solvents were purchased from Sigma-Aldrich (St. Louis, MO, USA) whereas Rink amide ChemMatrix resin was obtained from Biotage.

Rink Amide ChemMatrix resin (loading 0.44–0.48 mmol/g) was used to obtain peptides with an amidated C-terminus and each synthesis was scaled to 0.165 mmol. The resin was initially swelled at 70 °C for 20 min. Peptide synthesis was performed by coupling the Fmoc-amino acids (0.5 M in DMF, 4 equiv.) using the coupling reagent O-(6-chlorobenzotriazol-1-yl)-*N,N,N′,N′*-tetramethyluronium hexafluorophosphate (HCTU, 0.6 M in *N,N*-dimethylformamide (DMF), 3.92 equiv.), and the base *N,N*-diisopropylethylamine (DIEA, 2.0 M in *N*-methylpyrrolidone (NMP), 8 equiv.). The coupling reactions were performed with microwave heating (75 °C) and coupling times of 5 min. Coupling of Fmoc-Arg(Pbf)-OH (0.5 M in DMF, 4 equiv.) was done at room temperature for 60 min for peptides

StAMP-9, **-10** and **-11** and the coupling time of the remaining Fmoc-amino acids was increased from 5 to 10 min (microwave heating, 75 °C) due to the high lipophilicity of the fully side-chain protected peptides. After each coupling step, the temporary Fmoc-protecting group was cleaved using a solution of 20% piperidine in DMF (4.5 mL) at room temperature for 3 min and then repeated for 10 min. When the synthesis was completed the resin with peptide attached was washed with dichloromethane (DCM, 4.5 mL, 6 times, 45 s), followed by washing the resin with diethyl ether (4.5 mL, 3–4 times) using a vacuum manifold, and then dried in a vacuum desiccator overnight. The removal of protecting groups and cleaving the peptide from the resin was performed using a cleavage cocktail consisting of 95% trifluoroacetic acid (TFA, Sigma-Aldrich), 2.5% triisopropyl silane (TIS, Sigma-Aldrich), and 2.5% H_2O (total volume 10 mL) for 1 h and then repeated for 3 h. A vacuum manifold was used to isolate the cleaved peptide solution by filtration. The peptide filtrates were pooled, and the volume reduced in vacuo before the crude peptide was precipitated by the addition of ice-cold diethyl ether. The ether solution was decanted, and the procedure repeated twice by washing with ice cold diethyl ether. After the final decantation, the precipitated crude peptide was dried in vacuo prior to purification.

3.3. Peptide Purification and Verification

The synthesized peptides were purified by reversed-phase high-performance liquid chromatography (RP-HPLC) using a Waters preparative HPLC system equipped with a photodiode array (PDA) detector and an XBridge C_{18}, 5 μm, 10 × 250 mm column (Waters Associates, Milford, MA, USA). The separation was performed using linear gradients of acetonitrile (95% in water) and water, and both eluents containing 0.1% TFA (Sigma-Aldrich) with a flow rate of 10 mL/min. The purity of the peptides (>95%) was determined by an analytical UPLC-PDA system using an Acquity C_{18}, 1.7 μm, 2.1 × 50 mm column (Waters) with the same conditions as described above, but with a flow rate of 0.6 mL/min. Molecular weight and purity of the peptides (Table S2) were confirmed using a high-resolution 6540B quadrupole time-of-flight (Q-ToF) mass spectrometer with a dual electrospray ionization (ESI) source, coupled to a 1290 Infinity UHPLC system, controlled by MassHunter software (Agilent, Santa Clara, CA, USA). The peptides were separated using a Zorbax Eclipse Plus C_{18}, 1.8 μm, 2.1 × 50 mm column (Agilent). A gradient running from 3–20% acetonitrile containing 0.1% formic acid over 15 min with a flow rate of 0.4 mL/min was applied for the determination of the hydrophobicity (retention times) of the peptides.

3.4. Antibacterial Assay (Growth Inhibition)

The synthesized peptides were screened for antibacterial activity against five strains of G+ bacteria: *B. subtilis* (Bs, ATCC 23857), *C. glutamicum* (Cg, ATCC 13032), *S. aureus* (Sa, ATCC 9144), *Micrococcus luteus* (Ml), *B. megaterium* (Bm) (the last two were obtained from professor Olaf B. Styrvold, UiT The Arctic University of Norway).

Two strains of G- bacteria, *P. aeruginosa* (Pa, ATCC 27853) and *E. coli* (Ec, ATCC 25922), were also used. Cultures stored at -80 °C in glycerol were transferred to Müller–Hinton plates (MH, Difco Laboratories, Detroit, MI, USA) and incubated for 24 h at 35 °C. Colonies of each strain were transferred to 5 mL liquid MH medium and left shaking (600 rpm) at room temperature overnight. An aliquot of actively growing bacteria (20 μL) was inoculated in 5 mL MH medium and left shaking for 2 h at room temperature. In order to have a sensitive bioassay, the bacterial cultures were diluted with medium to only 2.5–3 × 10^4 bacteria/mL and an aliquot of 50 μL was added to each well in 96 microwell plates (Thermo Fisher Scientific, Roskilde, Denmark) preloaded with peptide solution (50 μL). The antibacterial assays were performed as previously described [49]. The microtiter plates were incubated for 24 h at 35 °C with optical density (595 nm) recorded every hour using an Envision 2103 multilabel reader, controlled by a Wallac Envision manager (PerkinElmer, Waltham, MA, USA). The minimum inhibitory concentration (MIC) was defined as the sample concentration showing an optical density less than 10% of the negative (growth) control, consisting of bacteria and MQ-H_2O. Oxytetracycline (concentrations ranging from 20–0.02 μg/mL, Sigma-Aldrich) and indolicidin (concentration ranging from 200–0.2 μg/mL, Sigma-Aldrich) served as a positive (inhibition) control.

The synthetic peptides were tested for antibacterial activity in concentrations ranging from 250 to 0.5 μg/mL in two-fold dilutions. All tests were performed in triplicates.

A killing experiment was performed on **StAMP-9** by using actively growing cultures of *B. subtilis* (ATCC 23857) and *E. coli*. (ATCC 25922). The procedure was performed as previously described [50]. Both tests were performed in triplicates.

3.5. Real-Time Assay Measuring Immediate Bacteria Membrane Disruption

The real-time bacterial membrane integrity assay was performed using *B. subtilis* 168 (ATCC 23857) and *E. coli* K12 (ATCC MC1061), both carrying the plasmid pCSS962 with the eukaryotic luciferase gene *lucGR*. Luciferase is dependent on D-luciferin as substrate to emit light, a substrate that does not penetrate intact cell membranes. The assay is a modification of a previously described protocol [44] and was conducted as previously described [24]. The bacteria ($\sim 5 \times 10^7$ bacteria/mL) were subjected to ranging concentrations of **StAMP-6-10** (50–3.1 μg/mL) and the positive control to chlorhexidine acetate (assay concentrations 100–1.6 μg/mL, Fresenius Kabi, Halden, Norway). Three independent measurements were conducted, and measurements were normalized to the untreated water controls.

3.6. Real-Time Assay Measuring Immediate Bacterial Cell Viability

A real-time cell viability assay (modified from [51]) was performed using *B. subtilis* 168 carrying an optimized *lux*ABCDE operon controlled by the promoter P*veg* [52], and *E. coli* K12 carrying the plasmid pCGLS-11 [53] with the *lux*CDABE operon from *Xenorhabdus luminescence*. The procedure was conducted as previously described [24]. The bacteria ($\sim 5 \times 10^7$ bacteria/mL) were subjected to ranging concentrations of **StAMP-6-10** (50–3.1 μg/mL) and the positive control to chlorhexidine acetate (assay concentrations 100–1.6 μg/mL). MQ-H$_2$O was used as a negative control. Three independent measurements were conducted, and measurements were normalized to the untreated water controls.

3.7. Antifungal Assay

StAMP-1–11 were screened for antifungal activity against *C. albicans* (Ca, ATCC 10231), *A. pullulans* (Ap) and *Rhodotorula* sp. (Rh) (the last two were obtained from professor Arne Tronsmo, The Norwegian University of Life Sciences, Ås, Norway). The antifungal assay was performed as previously described [54] with a few modifications. Briefly, fungal spores were dissolved in potato dextrose broth (Difco Laboratories) with 2% D(+)-glucose (Merck, Darmstadt, Germany) to a concentration of 4×10^5 spores/mL. The spores (50 μL) were inoculated on 96 microwell plates (Thermo Fisher Scientific) containing the synthetic peptides (50 μL) and controls (water or antibiotic). The peptides were diluted in MQ-H$_2$O at final concentrations ranging from 250–3.9 μg/mL in two-fold serial dilutions. Triclosan (Sigma-Aldrich, Steinheim, Germany) was used as a positive (antifungal) control (32–0.25 μg/mL), and MQ-H$_2$O as a negative (growth) control. Cultures were grown in room temperature for 24 h (Ca) and 48 h (Ap and Rh). Growth inhibition was determined by measuring OD values at 600 nm by a microplate reader (Synergy H1 Hybrid Multi-Mode Reader, BioTek, Winooski, VT, USA). The MIC values were defined as the lowest concentration of the peptides that showed >90% inhibition compared to the negative growth control (as measured by OD). All experiments were done in triplicate.

3.8. Hemolytic Activity Assay

The hemolytic activity assays were performed as previously described [23], but instead of using human red blood cells, defibrinated sheep blood (Thermo Scientific, No. R54016) was used. Briefly, the blood was centrifuged (450× *g*) for 10 min, the supernatant removed, and the pellet dissolved in phosphate-buffered saline (PBS; 320 mOSM, pH 7.4). This was done three times before the pellet was adjusted in PBS to a suspension containing 10% red blood cells (RBC). An aliquot of 10 μL of the RBC suspension was added to each well in 96 microwell plates with round bottom (Nunc, Thermo Fisher Scientific), preloaded with 90 μL of the synthetic peptides and controls (PBS or Triton). The peptides were diluted in PBS at final concentrations ranging from 250–2 μg/mL in twofold dilutions. As a

positive (hemolysis) control, Triton X-100 (Sigma-Aldrich, Saint Louis, MO, USA) was used at a final concentration of 0.05%, and PBS was used as a negative control. The plates were incubated at 37 °C for 1 h on a shaker, and afterwards centrifuged at 450× *g* for 10 min. The supernatants were transferred to 96 microwell plates with flat bottom (Thermo Fisher Scientific), and the absorbance was measured at 550 nm. The percent hemolysis was calculated using the formula $[(A_{sample} - A_{baseline})/(A_{triton} - A_{baseline})] \times 100$, where the PBS was used as baseline and Triton X-100 (Sigma-Aldrich) as 100% hemolysis. The experiment was performed in triplicate.

3.9. Human Cell Viability Assay

The human melanoma cell line A2058 (ATTC CRL-11144) and the non-malignant human lung fibroblast cell line MRC-5 (ATTC CCL-171) were assayed for sensitivity against **StAMP-1-11** at ranging concentrations between 100 and 5 µg/mL in a two-fold dilution series. The assays were performed as previously described [55]. Both assays were performed in triplicate in two independent experiments.

3.10. Anti-Inflammatory Activity Assay

The ability of **StAMP-1-11** to inhibit LPS induced TNF-α production by the human acute leukemia monocytic THP-1 cell line (ATCC TIB-202) was assayed as previously described [56]. Cells were added with 100 µg/mL of **StAMP-1-11**. The experiment was conducted in triplicate in two independent experiments.

4. Conclusions

The overall most potent antimicrobial peptide **StAMP-9** has several advantages, including potent antimicrobial activity, immediate effect on bacterial membranes, and high selectivity (non-hemolytic, non-cytotoxic), and it has a short sequence consisting of 10 natural amino acids. Although **StAMP-9** might be prone to proteolytic digestion, its simple sequence should facilitate rapid production, at low cost, and accelerate further studies and development into a clinical drug candidate. Proteolytic resistance might be improved by the insertion of D-amino acids or other chemically modified amino acids, or by cyclization [57]. This study also illustrates the potential for combining web-based and computational resources with a rational design of short antimicrobial peptides derived from larger peptides or proteins of natural origin. Future studies should be aimed at checking and/or improving the proteolytic stability of StAMP-9 as well as studying its efficacy in vivo, for instance, in a mouse infection model.

Supplementary Materials: The following are available online at http://www.mdpi.com/1422-0067/21/15/5460/s1, Figure S1. Antimicrobial effect on membrane integrity as measured by RLU in *B. subtilis* (pCSS962) treated with chlorhexidine and different concentration of **StAMP-8**, Figure S2. Antimicrobial effect on membrane integrity as measured by RLU in *B. subtilis* (pCSS962) treated with chlorhexidine and different concentration of **StAMP-9**, Figure S3. Antimicrobial effect on membrane integrity as measured by RLU in *B. subtilis* (pCSS962) treated with chlorhexidine and different concentration of **StAMP-10**, Figure S4. Antimicrobial effect on membrane integrity as measured by RLU in *E. coli* (pCSS962) treated with chlorhexidine and different concentration of **StAMP-8**, Figure S5. Antimicrobial effect on membrane integrity as measured by RLU in *E. coli* (pCSS962) treated with chlorhexidine and different concentration of **StAMP-9**, Figure S6. Antimicrobial effect on membrane integrity as measured by RLU in *E. coli* (pCSS962) treated with chlorhexidine and different concentration of **StAMP-10**, Figure S7. Antimicrobial effect on viability as measured by RLU in *B. subtilis* (pCGLS-11) treated with chlorhexidine and different concentration of **StAMP-8**, Figure S8. Antimicrobial effect on viability as measured by RLU in *B. subtilis* (pCGLS-11) treated with chlorhexidine and different concentration of **StAMP-9**, Figure S9. Antimicrobial effect on viability as measured by RLU in *B. subtilis* (pCGLS-11) treated with chlorhexidine and different concentration of **StAMP-10**, Figure S10. Antimicrobial effect on viability as measured by RLU in *E. coli* (pCGLS-11) treated with chlorhexidine and different concentration of **StAMP-8**, Figure S11. Antimicrobial effect on viability as measured by RLU in *E. coli* (pCGLS-11) treated with chlorhexidine and different concentration of **StAMP-9**, Figure S12. Antimicrobial effect on viability as measured by RLU in *E. coli* (pCGLS-11) treated with chlorhexidine and different concentration of **StAMP-10**, Figure S13. Antimicrobial effect on membrane integrity as measured by RLU in *B. subtilis* (pCSS962) treated with different concentrations of chlorhexidine, Figure S14. Antimicrobial effect on membrane integrity as measured by RLU in *E. coli* (pCSS962) treated with different concentrations of chlorhexidine, Figure S15. Antimicrobial effect on viability as measured by RLU in *B. subtilis* (pCGLS-11) treated with different concentrations of chlorhexidine, Figure S16. Antimicrobial effect on viability as measured by RLU in *E. coli*

(pCGLS-11) treated with different concentrations of chlorhexidine, Table S1. Antimicrobial activity prediction of the designed StAMPs.

References

1. Hassan, M.; Kjos, M.; Nes, I.F.; Diep, D.B.; Lotfipour, F. Natural antimicrobial peptides from bacteria: Characteristics and potential applications to fight against antibiotic resistance. *J. Appl. Microbiol.* **2012**, *113*, 723–736. [CrossRef] [PubMed]
2. Domalaon, R.; Zhanel, G.G.; Schweizer, F. Short antimicrobial peptides and peptide scaffolds as promising antibacterial agents. *Curr. Top. Med. Chem.* **2016**, *16*, 1217–1230. [CrossRef] [PubMed]
3. Ramesh, S.; Govender, T.; Kruger, H.G.; Torre, B.G.; Albericio, F. Short AntiMicrobial Peptides (SAMPs) as a class of extraordinary promising therapeutic agents. *J. Pept. Sci.* **2016**, *22*, 438–451. [CrossRef] [PubMed]
4. DeNegre, A.A.; Ndeffo Mbah, M.L.; Myers, K.; Fefferman, N.H. Emergence of antibiotic resistance in immunocompromised host populations: A case study of emerging antibiotic resistant tuberculosis in AIDS patients. *PLoS ONE* **2019**, *14*, e0212969. [CrossRef] [PubMed]
5. Dumford, D.M.; Skalweit, M. Antibiotic-resistant infections and treatment challenges in the immunocompromised host. *Infect. Dis. Clin. N. Am.* **2016**, *30*, 465–489. [CrossRef] [PubMed]
6. Teillant, A.; Gandra, S.; Barter, D.; Morgan, D.J.; Laxminarayan, R. Potential burden of antibiotic resistance on surgery and cancer chemotherapy antibiotic prophylaxis in the USA: A literature review and modelling study. *Lancet Infect. Dis.* **2015**, *15*, 1429–1437. [CrossRef]
7. O'Neill, J. *Tackling Drug-Resistant Infections Globally: Final Report and Recommendations. The Review on Antimicrobial Resistance*; HM Government and the Wellcome Trust: London, UK, 2016.
8. Simpkin, V.L.; Renwick, M.J.; Kelly, R.; Mossialos, E. Incentivising innovation in antibiotic drug discovery and development: Progress, challenges and next steps. *J. Antibiot.* **2017**, *70*, 1087–1096. [CrossRef]
9. Bahar, A.A.; Ren, D. Antimicrobial peptides. *Pharmaceuticals* **2013**, *6*, 1543–1575. [CrossRef]
10. Shabir, U.; Ali, S.; Magray, A.R.; Ganai, B.A.; Firdous, P.; Hassan, T.; Nazir, R. Fish antimicrobial peptides (AMP's) as essential and promising molecular therapeutic agents: A review. *Microb. Pathog.* **2018**, *114*, 50–56. [CrossRef]
11. Splith, K.; Neundorf, I. Antimicrobial peptides with cell-penetrating peptide properties and vice versa. *Eur. Biophys. J.* **2011**, *40*, 387–397. [CrossRef]
12. Hancock, R.E.W.; Sahl, H.-G. Antimicrobial and host-defense peptides as new anti-infective therapeutic strategies. *Nat. Biotechnol.* **2006**, *24*, 1551–1557. [CrossRef]
13. Semreen, M.H.; El-Gamal, M.I.; Abdin, S.; Alkhazraji, H.; Kamal, L.; Hammad, S.; El-Awady, F.; Waleed, D.; Kourbaj, L. Recent updates of marine antimicrobial peptides. *Saudi Pharm. J.* **2018**, *26*, 396–409. [CrossRef]
14. Arias, M.; Piga, K.B.; Hyndman, E.M.; Vogel, H.J. Improving the activity of Trp-rich antimicrobial peptides by Arg/Lys substitutions and changing the length of cationic residues. *Biomolecules* **2018**, *8*, 19. [CrossRef] [PubMed]
15. Zasloff, M. Antimicrobial peptides of multicellular organisms. *Nature* **2002**, *415*, 389–395. [CrossRef] [PubMed]

16. Tincu, J.A.; Taylor, S.W. Antimicrobial peptides from marine invertebrates. *Antimicrob. Agents Chemother.* **2004**, *48*, 3645–3654. [CrossRef] [PubMed]

17. Fjell, C.D.; Hiss, J.A.; Hancock, R.E.W.; Schneider, G. Designing antimicrobial peptides: Form follows function. *Nat. Rev. Drug Discov.* **2012**, *11*, 37–51. [CrossRef]

18. Greber, K.E.; Dawgul, M. Antimicrobial peptides under clinical trials. *Curr. Top. Med. Chem.* **2017**, *17*, 620–628. [CrossRef]

19. Mikut, R.; Ruden, S.; Reischl, M.; Breitling, F.; Volkmer, R.; Hilpert, K. Improving short antimicrobial peptides despite elusive rules for activity. *BBA Biomembr.* **2016**, *1858*, 1024–1033. [CrossRef]

20. Cherkasov, A.; Hilpert, K.; Jenssen, H.; Fjell, C.D.; Waldbrook, M.; Mullaly, S.C.; Volkmer, R.; Hancock, R.E.W. Use of artificial intelligence in the design of small peptide antibiotics effective against a broad spectrum of highly antibiotic-resistant superbugs. *ACS Chem. Biol.* **2009**, *4*, 65–74. [CrossRef]

21. Knappe, D.; Henklein, P.; Hoffmann, R.; Hilpert, K. Easy strategy to protect antimicrobial peptides from fast degradation in serum. *Antimicrob. Agents Chemother.* **2010**, *54*, 4003–4005. [CrossRef]

22. Strøm, M.B.; Rekdal, Ø.; Svendsen, J.S. The effects of charge and lipophilicity on the antibacterial activity of undecapeptides derived from bovine lactoferricin. *J. Pept. Sci.* **2002**, *8*, 36–43. [CrossRef] [PubMed]

23. Paulsen, V.S.; Blencke, H.-M.; Benincasa, M.; Haug, T.; Eksteen, J.J.; Styrvold, O.B.; Scocchi, M.; Stensvåg, K. Structure-activity relationships of the antimicrobial peptide arasin 1-and mode of action studies of the N-terminal, proline-rich region. *PLoS ONE* **2013**, *8*, e53326. [CrossRef] [PubMed]

24. Hansen, I.K.Ø.; Isaksson, J.; Poth, A.G.; Hansen, K.Ø.; Andersen, A.J.C.; Richard, C.S.M.; Blencke, H.-M.; Stensvåg, K.; Craik, D.J.; Haug, T. Isolation and characterization of antimicrobial peptides with unusual disulfide connectivity from the colonial ascidian *Synoicum turgens*. *Mar. Drugs* **2020**, *18*, 51. [CrossRef]

25. Waghu, F.H.; Barai, R.S.; Gurung, P.; Idicula-Thomas, S. CAMPR3: A database on sequences, structures and signatures of antimicrobial peptides. *Nucleic Acids Res.* **2016**, *44*, D1094–D1097. [CrossRef]

26. Lee, H.-T.; Lee, C.-C.; Yang, J.-R.; Lai, J.Z.C.; Chang, K.Y. A large-scale structural classification of antimicrobial peptides. *Biomed Res. Int.* **2015**, *2015*, 475062. [CrossRef] [PubMed]

27. Björn, C.; Håkansson, J.; Myhrman, E.; Sjöstrand, V.; Haug, T.; Lindgren, K.; Blencke, H.-M.; Stensvåg, K.; Mahlapuu, M. Anti-infectious and anti-inflammatory effects of peptide fragments sequentially derived from the antimicrobial peptide centrocin 1 isolated from the green sea urchin, *Strongylocentrotus droebachiensis*. *AMB Express* **2012**, *2*, 67. [CrossRef]

28. Liu, S.; Fan, L.; Sun, J.; Lao, X.; Zheng, H. Computational resources and tools for antimicrobial peptides. *J. Pept. Sci.* **2017**, *23*, 4–12. [CrossRef]

29. Zhang, Z.; Zhu, S. Comparative genomics analysis of five families of antimicrobial peptide-like genes in seven ant species. *Dev. Comp. Immunol.* **2012**, *38*, 262–274. [CrossRef]

30. Chan, D.I.; Prenner, E.J.; Vogel, H.J. Tryptophan- and arginine-rich antimicrobial peptides: Structures and mechanisms of action. *BBA Biomembr.* **2006**, *1758*, 1184–1202. [CrossRef]

31. Strøm, M.B.; Haug, B.E.; Skar, M.L.; Stensen, W.; Stiberg, T.; Svendsen, J.S. The pharmacophore of short cationic antibacterial peptides. *J. Med. Chem.* **2003**, *46*, 1567–1570. [CrossRef]

32. Joo, H.; Chavan, A.G.; Phan, J.; Day, R.; Tsai, J. An amino acid packing code for α-helical structure and protein design. *J. Mol. Biol.* **2012**, *419*, 234–254. [CrossRef] [PubMed]

33. Ouellette, A.J.; Satchell, D.P.; Hsieh, M.M.; Hagen, S.J.; Selsted, M.E. Characterization of luminal paneth cell alpha-defensins in mouse small intestine. Attenuated antimicrobial activities of peptides with truncated amino termini. *J. Biol. Chem.* **2000**, *275*, 33969–33973. [CrossRef] [PubMed]

34. Zelezetsky, I.; Tossi, A. Alpha-helical antimicrobial peptides-using a sequence template to guide structure-activity relationship studies. *BBA Biomembr.* **2006**, *1758*, 1436–1449. [CrossRef] [PubMed]

35. Gabere, M.N.; Noble, W.S. Empirical comparison of web-based antimicrobial peptide prediction tools. *Bioinformatics* **2017**, *33*, 1921–1929. [CrossRef]

36. Boman, H.G. Antibacterial peptides: Basic facts and emerging concepts. *J. Intern. Med.* **2003**, *254*, 197–215. [CrossRef]

37. Jiang, Z.; Vasil, A.I.; Hale, J.D.; Hancock, R.E.W.; Vasil, M.L.; Hodges, R.S. Effects of net charge and the number of positively charged residues on the biological activity of amphipathic α-helical cationic antimicrobial peptides. *Pept. Sci.* **2008**, *90*, 369–383. [CrossRef]

38. Takahashi, D.; Shukla, S.K.; Prakash, O.; Zhang, G. Structural determinants of host defense peptides for antimicrobial activity and target cell selectivity. *Biochimie* **2010**, *92*, 1236–1241. [CrossRef]

39. Juretić, D.; Chen, H.-C.; Brown, J.H.; Morell, J.L.; Hendler, R.W.; Westerhoff, H.V. Magainin 2 amide and analogues. Antimicrobial activity, membrane depolarization and susceptibility to proteolysis. *FEBS Lett.* **1989**, *249*, 219–223. [CrossRef]

40. Wang, G.; Li, X.; Wang, Z. APD3: The antimicrobial peptide database as a tool for research and education. *Nucleic Acids Res.* **2016**, *44*, D1087–D1093. [CrossRef]

41. Chen, Y.; Guarnieri, M.T.; Vasil, A.I.; Vasil, M.L.; Mant, C.T.; Hodges, R.S. Role of peptide hydrophobicity in the mechanism of action of α-helical antimicrobial peptides. *Antimicrob. Agents Chemother.* **2007**, *51*, 1398–1406. [CrossRef]

42. Kyte, J.; Doolittle, R.F. A simple method for displaying the hydropathic character of a protein. *J. Mol. Biol.* **1982**, *157*, 105–132. [CrossRef]

43. Wolfenden, R.; Lewis, C.A.; Yuan, Y.; Carter, C.W. Temperature dependence of amino acid hydrophobicities. *Proc. Natl. Acad. Sci. USA* **2015**, *112*, 7484–7488. [CrossRef] [PubMed]

44. Virta, M.; Åkerman, K.E.O.; Saviranta, P.; Oker-Blom, C.; Karp, M.T. Real-time measurement of cell permeabilization with low-molecular-weight membranolytic agents. *J. Antimicrob. Chemother.* **1995**, *36*, 303–315. [CrossRef]

45. Igumnova, E.M.; Mishchenko, E.; Haug, T.; Blencke, H.-M.; Sollid, J.U.E.; Fredheim, E.G.A.; Lauksund, S.; Stensvåg, K.; Strøm, M.B. Synthesis and antimicrobial activity of small cationic amphipathic aminobenzamide marine natural product mimics and evaluation of relevance against clinical isolates including ESBL–CARBA producing multi-resistant bacteria. *Bioorgan. Med. Chem.* **2016**, *24*, 5884–5894. [CrossRef]

46. Igumnova, E.M.; Mishchenko, E.; Haug, T.; Blencke, H.-M.; Sollid, J.U.E.; Fredheim, E.G.A.; Lauksund, S.; Stensvåg, K.; Strøm, M.B. Amphipathic sulfonamidobenzamides mimicking small antimicrobial marine natural products; investigation of antibacterial and anti-biofilm activity against antibiotic resistant clinical isolates. *Bioorgan. Med. Chem.* **2018**, *26*, 4930–4941. [CrossRef]

47. McDonnell, G.; Russell, A.D. Antiseptics and Disinfectants: Activity, Action, and Resistance. *Clin. Microbiol. Rev.* **1999**, *12*, 147–179. [CrossRef]

48. Schmitt, P.; Rosa, R.D.; Destoumieux-Garzón, D. An intimate link between antimicrobial peptide sequence diversity and binding to essential components of bacterial membranes. *BBA Biomembr.* **2016**, *1858*, 958–970. [CrossRef]

49. Sperstad, S.V.; Haug, T.; Vasskog, T.; Stensvåg, K. Hyastatin, a glycine-rich multi-domain antimicrobial peptide isolated from the spider crab (*Hyas araneus*) hemocytes. *Mol. Immunol.* **2009**, *46*, 2604–2612. [CrossRef]

50. Solstad, R.G.; Johansen, C.; Stensvåg, K.; Strøm, M.B.; Haug, T. Structure-activity relationship studies of shortened analogues of the antimicrobial peptide EeCentrocin 1 from the sea urchin *Echinus esculentus*. *J. Pept. Sci.* **2020**, *26*, e3233. [CrossRef]

51. Vesterlund, S.; Paltta, J.; Lauková, A.; Karp, M.; Ouwehand, A.C. Rapid screening method for the detection of antimicrobial substances. *J. Microbiol. Meth.* **2004**, *57*, 23–31. [CrossRef]

52. Radeck, J.; Kraft, K.; Bartels, J.; Cikovic, T.; Dürr, F.; Emenegger, J.; Kelterborn, S.; Sauer, C.; Fritz, G.; Gebhard, S.; et al. The Bacillus BioBrick Box: Generation and evaluation of essential genetic building blocks for standardized work with *Bacillus subtilis*. *J. Biol. Eng.* **2013**, *7*, 29. [CrossRef] [PubMed]

53. Frackman, S.; Anhalt, M.; Nealson, K.H. Cloning, organization, and expression of the bioluminescence genes of *Xenorhabdus luminescens*. *J. Bacteriol.* **1990**, *172*, 5767–5773. [CrossRef] [PubMed]

54. Sperstad, S.V.; Haug, T.; Paulsen, V.; Rode, T.M.; Strandskog, G.; Solem, S.T.; Styrvold, O.B.; Stensvåg, K. Characterization of crustins from the hemocytes of the spider crab, *Hyas araneus*, and the red king crab, *Paralithodes camtschaticus*. *Dev. Comp. Immun.* **2009**, *33*, 583–591. [CrossRef] [PubMed]

55. Hansen, K.Ø.; Andersen, J.H.; Bayer, A.; Pandey, S.K.; Lorentzen, M.; Jørgensen, K.B.; Sydnes, M.O.; Guttormsen, Y.; Baumann, M.; Koch, U.; et al. Kinase chemodiversity from the Arctic: The breitfussins. *J. Med. Chem.* **2019**, *62*, 10167–10181. [CrossRef] [PubMed]

56. Michael, P.; Hansen, E.; Isaksson, J.; Andersen, J.H.; Hansen, K.Ø. Dendrobeaniamine A, a new alkaloid from the Arctic marine bryozoan *Dendrobeania murrayana*. *Nat. Prod. Res.* **2019**, 1–6. [CrossRef]

57. Li, H.; Anuwongcharoen, N.; Malik, A.A.; Prachayasittikul, V.; Wikberg, J.E.; Nantasenamat, C. Roles of d-amino acids on the bioactivity of host defense peptides. *Int. J. Mol. Sci.* **2016**, *17*, 1023. [CrossRef]

Supporting information

Antimicrobial activity of small synthesized synthetic peptides based on the marine peptide turgencin A: prediction of antimicrobial peptide sequences in a natural peptide and strategy for optimization of potency

Ida K. Ø. Hansen [1,*], Tomas Lövdahl [2], Danijela Simonovic [2], Kine Ø. Hansen [3], Aron J. C. Andersen [1], Hege Devold [1], Céline S. M. Richard [1], Jeanette H. Andersen [3], Morten B. Strøm [2] and Tor Haug [1,*]

[1] Norwegian College of Fishery Science, Faculty of Biosciences, Fisheries and Economics, UiT The Arctic University of Norway, 9037 Tromsø, Norway; ajca@dtu.dk (A.J.C.A.); hege.devold@uit.no (H.D.); celine.s.richard@uit.no (C.S.M.R.)

[2] Department of Pharmacy, Faculty of Health Sciences, UiT The Arctic University of Norway, 9037 Tromsø, Norway; tlovdahl88@hotmail.com (T.L.); danijela.simonovic@uit.no (D.S.); morten.strom@uit.no (M.B.S.)

[3] Marbio, Faculty of Biosciences, Fisheries and Economics, UiT The Arctic University of Norway, Breivika, N-9037, Tromsø, Norway; kine.o.hanssen@uit.no (K.Ø.H.); jeanette.h.andersen@uit.no (J.H.A.)
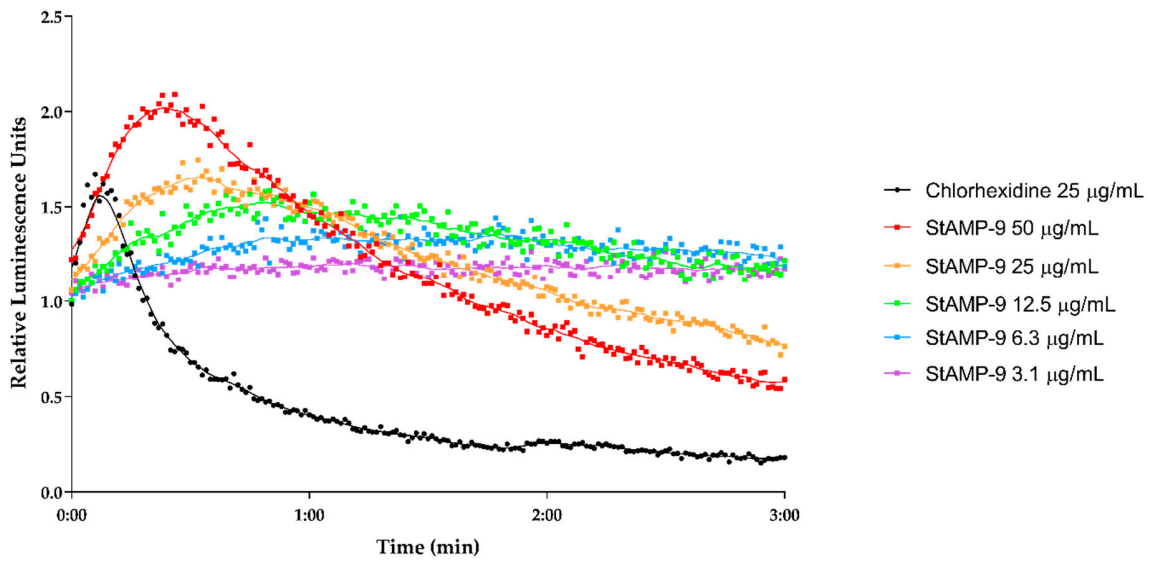
Table of contents

Figure S1. Kinetic of the antimicrobial effect on membrane integrity as measured by relative luminescence in *B. subtilis* (pCSS962) treated with chlorhexidine and different concentration of **StAMP-8**.

Figure S2. Kinetic of the antimicrobial effect on membrane integrity as measured by relative luminescence in *B. subtilis* (pCSS962) treated with chlorhexidine and different concentration of **StAMP-9**.
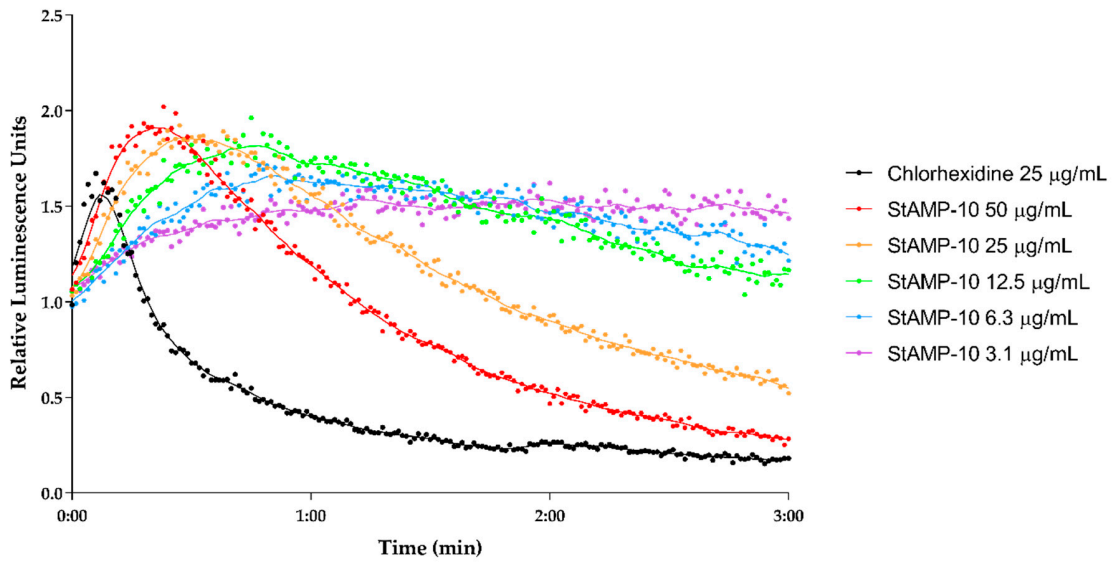
Figure S3. Kinetic of the antimicrobial effect on membrane integrity as measured by relative luminescence in *B. subtilis* (pCSS962) treated with chlorhexidine and different concentration of **StAMP-10**.

Figure S4. Kinetic of the antimicrobial effect on membrane integrity as measured by relative luminescence in *E. coli* (pCSS962) treated with chlorhexidine and different concentration of **StAMP-8**.

Figure S5. Kinetic of the antimicrobial effect on membrane integrity as measured by relative luminescence in *E. coli* (pCSS962) treated with chlorhexidine and different concentration of **StAMP-9**.

Figure S6. Kinetic of the antimicrobial effect on membrane integrity as measured by relative luminescence in *E. coli* (pCSS962) treated with chlorhexidine and different concentration of **StAMP-10**.

Figure S7. Kinetic of the antimicrobial effect on viability as measured by relative luminescence in *B. subtilis* (pCGLS-11) treated with chlorhexidine and different concentration of **StAMP-8**.

Figure S8. Kinetic of the antimicrobial effect on viability as measured by relative luminescence in *B. subtilis* (pCGLS-11) treated with chlorhexidine and different concentration of **StAMP-9**.

Figure S9. Kinetic of the antimicrobial effect on viability as measured by relative luminescence in *B. subtilis* (pCGLS-11) treated with chlorhexidine and different concentration of **StAMP-10**.
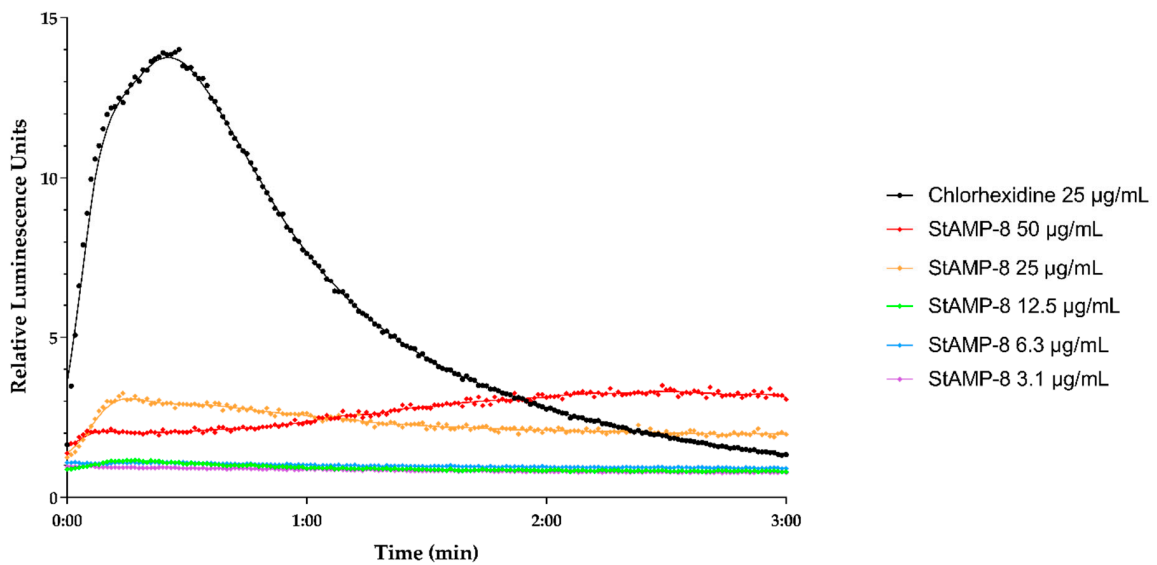

Figure S10. Kinetic of the antimicrobial effect on viability as measured by relative luminescence in *E. coli* (pCGLS-11) treated with chlorhexidine and different concentration of **StAMP-8**.

Figure S11. Kinetic of the antimicrobial effect on viability as measured by relative luminescence in *E. coli* (pCGLS-11) treated with chlorhexidine and different concentration of **StAMP-9**.

Figure S12. Kinetic of the antimicrobial effect on viability as measured by relative luminescence in *E. coli* (pCGLS-11) treated with chlorhexidine and different concentration of **StAMP-10**.
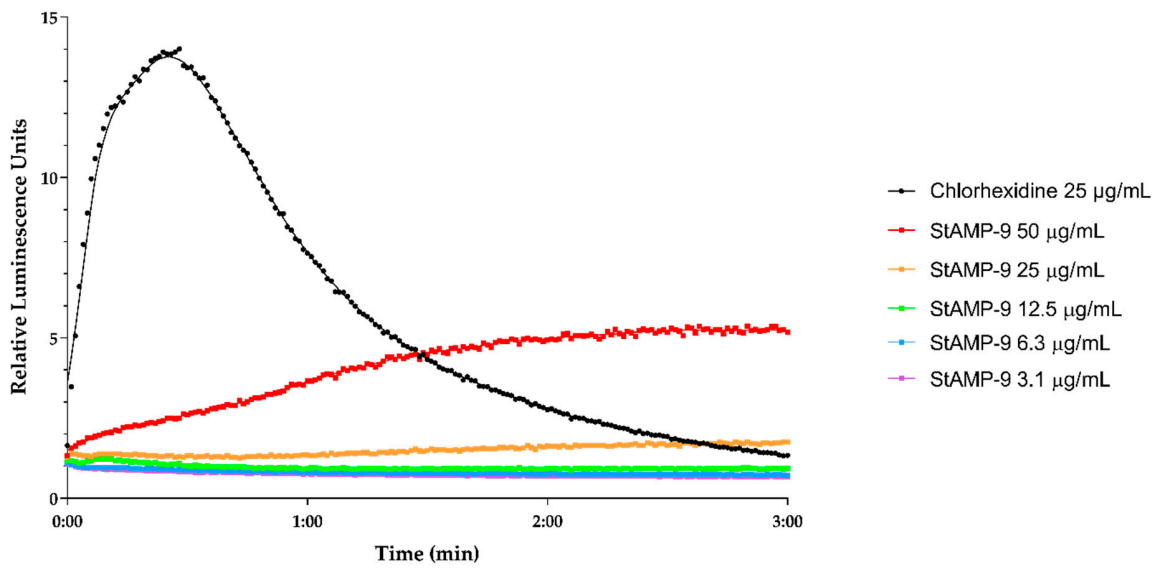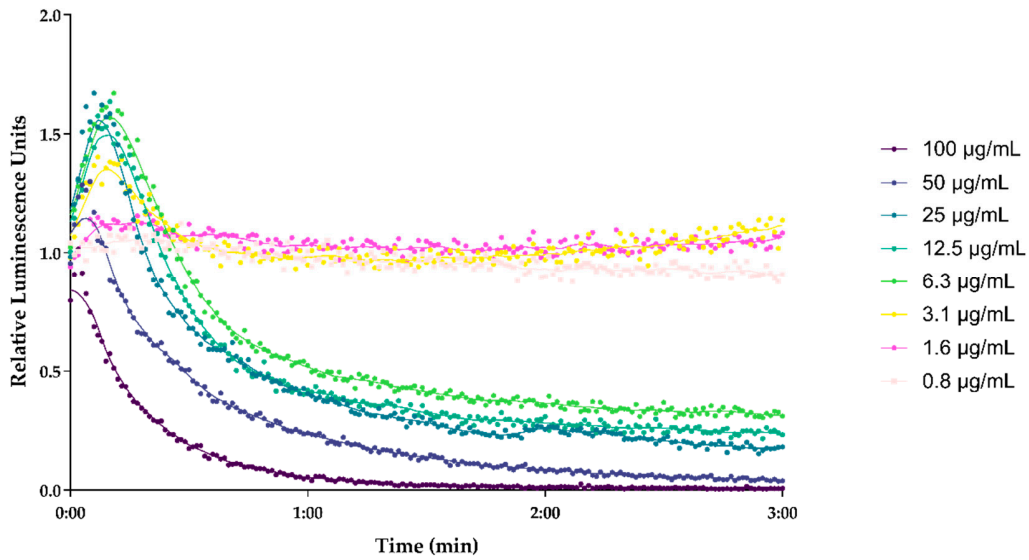
Figure S13. Kinetic of the antimicrobial effect on membrane integrity as measured by relative luminescence in *B. subtilis* (pCSS962) treated with different concentration of chlorhexidine.
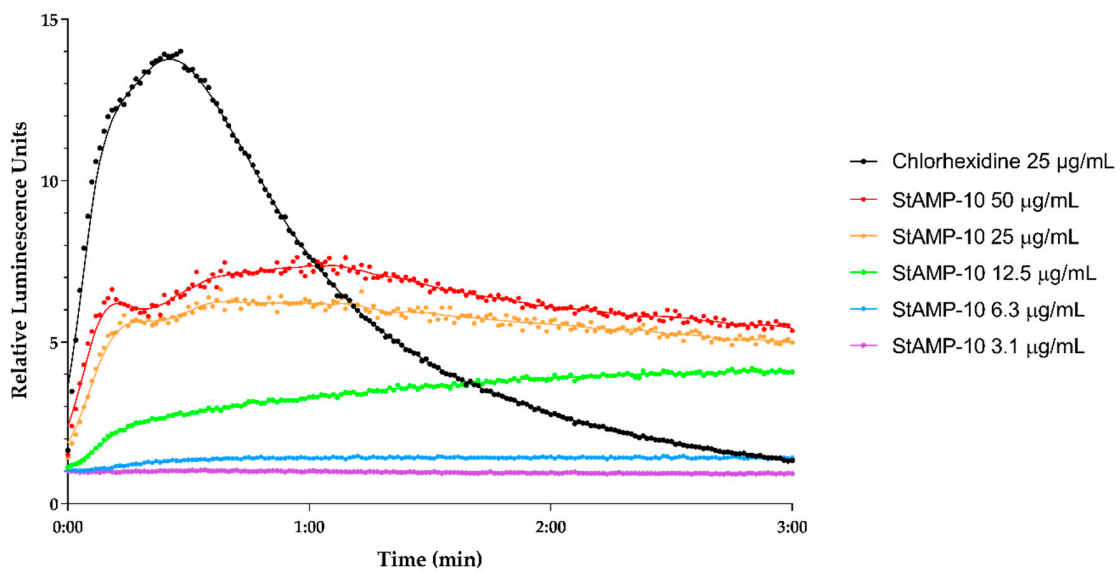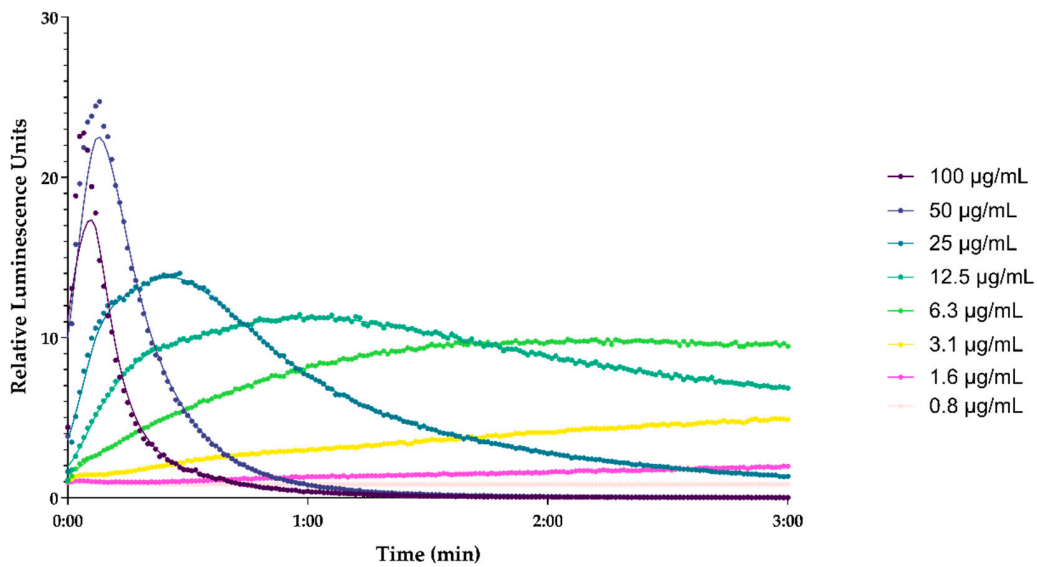

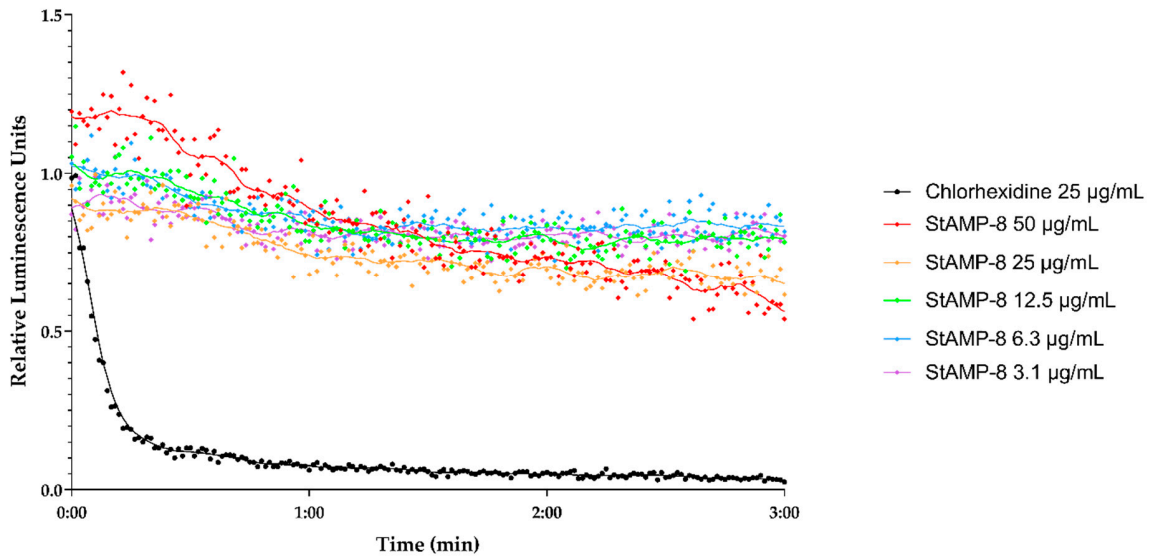**Figure S14**. Kinetic of the antimicrobial effect on membrane integrity as measured by relative luminescence in *E. coli* (pCSS962) treated with different concentration of chlorhexidine.
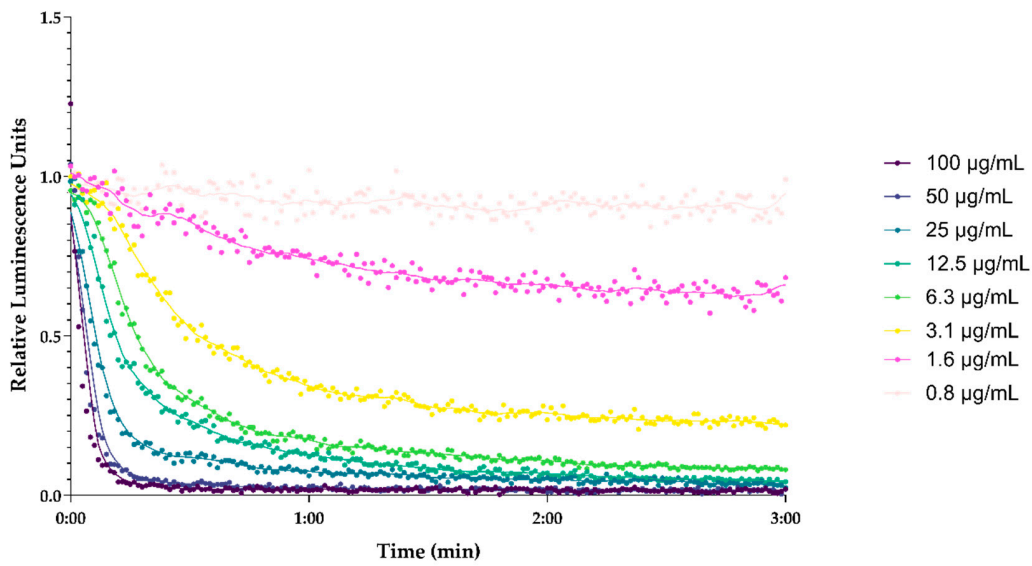
Figure S15. Kinetic of the antimicrobial effect on viability as measured by relative luminescence in *B. subtilis* (pCGLS-11) treated different concentration of chlorhexidine.
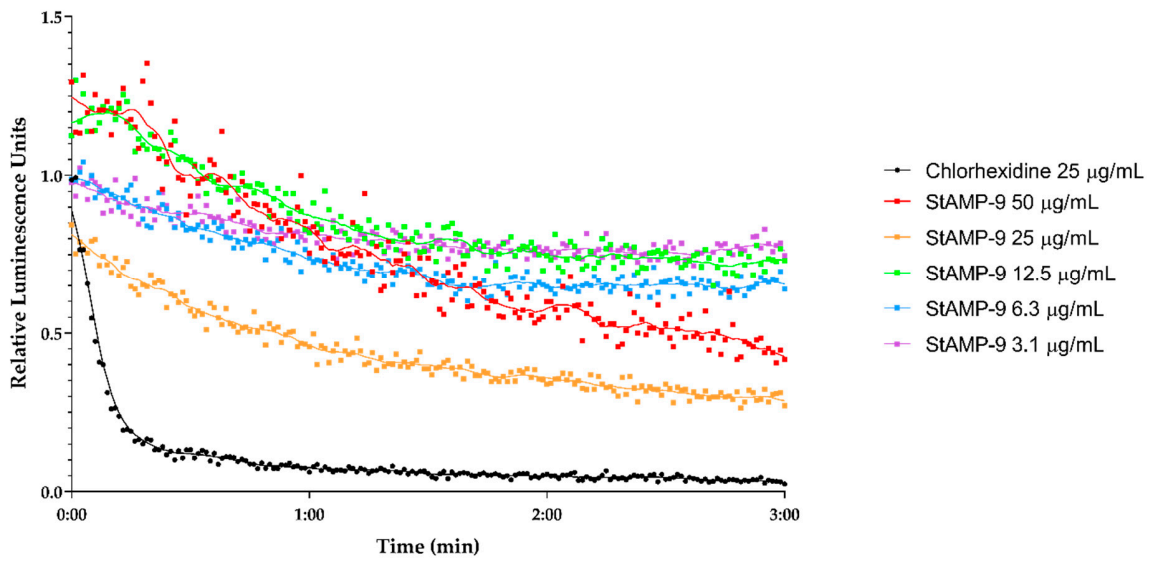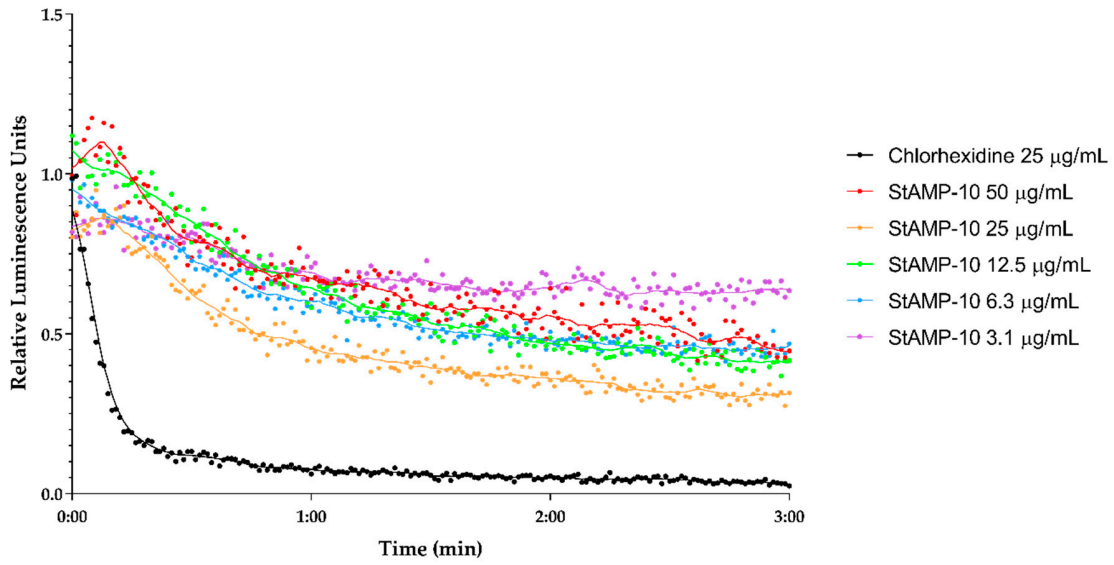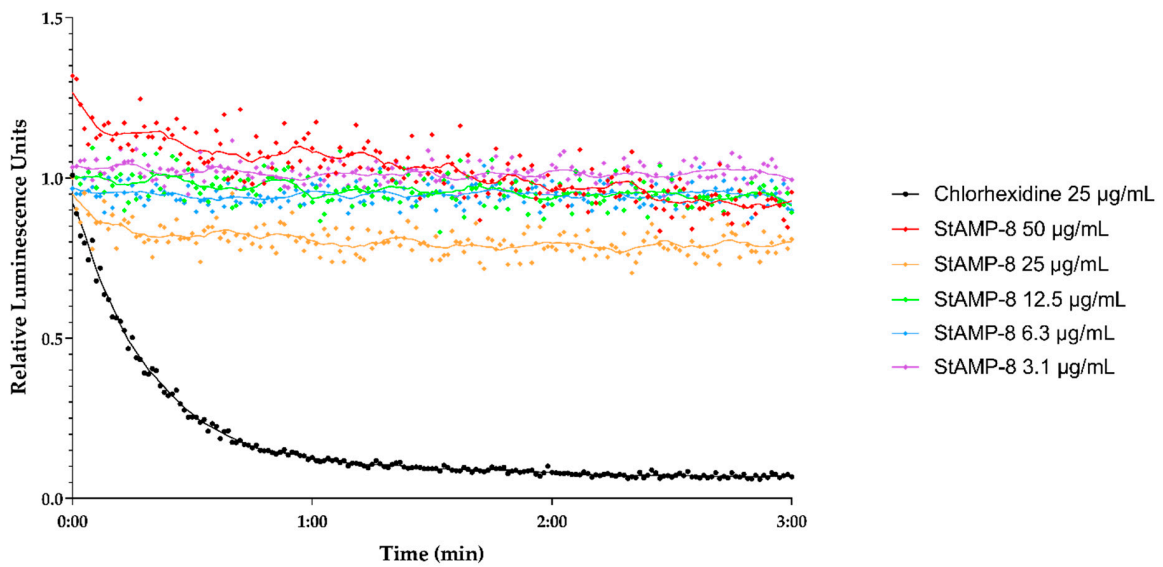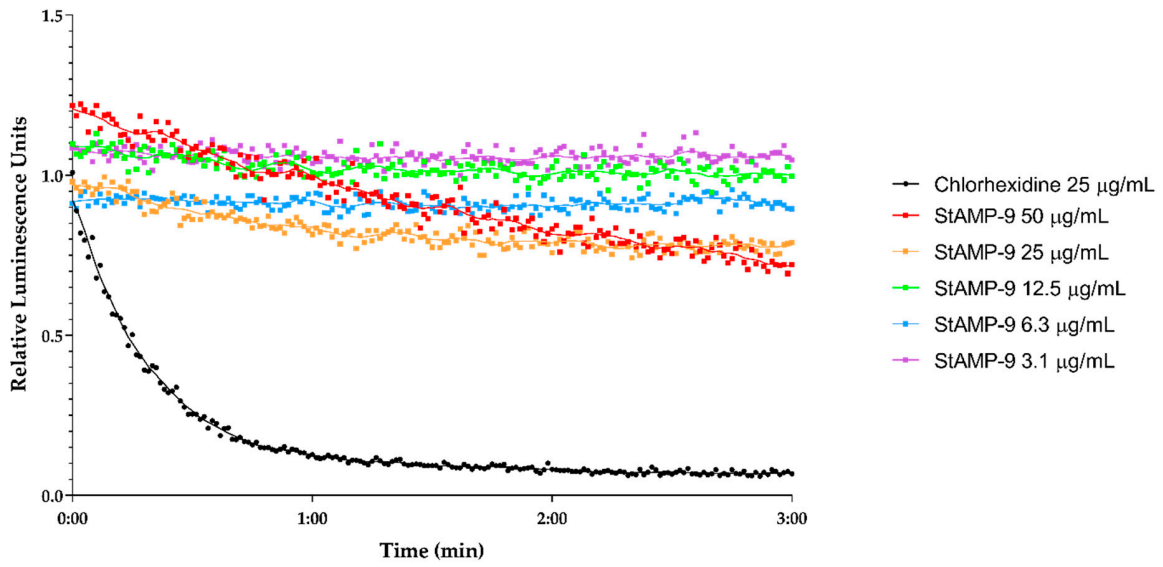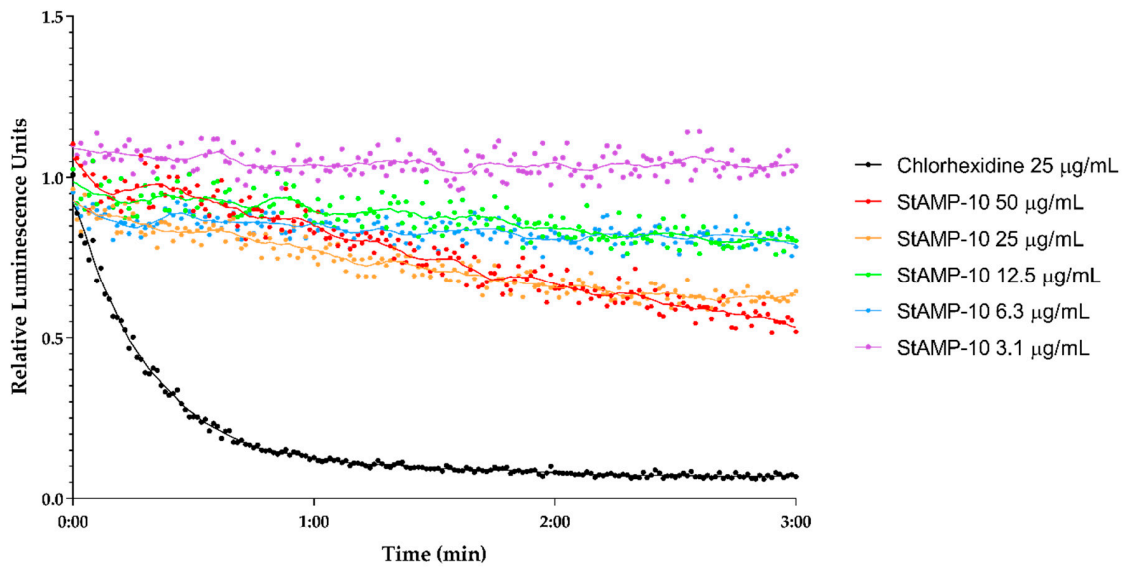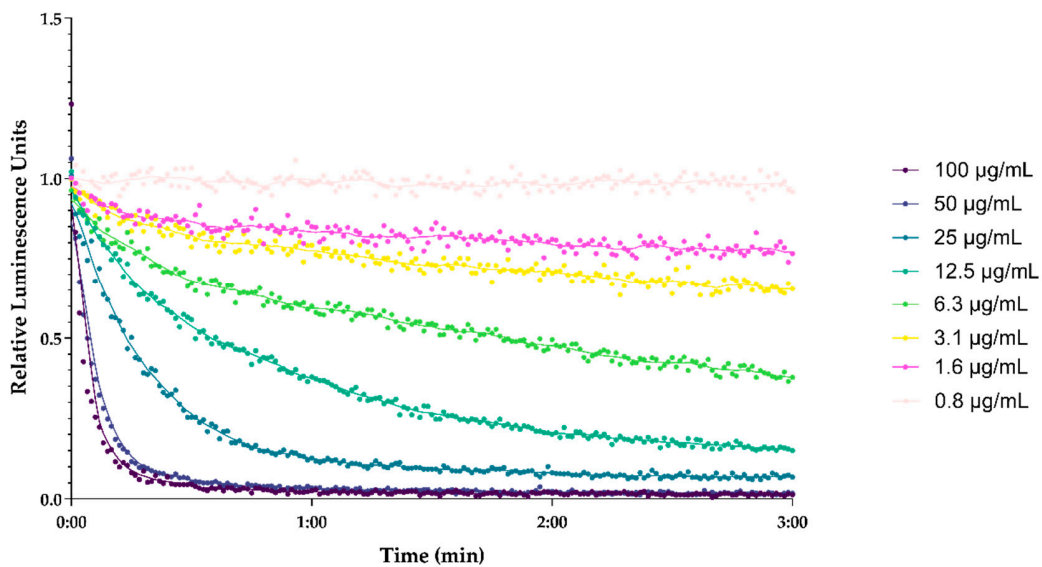

Figure S16. Kinetic of the antimicrobial effect on viability as measured by relative luminescence in *E. coli* (pCGLS-11) treated different concentration of chlorhexidine.

Table S1. Antimicrobial activity prediction of the designed StAMPs. SVM: support vector machines; RF: random forests; ANN: artificial neural networks; and DA: discriminant analysis.

Peptide	Sequence	CAMP$_{R3}$				ADAM
		SVM	RF	ANN	DA	SVM
StAMP-1	GKKPGGWKAK	0.968	0.559	AMP	0.884	2.85
StAMP-2	GKKWGGWKAK	0.998	0.533	AMP	0.887	3.23
StAMP-3	GKKPWGWKAK	0.999	0.625	AMP	0.979	2.85
StAMP-4	GKKPGWWKAK	0.997	0.623	AMP	0.979	2.85
StAMP-5	GKKWWGWKAK	1.000	0.605	AMP	0.980	3.14
StAMP-6	GKKWGWWKAK	1.000	0.605	AMP	0.980	3.14
StAMP-7	GKKPWWWKAK	1.000	0.724	AMP	0.997	2.79
StAMP-8	GKKWWWWKAK	1.000	0.830	AMP	0.998	2.90
StAMP-9	GRRPWWWRAR	0.999	0.634	AMP	0.993	1.36
StAMP-10	GRRWWWWRAR	1.000	0.649	AMP	0.995	1.97
StAMP-11	GRRPLLLRAR	0.918	0.583	AMP	0.907	1.82

Table S2. Molecular weight and purity of the StAMPs.

Peptide	Molecular weight (g/mol)	Purity (%)
StAMP-1	1055.28	97
StAMP-2	1144.37	98
StAMP-3	1184.44	98
StAMP-4	1184.44	98
StAMP-5	1273.53	95
StAMP-6	1273.53	98
StAMP-7	1313.59	99
StAMP-8	1402.69	100
StAMP-9	1425.65	100
StAMP-10	1514.74	100
StAMP-11	1206.49	97

Paper III

Isolation and characterization of St-CRPs: Cysteine-rich peptides from the Arctic marine ascidian *Synoicum turgens*.

Ida K. Ø. Hansen [1,*], Philip B. Rainsford [2], Johan Isaksson [2], Kine Ø. Hansen [3], Klara Stensvåg [1], Anastasia Albert [4], Terje Vasskog [5] and Tor Haug [1,*]

[1] The Norwegian College of Fishery Science, Faculty of Biosciences, Fisheries and Economics, UiT The Arctic University of Norway, Breivika, N-9037 Tromsø, Norway; klara.stensvag@uit.no (K.S.)

[2] Department of Chemistry, Faculty of Science and Technology, UiT The Arctic University of Norway, Breivika, N-9037 Tromsø, Norway; philip.rainsford@uit.no (P.B.R.); johan.isaksson@uit.no (J.I.)

[3] Marbio, UiT The Arctic University of Norway, N-9037, Tromsø, Norway; kine.o.hanssen@uit.no

[4] Norce, Siva Innovasjonssenter, Sykehusveien 21, 9019 Tromsø; anastasia.albert@norut.no (A.A.)

[5] Department of Pharmacy, Faculty of Health Sciences, UiT The Arctic University of Norway, Breivika, N-9037 Tromsø, Norway; terje.vasskog@uit.no (T.V.)

* Correspondence: ida.k.hansen@uit.no; Tel.: +47-77-64-92-66 (I.K.Ø.H.), tor.haug@uit.no; Tel.: +47-77-64-60-71 (T.H.)

Abstract

Ascidians are a group of marine invertebrates where most are sessile and soft bodied. Their absence of an adaptive immune system makes them rely on innate immune responses to detect and eliminate invading microbes. Antimicrobial peptides (AMPs) play an essential part in this process. In this paper, we present the isolation, structure elucidation and bioactivities of two new cysteine-rich peptides (CRPs) from the Arctic marine ascidian *Synoicum turgens*. The sequences and structures of the peptides were solved with Edman degradation sequencing, mass spectrometry, and NMR analysis. This revealed two novel 2 kDa peptides, St-CRP-1 and St-CRP-2, with neutral net charge, and C-terminal amidation. St-CRP-1 consisted of 18 amino acids and inhibited growth of two Gram-positive bacterial strains (*Bacillus subtilis* and *Corynebacterium glutamicum*) at 24.6 µM, whereas St-CRP-2 consisted of 19 amino acids and inhibited the growth of *B. subtilis* at 49.2 µM. St-CRP-1 had no effect on two mammalian cell lines or the brine shrimp *Artemia salina* at the highest concentration tested. Structural analysis of the St-CRPs indicated a Cys1-Cys6, Cys2-Cys4, and Cys3-Cys5 disulfide connectivity, which is also found in alpha-defensins. The results from this study show that Arctic marine ascidians are a rich source of novel bioactive peptides.

1. Introduction

Peptides are ubiquitous natural products, widely abundant and found in all living organisms, from prokaryotes to mammals. Many small peptides (<50 amino acids) are bioactive, displaying various activities such as analgetic, anticancer, antihypertensive, antimicrobial, antioxidative, antiviral and immunomodulatory properties [1]. Many peptides also show high potency and selectivity, and low toxicity against normal human cells [2]. Furthermore, most peptides are usually less allergenic compared to larger proteins when administered in mammals [3]. Natural peptides are therefore interesting candidates for pharmaceutical research by serving as templates for developing new therapeutic drugs. There are currently around 60 peptide drugs on the global market, and more than 400 different peptides are in clinical development or in preclinical studies, many of which are derived from natural sources [4].

Antimicrobial peptides (AMPs), also referred to as host defense peptides, are produced by all living organisms, in eukaryotes - as an important part of their innate immune system [5,6]. Because of their natural properties as antibiotic agents, AMPs are promising candidates to overcome the growing problem of antibiotic resistant pathogenic bacteria. AMPs are considered particularly favorable due to their broad-spectrum antimicrobial properties and the low-tendency of resistance development towards them [7]. One group of diverse AMPs are called the defensins. Defensins are a family of cysteine-rich AMPs, and are found in vertebrates, invertebrates, plants and fungi. They consist of a characteristic β-sheet core structure, and are most often stabilized with six disulfide-linked cysteines [8]. Defensins exhibit a broad-spectrum antimicrobial activity, displaying effects against both bacteria, fungi and viruses [9].

While linear peptides show limited promise as both orally and parentally administered drugs because of poor *in vivo* stability (due to e.g. proteolytic degradation) and limited membrane permeability [2], cysteine-rich peptides (CRPs) are emerging as a promising class of drug lead candidates and/or templates for drug development [10]. Introduction of disulfide bonds in peptides seems to be among nature´s solutions to the problem of proteolytic degradation. Disulfide bonds effectively constrains peptide topology, resulting in increased structural rigidity and proteolytic resistance [11,12]. Cysteine knot peptides (defined by its three disulfide bridges) and small cysteine-rich proteins are a special sort of peptides containing diverse structures and displaying a wide variety of bioactivities [13].

Marine invertebrates are an increasingly interesting source of novel bioactive peptides because of their ability to thrive in the bacteria-rich-environment without the presence of an adaptive immune system [14-16]. Ascidians (also known as sea squirts) belong to the phylum of Chordata and the subphylum Urochordata (tunicates), and have been a prolific source of bioactive peptides [14]. A variety of bioactive peptides showing anticancer, antineoplastic, antiviral, antidiabetic, antioxidant, and immunomodulatory properties,

have been isolated from ascidians. Several of these peptides have been explored as drugs candidates including a few in clinical trials [17].

As part of our ongoing search for novel AMPs from Arctic marine organisms, two novel cysteine-rich AMPs, turgencin A and turgencin B, were isolated from the colonial ascidian *Synoicum turgens* [18]. The peptides were 35-36 amino acids in length (3.5-3.7 kDa), containing 3 disulfide bridges with an unusual disulfide connectivity of Cys1-Cys6, Cys2-Cys5, and Cys3-Cys4. During the isolation of these peptides, we recognized a series of 2 kDa peptides in the same extract, with putative antimicrobial properties. Preliminary mass spectrometric analysis indicated the presence of multiple cysteines in these peptides. In this study, two small AMPs (18-19 amino acids in length) having 3 disulfide bridges, were isolated from *S. turgens*. St-CRP-1 was sequenced using Edman degradation and LC-MS/MS fragmentation and its structure was confirmed by NMR analysis. The sequence and structure of St-CRP-2 was solved solely with LC-MS/MS. This revealed, for both peptides, a disulfide connectivity similarity to alpha-defensins, a Cys1-Cys6, Cys2-Cys4, and Cys3-Cys5 connectivity.

2. Materials and Methods

2.1. Materials

The colonial sea squirt *S. turgens* (Phipps, 1774) was collected off the coast of Svalbard in August 2016 (79°33′ N, 18°37′ E) by divers at 20-30 m depth. The sample was identified by Robert A. Johansen, Marbank, Norway (http://www.imr.no/marbank/en), and subsequently frozen at -20 °C at sea. The biomass was lyophilized and kept frozen until further processing.

2.2. Extraction

Lyophilized samples of the ascidian (100 g) were pulverized and extracted with 5 volumes (v/w) of 60% acetonitrile (MeCN, HPLC-grade, Sigma-Aldrich, Steinheim, Germany) containing 0.1% trifluoroacetic acid (TFA, HPLC-grade, Sigma-Aldrich) dissolved in Milli-Q H_2O (Millipore, Burlington, MA, USA) for 24 hours at 4 °C. The mixture was centrifuged, and the supernatant was collected and stored at 4 °C before the residue was extracted once more under the same conditions. Supernatants were pooled and incubated at -20 °C for 1-2 h, causing the formation of two liquid phases, an organic MeCN-rich phase and an aqueous salt-rich phase. The aqueous phase was dried in a ScanSpeed 40 vacuum centrifuge (Labogene ApS, Lillerød, Denmark), and afterwards dissolved in 0.05% TFA/ H_2O (v/v) to a concentration of 100 mg/mL. To remove salt form the sample, solid phase extraction (SPE) was performed using reversed-phase C18 35 cc Sep-Pak Vac cartridges (Waters, Milford, MA, USA), as described by Haug et al. [19] with some modifications. Briefly, the cartridge was conditioned in MeCN and equilibrated with 0.05% TFA/H_2O (v/v)

before adding the aqueous phase. After washing the loaded extract with acidified water, a five-step elution was done with 10, 20, 30, 40, and 80% (v/v) MeCN containing 0.05% TFA (v/v). The collected SPE eluates were dried in a ScanSpeed 40 vacuum centrifuge and kept frozen at -20 °C until further analysis.

The SPE fractions were resuspended in Milli-Q H_2O to a concentration of 10 mg/mL. Non-dissolved material was removed by centrifugation, and the supernatant was tested for antibacterial activity.

2.3. Peptide Purification and Identification

Active SPE fractions were submitted to purification by preparative reversed-phase high-performance liquid chromatography (RP-HPLC). The separation was performed using an Agilent 218 Preparative gradient LC system coupled to an Agilent 1260 infinity DAD and an Agilent 440-LC fraction collector (Matriks, Oslo, Norway). The column used was an XBridge BEH C18 Prep column (10 × 250 mm, 5 µm, Waters). The mobile phase consisted of A: H_2O with 0.05% TFA and B: MeCN with 0.05% TFA, where the method was set to run mobile phase A for 10 min, then a gradient of 0-60% of mobile phase B from 10-70 min, with a flow rate of 6 mL/min. One-minute fractions were collected throughout the analysis, vacuum dried separately and redissolved in 500 µL Milli-Q H_2O, before testing for antibacterial activity. All SPE fractions, and the active HPLC fractions were submitted to high-resolution mass spectrometry (HR-MS) analysis, using an Agilent 1290 Infinity UHPLC-DAD system and an Agilent 6540B quadrupole time-of-flight (Q-ToF) mass spectrometer coupled with a dual electrospray ionization (ESI) source. The data was acquired and analyzed by using the Agilent MassHunter software (Data Acquisition B.06.01, SP1, and Qualitative Analysis B.07.00, SP2)) (all instruments and software were from Matriks). A standard method was used, running a gradient from 5-100% MeCN with 0.1% formic acid over 8 min with a flow rate of 0.3 mL/min. The separation was done using an Agilent Zorbax Eclipse Plus C18 column (2.1 × 50 mm , 1.8 µM, Matriks).

The HR-MS analysis confirmed the presence of the small (ca. 2 kDa) peptides in some of the antibacterial HPLC fractions, derived from the 40% MeCN SPE fraction. In order to isolate these peptides, the SPE fraction was repeatedly injected on the preparative RP-HPLC system, using an optimized RP-HPLC method. The mobile phase consisted of the same constituents as described above, However, elution was performed by running 20% of mobile phase B for 5 min, then a gradient of 20-45% of mobile phase B from 5-35 min, with a flow rate of 6 mL/min. The peptides were isolated by triggering collection at predetermined timepoints during the run. Each fraction was analyzed using the Agilent HR-MS system, and fractions containing pure peptides were pooled, lyophilized, and kept frozen at -20 °C until further analysis.

2.4. Sequence Analysis

Primary structure determination of St-CRP-1 was performed with Edman degradation sequencing at Eurosequence (Groningen, The Netherlands, www.eurosequence.nl). For *de novo* MS sequencing of St-

CRP-2, 2 μL 0.5 mM peptide was added 20 μL 0.1 M Tris[2-carboxyethyl] phosphine (TCEP, Sigma-Aldrich, St. Louis, MO, USA) and 50 μL 1 mM ammonium format buffer adjusted to pH 3 with formic acid. The solution was incubated at room temperature for one hour for full reduction of the peptide. The reduced peptide was analyzed on an Acquity I-class UPLC with a Waters Xevo QToF G2 mass spectrometer (Waters). The separation was performed using an Acquity BEH C18 column (2.1 × 100 mm, 1.7 μm, Waters), and a mobile phase gradient consisting of A: water + 0.1% formic acid and B: MeCN + 0.1% formic acid. Fragmentation spectra were obtained by CID fragmentation with a collision energy ramp of 20-50 eV. The fragment spectra gave full coverage of the peptide sequence, and for confirmation, the proposed sequence was inserted in MS-product from UCSF (http://prospector.ucsf.edu/prospector/cgi-bin/msform.cgi?form=msproduct) to induce peptide fragmentation. Isoelectric points (pI) were calculated using Innovagen's peptide property calculator app (http://www.innovagen.com). Sequence similarity searches were performed using the Basic Local Alignment Search Tool (BLAST, https://blast.ncbi.nlm.nih.gov/Blast.cgi), provided by the National Centre for Biotechnological Information (NCBI).

2.5. NMR Spectroscopy and Calculations

NMR experiments were acquired on an Avance III HD spectrometer equipped with an inverse four-channel probe with cryogenic enhancement for ^{1}H, ^{2}H and ^{13}C (TCI) operating at 600 MHz for ^{1}H (Bruker Biospin, Fällanden, Switzerland).

The sample of St-CRP-1 was prepared by dissolving 0.8 mg of material in 120 μL of H$_2$O/D$_2$O solution (95/5) in a D$_2$O matched 3 mm Shigemi tube. The following experiments were acquired for the elucidation of St-CRP-1: ^{1}H (excitation sculpting), ^{13}C, ^{15}N-HSQC, ^{13}C-HSQC, HMBC (including selective carbonyl HMBC), HSQCTOCSY (80 ms DIPSI), NOESY (100, 200, 300 ms mixing time), ROESY (100 ms spinlock), DQF-COSY, E.COSY and TOCSY (60, 100 ms DIPSI). Where applicable, gradient-selection and adiabatic pulse sequences were used. Acquisition and processing were done in Topspin 3.5pl7 using standard pulse sequences (Bruker Biospin). Spectral assignment and integration were done in CARA 1.8.4.2.

Starting structures were created as extended chains and folded using standard simulated annealing protocol (2000 K, 20000 cooling steps *in vacuo*) using observed NMR parameters, and with an absence of disulfide connectivity. Low energy folds from the previous step were used to generate disulfide connected starting structures for the final refinements. Finally, production runs of 500 cycles of simulated annealing generated the reported structure ensemble. Structures were generated using XPLOR-NIH 2.52 and secondary structure prediction made in TALOS+ (https://spin.niddk.nih.gov/NMRPipe/talos/). The NMR data is available at the Biological Magnetic Resonance Data Bank (https://bmrb.io/) under accession number 50547.

2.6. Reduction and Alkylation of the Peptides

To determine the disulfide connectivity in the peptides a reduction and alkylation method by Albert et al. was employed [20]. All chemicals used in this method were purchased from Sigma-Aldrich. The protocols for St-CRP-1 and St-CRP-2 were optimized individually, using the described method as a template. An overview of the analytical method and details on the reduction and alkylation procedures will be given here.

St-CRP-1: The SPE column (Empore C18, 3M, St. Paul, MN, USA) was activated with 250 µL MeCN and subsequently equilibrated with 500 µL ammonium formate buffer (50 mM, pH 3). The peptide was dissolved in the same buffer to a concentration of 0.5 mM and a volume of 500 µL was applied to the column. A volume of 100 µL 0.1 M TCEP was loaded onto the column to selectively reduce available cysteine bridges and the mixture on the column was incubated for 1 min before the column was washed 3 times with 300 µL of ammonium formate buffer/MeCN 90:10 (v/v), and once with 250 µL of the same buffer. Immediately after, the peptide was alkylated by adding 20 µL 0.5 M *N*-methylmaleimide (NMM) dissolved in buffer and the solution was left to incubate for 1 hour. The sample was eluted from the column with 300 µL 80% MeCN, and MeCN was removed under a gentle stream of nitrogen at 55 °C. To remove excess NMM, 100 µL of 0.5 M thiosalicylic acid (TA) was added and left to react with remaining NMM for 30 min. The sample was loaded onto a freshly equilibrated SPE column and washed 3 times with 300 µL 10% MeCN and once with buffer. For the second reduction, 100 µL of 0.1 M TCEP was again added and left to incubate for 1 min before the column was washed 3 times with 300 µL 10% MeCN and once with 300 µL buffer. The peptides were alkylated for the second time by adding 20 µL of a 0.5 M solution of *N*-ethylmaleimide (NEM) and the solution was left to incubate for 1 hour before the column was washed, as described above. Excess NEM was removed with TA as described for NMM and after washing and eluting from the column 20 µL of 0.1 M TCEP was added to the solution and left to incubate for 1 hour. The final alkylation was performed by adding 20 µL 0.12 M *N*-cyclohexyl maleimide (NCM) and the solution was left to incubate for 3 hours.

St-CRP-2: In general, the same alkylation protocol was used for St-CRP-2, but with some modifications. The peptide was dissolved in the same buffer, but 450 µL of a 0.5 mM peptide solution was added to the column. A volume of 50 µL 0.1 M TCEP was added to the column to selectively reduce available cysteine bridges. After incubation, the column was washed with 500 µL 20% MeCN. Immediately afterwards, 10 µL of a 0.5 M NMM solution was added to alkylate the reduced cysteines and the solution was incubated for 1 hour. To remove excess NMM the column was washed 5 times with 500 µL 20% MeCN. The second reduction and alkylation were done by adding 50 µL of 0.1 M TCEP to the peptide solution before incubation for 1 min. The column was then washed with 500 µL 20% MeCN and immediately loaded with 10 µL 0.5 M NEM which was left to incubate for 1 hour. A volume of 50 µL 0.5 M TA was added to the column and

left to incubate for 0.5 hour to react with excess NEM before the column was washed 3 times with 500 μL 20% MeCN. The third and final reduction and alkylation was done in solution by eluting the peptide from the column with 300 μL 80% MeCN before 20 μL 0.1 M TCEP was added and left to incubate for 1 hour to reduce the remaining disulfide bridges. Then 20 μL of a 0.12 M NCM solution was added to complete the alkylation of the last cysteines.

Reduced and alkylated peptides were analyzed using the same MS instrument, column and mobile phase as described in the sequence analysis method. Mass spectrometric identification parameters were similar as for Albert et al. [20]. For both peptides a collision energy ramp of 26-58 eV was used for optimal fragmentation.

2.7. Antibacterial Activity Assay

All MeCN SPE fractions and HPLC fractions collected from the 40% MeCN SPE, as well as the isolated St-CRPs were screened for activity against *Escherichia coli* (ATCC 25922), *Pseudomonas aeruginosa* (ATCC 27853), *Staphylococcus aureus* (ATCC 9144), *Corynebacterium glutamicum* (ATCC 13032) and *Bacillus subtilis* (ATCC 23857). All isolates were grown in Mueller-Hinton (MH) broth (Difco Laboratories, Detroit, MI, USA) at room temperature. The assays were performed in 96 microwell plates (Thermo Fisher Scientific, Roskilde, Denmark) as previously described [21], but with a few exceptions; the cultures were diluted in MH broth to a concentration of $2.5\text{-}3.0\times10^4$ bacteria/mL, and 50 μL was added to each well in a plate preloaded with 50 μL of either SPE in a dilution series, HPLC fractions, or a dilution series of St-CRPs and controls. The purified peptides (>95% purity based on UHPLC-DAD-MS analysis) were dissolved in DMSO (Sigma-Aldrich), vortexed, and added MQ-H_2O to end up with a stock solution of 500 μg/mL containing 2.5% DMSO. The stock solution was diluted in MQ-H_2O to obtain final test concentrations ranging from 2.5-100 μg/mL. Oxytetracycline (Sigma-Aldrich) was used as a positive (antibacterial) control (0.04-40 μM), MQ-H_2O as a negative (growth) control, and a DMSO control was made using the highest tested concentration of DMSO (0.25% DMSO). All experiments were done in technical triplicates. The bacterial growth at 35 ˚C was monitored with an EnVision Multilable Reader (PerkinElmer, Llantrisant, United Kingdom), where the optical density (OD$_{595}$) was measured every hour for 24 hours. The minimum inhibitory concentration (MIC) was defined as the concentration resulting in >90% reduction in OD$_{595}$ after 24 hours compared to the negative (bacterial growth) control.

2.8. Human Cell Viability Assay

The cytotoxic activities of St-CRP-1 was tested on two cell lines: A2058 (a human melanoma cancer cell line, ATCC CRL-11147TM) and MRC-5 (a non-malignant human fibroblast cell line, ATCC CCL-171). The peptides were assayed using a two-fold dilution series, ranging from 5-100 μg/mL. The assays were performed as previously described [22]. Cell viability calculation: cell survival (%) = (absorbance treated

wells − absorbance positive control)/(absorbance negative control − absorbance positive control) × 100. Both assays were performed in technical triplicates in two independent experiments.

2.9. Brine Shrimp Lethality Assay

St-CRP-1 was tested for toxic effect against *Artemia salina* nauplii as previously described by Haug et al. [23], with some modifications. Sterile filtered (0.22 μm) seawater was added to an illuminated petri dish with a teaspoon of dried brine shrimp eggs and incubated at 22-24 ˚C. After 48 hours of incubation, 100 μL of seawater containing 10-20 freshly hatched nauplii was added to separate wells in 96 microwell plates (Thermo Fisher Scientific). Three dilutions of the peptide were added to the wells (in duplicates) at final concentrations of 100, 50 and 25 μg/mL. The plates were incubated with illumination at 22-24 ˚C, and dead nauplii were counted after 6 (acute toxicity) and 24 hours (chronic toxicity). MQ-H_2O was used as negative control, and potassium dichromate ($K_2Cr_2O_7$, Sigma, 10-1000 ppm) was used as a positive control.

3. Results and Discussion

3.1. Peptide Purification and Mass Spectrometry Analysis

Colonies of *S. turgens*, collected from the coast of Svalbard, were lyophilized, crunched, and extracted with 60% acidified MeCN. After removing the sediment, the extract was separated into an organic phase and an aqueous phase (containing a high concentration of salt). The aqueous phase was subjected to SPE to remove the salt content, and to gain a rough compound separation based on their polarity. Antibacterial screening was done on the organic phase and the 5 fractions obtained after solid phase extraction. All fractions tested displayed antibacterial activity, but the 40% MeCN SPE fraction was the most potent fraction, but mainly against the Gram-positive strains *C. glutamicum* and *B. subtilis* (Table S1 in the SI). This fraction was therefore subjected to further fractionation by preparative RP-HPLC, and the collected one-minute HPLC fractions were tested against the same panel of bacteria as the SPE fractions to get a pointer towards which fractions/compounds might be causing the antibacterial effect. Such bioassay-guided purification has proven effective when discovering and isolating novel marine AMPs [21,24,25]. Several of the obtained HPLC fractions (fractions 40-52), containing compounds eluting at approximately 30-40% MeCN, displayed antibacterial activity against several of the test strains (Figure 1).

HR-MS analysis of the active fractions proved that many of them (fractions 42-43 and 47-51) contained the previously described AMPs turgencin A and B, both also having various oxidized versions (Figure 1) [18]. The turgencins (3.5-3.7 kDa) was originally isolated from the 80% MeCN SPE fraction due to much higher abundance of these peptides in that SPE fraction [18]. In the present study, HPLC fraction 44 (displaying

activity against all test strains), contained only minor amounts of the previously described AMP turgencin A_{Mox1} [18], indicating that another compound or compounds might be responsible for the activity observed. The most abundant molecule in this fraction was a smaller peptide that we later named, St-CRP-1. Mass-to-charge (m/z) ions recorded for this peptide were m/z 1019.8 and m/z 680.2, corresponding to $[M + 2H]^{2+}$ and $[M + 3H]^{3+}$, respectively. The monoisotopic mass of St-CRP-1 was determined to be 2037.67 Da by doing deconvolution of the isotopes.

Another peptide with similar size as St-CRP-1 was discovered in the broad-spectrum antibacterial HPLC fraction 48 (Figure 1). This peptide was named St-CRP-2. m/z ions recorded for this peptide were m/z 1003.9 and m/z 669.6, corresponding to $[M + 2H]^{2+}$ and $[M + 3H]^{3+}$, respectively. The monoisotopic mass of St-CRP-2 was determined to be 2005.75 Da. However, the most abundant molecule in this active HPLC fraction was the AMP turgencin B_{Mox2}. The peaks containing the St-CRPs are marked in bold in the RP-HPLC-DAD chromatogram in Figure 1.
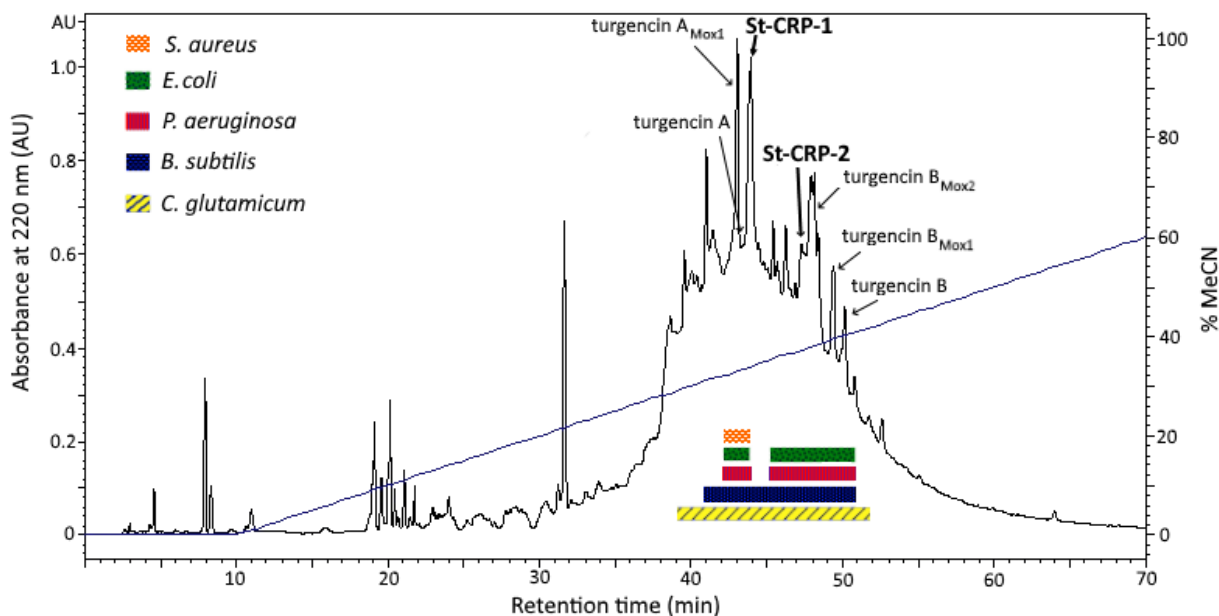
Figure 1. Preparative RP-HPLC-DAD chromatogram (recorded at 220 nm) of the 40% MeCN SPE fraction of *Synoicum turgens*. The peak fractions containing the St-CRP peptides and the turgencins are marked with arrows. HPLC fractions displaying antibacterial activity are marked with colored boxes below the chromatogram. The blue line shows the linear gradient (0-60%) of MeCN containing 0.05% TFA.

The St-CRPs proved to be challenging to purify as they coeluted with several other peptides with similar hydrophobicity. Another obstacle was the poor solubility after drying the isolated peptides. A prolonged process of optimizing the RP-HPLC method provided enough material of St-CRP-1 (1.2 mg) for nuclear

magnetic resonance (NMR) and bioactivity analysis. The amount of pure St-CRP-2 (0.6 mg) was only sufficient for the antibacterial assays and MS analysis. UPLC-DAD analysis of the isolated peptides indicated a purity of >95% for both the St-CRPs (Figure S1 and S2 in the SI).

3.2. Sequence Analysis

Edman degradation analysis of St-CRP-1 revealed an 18-residue N-terminal sequence (CCDQCYGFCRLVDNCCNS). The calculated monoisotopic mass of this sequence, assuming the six cysteines forms three disulfide bridges, is 2038.70 Da. The mass difference between measured and calculated mass of around -1 Da can be explained by a C-terminally amidated serine. C-terminal amidation occurs in all previously sequenced peptides from *S. turgens* [18], and is a known feature in antimicrobial peptides from eukaryotic organisms [26]. The sequence was confirmed by NMR analysis.

The sequence of St-CRP-2 was obtained by *de novo* sequencing using MS/MS. The peptide was treated with TCEP in acidic pH to break the disulfide bonds and subsequently analyzed on a UPLC-QToF-MS apparatus. This analysis resulted in a good sequence coverage, providing a 19-residue sequence (SCCEYCSXSCXVSGXXCCQ) with a C-terminally amidated glutamine (Figure S3 in the SI). The proposed fragments from MS-product (UCSF, ProteinProspector v.6.3.1, http://prospector.ucsf.edu) corresponded to the observed fragments in the MS/MS analysis and confirmed the sequence. Four amino acids in the MS/MS spectra were determined to be either leucine or isoleucine (both having a monoisotopic mass of 113.08 Da), but the method used could not distinguish between them, hence the X positions noted in the sequence. The calculated monoisotopic mass of this sequence, assuming three disulfide bridges, C-terminal amidation, and replacing X with leucine, is 2005.75 Da – the same mass as measured HR-MS.

Sequence alignment of the St-CRPs illustrates the similarities between the two peptides (Figure 2). They share the same cysteine pattern (CC-C-C-CC), are both C-terminally amidated, and neutrally charged with a calculated pI of 6.94 (St-CRP-1) and 6.58 (St-CRP-2). NCBI BLAST analyses revealed no sequence similarities to other known peptides or proteins. In addition, no similarities were found to any of the major AMP families present in the CAMP$_{R3}$ database by using the CAMPSign tool [27]. Furthermore, only 191 of the 3346 antimicrobial peptides registered at APD3 have a net charge of 0, whereof 41 have structures with 3 disulfide bonds. Most of these cysteine rich neutral peptides comes from plants (38 out 41), and their size differs between 26-46 amino acids [28].

Figure 2. Sequence alignment of St-CRP-1 and St-CRP-2. Gaps (_) are introduced to maximize the alignment. Residues: yellow = Cys, red = acidic amino acids, blue = basic amino acid, X = Ile/Leu.

Knowledge obtained of the structures gave some clues about the solubility obstacles. Prior to this current information, the peptides were subjected to be dissolved in pure water, but with variable result. The solubility of the peptides improved when adding a small amount of DMSO first, before diluting the DMSO concentration considerably with water. DMSO at high concentrations has been known to interfere with bioassays, and the final concentration needs be kept at a minimum, with appropriate controls, to avoid false positives [29].

3.3. Structure Determination

The water-suppressed ^{1}H spectra of St-CRP-1 was clean, with no impurities above 5 mol%, and well-resolved. ^{15}N-HSQC and TOCSY spectra enabled the unambiguous assignment of all 18 amino acid residues (Table S2 and S3 in the SI). The sequence was assigned by NOE hopping supported by high resolution HMBC correlations through the backbone carbonyls where possible. In total 69 inter-residue backbone-backbone and backbone-sidechain through-space correlations could be extracted from the collected 100, 200 and 400 ms mixing time NOESYs. These NOEs were consistent with the sequence for St-CRP-1 (Figure 3).
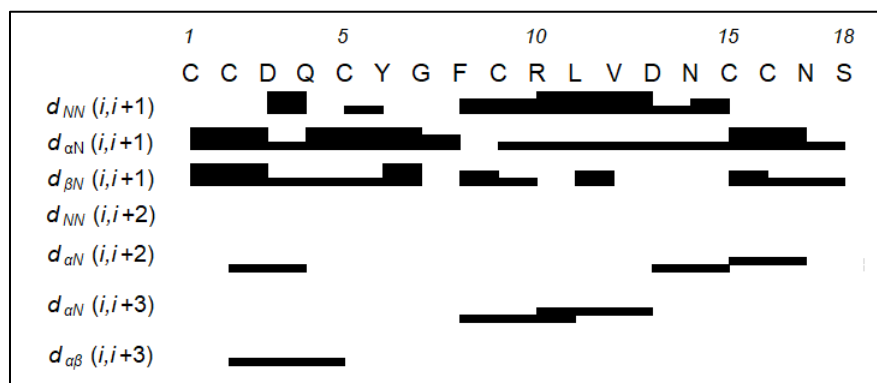
Figure 3. Inter-residual NOEs for St-CRP-1 between adjacent residues extracted from 100, 200, and 300 ms NOESY NMR experiments. The line thickness for the 'i, i+1' couplings indicate the strength of the correlation: the thicker the line, the stronger the crosspeak. For 'i, i+2' and greater, the lines indicate which two residues dipolar couplings can be identified between specified backbone residues.

An additional 144 non-sequential inter- and intra-residual NOEs were extracted, to a combined total of 213 unique NOEs. The NOEs were qualitatively classified as one of four categories: Strong, Medium, Weak, Very Weak based on their intensities and correspond with upper limit distance constraints of 2.7, 3.5, 5.0, and 6.0 Å respectively.

Three dimensional structures were generated by simulated annealing protocols to produce a series of energetically minimized structures. First, structures were generated from an extended chain without any designation of disulfide bonds, applying only the distance constraints to fold the peptide. Three iterations were calculated, where any violations of interatomic distances due to overlaps or other sources of erroneous input were resolved to refine the fold. A batch production run of 500 structures was generated using the iterated constraints, and the 10 most energetically favorable structures were selected, and the sulfur-sulfur interatomic distances were plotted (Figure 4). By comparing the distances between each cysteine sulfur, the nearest and therefor most likely bonding partners were identified. The determined disulfide bridge partners were Cys1-Cys16, Cys2-Cys9, Cys5-Cys15, giving a C1-C6/C2-C4/C3-C5 disulfide pattern.
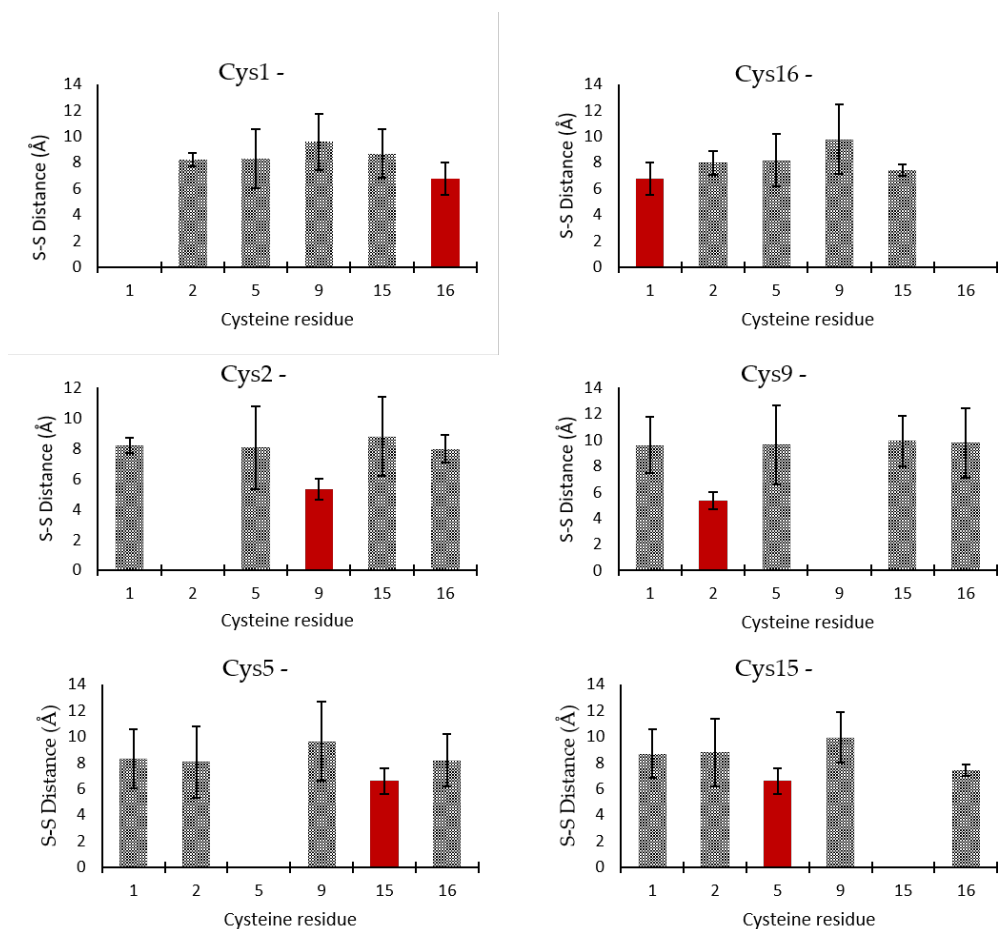
Figure 4. Average inter-sulfur distances for the six cysteines identified in St-CRP-1. The shortest distance is highlighted in red, being consistent with a C1-C6/C2-C4/C3-C5 disulfide pattern.

A final production batch was calculated with the C1-C6/C2-C4/C3-C5 disulfide pattern, using the same simulated annealing protocol together with the refined distance constraints, adding also dihedral bond angle constraints predicted from the H, N, C, CA, CB, HA and HB chemical shifts using TALOS+. The lowest energy structures (energies below 2 kcal) were selected for analysis, representing 38 of the 500 structures. Evaluation of the structures revealed that the structures adopt one of two energetically equivalent conformations – an open fold with a small stretch of helix (Figure 5a and b – 21/38 structures), and a knot conformation (Figure 5c and d – 17/38 structures).

(a)   (b)   (c)   (d)
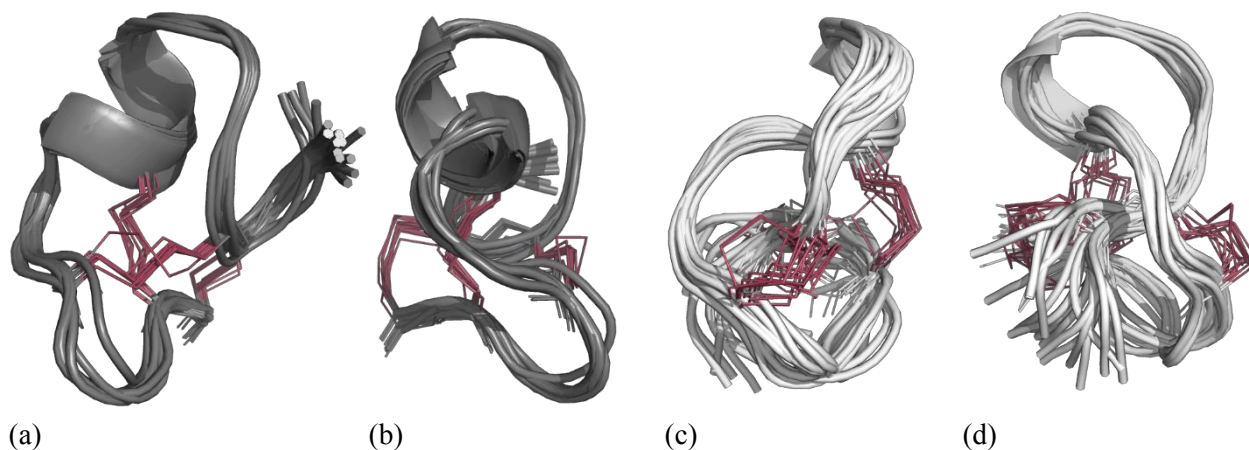
Figure 5. The lowest energy structures generated from the simulated annealing of St-CRP-1 with a defined disulfide bridge pattern of C1-C6/C2-C4/C3-C5 in combination with NOE constraints and TALOS+ predicted dihedrals. The open structure (a), and the 90-degree rotated view (b), compared to the knot structure (c) and its rotated view (d).

Both these structures satisfied the experimental constraints equally well. The structures were evaluated for correlations that would be expected according to the conformation adopted but were absent in the data set – indicating if one conformation is more or less supported by the acquired data. The knot structure is more condensed and if this conformation was populated one would expect to observe a range of correlations between the C-terminus and residues 6-9 where the knot is formed. The clearest example was between HA-Tyr6 and HA-Cys16 (a distance of 4 Å). Since this correlation was not observed in the data and no clear inconsistencies with the open conformation could be found, we introduced a repulsion between HA Tyr6 and HA Cys16 and recalculated the structures. This abolished the knot conformation and resulted in a final structure ensemble presented in Figure 6. Three out of the 31 lowest energy structures had a backbone RMSD of more than 2.5 Å from the lowest energy structure and these were omitted from the graphical representation as a minor outlying conformation for visual clarity. The backbone RMSD of the other 28 structures were all 1.0 Å or less (Table S4 in the SI).

A short alpha-helical loop stretches between Cys9 and Val12 could be identified and was amply represented in the calculated structure ensemble (15 out of 19 in the final ensemble). Strong NH(i)-NH(i+1), and medium strength αH(i)- NH(i+1) NOEs were recorded for this stretch, which is consistent with an alpha-helical conformation being populated. Furthermore, two NH(i)-NH(i+3) correlations were also identified from residues 8 to 11 and 10 to 13, which is consistent with an alpha helix.

(a)   (b)
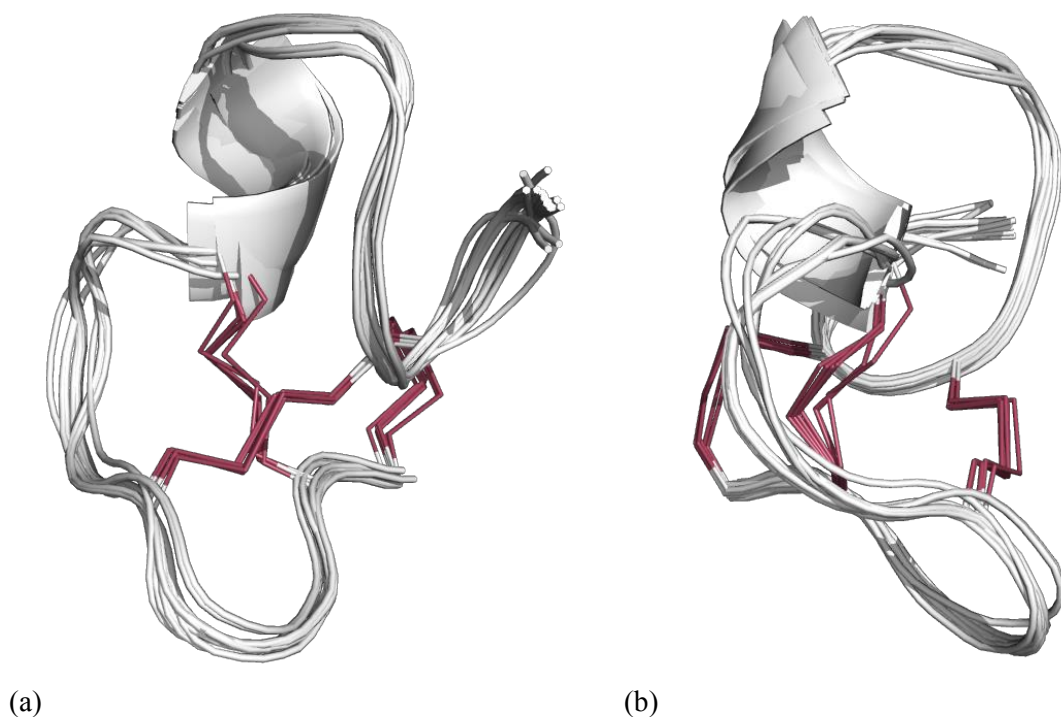
Figure 6. The 19 lowest energy structure ensembles generated from the simulated annealing of St-CRP-1 with the defined disulfide bridge pattern of C1-C6/C2-C4/C3-C5 in combination with NOE constraints and TALOS+ predicted dihedrals (a), and the 90-degree rotated view (b).

The disulfide bridge pattern for both peptides was confirmed with LC-MS/MS by using a sequential alkylation method, introduced by Albert et al. [20]. The peptides were reduced and alkylated with different maleimides on solid phase before sequencing. The reduction and alkylation process resulted in a mixture of different alkylation patterns where the number of cysteines with different alkylating agents were 2xNMM + 4xNEM, 4xNMM + 2xNEM, 2xNMM + 4xNCM, 4xNMM + 2xNCM, 2xNEM + 4xNCM, 4xNEM + 2xNCM, 2xNMM + 2xNEM + 2xNCM, 2xNMM and 4xNMM without further alkylation, and 6xNMM for both peptides. In addition, St-CRP-1 got a pattern of 2xNMM+ 2xNEM without further reduction and alkylation that was not seen for St-CRP-2. Several of the alkylation patterns could be used to determine the disulfide connectivity, but the most convenient pattern was the 2xNMM + 2xNEM + 2xNCM, where each

bridge results in a pair of cysteines with the same alkylating agent. The other alkylating patterns were used to confirm the findings from this pattern.

To determine cysteine connectivity by MS/MS analysis, the $[M+2H]^{2+}$ ion and the corresponding acetylated ion was used for both peptides. The m/z value of this ion differs depending on the alkylation pattern, but for the 2xNMM + 2xNEM + 2xNCM pattern the St-CRP-1 peptide gave m/z = 1438.04 (acetylated m/z = 1459.05 (Figure 7) and the St-CRP-2 peptide gave m/z = 1422.08 (acetylated m/z = 1443.09) (Figure 8). The observed b- and y-ions of the acetylated $[M+2H]^{2+}$ of St-CRP-1 indicates that Cys1 and Cys16 are alkylated with maleimide NEM, Cys2 and Cys9 with NMM, and Cys5 and Cys15 with NCM (Figure 7). This verifies the C1-C6/C2-C4/C3-C5 connectivity for St-CRP-1 obtained by NMR.
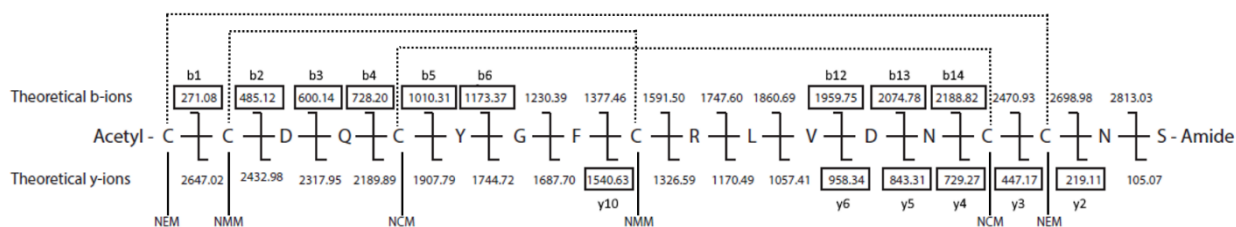
Figure 7. The alkylation pattern 2xNEM + 2xNMM + 2xNCM of the acetylated doubly charged $[M+2H]^{2+}$ molecular ion of St-CRP-1. The framed masses are b- and y-ions identified in the MS/MS spectra. The dotted lines illustrate the disulfide bridges.

St-CRP-2 showed the same disulfide bridge pattern as St-CRP-1. From the acetylated $[M+2H]^{2+}$ ion of St-CRP-2, two spectra showed the 2xNMM + 2xNEM + 2xNCM pattern. The observed b-ions, b-ions with water loss, y-ions, and y-ions with ammonia loss identified Cys1 and Cys16 to be alkylated with maleimide NCM, Cys2 and Cys9 with NEM, and Cys5 and Cys15 with NMM (Figure 8).
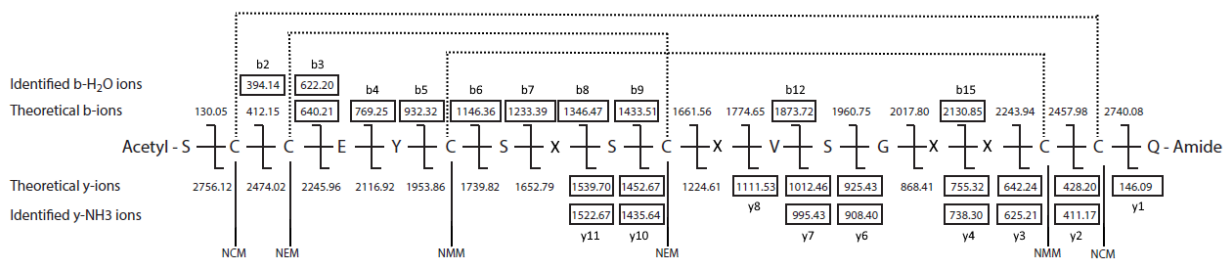
Figure 8. The alkylation pattern 2xNCM + 2xNEM + 2xNMM of the acetylated doubly charged $[M+2H]^{2+}$ molecular ion of St-CRP-2. The framed masses are b-, b-H_2O, y- and y-NH_3 ions identified in the MS/MS spectra. The dotted lines illustrate the disulfide bridges. The X in the sequence is either I or L.

The same cysteine connectivity was confirmed in another spectrum of St-CRP-2, where the identified fragments showed Cys1 and Cys16 to be alkylated with maleimide NEM, Cys2 and Cys9 with NMM, and Cys5 and Cys15 with NCM (Figure S4 in the SI). This gave the same cysteine pattern as for St-CRP-1, a C1-C6/C2-C4/C3-C5 connectivity. In contrast, the turgencins have a C1-C6/C2-C5/C3-C4 connectivity [18]. The St-CRPs share the same cysteine connectivity as mammalian alpha-defensins [8], and other AMPs such as aurelin from the jellyfish *Aurelia aurita* [30] and damicornin from the coral *Pocillopora damicornis* [31]. Other than the cysteine connectivity, these peptides share few similarities with the St-CRPs. They are all cationic peptides (damicornin with as much as 9 charges) and bigger in size (<30 amino acids), while the St-CRPs have a neutral net charge and less than 20 amino acids.

Another peptide family that has a C1-C6/C2-C4/C3-C5 connectivity is the M2 family of the conotoxins. In addition, the majority of the entire M family share the same cysteine pattern (CC-C-C-CC) as the St-CRPs [32]. These cysteine pattern similarities are interesting, but other than that, no relations can be drawn between the M2-family and the St-CRPs based on the information that is available. Many conotoxin families are well described in literature, but there are limited published data on the biological targets and mechanism of action of the peptides coming from the M2 branch. It has been reported that some of these peptides gives a strong excitatory behavior in mice [32].

3.4. Biological Activity

As the HPLC-fractions containing the St-CRPs possessed antibacterial properties (Figure 1), the purified peptides were tested against the same panel of bacteria to verify the antibacterial activity. In addition, St-CRP-1 was tested for toxicity against the brine shrimp *A. salina*, and for cytotoxic activity against a human melanoma cancer cell line A2058, and a non-malignant human fibroblast cell line MRC-5. The St-CRPs showed only moderate activity against a few bacterial strains. St-CRP-1 displayed a MIC-value of 50 µg/mL (24.6 µM) against *C. glutamicum* and *B. subtilis*, whereas St-CRP-2 displayed a MIC-value of 100 µg/mL (49.2 µM) *B. subtilis* (Table 1). None of the peptides were active against the Gram-negative bacterial strains at the highest concentration tested (100 µg/mL), which equals to 49.1 µM for St-CRP-1 and 49.2 µM for St-CRP-2, respectively. Also, St-CRP-1 showed no activity in any of the toxicity assays at the highest concentration tested. This conforms well with other neutral CRPs found in the APD3, whereof half of these peptides have unknown bioactivity [28]. In some cases, like with the varv peptides from the plant *Viola arvensis*, the plant produces several neutral CRPs with both known bioactivity (varv peptide A – anticancer, and varv peptide E – antiviral and hemolytic) and unknown bioactivity (varv peptide C and D) [33,34].

Table 1. Antimicrobial and cytotoxic activity of St-CRPs.

Peptide	Antimicrobial activity (MIC; µg/mL)					Brine shrimp toxicity (LC$_{50}$; µg/mL)	Cytotoxic activity (IC$_{50}$; µg/mL)	
	Cg	Bs	Sa	Ec	Pa	As	A2058	MRC-5
St-CRP-1	50	50	>100	>100	>100	>100	>100	>100
St-CRP-2	>100	100	>100	>100	>100	N.t	N.t	N.t

Cg - *Corynebacterium glutamicum*, Bs - *Bacillus subtilis*, Sa - *Staphylococcus aureus*, Ec - *Escherichia coli, Pa – Pseudomonas aeruginsa,* As - *Artemia salina*. N.t : Not tested

Compared to some of the turgencins [18], which in general showed much higher antibacterial activity against the same panel of bacteria, one could assume that the main function of the St-CRPs is not to interfere with (inhibit the growth of or kill) bacteria directly. Here we have tested purified peptides alone *in vitro* against standard laboratory bacteria. It is plausible that the peptides would be more potent towards marine pathogenic bacteria, which is a bigger threat to the animal than the terrestrial strains tested. This have been observed in other studies of marine derived antimicrobial peptides [24]. However, the peptides might also have other host defense functions *in vivo*. Perhaps the St-CRPs generates a synergistic effect together with the turgencins or other compounds from the ascidian. The HPLC-fraction containing St-CRP-1 was active against all bacteria tested, and the fraction containing St-CRP-2 was active against 4 out of 5 strains tested. The St-CRPs was the dominant compounds in their respective HPLC-fractions. Since the St-CRPs showed no activity at 100 µg/mL against the Gram-negative bacterial strains tested (*E. coli* and *P. aeruginosa*) as well as against *S. aureus*, the activity had to come from other compounds in the fractions or be due to synergistic effect between the St-CRPs and other compounds. Many organisms produce cocktails of different AMPs to fight for their survival, and the main function of many of these peptides are yet to be explored [34].

4. Conclusions

The world-wide spread of antibiotic resistance has fueled the search for and discovery of novel antibacterial molecules. AMPs are promising candidates because of their broad-spectrum antimicrobial properties and fewer cases of antimicrobial resistance developed towards them. In addition, cysteine-rich AMPs (or CRPs) are generally also less prone to proteolytic degradation. In the present study, two novel cystine-rich peptides, St-CRP-1 and St-CRP-2, were isolated from the Arctic ascidian, *S. turgens*. The peptides consist of 18-19 amino acids, are neutrally charged, and share the same cysteine connectivity as alpha-defensins and M2 family of the conotoxins, a C1-C6/C2-C4/C3-C5 connectivity. A gene characterization of the St-CRPs could reveal the evolutionary relationship between them and other CRPs. The St-CRPs showed moderate

antibacterial activity, and no cytotoxicity against mammalian cells. Ascidians have proven to be a promising resource for finding novel peptides - potential templates for drug development.

Conflict of Interest: The authors declare no conflict of interest.

References

1. Cheung, R.C.F.; Ng, T.B.; Wong, J.H. Marine peptides: Bioactivities and applications. *Mar. Drugs* **2015**, *13*, 4006-4043, https://doi.org/10.3390/md13074006
2. Fosgerau, K.; Hoffmann, T. Peptide therapeutics: current status and future directions. *Drug Discov. Today* **2015**, *20*, 122-128, https://doi.org/10.1016/j.drudis.2014.10.003
3. Høst, A.; Halken, S. Hypoallergenic formulas – when, to whom and how long: after more than 15 years we know the right indication! *Allergy* **2004**, *59*, 45-52, https://doi.org/10.1111/j.1398-9995.2004.00574.x
4. Lau, J.L.; Dunn, M.K. Therapeutic peptides: Historical perspectives, current development trends, and future directions. *Bioorgan. Med. Chem.* **2018**, *26*, 2700-2707, https://doi.org/10.1016/j.bmc.2017.06.052
5. Ganz, T. The role of antimicrobial peptides in innate immunity. *Integr. Comp. Biol.* **2003**, *43*, 300-304, http://dx.doi.org/10.1093/icb/43.2.300
6. Hancock, R.E.W.; Sahl, H.-G. Antimicrobial and host-defense peptides as new anti-infective therapeutic strategies. *Nat. Biotechnol.* **2006**, *24*, 1551-1557, http://dx.doi.org/10.1038/nbt1267
7. Hancock, R.; Patrzykat, A. Clinical development of cationic antimicrobial peptides: from natural to novel antibiotics. *Curr. Drug. Targets. Infect. Disord.* **2002**, *2*, 79-83, https://doi.org/10.2174/1568005024605855
8. Ganz, T. Defensins: antimicrobial peptides of innate immunity. *Nat. Rev. Immunol.* **2003**, *3*, 710-720, https://doi.org/10.1038/nri1180
9. Raj, P.A.; Dentino, A.R. Current status of defensins and their role in innate and adaptive immunity. *FEMS Microbiol. Lett.* **2002**, *206*, 9-18, https://doi.org/10.1111/j.1574-6968.2002.tb10979.x
10. Muttenthaler, M.; King, G.F.; Adams, D.J.; Alewood, P.F. Trends in peptide drug discovery. *Nat. Rev. Drug Discov.* **2021**, *20*, 309-325, https://doi.org/10.1038/s41573-020-00135-8
11. Wang, C.K.; Craik, D.J. Designing macrocyclic disulfide-rich peptides for biotechnological applications. *Nat. Chem. Biol.* **2018**, *14*, 417-427, https://doi.org/10.1038/s41589-018-0039-y
12. Tombling, B.J.; Wang, C.K.; Craik, D.J. EGF-like and other disulfide-rich microdomains as therapeutic scaffolds. *Angew. Chem. Int. Edit.* **2020**, *59*, 11218-11232, https://doi.org/10.1002/anie.201913809
13. Schwarz, E. Cystine knot growth factors and their functionally versatile proregions. *Biol. Chem.* **2017**, *398*, 1295-1308, https://doi.org/10.1515/hsz-2017-0163
14. Wu, R.; Patocka, J.; Nepovimova, E.; Oleksak, P.; Valis, M.; Wu, W.; Kuca, K. Marine invertebrate peptides: Antimicrobial peptides. *Front. Microbiol.* **2021**, *12*, 785085, https://doi.org/10.3389/fmicb.2021.785085

15. Casertano, M.; Menna, M.; Imperatore, C. The ascidian-derived metabolites with antimicrobial properties. *Antibiotics* **2020**, *9*, 510, https://doi.org/10.3390/antibiotics9080510

16. Pavlicevic, M.; Maestri, E.; Marmiroli, M. Marine bioactive peptides-An overview of generation, structure and application with a focus on food sources. *Mar. Drugs* **2020**, *18*, 424, https://doi.org/10.3390/md18080424

17. Arumugam, V.; Venkatesan, M.; Ramachandran, S.; Sundaresan, U. Bioactive peptides from marine ascidians and future drug development–A review. *Int. J. Pept. Res. Ther.* **2018**, *24*, 13-18, https://doi.org/10.1007/s10989-017-9662-9

18. Hansen, I.K.Ø.; Isaksson, J.; Poth, A.G.; Hansen, K.Ø.; Andersen, A.J.C.; Richard, C.S.M.; Blencke, H.-M.; Stensvåg, K.; Craik, D.J.; Haug, T. Isolation and characterization of antimicrobial peptides with unusual disulfide connectivity from the colonial ascidian *Synoicum turgens*. *Mar. Drugs* **2020**, *18*, 51, https://doi.org/10.3390/md18010051

19. Haug, T.; Kjuul, A.K.; Stensvåg, K.; Sandsdalen, E.; Styrvold, O.B. Antibacterial activity in four marine crustacean decapods. *Fish Shellfish Immunol.* **2002**, *12*, 371-385, http://dx.doi.org/10.1006/fsim.2001.0378

20. Albert, A.; Eksteen, J.J.; Isaksson, J.; Sengee, M.; Hansen, T.; Vasskog, T. General approach to determine disulfide connectivity in cysteine-rich peptides by sequential alkylation on solid phase and mass spectrometry. *Anal. Chem.* **2016**, *88*, 9539-9546, https://doi.org/10.1021/acs.analchem.6b02115

21. Solstad, R.G.; Li, C.; Isaksson, J.; Johansen, J.; Svenson, J.; Stensvåg, K.; Haug, T. Novel antimicrobial peptides EeCentrocins 1, 2 and EeStrongylocin 2 from the edible sea urchin *Echinus esculentus* have 6-br-trp post-translational modifications. *PloS One* **2016**, *11*, e0151820, https://doi.org/10.1371/journal.pone.0151820

22. Hansen, K.Ø.; Andersen, J.H.; Bayer, A.; Pandey, S.K.; Lorentzen, M.; Jørgensen, K.B.; Sydnes, M.O.; Guttormsen, Y.; Baumann, M.; Koch, U.; Klebl, B.; Eickhoff, J.; Haug, B.E.; Isaksson, J.; Hansen, E.H. Kinase chemodiversity from the Arctic: The breitfussins. *J. Med. Chem.* **2019**, *62*, 10167-10181, https://doi.org/10.1021/acs.jmedchem.9b01006

23. Haug, T.; Stensvåg, K.; Olsen, Ø.M.; Sandsdalen, E.; Styrvold, O.B. Antibacterial activities in various tissues of the horse mussel, *Modiolus modiolus*. *J. Invertebr. Pathol.* **2004**, *85*, 112-119, https://doi.org/10.1016/j.jip.2004.02.006

24. Moe, M.K.; Haug, T.; Sydnes, M.O.; Sperstad, S.V.; Li, C.; Vaagsfjord, L.C.; de la Vega, E.; Stensvåg, K. Paralithocins, antimicrobial peptides with unusual disulfide connectivity from the red king crab, *Paralithodes camtschaticus*. *J. Nat. Prod.* **2018**, *81*, 140-150, https://doi.org/10.1021/acs.jnatprod.7b00780

25. Stensvåg, K.; Haug, T.; Sperstad, S.V.; Rekdal, Ø.; Indrevoll, B.; Styrvold, O.B. Arasin 1, a proline–arginine-rich antimicrobial peptide isolated from the spider crab, *Hyas araneus*. *Dev. Comp. Immunol.* **2008**, *32*, 275-285, https://doi.org/10.1016/j.dci.2007.06.002

26. Merkler, D.J. C-terminal amidated peptides: production by the in vitro enzymatic amidation of glycine-extended peptides and the importance of the amide to bioactivity. *Enzyme Microb. Tech.* **1994**, *16*, 450-456, https://doi.org/10.1016/0141-0229(94)90014-0

27. Waghu, F.H.; Barai, R.S.; Idicula-Thomas, S. Leveraging family-specific signatures for AMP discovery and high-throughput annotation. *Sci. Rep.* **2016**, *6*, 24684, https://doi.org/10.1038/srep24684

28. Wang, G.; Li, X.; Wang, Z. APD3: the antimicrobial peptide database as a tool for research and education. *Nucleic Acids Res.* **2015**, *44*, D1087-D1093, https://doi.org/10.1093/nar/gkv1278

29. Ansel, H.C.; Norred, W.P.; Roth, I.L. Antimicrobial activity of dimethyl sulfoxide against *Escherichia coli*, *Pseudomonas aeruginosa*, and *Bacillus megaterium*. *J. Pharm. Sci.* **1969**, *58*, 836-839, https://doi.org/10.1002/jps.2600580708

30. Ovchinnikova, T.V.; Balandin, S.V.; Aleshina, G.M.; Tagaev, A.A.; Leonova, Y.F.; Krasnodembsky, E.D.; Men'shenin, A.V.; Kokryakov, V.N. Aurelin, a novel antimicrobial peptide

from jellyfish *Aurelia aurita* with structural features of defensins and channel-blocking toxins. *Biochem. Bioph. Res. Co.* **2006**, *348*, 514-523, https://doi.org/10.1016/j.bbrc.2006.07.078

31. Vidal-Dupiol, J.; Ladrière, O.; Destoumieux-Garzón, D.; Sautière, P.-E.; Meistertzheim, A.-L.; Tambutté, E.; Tambutté, S.; Duval, D.; Fouré, L.; Adjeroud, M.; Mitta, G. Innate immune responses of a scleractinian coral to vibriosis. *J. Biol. Chem.* **2011**, *286*, 22688-22698, https://doi.org/10.1074/jbc.M110.216358

32. Jacob, R.B.; McDougal, O.M. The M-superfamily of conotoxins: a review. *Cell. Mol. Life Sci.* **2010**, *67*, 17-27, https://doi.org/10.1007/s00018-009-0125-0

33. Svangård, E.; Göransson, U.; Hocaoglu, Z.; Gullbo, J.; Larsson, R.; Claeson, P.; Bohlin, L. Cytotoxic cyclotides from *Viola tricolor*. *J. Nat. Prod.* **2004**, *67*, 144-147, https://doi.org/10.1021/np0301011

34. Göransson, U.; Luijendijk, T.; Johansson, S.; Bohlin, L.; Claeson, P. Seven novel macrocyclic polypeptides from *Viola arvensis*. *J. Nat. Prod.* **1999**, *62*, 283-286, https://doi.org/10.1021/np9803878

Supporting information

Isolation and characterization of St-CRPs: Cysteine-rich peptides from the Arctic marine ascidian *Synoicum turgens*

Ida K. Ø. Hansen [1], Philip B. Rainsford [2], Johan Isaksson [2], Kine Ø. Hansen[3], Klara Stensvåg [1], Anastasia Albert [4], Terje Vasskog [5] and Tor Haug [1,*]

[1] The Norwegian College of Fishery Science, Faculty of Biosciences, Fisheries and Economics, UiT The Arctic University of Norway, Breivika, N-9037 Tromsø, Norway; klara.stensvag@uit.no (K.S.)

[2] Department of Chemistry, Faculty of Science and Technology, UiT The Arctic University of Norway, Breivika, N-9037 Tromsø, Norway; philip.rainsford@uit.no (P.B.R.); johan.isaksson@uit.no (J.I.)

[3] Marbio, UiT The Arctic University of Norway, N-9037, Tromsø, Norway; kine.o.hanssen@uit.no

[4] Norce, Siva Innovasjonssenter, Sykehusveien 21, 9019 Tromsø; anastasia.albert@norut.no (A.A.)

[5]Department of Pharmacy, Faculty of Health Sciences, UiT The Arctic University of Norway, Breivika, N-9037 Tromsø, Norway

* Correspondence: ida.k.hansen@uit.no; Tel.: +47-77-64-92-66 (I.K.Ø.H.), tor.haug@uit.no; Tel.: +47-77-64-60-71 (T.H.)

Table of contents

Figure S.1. UPLC-PDA chromatogram (detection wavelength, 280 nm) to determine the purity (97%) of St-CRP-1 isolated from *S. turgens*.

Figure S.2. UPLC-PDA chromatogram (detection wavelength, 280 nm) to determine the purity (100%) of St-CRP-2 isolated from *S. turgens*.

Identified fragments from *de novo* sequencing

Identified a-ions				558.17													
Identified b-H₂O ions	173.04			568.15		758.19	871.28		1061.32	1174.40	1273.47			1530.61			
Theoretical b-ions	191.05	294.06	423.10	586.16	689.17	776.21	889.29	976.32	1079.33	1192.41	1291.48	1378.52	1435.54	1548.62	1661.70	1764.71	1867.72

Sequence: S — C — C — E — Y — C — S — X — S — C — X — V — S — G — X — X — C — C — Q - Amide

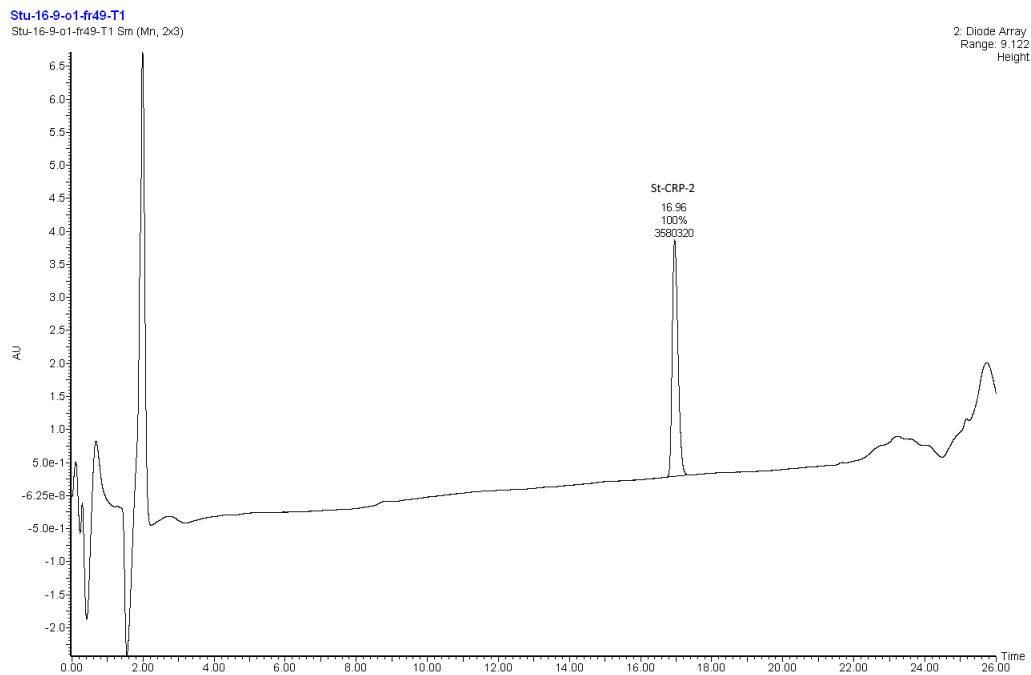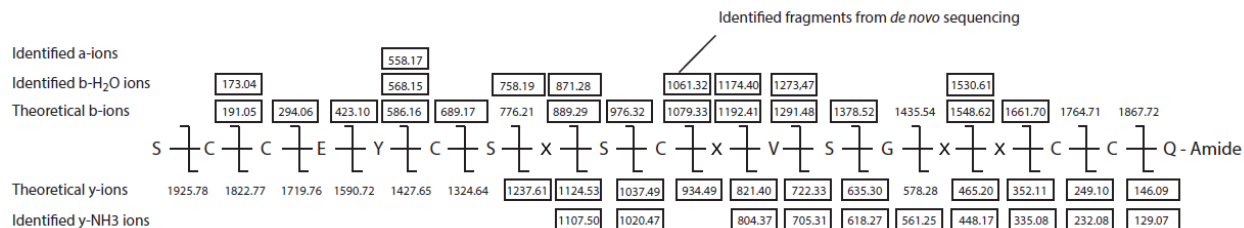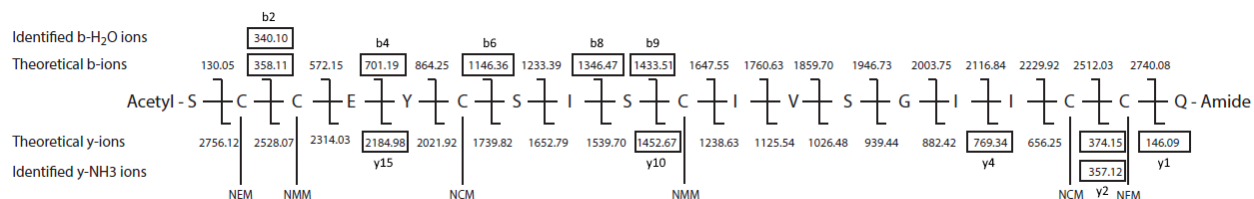|																	
Theoretical y-ions	1925.78	1822.77	1719.76	1590.72	1427.65	1324.64	1237.61	1124.53	1037.49	934.49	821.40	722.33	635.30	578.28	465.20	352.11	249.10	146.09
Identified y-NH3 ions							1107.50	1020.47		804.37	705.31	618.27	561.25		448.17	335.08	232.08	129.07

Figure S3. *De novo* sequencing of St-CRP-2 isolated from *S. turgens*, showing the identified a-, b-, b-H₂O, y- and y-NH₃ ions in frames. X = I/L. The sequencing was done on a Xevo G2-XS QToF MS (Waters).

	b2			b4		b6		b8	b9									
Identified b-H₂O ions	340.10																	
Theoretical b-ions	130.05	358.11	572.15	701.19	864.25	1146.36	1233.39	1346.47	1433.51	1647.55	1760.63	1859.70	1946.73	2003.75	2116.84	2229.92	2512.03	2740.08

Sequence: Acetyl - S — C — C — E — Y — C — S — I — S — C — I — V — S — G — I — I — C — C — Q - Amide

				y15					y10					y4			y1
Theoretical y-ions	2756.12	2528.07	2314.03	2184.98	2021.92	1739.82	1652.79	1539.70	1452.67	1238.63	1125.54	1026.48	939.44	882.42	769.34	656.25	374.15	146.09
Identified y-NH3 ions																	357.12	

NEM   NMM   NCM   NMM   NCM y2 NEM

Figure S4. The alkylation pattern 2xNEM + 2xNMM + 2xNCM of the acetylated [M+2H]²⁺ of St-CRP-2, isolated from *S. turgens*. The framed masses are b-, b-H₂O, y- and y-NH₃ ions identified in the MS/MS spectra. The X in the sequence is either I or L. The sequencing was done on a Xevo G2-XS QToF MS (Waters).

Table S1. Antimicrobial activity given as minimal inhibitory concentrations (MIC) of solid phase extract (SPE) fractions and the organic extract of *S. turgens*. The measurements were end point values of OD₅₉₅ after 24 h at 35˚C. Bacterial test strains: *C. g.* - *Corynebacterium glutamicum*, *B. s.* - *Bacillus subtilis*, *S. a.* - *Staphylococcus aureus*, *E. c.* - *Escherichia coli*, *P. a.* - *Pseudomonas aeruginosa*.

	Antimicrobial activity (MIC; mg/mL)				
Extract	*C. g.*	*B. s.*	*S. a.*	*E. c.*	*P. a.*
10% SPE	1.25	5.00	5.00	10.00	5.00
20% SPE	2.50	2.50	5.00	5.00	5.00
30% SPE	0.16	0.16	2.50	5.00	5.00
40% SPE	0.04	0.08	2.50	5.00	2.50
80% SPE	0.31	0.31	2.50	5.00	2.50
Organic	2.50	2.50	10.00	>10.00	>10.00

Table S2. Proton (^1H) NMR and chemical shift assignments for St-CRP-1, isolated from *S. turgens*.

Residue	N^{1}H (ppm) 600 MHz, H$_2$O	α^{1}H (ppm) 600 MHz, H$_2$O	β^{1}H (ppm) 600 MHz, H$_2$O	γ^{1}H (ppm) 600 MHz, H$_2$O	other ^{1}H (ppm) 600 MHz, H$_2$O
CYS*1*	8.80	4.349	3.038, 2.875	-	-
CYS*2*	9.003	4.835	3.323	-	-
ASP*3*	9.028	4.262	2.698	-	-
GLN*4*	7.866	4.347	1.884, 1.944	2.229	6.785, 7.416
CYS*5*	8.793	4.676	2.895, 3.018	-	-
TYR*6*	7.581	4.596	2.812, 3.027	-	εCH: 6.772 δCH:6.926
GLY*7*	8.686	3.703, 3.849	-	-	-
PHE*8*	8.766	4.108	2.928, 3.182	-	εCH: 7.196 δCH: 7.233 ζCH: 7.147
CYS*9*	8.244	3.985	3.075, 3.371	-	-
ARG*10*	6.803	4.031	1.348, 1.632	1.439, 1.463	δCH$_2$: 3.060 εNH: 7.046
LEU*11*	7.712	3.963	1.585, 1.598	1.487	δCH$_3$: 0.780, 0.810
VAL*12*	7.234	4.226	2.188	0.470, 0.569	-
ASP*13*	7.743	4.438	2.639, 4.438	-	-
ASN*14*	8.222	5.150	2.293, 2.777	NH$_2$: 6.760, 7.355	-
CYS*15*	8.656	4.814	3.228, 3.257	-	-
CYS*16*	8.716	4.426	2.585, 3.155	-	-
ASN*17*	8.750	4.639	2.673, 2.752	NH2: 6.792, 7.504	-
SER*18*	8.199	4.295	3.758, 3.826	-	-

*Bruker Avance III HD spectrometer operating at 600 MHz for protons, equipped with an inverse detected TCI probe cryogenically enhanced for 1H, 13C and 2H.

Table S3. Carbon (^{13}C) NMR and chemical shift assignments for St-CRP-1, isolated from *S. turgens*.

Residue	^{13}C (ppm) 150 MHz, H$_2$O	α^{13}C (ppm) 150 MHz, H$_2$O	β^{13}C (ppm) 150 MHz, H$_2$O	γ^{13}C (ppm) 150 MHz, H$_2$O	Other (^{13}C (ppm) 150 MHz, H$_2$O)
CYS*1*	-	51.05	38.73	-	-
CYS*2*	-	51.38	42.86	-	-
ASP*3*	-	53.25	36.64	-	-
GLN*4*	-	51.97	25.81	30.69	177.75
CYS*5*	-	51.25	32.72	-	-
TYR*6*	-	53.52	37.87	127.02	δC: 130. 58 εC: 115.47 ζC: 154.94
GLY*7*	-	43.56	-	-	-
PHE*8*	-	58.57	36.21	135.21	δC: 128.86 εC: 127.55 ζC: 129.01
CYS*9*	-	56.47	41.35	-	-
ARG*10*	-	55.58	27.39	24.30	δC: 40.625 ζC: 156.651
LEU*11*	-	54.93	39.24	23.92	δC: 21.079, 21.601
VAL*12*	-	57.88	27.79	15.74, 18.32	-
ASP*13*	-	51.06	36.53	-	-
ASN*14*	-	48.63	37.87	-	-
CYS*15*	-	53.28	35.99	-	-
CYS*16*	-	52.66	36.50	-	-
ASN*17*	-	50.47	36.09	-	-
SER*18*	174.32	55.59	61.02	-	-

* Bruker Avance III HD spectrometer operating at 600 MHz for protons, equipped with an inverse detected TCI probe cryogenically enhanced for 1H, 13C and 2H

Table S4. RMSD of top St-CRP-1 structures generated through final simulated annellation constraints

Structure Name	All atom RMSD	Backbone RMSD	Carbon RMSD	Heavy atom RMSD
SA_252	0	0	0	0
SA_463	1.215	0.323	0.217	0.675
SA_6	1.624	0.355	0.258	0.628
SA_37	1.725	0.63	0.793	0.936
SA_372	1.749	0.526	0.513	0.852
SA_487	1.776	0.527	0.546	0.816
SA_48	1.793	0.658	0.75	0.963
SA_401	1.802	0.355	0.249	0.628
SA_382	1.872	0.531	0.517	0.869
SA_202	1.874	0.602	0.73	1.003
SA_495	1.885	0.512	0.502	0.867
SA_78	1.899	0.737	0.691	1.078
SA_238	1.927	0.541	0.519	0.905
SA_20	1.967	0.924	0.917	1.182
SA_113	1.974	1.004	1.111	1.412
SA_199	1.985	0.706	0.838	0.989
SA_100	2.074	0.533	0.48	0.925
SA_11	2.101	0.781	0.704	1.028
SA_462	2.178	0.532	0.506	0.906
SA_215	2.214	0.531	0.551	0.815
SA_80	2.215	0.538	0.552	0.802
SA_221	2.239	0.612	0.668	1.025
SA_76	2.259	0.766	0.854	0.948
SA_427	2.309	0.665	0.665	0.87
SA_97	2.374	0.635	0.686	0.932
SA_226	2.433	0.732	0.815	1.03
SA_412	2.509	0.87	0.968	1.059
SA_367	3.521	2.788	3.216	2.919
SA_488	3.726	2.88	3.347	3.047
SA_338	3.989	3.211	3.657	3.364
SA_436	4.13	3.192	3.645	3.307